FACTORS CONTROLLING PHYTOPLANKTON SEASONAL SUCCESSION IN MT BOLD RESERVOIR, SOUTH AUSTRALIA.

by

Roderick L. Oliver B.Sc.(Hons)(Adel.)

Department of Botany

University of Adelaide

A thesis submitted to the University of Adelaide in fulfilment of the requirements for the degree of Doctor of Philosophy.

December 1981

This thesis contains no material which has been accepted for the award of any other degree or diploma in any university and, to the best of my knowledge, contains no material previously published or written by another person, except where due reference is made in the text.

SUMMARY

The thesis describes an investigation of factors controlling phytoplankton seasonal succession in Mt Bold Reservoir, South Australia (35°07'S, 138°43'E, maximum surface area = 3.08 km^2, maximum depth = 47 m) a warm, monomictic lake.

An extensive monitoring programme provided data on seasonal variations in species composition, phytoplankton biomass, integral photosynthesis and changes in the chemical and physical environments.

Investigation of the light regime indicated severe competition for radiation between the phytoplankton and other suspended and dissolved compounds of the water column. High levels of "gelbstoff" caused rapid modification of light intensity, and spectral quality with depth, an effect amplified by the high turbidity. This had important consequences for biomass levels and integral photosynthesis, and in conjunction with mixing resulted in very low winter biomass levels despite relatively warm water temperatures.

Phytoplankton growth was initiated by the reduction of mixing depth caused by the onset of thermal stratification in spring. Biomass increase was linearly related to the irradiance absorbed per unit chlorophyll *a* up to a critical value, where apparently growth was light saturated. On attaining this value the typical spring bloom occurred.

The general successional sequence, cryptomonads → diatoms → chlorophytes → cyanophytes followed the temporal gradient of decreasing water turbulence with the cyanophytes dominating the period influenced

by an intense thermocline. The rapidity with which the water column stabilized, controlled the temporal extent of the successional sequence. When thermocline formation occurred rapidly growth of diatoms and cyanophytes began simultaneously, however diatoms soon disappeared from the stable water column, implicating variations in sinking rate as a determinant.

The assessment of morphological and physiological adaptations to sinking rate has been impeded by an inability to measure phytoplankton cellular densities. A technique was developed using density gradient centrifugation which enabled the magnitude and distribution of population cellular densities to be measured, and the effect of phytoplankton morphology on sinking rates to be assessed from simultaneous sinking experiments. Application of the technique to field populations provided data on the role of sinking rate in seasonal succession.

Chemical data showed that algal growth resulted in marked decreases in nutrient concentrations of the epilimnion. To provide direct data on the availability of nutrients to the phytoplankton, the biological growth potential of filtered water samples was assessed using inocula of the *in situ* phytoplankton assemblage. During the summer a large vertical separation developed between available light and available nutrients, a situation intensified by the rapid attenuation of light in the highly coloured, turbid water.

Environmental and biological determinants of photosynthesis were investigated using measured photosynthesis - irradiance relationships, and an empirical model which closely estimated integral photosynthesis (Talling 1957b). The turbidity of the reservoir focussed attention on the importance of phytoplankton irradiance absorption, and the

integral model was recast into more functional units which partitioned integral photosynthesis into components of light absorption and quantum yield. Application of this model to data from two lakes illustrated its ability to compare diverse aquatic environments. Results showed integral photosynthesis to be proportional to the light absorbed by phytoplankton up to a "critical" level, above which quantum yield and integral photosynthesis declined.

Derived functions describing phytoplankton light absorption demonstrated the potential role of this factor in influencing phytoplankton seasonal succession.

ACKNOWLEDGEMENTS

This project was carried out in the Department of Botany, University of Adelaide, with financial support provided by an Adelaide University Research Grant.

I thank my supervisor, Dr G. G. Ganf, for his continual guidance, encouragement and support.

I have benefited substantially from discussion and information provided by members of staff, particularly Dr J. Wiskich, Dr. R. Sinclair and Prof. G. Martin.

I am indebted to Brian Rowlands, Richard Norrish and Tony Fox for their technical advice.

To my friends, who rallied around me in the final stages of thesis preparation, and laboured so hard and long, all I can say is 'thank you'; to Cathie Buddle for the majority of diagrams, Joy Fox for diagrams and assistance with collating and corrections, and to Russell Shiel for his patience with the long hours of typing.

My thanks also to Carol Grose for typing two of the chapters.
The Engineering and Water Supply Department allowed access to Mt Bold Reservoir and provided boating facilities. I am most grateful for this and for the background data provided by the Boliver Laboratories, which was invaluable.

Finally I thank my wife Estelle, for her support, patience and understanding, without which this would not have been achieved.

TABLE OF CONTENTS

SYMBOLS

		Units
A	General symbol for thermal eddy conductivity and vertical eddy diffusivity	$cm^2\ s^{-1}$
A_Z	Vertical eddy conductivity at depth Z	$cm^2\ s^{-1}$
A(Z)	Irradiance absorbed by all components at depth Z	$\mu E\ m^{-3}s^{-1}$
A*(Z)	Irradiance absorbed by phytoplankton at depth Z	$\mu E\ m^{-3}s^{-1}$
$A_b^*(Z)$	Irradiance absorbed by phytoplankton per unit chlorophyll a	$\mu E\ mgchla^{-1}s^{-1}$
$\bar{A}^*$	Average light absorbed per unit chlorophyll a in mixed zone	$\mu E\ mgchla^{-1}s^{-1}$
B	Total phytoplankton cell volume	$mm^3\ \ell^{-1}$
bi	Cell volume of species i	$mm^3\ \ell^{-1}$
b	Chlorophyll a concentration	$mg\ chla\ m^{-3}$
$\bar{b}$	Growing season average chlorophyll a concentration of euphotic zone samples	$mg\ chla\ m^{-3}$
b_b	Backscattering coefficient	$\ell n\ unit\ m^{-1}$
b_b^1	Asymptotic backscattering coefficient	$\ell n\ unit\ m^{-1}$
D	Nominal diameter of a non-spherical body defined as the diameter of a sphere of equal volume	cm
E	Einstein	
F_{SZ}	Mean flux of substance S in vertical direction	$quantity\ cm^{-2}s^{-}$
g	Acceleration due to gravity	$cm\ s^{-2}$
H_ω	Thermal energy flux	$calorie\ cm^{-2}s^{-1}$
I_Z	Irradiance intensity at depth Z (PAR)	$\mu E\ m^{-2}s^{-1}$
I_o^1	Incident irradiance intensity corrected for surface reflection (PAR)	$\mu E\ m^{-2}s^{-1}$
$\bar{I}_o^1$	Daily average incident irradiance corrected for surface reflection (PAR)	$\mu E\ m^{-2}s^{-1}$
$I_{o\lambda}^1$	Incident irradiance at wavelength λ	$\mu E\ m^{-2}s^{-1}$
$\bar{I}$	Mean total irradiance of the mixed zone	$MJ\ m^{-2}d^{-1}$
I_o	Average daily total incident irradiance calculated over a week	$MJ\ m^{-2}d^{-1}$

I_k	Light intensity characterising the onset of light saturation of photosynthesis	$\mu E\ m^{-2}s^{-1}$
I_k*	Absorbed irradiance per unit chlorophyll a characterising the onset of light saturation of photosynthesis	$\mu E\ mgchla^{-1}s^{-1}$
I_U, I_D	Upwelling and downwelling irradiance respectively	$\mu E\ m^{-2}s^{-1}$
K_{SZ}	Vertical eddy diffusivity	$cm^{-2}s^{-1}$
$\overline{OP}$	Growing season average orthophosphate-P concentration of surface samples	$\mu g\ \ell^{-1}$
P_o, P_t	Cell number within the epilimnion at time zero and time t	
P_m	Maximum specific rate of photosynthesis (photosynthetic capacity	$mgC\ mgchla^{-1}h^{-1}$
P(Z)	Specific rate of photosynthesis at depth Z	$mgC(mgO_2)mg_{chla^{-1}h^{-}}$
$\overline{PP}$	Growing season average particulate phosphate concentration of surface samples	$\mu g\ \ell^{-1}$
ΣP	Hourly integral rate of photosynthesis	$mgC\ m^{-2}h^{-1}$
$\Sigma\Sigma P$	Daily integral rate of photosynthesis	$mgC\ m^{-2}d^{-1}$
P^1	Phytoplankton cellular density	$g\ cm^{-3}$
P	Density of lake water	$g\ cm^{-3}$
R	Reflectance, ratio of upwelling to downwelling irradiance	
R_A	Asymptotic reflectance	
R^1	Specific rate of respiration	$mgC(mgO)mgchla^{-}h^{-1}$
$\Sigma\Sigma R$	Daily integral respiration rate	$mgC(mgO_2)m^{-2}d^{-1}$
r	Ratio of specific respiration rate (R) to maximum rate of photosynthesis (P_m)	
S	Extinction coefficient due to light scattering	$\ell n\ unit\ m^{-1}$
S.D.	Summed difference index of succession rate (equation 5.3)	d^{-1}
$\frac{\partial S}{\partial Z}$	Vertical concentration gradient of substance S	$weight\ cm^{-3}$

$\overline{TN}$	Growing season average total nitrogen concentration of surface samples	$\mu g\ \ell^{-1}$
$\overline{TP}$	Growing season average total phosphorus concentration of surface samples	$\mu g\ \ell^{-1}$
$\overline{TDP}$	Growing season average total dissolved phosphorus concentration of surface samples	$\mu g\ \ell^{-1}$
t	Time	
V	Terminal sinking velocity of a non-spherical body	$cm\ s^{-1}$
V^1	Average sinking rate from epilimnion	$m\ d^{-1}$
Z_{eu}	Depth of euphotic zone	m
Z	Depth of mixed zone	m
α	Initial slope of photosynthesis irradiance curve	$mgCmgchla^{-1}h^{-1}(\mu E\ m^{-2}s^{-1})^{-1}$
α^1	" " " " " "	mgC mgchla^{-1} per E m^{-2}
α_m^*	" " " " irradiance absorption curve	mgC per E
Δ	Daylength	h
ε	Vertical extinction coefficient	ℓn units m^{-1}
ε_G	" " " - dissolved colour	" " "
ε_ω	" " " - water	" " "
ε_p	" " " - suspended particulate matter	" " "
ε_q	Sum of ε_G, ε_ω and ε_p	" " "
$\varepsilon_{G+\omega}$	Dissolved colour and water	" " "
$\varepsilon\lambda$	Wavelength λ	" " "
$\varepsilon_s b$	Phytoplankton	" " "
$\overline{\varepsilon}p$		
$\overline{\varepsilon}_s b$	As above, but measured in a non-scattering medium	" " "
$\overline{\varepsilon}_{G+\omega}$		
ε_s	Specific extinction coefficient per unit chlorophyll a	m^2 mgchla^{-1}
η	Viscosity of water	poise
θ	Temperature	^oC
θ_H	Average temperature of 1 metre layer midway through spring heating period	^oC

θ_o	Initial temperature	^oC
θ_t	Temperature after time t	^oC
ϕ	Quantum yield	mole C per Einstein absorbed
ϕ_m	Maximum quantum yield	"
$\overline{\phi}$	Average quantum yield in the euphotic zone	"
ϕ_f	Coefficient of form resistance	

INTRODUCTION

1.1 Project Rationale and Aims

A fundamental aim of limnological research is the understanding and prediction of phytoplankton seasonal biomass patterns and species succession. The factors influencing phytoplankton dynamics have not only theoretical interest, but also practical importance to the successful management of water bodies. The necessity for such knowledge is amplified in South Australia by the general aridity of the state, and the seasonal occurrence of problematic blue-green algal blooms in many of the reservoirs. Despite the apparent need for such research, there are no published accounts on phytoplankton ecology for South Australian water bodies, and limited documentation available on either freshwater or marine habitats for Australia generally. This dearth of basic data precludes the formulation of all but the most general hypotheses based on results from water bodies overseas. Furthermore the applicability of models describing phytoplankton photosynthesis and biomass fluctuations in lakes of the northern hemisphere, must be critically assessed with relevant data before accepted. Consequently a primary aim of this project was to provide fundamental information necessary for the formulation of hypotheses, design of experiments and testing of imported models. Only with such data can we begin to understand the functioning of our water bodies, and constructively participate in the fundamental science.

The extensive literature on phytoplankton ecology identifies numerous environmental variables which potentially affect the size and

composition of phytoplankton populations (Lund 1965; Hutchinson 1967; Round 1971; Kalff & Knoechel 1978; Reynolds 1980). The measurement of all such variables is physically impossible without extensive resources, and potentially fruitless without the guidance of a fundamental data base on which to erect hypotheses (Kalff & Knoechel 1978). The problem faced when undertaking study of an unknown area is therefore selection of those factors likely to play a primary role in determining biomass and species fluctuations of the phytoplankton population. To this end a short review of relevant literature is presented as rationale for the specific topics investigated.

The annual cycle of algae in temperate lakes, deep enough to stratify, is intimately related to the seasonal changes in thermal stratification (Lund 1965; Round 1971; Kalff & Knoechel 1978). Peak biomass concentrations frequently occur in spring and autumn, separated by reduced concentrations during summer and winter (Round 1971). In general the spring increase closely correlates with the onset of thermal stratification, and the autumn maximum with the beginning of autumnal overturn. Characteristic of many temperate waters is the spring occurrence of diatoms, and the summer occurrence of green and blue-green algae (Pearsall 1932; Lund 1965; Kalff & Knoechel 1978; Reynolds 1980).

In optically deep lakes the low winter biomass levels are associated with light limitation, due to the length of time the phytoplankton are forced to stay in the unilluminated regions of the water column by turbulent mixing. The influence of light on phytoplankton growth is

mediated through the reactions of photosynthesis, and a significant mathematical framework has been derived describing photosynthesis-irradiance relationships. Early models assumed rate of photosynthesis to be proportional to light intensity and so to decrease exponentially with depth (Sverdrup 1953). The concept of light saturation of photosynthesis was later recognized and Talling (1957a, b) described the change in rate of photosynthesis with depth based on the photosynthesis-irradiance relationship of Smith (1936).

A further complication arose from the observation of light inhibition at high irradiance intensities and substantial effort has been expended on investigating functions to describe the total photosynthesis-irradiance curve (Steele 1962; Vollenweider 1965; Fee 1969, 1973a; Platt et al. 1980).

The variable of primary interest when considering population fluctuations is the areal rate of photosynthesis, obtained from the depth integral of the photosynthesis-depth curve. Talling (1957b) derived a depth integral based on the photosynthesis-irradiance relationship of Smith (1936), and this has been successfully applied to a broad range of aquatic habitats (Talling 1965; Bindloss 1974; Ganf 1975; Jewson 1979; Harris et al. 1980). The success of this model, despite its neglect of surface inhibition, coupled with the difficulty in applying and interpreting the more complex models, has reduced the practical use of functions incorporating surface inhibition.

The model proposed by Talling (1957b) assumes a homogeneous water mass.

For cases of marked vertical inhomogeneity Fee (1973b) has provided a computer program to numerically calculate daily integral photosynthesis from daily rates estimated for a series of small vertical layers.

The concept of a critical mixing depth which inhibits phytoplankton growth by light limitation appeared early in the literature (Gran & Braarud 1935; Riley 1942; Sverdrup 1953). It is defined as the depth to which the phytoplankton must be circulated for integral photosynthesis and integral respiration to balance over a 24h period. Incorporation of the photosynthesis-depth integral of Talling (1957b), into a model inter-relating photosynthesis and respiration with the optical properties of the water column and the ratio of euphotic to mixed depth, provided a basis for assessing the suitability for growth of the light regime of the mixed water column (Talling 1957b, 1971; Steel 1973, 1980).

Available data on the light regime of Australian inland waters (Kirk 1976b, 1977, 1979; Ganf 1976, 1980; Bowles et al. 1979) has demonstrated their extreme turbidity. This attribute, coupled with the monomictic thermal pattern which appears typical of Australian lakes and reservoirs (Williams & Wan 1972), suggests that irradiance and thermal stratification might be significant factors determining biomass fluctuations.

In the field of phytoplankton ecology interest in photosynthesis measurements has not only centred on determination of integral photosynthesis, but also the study of adaptation to changing irradiance

(Jorgensen & Steeman Nielsen 1966; Yentsch & Lee 1966; Vollenweider 1970; Steeman Nielsen 1974; Jones 1978; Harris et al. 1980). Adaptations, or physiological adjustments (Beardall & Morris 1976) of photosynthetic efficiency and capacity are of interest to studies of seasonal succession as they may reflect the relative capability of different algal groups to utilize the light regime (Falkowski & Owens 1980). In turbid waters where suspended particles and dissolved colour competitively absorb the available light, such adaptations may be of particular importance. Fundamentally the question of phytoplankton adaptation to variations in irradiance is one of light absorption, however, only recently have algal light absorption capabilities been specifically incorporated in photosynthesis models (Bannister 1974; Smith 1980).

The frequently observed decline in nutrient concentrations following vernal increase in phytoplankton biomass, has led to the view that nutrients are a major factor limiting population size, and a driving force to species succession (Pearsall 1932; Lund 1950, 1965). It has been demonstrated that a wide range of nutrients may potentially act to limit phytoplankton growth (Lund 1950; Droop 1970; Goldman 1972; Smayda 1974), however nitrogen and phosphorus have long been considered major determinants (Lund 1965). The development of chlorophyll-phosphorus models has confirmed the significant role of phosphorus in determining biomass levels for a large number of northern hemisphere lakes (Sakamoto 1966; Vollenweider 1970; Dillon & Rigler 1974). The extension of these models to include the effect of nitrogen availability on the utilization of available phosphorus, has further refined predictions (Smith 19-), and

demonstrated the importance of nitrogen in lakes with relatively high phosphorus concentrations. However these models provide no insight to the timing and magnitude of potential blooms, or to species succession.

The determination of growth limiting nutrients *in situ* is far from simple. Chemical analyses of water samples may in some cases provide the necessary information (Schelske et al. 1978; Forsberg et al. 1978), but frequently ambient concentrations do not reflect the resource supply (Stewart et al. 1978). Smayda (1974) bioassayed water samples using the marine diatom *Thalassiosira pseudonana* and demonstrated that routine chemical analysis could not be used to predict the growth and succession of species in Narragansett Bay.

Although bioassays represent an important technique for determining nutrient availability (Smayda 1974; O'Brien & de Noyelles 1976; Schelske et al. 1978) the water sample is usually cut off from sources of nutrient supply such as re-cycling. Consequently the absence of detectable levels of nutrients cannot necessarily be equated with nutrient limitation.

Healey (1975) reviewed the literature on cellular composition under varying nutrient conditions and suggested a number of physiological changes useful as indicators of nutrient limitation, and providing a direct means of assessing the *in situ* nutrient supply. The use of these indices is dependent upon measuring cellular attributes of the phytoplankton, this is frequently difficult as algae comprise only a fraction of the seston.

The many problems associated with determining *in situ* availability of nutrients has resulted in few unambiguous examples of the dependence of phytoplankton growth on the resource supply.

Lund (1950) correlated the decline in spring diatom-growth with silica depletion, a result supported in some lakes (Kilham 1971) but not others (Talling 1966). Knoechel and Kalff (1975) demonstrated that the shift in dominance from diatoms to blue-green algae in Lac Hertel resulted from the decline of the population through sedimentation.

Unequivocal evidence for the potential influence of nutrient availability on species succession comes from laboratory experiments on nutrient uptake kinetics (Kilham 1971; Droop 1974; Tilman & Kilham 1976). These have demonstrated variation in the capability of phytoplankton species to utilize different concentrations of nutrients. Titman (1976) experimentally confirmed the resource based competition theory, and successfully described the distribution and relative abundance of two diatom species along a transect in Lake Michigan on the basis of their ability to use silicate or phosphate. In general however, application of the steady-state laboratory results to the field situation is fraught with difficulty (Harris 1980), and interpretation of the significance of different uptake rates to biomass development and species succession obtuse (Kalff & Knoechel 1978).

Despite the problems of interpreting nutrient measurements the literature suggests that in stratified lakes nutrient depletion resulting from extensive algal growth in the epilimnion is likely to

limit summer biomass levels.

Kalff & Knoechel (1978) emphasized the importance of loss factors to fluctuations in phytoplankton populations, and the need for a better understanding of loss processes. In a water body which thermally stratifies, turbulence will show marked seasonal variation. Hutchinson (1967) after considering the hydromechanics of the plankton, concluded,

> "It is quite possible that much of the seasonal succession of the phytoplankton is due to this interrelation between turbulence and sinking speed".

Phytoplankton sinking rates have been extensively studied with a view to assessing adaptations to suspension (Smayda & Boleyn 1965, 1966a, b; Eppley et al. 1967; Smayda 1970; Reynolds & Walsby 1975; Titman & Kilham 1976). Historically the diverse shapes of planktonic organisms focused attention on morphological adaptations to flotation (Smayda 1970), however it became evident that sinking rates frequently varied independently of changes in cell morphology (Smayda & Boleyn 1965, 1966a, b; Eppley et al. 1967; Titman & Kilham 1976).

These results implied that cellular density changes were important determinants of phytoplankton sinking rates, and that adaptations to suspension could only be assessed when density and morphological factors were discriminated. The lack of a technique to readily measure phytoplankton cellular densities has severely handicapped investigation of adaptations to suspension. Only studies of the gas-

vacuolate blue-green algae, which undergo extreme density variations, have continued successfully (Walsby 1971, 1978; Reynolds & Walsby 1975; Allison & Walsby 1981).

Recently, the major factors described in the preceeding paragraphs have been combined into a general hypothesis of phytoplankton succession. Lewis (1978a) suggested a hypothetical time tract for the succession of algal species in tropical Lake Lanao which involved the interplay between water turbulence, mixing depth, light and nutrient availability. The successional sequence described, commenced with diatoms during periods of low light availability, high nutrients, deep mixing and high turbulence. Pulses of green algae, blue-green algae and finally dinoflagellates occurred successively as mixing and turbulence decreased, light availability increased, and nutrient availability decreased. Reynolds (1980) has produced a similar successional sequence for a number of English lakes.

Based on the general concepts embodied in the literature the following areas were delineated for detailed research to be carried out on one of Adelaide's metropolitan reservoirs, Mt. Bold Reservoir.

a) Investigate the optical properties with particular reference to the significance of turbidity and dissolved colour on light attenuation.

b) Describe the seasonal thermal regime and assess its effect on biomass patterns.

c) Determine the availability of nutrients and their influence on phytoplankton growth.

d) Describe the seasonal variation in phytoplankton biomass and species succession.

e) Measure the seasonal variation in phytoplankton photosynthesis and assess the effect of variations in phytoplankton irradiance absorption capabilities.

f) Investigate phytoplankton adaptations to suspension.

DESCRIPTION OF THE STUDY AREA

1.2 General Introduction

The Mt. Lofty Ranges rise to the east of Adelaide in a series of steep scarps terminating in several levels of benches and high planes. The summit plain stands at 300-400m, but residual remnants such as Mt. Lofty (727m) protrude above this level. The ranges have a dominating effect on the climate of the Adelaide region through orographic uplift of the easterly moving low pressure belt which influences the southern regions of the state in winter (Schwerdtfeger 1976). As a result the Adelaide region has a climate anomalous to the rest of the state, which in general is arid, some 80% having less than 250mm of precipitation annually (Fig. 1.1). In summer the southerly shift of the low pressure belt results in the Adelaide region experiencing prolonged dry periods typical of Mediterranean climates. The concomitant absence of cloud and extreme dryness of the air cause evaporation rates of 200mm per month in January compared to 40mm per month in July (Schwerdtfeger 1976). The average annual rate of 1500mm (Specht 1972), represents a potential loss equivalent to twice the average precipitation. The lack of summer rainfall and the general aridity of the state has necessitated the construction of large bulk storage reservoirs to serve the needs of

domestic, industrial and agricultural requirements. The Mt. Lofty Ranges constitute a major source of water and suitable storage sites, and provides a valuable water resource to the state.

1.3 General Characteristics of the Mt. Bold Reservoir Catchment

Mount Bold Reservoir (35°07'S, 138°43'E) was constructed in 1938 by impoundment of the Onkaparinga River. The catchment covers an area of 388km^2 most of which is drained by the Onkaparinga River and tributaries (Fig. 1.2 & 1.3).

The soils in the area are predominantly acidic duplex podzols underlayed by sandstone, slate, quartzite or schist (Northcote 1976). Of particular interest is the general deficiency of these soil types in nitrogen and phosphorus as well as some trace elements (eg. K, Zn and Cu).

The native vegetation of the catchment has been largely cleared, and only in the reserve around the reservoir is there any extensive area of the original sclerophyllous woodland remaining. This is dominated by *Eucalyptus* species (eg. *E. obliqua, E. baxteri, E. leucoxylon, E. camaldulensis*) with a heath type understory (mainly members of the Proteaceae, Epacridaceae, and Dilleniaceae).

Precipitation in the catchment is the highest in South Australia (Fig. 1.3) and until the 1950's provided the major input to the reservoir. However increased water demand led to the construction of a pipeline to carry water from the Murray River at Murray Bridge, to a point on

the Onkaparinga River just above Mt. Bold Reservoir. In recent times increasing use has been made of Murray River water to augment the natural supply.

As the catchment is an area of high rainfall in an otherwise arid region, agricultural exploitation began very early. Districts suitable for orchards and market gardening were discovered and still thrive with the use of artificial fertilizers. The addition of fertilizers has further enabled the extensive podzolic soils to be utilized for both agricultural and stock grazing purposes (Fig. 1.2, Table 1.2).

The advent of rapid transport combined with the close proximity of the ranges to metropolitan Adelaide has caused an increasing population pressure on the limited resources of the area. In 1971 the Engineering and Water Supply Dept. produced estimates of the population and land usage of the catchment for the O.E.C.D., these data are shown in Table 1.2. The total population of the area is now c. 28,000 (June 1980 estimate, Bureau of Statistics), having almost doubled in 9 years.

Despite the substantial impact that multiple land use is acknowledged to have on the trophic status of a water body, no extensive data on the biology of this reservoir has been published (Ganf 1980). This is particularly surprising as the Engineering and Water Supply Department annually spends a considerable sum of money on copper sulphate to control nuisance blooms of blue-green algae.

A considerable amount of unpublished data on physical and chemical characteristics of the reservoir has been collected during routine water quality monitoring by the E. & W.S., and access to this data provided valuable background to the present study.

THE LACUSTRINE ENVIRONMENT

1.4 General Description and Morphology

The reservoir is an initial impoundment for drinking water and used to feed lower-level service-storages, where the water is treated and supplied to townships in the southern Mt. Lofty Ranges, and to the Adelaide metropolitan reticulation system. At full service level the reservoir surface is 247m above sea level, extends 8km upstream from the dam wall and is c.1km across at the widest point with a dendritic morphology typical of flooded river valleys. The maximum depth of 47m occurs at the dam wall. Further morphometric and bathymetric data are presented in Table 1.1 and Fig. 1.4.

In general c.70% of the catchment rainfall occurs in the six month period during winter and spring (Schwerdtfeger 1976), resulting in marked annual variations in flow rates of rivers supplying the reservoir (Fig. 1.5a-c). This, combined with increased water consumption during the dry summer causes large annual oscillations in the reservoir level (Fig. 1.6), which are mediated to varying degrees by introduction of water from the Murray River.

Superimposed on the annual precipitation cycle is the frequent

occurrence of extended drought periods during which the supply of water from the catchment is markedly reduced. In 1976 and 1977 rainfall in the Mt. Lofty Ranges was c.75% of the expected annual average and monthly values showed a surprisingly uniform distribution (Fig. 1.7), with a large proportion (20-25%) of the precipitation falling during periods epitomized by high evaporative rates. Consequently catchment inflows to Mt. Bold Reservoir were low (Table 1.3) and substantial quantities of water comprising c.80-90% of the annual inflow were pumped from the Murray River (Table 1.3, Fig. 1.5a).

Precipitation in 1978 was only slightly below average (Fig. 1.7) but was insufficient to fill the reservoir after the two consecutive dry years (Fig. 1.6) and Murray River water was pumped during the summer (Fig. 1.5b) to maintain reserves (Table 1.3).

In 1979 precipitation exceeded the annual average (Fig. 1.7), and sufficient water was received from the catchment to fill the reservoir (Fig. 1.6, Table 1.3).

The variable rainfall therefore results in dramatic changes to the mixture of water held in storage. As water from the two sources is likely to be physically and chemically disimilar this will have important effects on the biology of the system.

It is noteworthy that significant river flow did not occur until June of each of the years 1976-1979 (Fig. 1.5), (Buckney 1979), even though 30-50% of the annual precipitation had been received (Fig. 1.7). Simple addition indicates that stream flow occurs after the average

rainfall of the area exceeds c.250mm (Table 1.4). The figure will vary depending on the location and timing of precipitation, however the similarity of the values suggests a replenishing of soil moisture removed during the dry summer period. As a result of this soil deficit, the occasional summer rainstorm which can deliver a significant quantity of water to the catchment area, rarely contributes to the reservoir supply.

Aquatic macrophytes are absent from the reservoir, and due to the large annual variation in water level it seems unlikely that rooted macrophytes will ever pose a serious problem. Phytoplankton therefore constitute the only autotrophic component, and extensive blue-green algal blooms are a regular summer occurrence.

Historically Mt. Bold Reservoir has been infrequently dosed with $CuSO_4$ and it was chosen as the study site partly for this reason. Unfortunately history did not repeat itself, and in two of the three seasons data sequences were interrupted by periods of dosing.

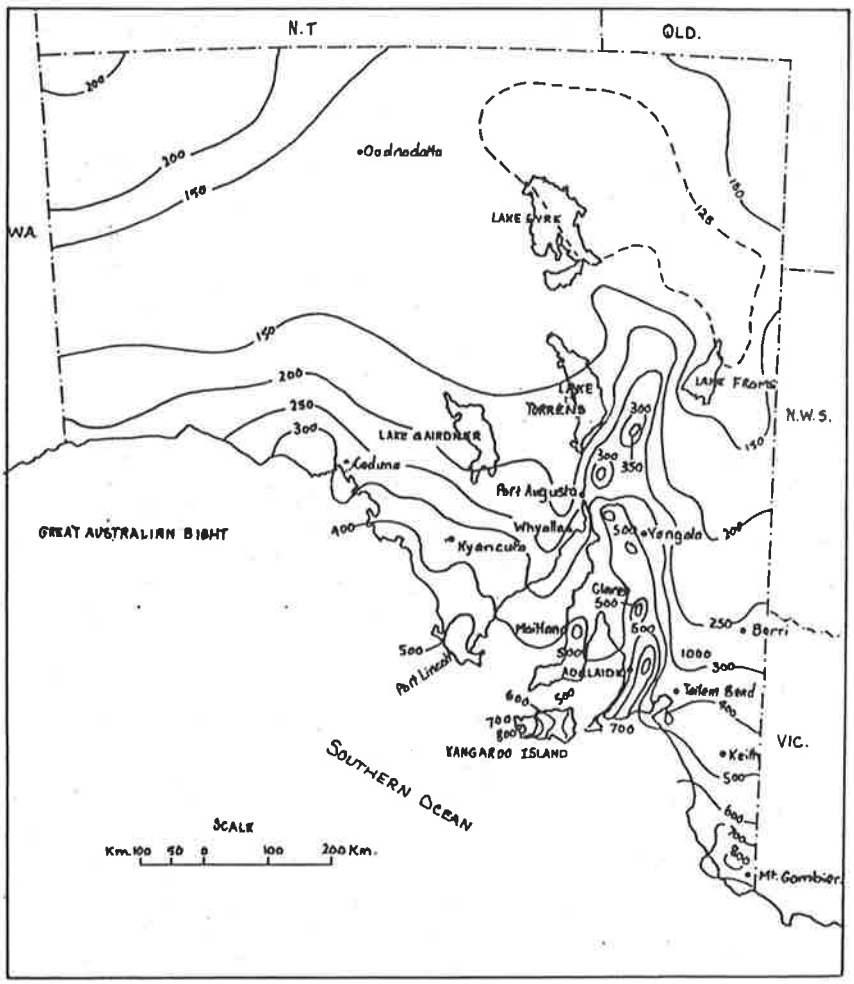

Fig. 1.1: Average annual rainfall for South Australia, (mm). (Specht 1972).

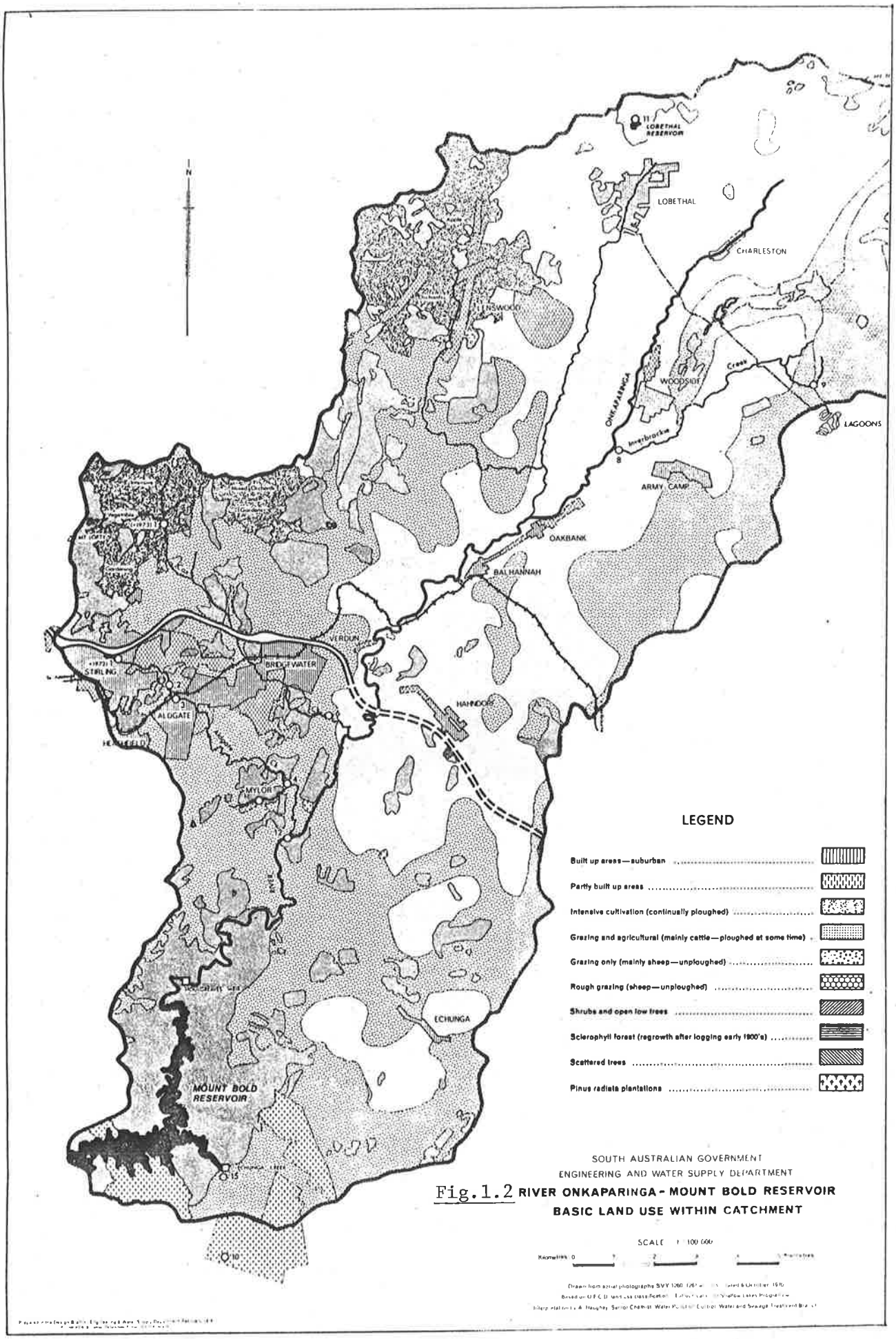
LOBETHAL RESERVOIR
LOBETHAL
CHARLESTON
LENSWOOD
WOODSIDE
ONKAPARINGA
Inverbrackie
LAGOONS
ARMY CAMP
OAKBANK
BALHANNAH
VERDUN
STIRLING
BRIDGEWATER
ALDGATE
HAHNDORF
MYLOR
ECHUNGA
MOUNT BOLD RESERVOIR
LEGEND
Built up areas—suburban
Partly built up areas
Intensive cultivation (continually ploughed)
Grazing and agricultural (mainly cattle—ploughed at some time)
Grazing only (mainly sheep—unploughed)
Rough grazing (sheep—unploughed)
Shrubs and open low trees
Sclerophyll forest (regrowth after logging early 1900's)
Scattered trees
Pinus radiata plantations
SOUTH AUSTRALIAN GOVERNMENT
ENGINEERING AND WATER SUPPLY DEPARTMENT
Fig.1.2 RIVER ONKAPARINGA - MOUNT BOLD RESERVOIR
BASIC LAND USE WITHIN CATCHMENT
SCALE 1 100 000

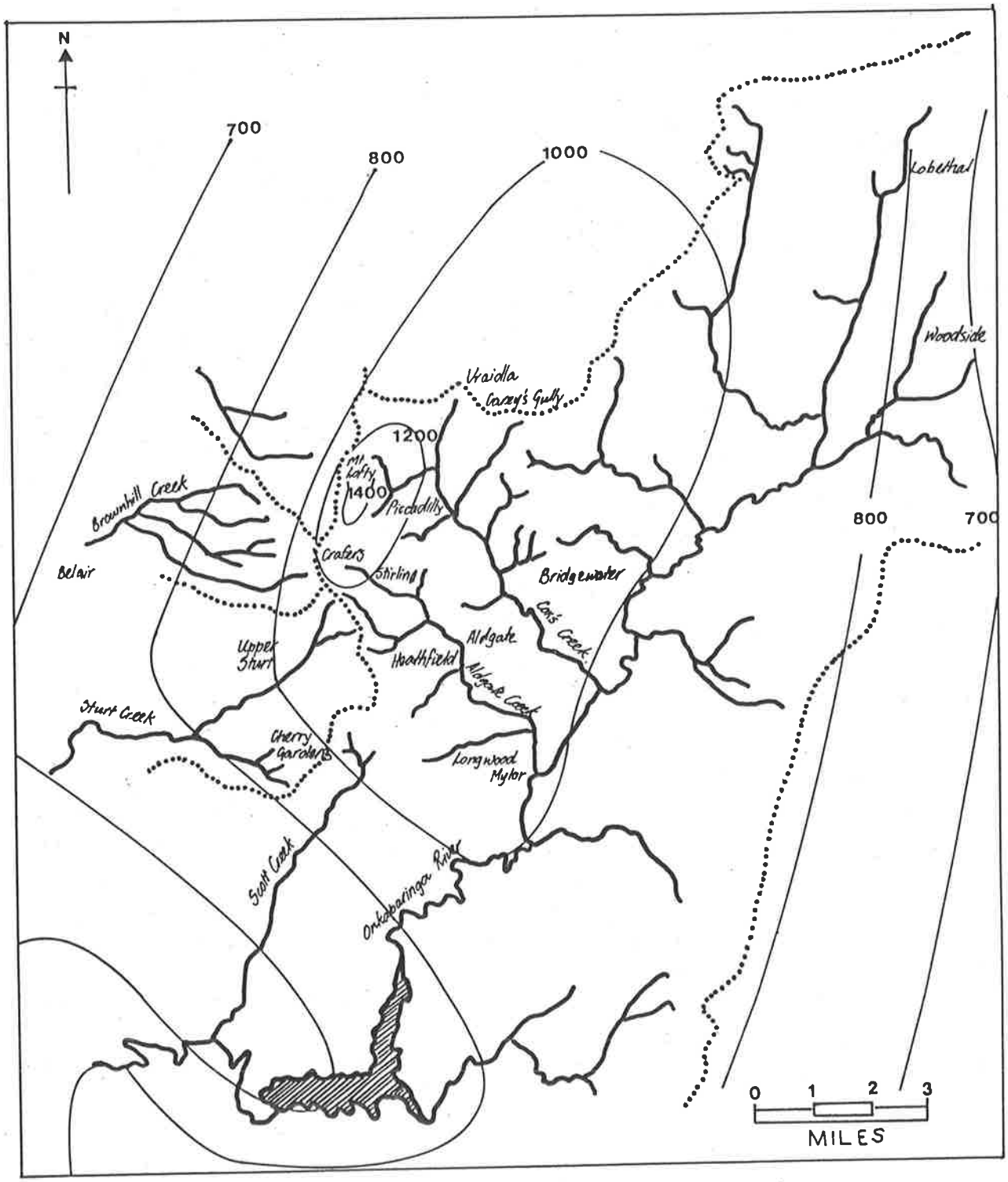

Fig. 1.3: Mt Bold Reservoir catchment area showing average annual rainfall (mm) and main watercourses (Schwerdtfeger 1972).

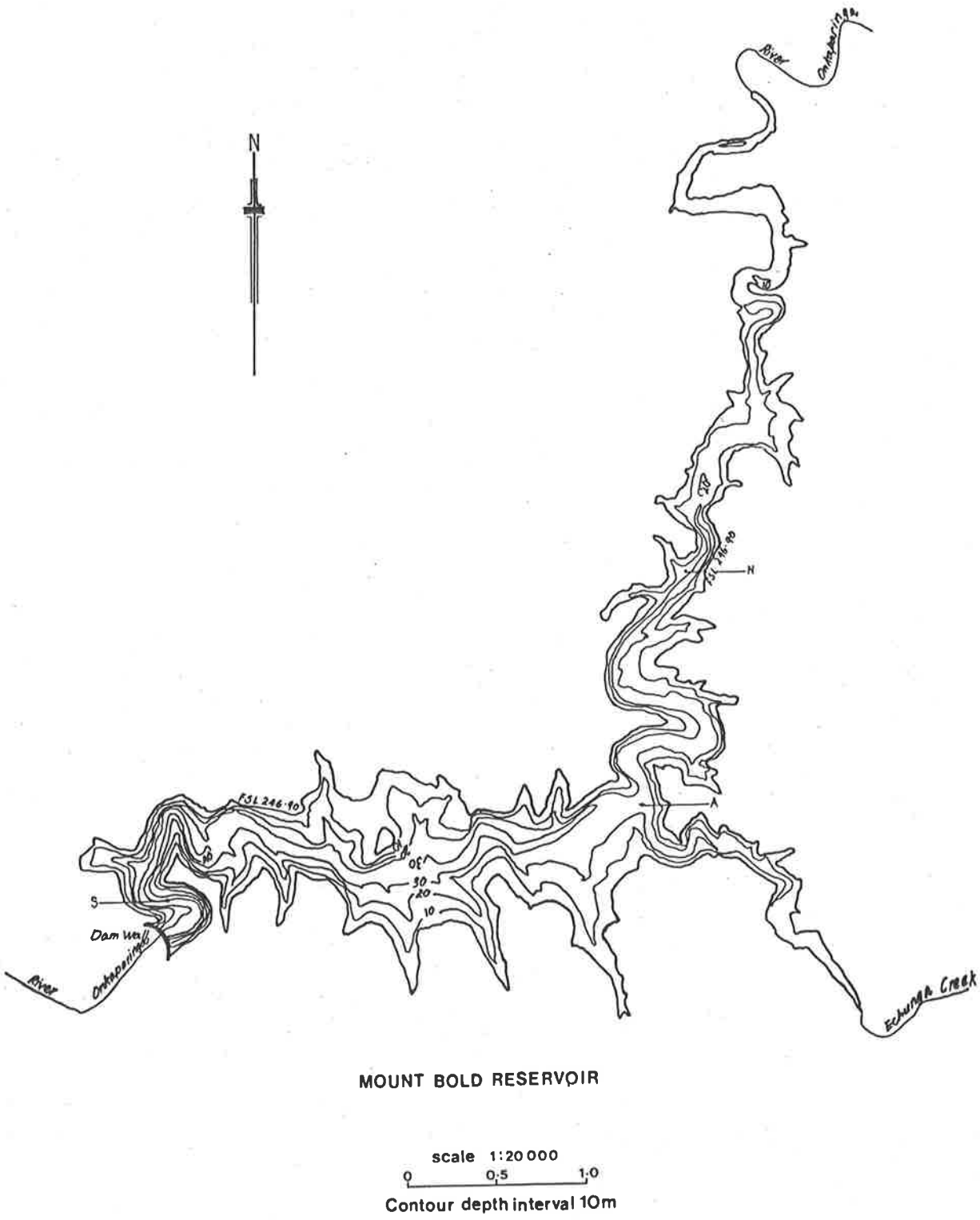

Fig. 1.4: Bathymetry of Mt Bold Reservoir (Engineering & Water Supply Dept) showing the north and south sampling sites and sampling site A.

Fig. 1.5: Daily inflow (megalitres) to Mt Bold Reservoir as measured at Houlgrave Weir on the Onkaparinga River, during the study period. Hatched areas denote River Murray water.

a 1977-78

b 1978-79

c 1979-80

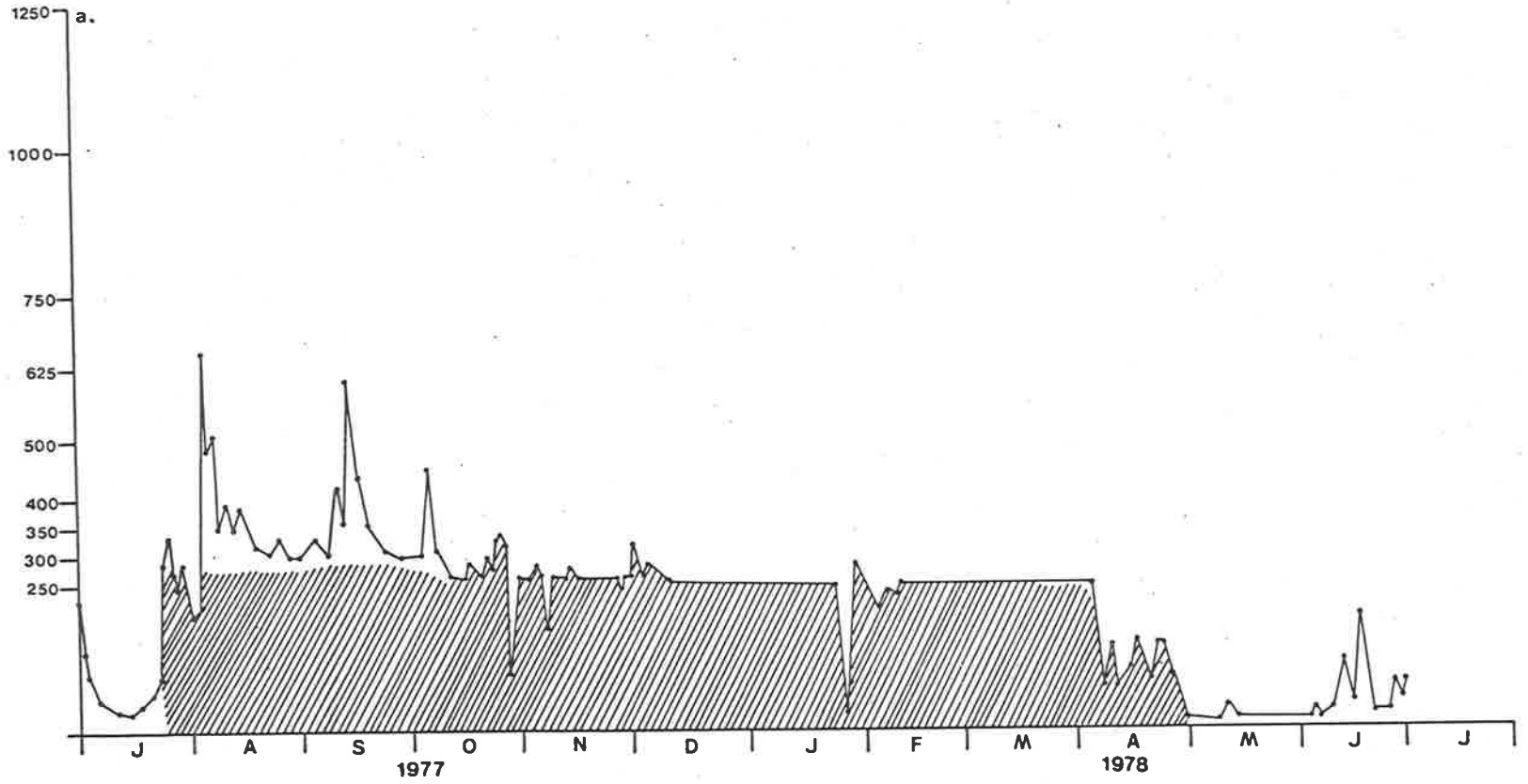
a.
1250
1000
750
625
500
400
350
300
250
J
A
S
O
N
D
J
F
M
A
M
J
J
1977
1978

Fig. 1.5

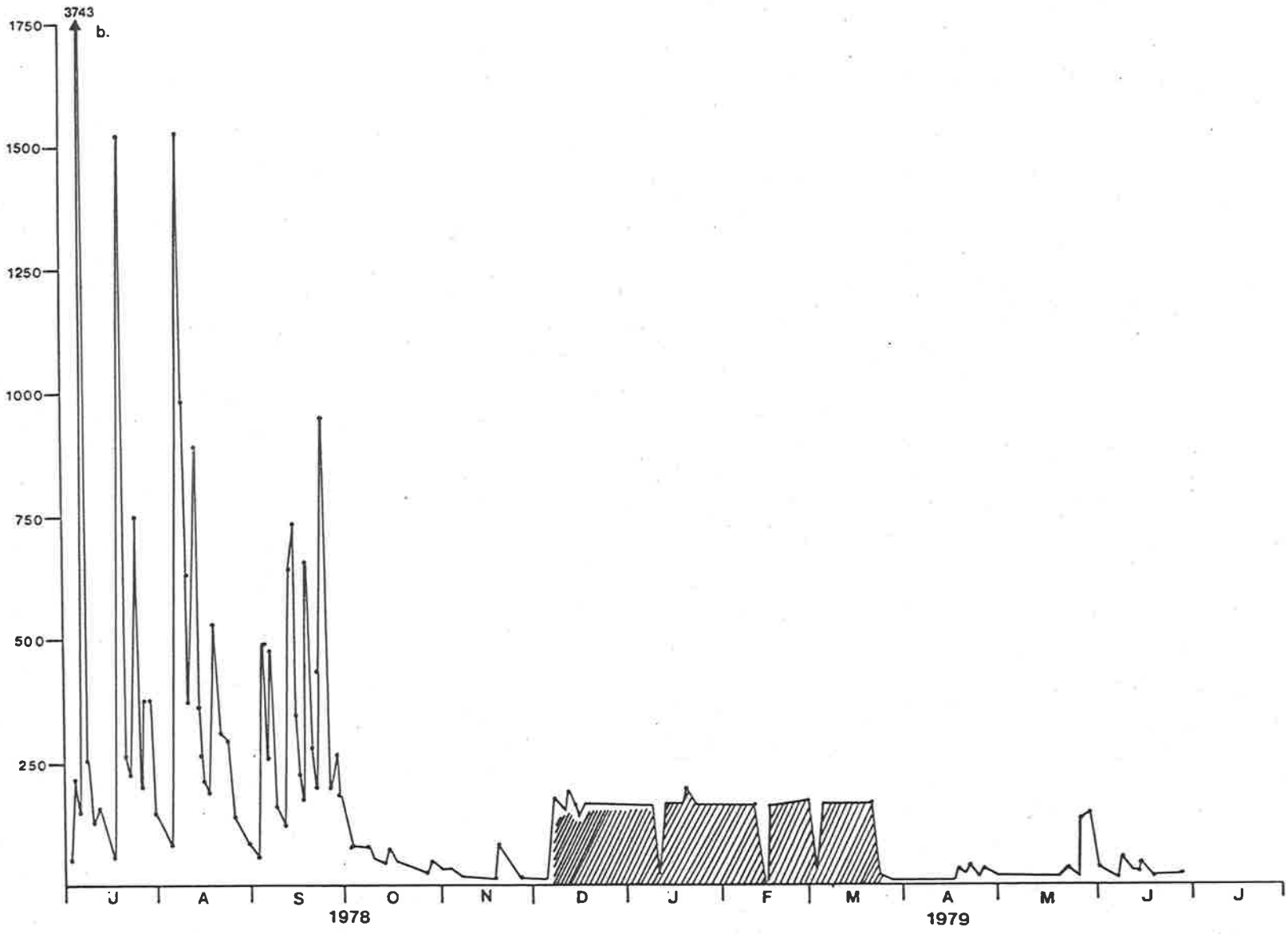
3743
b.
1750
1500
1250
1000
750
500
250
J
A
S
O
N
D
J
F
M
A
M
J
J
1978
1979

Fig. 1.5

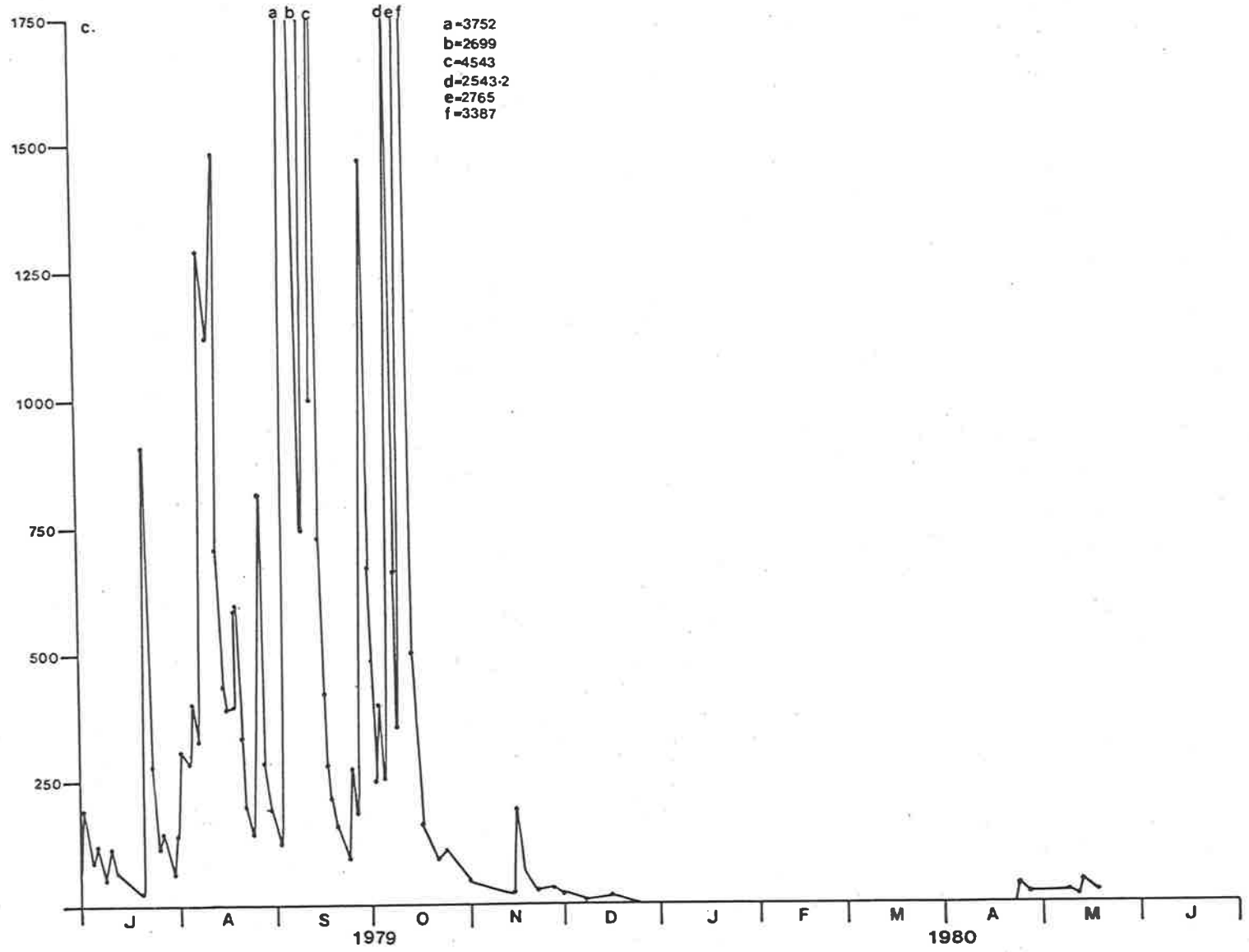
c.
a b c
d e f
a=3752
b=2699
c=4543
d=2543·2
e=2765
f=3387
1750
1500
1250
1000
750
500
250
J
A
S
O
N
D
J
F
M
A
M
J
1979
1980

Fig. 1.5

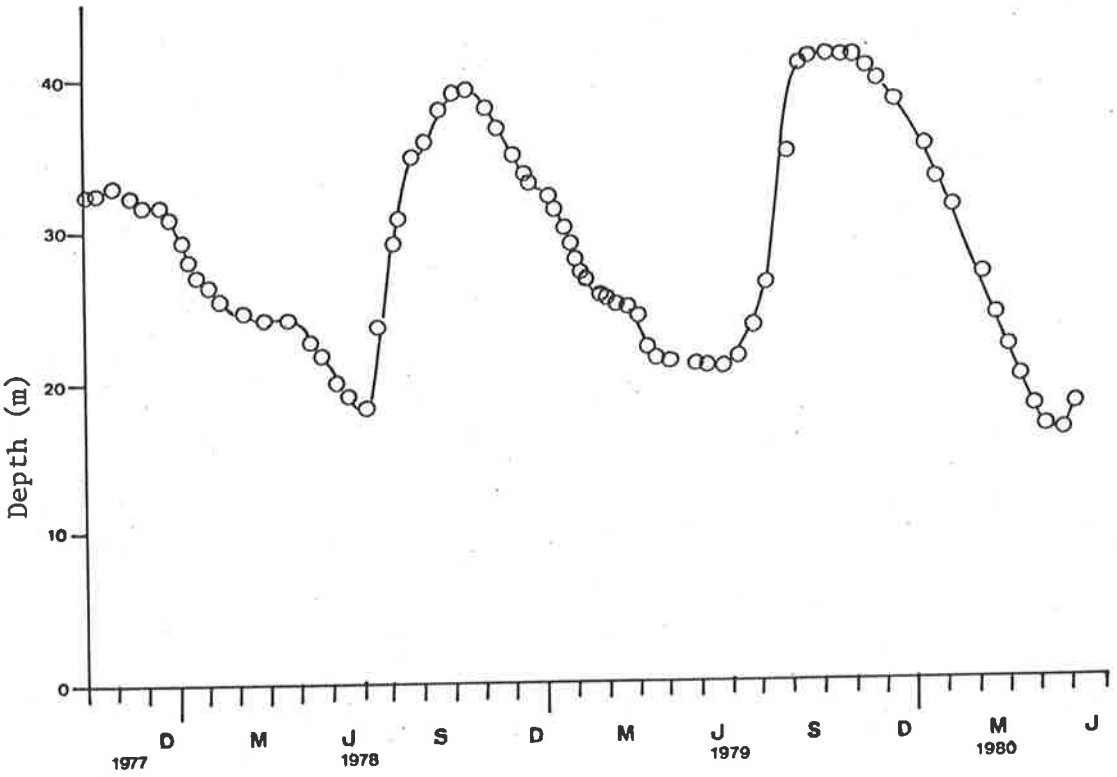

Fig. 1.6: Annual variation of water depth in Mt Bold Reservoir as measured at the dam wall for the period 1977-1980.

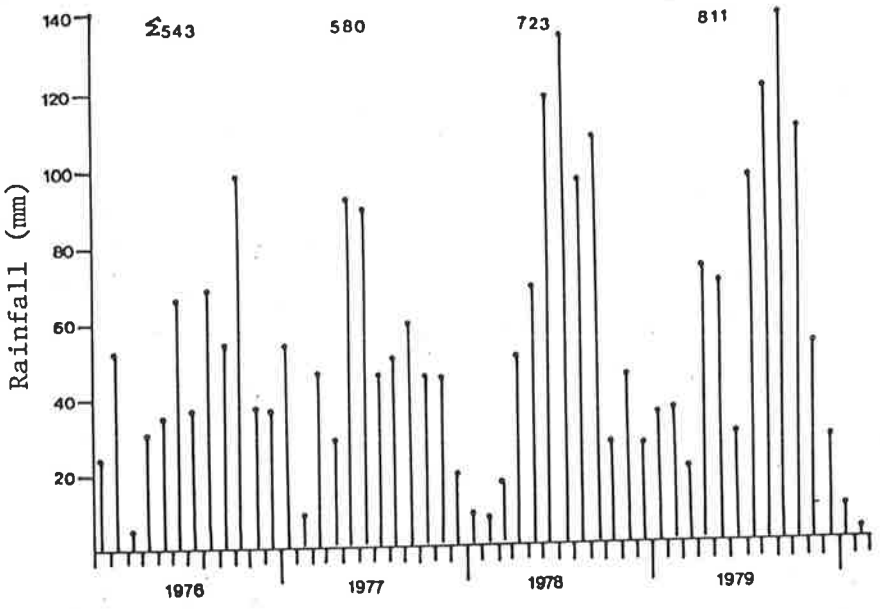

Fig. 1.7: Monthly rainfall (mm) in the area designated Mt Lofty Ranges (Monthly Weather Review, S.A. Bureau of Meteorology) for the period 1976-79. Annual average for the area is 736 mm. Annual totals shown above each year.

Surface area (m^2)	3.08×10^6
Maximum depth (m)	47
Mean depth (m)	25.4
Volume (m^3)	47.3×10^6
Length (m)	8000
Width (m)	1000

Table 1.1 Morphometric data for Mt Bold Reservoir at full storage level.

Table 1.2

Population

Total number of inhabitants 15,000 (1971 estimate)

Towns, villages and so on specified by inhabitants:

Bridgewater-Stirling-Aldgate-Crafers	5300
Woodside Army Camp	2000
Woodside	690
Lobethal	1380
Hahndorf	670
Uraidla-Summertown	610
Balhannah	320
Oakbank	210
Echunga	180
Mylor	90
Charleston	80
Lenswood	50
Carey Gully	50

The remaining 3350 live on farms in the watershed.

Land usage of catchment area:

industrial purposes		0.3%
urban (including streets,places)		4.8%
agricultural purposes		
pasture and fodder	} ploughed	41.0%
gardens and orchards		
open grazing	unploughed	35.6%
forest		
native		14.9%
exotic		1.6%
miscellaneous		1.0%
reservoir		0.8%

Sewage and effluent discharge:

Domestic

Lobethal (1380 population)- sewage pumped out of catchment for lagoon treatment.

Woodside Army Camp (up to 2000 pop.)- secondary treatment and chlorination of effluent before discharge to small stream.

Table 1.2 (cont.)

Remainder (c. 12,500 pop. on individual septic tanks	- quantity of effluent seeping to streams not known but effects detectable downstream of major population centres, especially in the wetter parts of the catchment (e.g. Aldgate Creek).
Industrial	
Lobethal Woollen Mills	- wastes pumped out of catchment and treated in lagoons with the domestic sewage from the township.
Rural	
Piggeries	- lagoon treatment for some 4000 of the 5000 pigs on catchment.
Dairies	- spray irrigation for some 7500 of the 8700 milking cows on catchment.
Poultry etc.	- dry collection and spread on pastures, gardens etc. or disposed of outside catchment for some 550,000 birds.

In addition to the above livestock some 21,000 cattle and 30,000 sheep and an estimated 2000 horses are also present within the watershed.

Table 1.2: Human and animal populations and land usage of the Mt Bold Reservoir catchment area as reported by the Engineering and Water Supply Department to the O.E.C.D. in 1971

	1976-1977	1977-1978	1978-1979	1979 -1980
Catchment	6921	657	37425	76133
River Murray	68354	76367	16631	-
% from River Murray	90	99	31	0

Table 1.3: Volume of water (megalitres) entering Mt Bold Reservoir, compared to the volume pumped from the River Murray, for annual periods July-June.

Year	Rainfall (mm)
1976	211
1977	317
1978	270
1979	268

Table 1.4: Catchment rainfall between January and the initiation of stream inflow to Mt Bold Reservoir via the Onkaparinga River (June in each year).

METHODS AND MATERIALS

2.1. Field Methods

Water samples were collected from discrete depths using a 1- or 2-litre Friedinger sampler, or on occasions with a submersible Otter pump connected to a 40m length of opaque tubing. Integrated euphotic zone samples were collected with a 2 or 4 m length of PVC piping, stoppered with a rubber bung prior to removal. Samples were stored in 1- or 2-litre acid washed polyethylene bottles and kept cool and dark in polystyrene boxes until arrival at the laboratory.

Integrated euphotic samples for protein and carbohydrate analysis were collected between 0900 and 1000 h and siphoned into 150 ml glass stoppered bottles containing 2 ml of 50% glacial acetic acid which acted as a preservative (cf. Gibson 1978). On return to the laboratory the water was filtered through coarse mesh netting to remove zooplankton and, depending on phytoplankton biomass, a 15-100 ml sample sedimented in a bench centrifuge for 10 min. The supernatant was discarded and the cells resuspended in 1 ml of distilled water and frozen until analyzed.

A continuous record of total incoming solar irradiance was graphically recorded using a solarimeter. Incoming irradiance during experimental periods was also measured with either a solarimeter (Kipp and Zonen, Holland) or a quantum sensor (Lambda Instruments, U.S.A.) connected to a volt-time integrator (Lintronic Ltd., U.K) recording 15 min. integrals. Underwater irradiance intensity was measured in opposite directions using two vertically held underwater quantum sensors (Lambda Instruments, U.S.A.)

secured in a cradle and lowered on a boom projecting 1 metre from the side of the boat (Kirk 1977). Upwelling and downwelling irradiance was measured every 0.2 m during two profiles of the euphotic zone. Each profile was performed rapidly under constant sky conditions.

The quantum sensors measured the waveband 400-700nm, which was taken to be equivalent to photosynthetically active radiation (PAR). Comparison of solarimeter and quantum sensor recordings over short time periods enabled daily total radiation to be converted to daily PAR values. PAR was usually ca. 46% of total radiation (Talling 1957*a*). Upwelling and downwelling extinction coefficients were calculated by linear regression from the logarithmic transformation of the Beer-Lambert law following graphical assessment. Water temperature was measured with a thermistor probe reading to 0.01°C, and oxygen concentration with an oxygen electrode (Martek Inst.).

Photosynthesis profiles were measured between 1000 and 1400h using either the ^{14}C or oxygen technique. An integrated euphotic zone water sample was siphoned into a series of duplicate borosilicate bottles (125 ml) in dim light. These were suspended horizontally at a number of depths over the euphotic zone. Bottles wrapped in aluminium foil were used to measure dark fixation of ^{14}C, or oxygen uptake. Exposure times varied from 1.25 - 4 h with the majority of experiments lasting 2 h.

Prior to incubation ^{14}C bottles were inoculated with 2.5 µCi $NaH^{14}CO_3$. These experiments were terminated by adding 1 ml of 4N H_2SO_4 which reduced the water sample to pH 2. Sub-samples (20-40 ml) were concentrated on Whatman GF/C (2.1 cm) filters and dried on planchets with 2 drops of 1% propionic acid. Filters were

then placed in scintillation vials and ^{14}C activity measured in a Packard Tri-carb liquid scintillation spectrometer, using 10 ml of a toluene based scintillation fluor (4g PPO and 0.2 g POPOP per litre of 2 : 1, Toluene : Brydet detergent). As a result of the heterogeneous nature of the sample correction for quenching could not be made using channels ratio, external standard or internal standards (Bush 1963; Pugh 1970; Bransome & Grower 1970). To correct for quenching and cell breakage, a range of volumes was filtered and the linear relationship between ^{14}C activity and small volumes used to correct for the apparent loss of activity in the experimental sub-samples (Arthur & Rigler 1967). The correction factor varied between 1.0 and 1.33 with the majority lying between 1.0 and 1.2. Assimilation rates were corrected for dark uptake of ^{14}C, but this rarely exceeded 1% of the maximum photosynthetic rate.

The specific activity of the ampoule of stock solution used for each experiment was determined by layering 0.025 ml of isotope on a Whatman GF/C filter to which had been applied 0.1 ml of 2N NaOH. The dried sample was counted in the same manner as experimental samples. Counts obtained from the layering technique were linear with volume up to at least 0.05 ml of isotope.

For determination of extracellular products filtrates were bubbled 10 min. with (99% N + 1% CO_2) and 5 min. with air. A 1.0 ml sample of filtrate was added directly to 10 ml of scintillation fluor. Counts were corrected for quenching by channels ratio.

Total inorganic carbon was determined by titration with 0.01N HCl as described by Golterman (1971).

Oxygen incubations were terminated by addition of Winkler reagents (Carpenter 1965), and oxygen concentrations determined by amperometric titration (Talling 1973) with 10 mM sodium thiosulphate.

Depth profiles of chlorophyll *a* concentration were obtained from *in situ* fluorescence measurements using a Turner Model III fluorometer fitted with a high volume flow through door, the recommended excitation and emittance filters (Turner Co.) and a red-sensitive photomultiplier. Continuous profiles were recorded on a Rikadenki chart recorder. Calibration of the fluorometer was achieved by taking frequent samples from the outflow for chlorophyll *a* analysis.

Chlorophyll *a* concentration was estimated spectrophotometrically after grinding a Whatman GFC filtered sample in 90% acetone and extracting cold for 12 h. Calculation followed the abbreviated equation of Talling & Driver (1963).

2.2 Laboratory methods

Phytoplankton samples were preserved with Lugols iodine solution (Vollenweider 1969) and subsequently counted using the inverted microscope technique described by Lund *et al* (1958). Average cell volumes were computed from microscopic measurements of cell dimensions using volume formulae of equivalent geometric shapes.

Bioassay experiments utilized the natural phytoplankton assemblage as test organisms. Water samples from discrete depths were filtered through prewashed, Whatman GF/C filters and 100 ml sub-samples of filtrate transferred to four 250 ml conical flasks for each depth. One flask acted as the control, while two flasks were

enriched to concentrations of 1150 µg NO_3 - N ℓ^{-1}, and 100 µg PO_4 - P ℓ^{-1} respectively. The final flask was enriched with both phosphate and nitrate to these same levels.

An integrated euphotic zone sample was filtered through a Millipore 0.45 µ filter and the algae resuspended in a small volume of filtrate using a stirring bar and magnetic stirrer. This concentrate was used to innoculate the 250 ml flasks to an initial concentration < 0.5 mg dry weight ℓ^{-1}. Flasks were incubated at 20°C in a 12 : 12 light dark cycle at 300 µEinsteins $m^{-2}s^{-1}$ for a 6-8 day period. Biomass changes were measured at least every two days by fluorescence measurement in the Turner fluorometer. The mean growth rate between the end of lag phase and the peak biomass level was used as a measure of the growth potential of the sample.

Carbohydrate analysis (Stone, unpublished thesis) was carried out colorimetrically using anthrone reagent standardized to D + glucose solutions, and all results expressed as glucose equivalents (Herbert *et al* 1971).

Protein was estimated (Stone, unpublished thesis) with the Folin - Ciocalteu phenol method, following the procedure of Halmann (1972), and referred to bovine serum albumen standards.

Chemical analyses of water samples was carried out by the Bolivar Laboratories of the Engineering and Water Supply Department as part of their routine water quality monitoring programme. Discrete water samples were taken from 10 m depth intervals at one or two weekly intervals.

The following list describes the basis of the techniques.

Ammonia: Determined colorimetrically by the reaction of alkaline phenol and hypochlorite with ammonia to form indophenol blue. Colour intensity was increased by addition of sodium nitroprusside. The method is based on Technicon method 154-71W.

Total Kjeldahl Nitrogen: Determined colorimetrically following formation of ammonium sulphate by digestion at 370°C with sulphuric acid and potassium sulphate. The digest was neutralised with NaOH and treated with alkaline phenol and hypochlorite to form indophenol blue. Colour intensity was increased by addition of sodium nitroprusside.

Nitrogen, nitrate - nitrite: Filtered samples (0.45 μ) were passed through a cadmium column to reduce nitrate to nitrite, which then reacted with sulphanilamide to form the diazo compound. Concentration was determined colorimetrically by formation of the azo dye. Separate nitrate and nitrite values were obtained by assaying filtered samples without cadmium reduction. The method is based on Technicon method 100-70W.

Dissolved reactive phosphorus: Filtered samples (0.45μ) were reacted with ammonium molybdate and antimony potassium tartrate in an acid medium to form a complex which was reduced to molybdenum blue by ascorbic acid. Concentration was determined colorimetrically. The automated method is based on Technicon method 155-71W.

Total phosphorus: Determined colorimetrically from the same digest as total Kjeldahl nitrogen, using the analysis described for reactive dissolved phosphorus. The automated method was based on Technicon method 327-74W.

Silicate : Determined colorimetrically following formation of molybdate complex in acid solution and reduction with stannous chloride.

Further specific methods are described in relevant sections.

PHYSICAL ENVIRONMENT

LIGHT CLIMATE

3.0 Introduction

Incoming solar radiation plays a major role in freshwater ecosystems through its effects on the thermal structure of the water column and its utilization in photosynthesis. In South Australia, clear summer skies ensure high incident irradiance levels (Fig. 3.19), however, the extent to which incident radiation penetrates the water column is a function of light attenuation and scattering by components of the medium including dissolved coloured compounds, suspended inorganic particulate matter, phytoplankton and water itself.

The available quantitative data (Kirk 1976b, 1977, 1979; Ganf 1976, 1980; Bowles *et al* 1979; Oliver and Ganf in press) suggests that many Australian inland waters are highly coloured and turbid. Previous measurements on Mt. Bold Reservoir showed rapid light attenuation, particularly after the entry of Murray River water (Ganf 1980). As turbidity and colour compete with phytoplankton for absorption of available light, high values restrict the levels of photosynthesis, growth and biomass which can be attained. To investigate these inter-relationships extensive light measurements were made during the study period using the techniques described in Chapter 2.

3.1 Extinction Coefficient and the Euphotic Zone

In a homogeneous, non-scattering solution the intensity of monochromatic light decreases exponentially with depth and is described by the Beer-Lambert law,

$$I_z = I_o^1 e^{-\varepsilon z} \qquad (3.1)$$

where I_z is the light intensity at depth z metres, I_o^1 the surface intensity, and ε the vertical extinction coefficient (ℓn units m^{-1}). In practise this relationship often adequately describes attenuation of photosynthetically active radiation (400-700 nm ≡ PAR) (Smith 1968; Kirk 1977). In such cases the vertical extinction coefficient (ε), determined from a semi-logarithmic plot of light intensity against depth, provides a useful parameter to compare light attenuation by water bodies.

Downwelling and upwelling irradiance in Mt. Bold Reservoir closely followed an exponential relationship with depth (Fig. 3.1), although slight deviations to 0.2m resulted from rapid attenuation of the most highly absorbed wavelengths. Linear regression analysis of semi-logarithmic graphs yielded regression coefficients (r^2) greater than 0.99 in all but a few cases. Duplicate values of extinction coefficients, estimated from the negative slope of the semi-logarithmic plots, rarely differed by more than 10% .

Extinction coefficients ranged from c. 1.0 - 17.0 (Fig. 3.2) with maximal values occurring at the northern sampling site during

periods of high stream inflow initiated by catchment rainfall (Fig. 1.5 & 3.2). The large difference in extinction coefficients between the northern and southern sampling sites indicates significant sedimentation of transported material. It is noteworthy, in the light of suggestions that Murray River water is a major contributor of turbidity to the reservoir (Ganf 1980), that extinction coefficients tended to fall during extended periods of pumping (1977-78), but increased dramatically with the inflow of catchment water (e.g. July 1978 Fig. 1.5 & 3.2).

The applicability of the Beer-Lambert law enables calculation of the depth of the euphotic zone (Z_{eu}), defined as that depth to which 1% of incident irradiance penetrates. Rearranging equation (1),

$$Z_{eu} = \frac{1}{\varepsilon} \ln \frac{100}{1} = \frac{4.605}{\varepsilon}$$

Direct field measurements of Z_{eu} are compared with calculated values in Fig. 3.3. The close agreement supports the use of the extinction coefficient to describe light attenuation in the water column of Mt. Bold. As expected from high extinction coefficients the euphotic zone is narrow, with an average depth of c. 1-2m (Fig. 3.4).

3.2 Components of the Extinction Coefficient

The total extinction coefficient can be partitioned into that due to each of the absorbing components of the water column,

$$\varepsilon = \varepsilon_s b + \varepsilon_\omega + \varepsilon_p + \varepsilon_G \qquad (3.2)$$

$\varepsilon_s b$ is the extinction due to phytoplankton, b representing the biomass, usually measured as chlorophyll *a* concentration (mg chl *a* m^{-3}), and ε_s the specific extinction coefficient per unit biomass (m^2 mg chl *a*$^{-1}$). ε_ω, ε_p and ε_G (ℓn units m^{-1}) are extinction coefficients due respectively to water, suspended particulate matter other than phytoplankton, and dissolved coloured compounds, which together comprise the background extinction coefficient ε_q,

$$\varepsilon = \varepsilon_s b + \varepsilon_q \qquad (3.3)$$

During periods when ε_s and ε_q remain constant, equation (3.3) describes a linear relationship between the total vertical extinction coefficient (ε) and the chlorophyll *a* concentration (b), from which *in situ* values of ε_s and ε_q may be estimated. This requirement was met during four periods (Fig. 3.5 (a)-(c)) and values for ε_s and ε_q calculated using linear regression (Table 3.1). All slopes differed from zero ($P<0.02$), but ε_s values of 0.0122, 0.0133 and 0.016 were not significantly different ($P>0.05$). ε_q values of 1.59 and 1.44 were significantly different at the 10% level and all others at 5%.

The ε_s values are compatible with previous estimates (Talling 1960; Bindloss 1974; Ganf 1974; Scott 1978; Megard *et al* 1979;) falling within the range c. 0.01 - 0.02 m^2 mg chl *a*$^{-1}$. The high background extinctions indicate the turbid nature of the water. A measure of the effect of ε_q values on the

availability of light for phytoplankton is the concentration of chlorophyll a required to attenuate half of the available light (Table 3.1), i.e. for $\varepsilon_s b = \varepsilon_q$. The high chlorophyll concentrations required, in Mt. Bold, to meet this stipulation are only briefly attained (Fig. 4.1) illustrating the dominance of ε_q in light attenuation.

During the winter period when chlorophyll concentration $<<10 mg\ m^{-3}$, ε_q is equivalent to the vertical extinction coefficient, while in summer $\varepsilon_q = \varepsilon - \varepsilon_s b$ (Table 3.3). The temporal variation in ε_q at the southern sampling site was considerable (1 - 4.5 $\ell n\ m^{-1}$, Fig. 3.6(a)) and as it accounted for the majority of vertical attenuation in all periods except February 1980, ε followed a similar pattern (Fig. 3.6(a)). To provide further insight to causes of variation in vertical light attenuation, data was obtained on the contributions of dissolved colour and light scattering.

3.3 The Role of Dissolved Colour in Light Attenuation

Water samples from the southern sampling site were filtered sequentially through Whatman GFC and 0.22 μm Millipore filters to remove suspended material (Kirk 1976b), and filtrate absorbances measured at 10ηm intervals between 400-700ηm in a Beckman Acta CIII spectrophotometer, using a 10cm cylindrical cuvette. A linear zero absorption line was set on water, double distilled in glass, using the inbuilt scale potentiometers. Extinction coefficients for dissolved colour (ε_G) (ℓn units m^{-1})

were calculated for each 10 ηm interval (Fig. 3.7) and the extinction coefficient for dissolved colour plus water ($\varepsilon_{G+\omega}$), (Table 3.3) obtained by adding the appropriate extinction for clear natural water (Smith & Tyler 1967).

To provide a reasonable estimate of the <u>in situ</u> value of $\varepsilon_{G+\omega}$ for total PAR it was necessary to estimate the spectral distribution of the incoming solar irradiance, the intensity of which was measured with a solarimeter (Chp. 2). A literature survey provided several sources of data on the spectral distribution of global irradiance on a horizontal plane, (Taylor & Kerr 1941 (Table 11, Col. C&D); Henderson & Hodgkiss 1963 (Table 1, Col. E2 & E3); Judd et al. 1964 (Table V, Correlated colour temperature 5500°K, 6500°K); Winch et al. 1966 (Table 1, Col. E1, E5 & E6); Thekaekara 1970). The percentage energy content of each 10ηm interval between 400-700ηm was calculated from the tabulated data (Fig. 3.8 (a)-(c)) and a mean distribution determined (Fig. 3.8(d), Table 3.2). The similarity of the various sets of results is marked, particularly when variation in location and methodology is considered. Kondratyev (1969, p.453) concluded that the spectral composition of global radiation received by a horizontal surface is practically independent of solar height and consequently remains constant throughout the day. The measured incoming PAR (c. 46% total radiation, see Chp. 2) was partitioned into 10ηm intervals on the basis of Table 3.2 and converted from energy to quanta using Planck's quantum equation. Application of the extinction coefficients due to dissolved colour and water for each 10ηm waveband enabled calculation of the spectral

distribution and remaining light intensity at various depths in a hypothetical column of filtered water.

The absorption of light by pure natural water (Fig. 3.9(a)) is maximal at the red end of the spectrum, decreases rapidly to a minimum in the blue and then increases again in the violet wavelengths. When the extinction due to dissolved coloured material is included (Fig. 3.9 (b)-(g)) the underwater light regime is strongly modified, particularly in the blue and ultraviolet regions. The absorption of blue light is due to the presence of dissolved yellow substances (gelbstoff≡gilvin; Kirk 1976b) considered to be heteropolycondensates of phenolic compounds (Hall & Lee 1974). The effect of increasing quantities of gelbstoff can be ascertained using the attenuation at 440ηm (ε_{440}, ℓn units m^{-1}) as a measure of gelbstoff concentration (Kirk 1976b).

The underwater light spectra in Fig. 3.9(c) (ε_{440} = 0.51) shows a distinct maximum penetration at λ=570ηm, which is reduced and shifted to λ=580ηm in Fig. 3.9(b) (ε_{440} = 1.84). With a further increase in gelbstoff concentration (Fig. 3.9(f), ε_{440} = 4.4) a small peak occurs at 590ηm, but the most penetrating wavelengths are situated in the red region of the spectrum (670-690ηm). In Fig. 3.9(e) (ε_{440} = 8.01) the most penetrating wavelength is 700ηm and virtually no light of wavelength less than 500ηm arrives at a depth of 1.0m. As a result of the important blue absorption bands in chloroplast pigments, the depletion of blue light due to gelbstoff will have

significant effects on phytoplankton photosynthesis.

Vertical extinction coefficients for total PAR penetrating a water column containing only dissolved coloured material were calculated from

$$\varepsilon_{G+\omega} = \frac{1}{z} \ln \left(\frac{I_z}{I_o^1}\right)$$

where

$$I_z = \Sigma_{\lambda=400}^{\lambda=700} I_{o\lambda}^1 \, e^{-\varepsilon_\lambda z}$$

I_o^1 is incident light intensity, $I_{o\lambda}^1$ incident light intensity for 10ηm wavebands, ε_λ the extinction due to water and gelbstoff in waveband λ, and I_z the calculated intensity remaining at depth z after passage through water and dissolved colour. ε_G was calculated in a similar manner, replacing ε_λ with $\varepsilon_{G\lambda}$. The proportion of light absorbed by gelbstoff in the two component system $\left(\frac{\varepsilon_G}{\varepsilon_{G+\omega}}\right)$ provides a measure of the significance of dissolved colour to light attenuation (Fig. 3.10, Table 3.3). At times gelbstoff absorbed >80% of available light.

In the two component system, where scattering is negligible, calculated extinction coefficients decreased with depth of calculation, as expected from the concomitant spectral shift to more penetrating wavelengths. This made the choice of a single descriptive extinction coefficient, comparable to a mean <u>in situ</u> value, difficult, particularly in samples with high attenuation. This problem would be alleviated by direct data on the mean

in situ spectral distribution of the euphotic zone, to which laboratory measured extinction coefficients could be applied. In the absence of such data the average calculated extinction over 2 metres has been used as an indicator of the variation in attenuation due to dissolved colour (Fig. 3.6(a)). Actual euphotic zone values would be smaller, as in situ spectral variations occur more rapidly due to the increased pathlength resulting from light scattering.

A comparison of the laboratory determined extinction due to dissolved colour and water ($\varepsilon_{G+\omega}$), with total vertical extinction (ε) and background extinction (ε_q) using equations (3.2) and (3.3) is not valid. The terms in these equations refer to apparent vertical extinction coefficients measured in situ, not to absorbances as measured in the laboratory situation. The difference between the two sets of values depends on the scattering of light in the water column. Increased scattering will effectively increase the apparent vertical extinction coefficients by increasing the actual pathlength travelled in traversing a fixed vertical depth. As a result each term in equation (3.2) and (3.3) is larger than the attenuation which would be measured in a non-scattering medium. If measurements made under non-scattering conditions are denoted by a bar (i.e. $\bar{\varepsilon}_{G+\omega}$) then,

$$\varepsilon = \bar{\varepsilon}_{G+\omega} + \bar{\varepsilon}_p + \bar{\varepsilon}_s b + S \qquad (3.4)$$

where ε is the apparent vertical attenuation measured in situ;

$\bar{\varepsilon}_{G+\omega}$, $\bar{\varepsilon}_p$ and $\bar{\varepsilon}_s b$ refer to the same components as in equation (3.2) but measured in a non-scattering medium, and S (ℓn unit m^{-1}) is, the extinction coefficient due to light scattering, or the total volume scattering coefficient (Duntley 1963). A comparison of $\bar{\varepsilon}_{G+\omega}$ values and *in situ* vertical extinction coefficients (ε) (Fig. 3.6(a)), particularly during periods when chlorophyll *a* concentration is very low and so $\bar{\varepsilon}_s b$ negligible, implies a large attenuation of light by particle absorption (ε_p) and scattering, S.

3.4 Measurement of Light Scattering in Natural Waters

In an attempt to assess scattering effects Kirk (1977) derived an expression relating the scattering properties of turbid waters to reflectance measurements. Reflectance (R) is the ratio of upwelling irradiance to downwelling irradiance ($\frac{I_u}{I_D}$) at a given depth, and is a function of both the light scattering properties of the water, and the extinction coefficient, the latter value determining the penetration of upward reflected light. When downwelling light penetrates the water column scattering causes the radiance distribution to become proportionately enriched at lower angles to the horizontal, and reflectance increases with depth (Kirk 1977; Duntley 1963), until eventually the radiance distribution takes up a fixed form dependent on the optical properties of the water. As this asymptotic radiance distribution is reached reflectance assumes a constant value (R_A) termed asymptotic reflectance. In turbid waters, for example Mt. Bold Reservoir, the asymptotic radiance distribution is rapidly attained (Fig. 3.11).

It will be noted that in many of the profiles reflectance tends to decrease after a period of rather constant value. As this always occurred when upwelling irradiance reached C. 1 $\mu E\ m^{-2}\ s^{-1}$ it is considered to be a result of receptor insensitivity at low light intensities. Asymptotic reflectance values varied over a considerable range (Fig. 3.6(b); Table 3.3) being particularly high in late 1977 and low in late 1978. (Results from the northern sampling site are shown in Fig. 3.13 for comparative purposes. Lack of data on $\varepsilon_{G+\omega}$ values for this site preclude it from full analysis.)

Kirk (1977) related asymptotic reflectance to a term described as the asymptotic backscattering coefficient (b_b^1). This is defined as the proportion of downward incident radiant flux scattered backward from an infinitely thin layer illuminated with light having the asymptotic radiance distribution typical of the water, divided by the thickness of the layer. As the normal backscattering coefficient b_b (Jerlov 1968) is defined in terms of a perpendicular, parallel beam of incident light, b_b^1 will be greater than b_b.

The relationship derived by Kirk (1977)

$$b_b^1 = 2\ \varepsilon R_A \qquad (3.5)$$

relates the asymptotic backscattering coefficient to the asymptotic reflectance and the vertical extinction coefficient, two easily

measured variables. Several assumptions are necessary in the use of this equation: (a) light attenuation must be sufficient for reflection from the bottom to be ignored. The optical depth of Mt. Bold ensured that this condition was met at all times at the southern sampling site. (b) ε is the extinction coefficient within the region where the asymptotic radiance distribution exists. In the turbid water of Mt. Bold ε did not vary greatly with depth and could be calculated from all data points. (c) ε describes the attenuation of both upwelling and downwelling irradiance. This condition was generally satisfied, however it is not a necessary requisite for calculating b_b^1, in that equation (3.5) can be modified to account for a difference between downwelling (ε) and upwelling (ε_u) extinction coefficients,

$$b_b^1 = R_A (\varepsilon + \varepsilon_u)$$

Kirk (1980) compared asymptotic backscattering coefficients with nepholometric turbidity measurements and found a linear relationship, providing evidence that b_b^1 is a measure of light scattering in natural waters. Using published data, theoretical calculations were used to determine the ratios of the asymptotic backscattering coefficient to the normal backscattering and total scattering coefficients (b_b and S).

To provide more direct evidence on the relationship between b_b^1 and the total volume scattering coefficient S, the present data was used to estimate S. If the vertical extinction coefficient ε, is described as in equation (3.4), then at times of very low

chlorophyll a concentrations,

$$\varepsilon = \bar{\varepsilon}_{G+\omega} + \bar{\varepsilon}_{p} + S.$$

$\bar{\varepsilon}_{G+\omega}$ has been estimated using laboratory absorbance measurements and an average spectral distribution for the incoming solar energy. As this distribution is likely to be similar to that occurring in the field (Spence et al 1971; Tyler & Smith 1970; Kondratyev 1969) the laboratory estimates of $\bar{\varepsilon}_{G+\omega}$ will vary from the field values by a factor related to the degree of shift in the spectral distribution due to selective absorption. As discussed earlier laboratory estimates will be slightly larger than average euphotic zone values, but assuming this difference is small,

$$\varepsilon - \bar{\varepsilon}_{G+\omega} = \bar{\varepsilon}_{p} + S$$

The scattering of light in turbid waters is mainly a function of the suspended particulate matter so that $\bar{\varepsilon}_{p}$ and S refer to the same component of the system. As separation of the absorbing and scattering roles is not possible with the present data it is assumed that absorption of light by the particulate fraction, which is composed largely of highly refractile mineral particles, is negligible compared to that of the dissolved colour, and

$$\varepsilon - \bar{\varepsilon}_{G+\omega} = S \qquad (3.6)$$

The two assumptions have opposing effects on the estimate of S. $\bar{\varepsilon}_{G+\omega}$ being a slight over-estimate decreases the calculated value

of S, while neglecting $\bar{\varepsilon}_p$ increases the value. Provided both effects are small and do not vary greatly over the considered turbidity range, a reasonable estimate of S should be obtained.

The total scattering coefficient is equivalent to the integral of the volume scattering function (Duntley 1963)

$$S = 2\pi \int_0^{\pi} \sigma(\nu) \, \mathrm{Sin}\, \nu \, d\nu$$

where ν is the scattering angle (that angle between the original direction of the light beam and its scattered direction) and $\sigma(\nu)$ the volume scattering function, defined as the proportion of incident irradiance which is scattered at angle ν from an infinitely small volume, divided by the volume. The backscattering coefficient is the integral of the volume scattering function in the back direction. Duntley (1963) illustrated the similar shape of volume scattering functions from a wide range of natural waters. Dealing here with a single water body in which the predominant scattering components are of a similar nature it is reasonable to assume that the volume scattering function will remain relatively constant. Kirk (1980) calculated theoretical total scattering coefficients for the zone of asymptotic irradiance distribution in waters with varying reflectance values, and found a linear relationship with nephelometric turbidity. As mentioned earlier a linear relationship was also found between turbidity and the asymptotic backscattering coefficient b_b^1. The conclusion implied by these results, but not stated, is that the asymptotic backscattering coefficient is linearly related to the total scattering coefficient

when the volume scattering function remains constant. If this is correct, and previous assumptions valid, then S values , calculated using equation (3.6) should be linearly related to b_b^1 values calculated from equation (3.5).

Equation (3.6) was derived, and used, for periods of low chlorophyll *a* concentration (<10 mg m^{-3}). To extend the available range of data for testing the linear relationship between b_b^1 and S, equation (3.6) was modified during periods of chlorophyll *a* concentration >10mg m^{-3}

$$\varepsilon - \bar{\varepsilon}_{G+\omega} - \varepsilon_s b = S$$

$\varepsilon_s b$ is the apparent *in situ* vertical extinction coefficient due to phytoplankton, calculated graphically from equation (3.3). Although this parameter is affected by the degree of light scattering in the water column, causing ε_s values to be higher than those measured in a non-scattering medium, the relative magnitude of ε_s and ε_q is such that 20-30 mg chl *a* m^{-3} are required before considerable errors occur. S, calculated from this equation, progressively underestimates the true value as chlorophyll concentration and scattering increases in the medium.

Except for two points, the relationship between estimated total scattering coefficient (equation (3.6)) and the asymptotic backscattering coefficient (equation (3.5)) is essentially linear as predicted (Fig. 3.12). In both disparate cases high chlorophyll concentrations and high asymptotic backscattering

coefficients prevailed (17/1/78: chla = 54 mg m^{-3}, b_b^1 = 1.49; 22/2/80: chla = 127.9 mg m^{-3}, b_b^1 = 1.24; Table 3.3). It is interesting that the data point for 4/12/79 fell on the line despite a chlorophyll a concentration of 106 mg m^{-3}. Presumably this is the result of the low b_b^1 value of 0.31. Excluding the two data points which obviously underestimate S, linear regression on the remaining 23 points yields the relationship,

$$S = 0.58 + 1.184\ b_b^1 \quad (r^2=0.84,\ S_{y.x}=0.28,\ S_c=0.09,\ S_s=0.12)$$

The line was expected to pass through zero, that it doesn't indicates S is over estimated, presumably as a result of ignoring the absorption by particulate matter. If this is the case then the linearity of the relationship suggests that increased particulate matter has a far greater effect on light scattering than on light absorption.

Tyler (1961) measured the ratio of backscattered to total scattered light ($\frac{b_b}{S}$) in distilled water and obtained a value of c. 0.14, while Kirk (1980) using the results of Petzold for water from San Diego Harbour suggested a value of 0.019. The slope of the line relating S to b_b^1 in the above results provides an estimate of $\frac{b_b^1}{S} = 0.84$. Kirk (1980) calculated a theoretical value for the ratio $\frac{b_b^1}{b_b}$ of c. 4.5 in water with reflectance value of c. 0.2. Based on these figures the data from Mt. Bold provides an estimate of $\frac{b_b}{S} = \frac{b_b^1}{S}\frac{b_b}{b_b^1} = \frac{0.85}{4.5} = 0.19$ which considering the crudity of the analysis is surprisingly close to the expected range, though probably far too large for such turbid water.

The linear relationship between S and b_b^1 provides support for use of the asymptotic backscattering coefficient as a measure of total scattering within a water body.

The backscattering coefficient calculated from equation (3.5) varied in a similar manner to ε (Fig. 3.6 (a) & (c)) during the period mid 1977 - mid 1978. As the extinction due to gelbstoff was relatively constant, this was expected and indicates the importance of light scattering during this period. By August 1978 scattering, as measured by b_b^1, had decreased to a low level, however the extinction coefficient maintained a value of c.2 due to increased gelbstoff concentrations (Fig. 3.6 (a) & (c)). During the summer of 1979-1980 gelbstoff concentration fell dramatically, and except for three peaks of increased scattering, caused a similar decrease in ε. The interplay of scattering and background absorption is particularly evident during this period.

3.5 Discussion

The extinction coefficients measured in Mt. Bold are of similar magnitude to those obtained in the more productive lakes of the northern hemisphere (e.g. Lake George, Loch Leven, Lough Neagh, Lake Kinneret; Lake Minnetonka; Table 3.4). In general the large extinction coefficients of these lakes result from light absorption by phytoplankton, and background extinctions are relatively small compared to those in Mt. Bold (Table 3.4). Noteworthy exceptions to this are Lake George (Ganf 1974) and Lough Neagh (Jewson 1977), both of which are shallow lakes,

(mean depth: Lough Neagh = 8.6m, Lake George = 2.5m) strongly influenced by wind, in which high ε_q values result from resuspension of sediments. This is unlikely to be a major turbidity source in Mt. Bold, which is deeper (average depth = 15.4m) and well protected from the wind by surrounding hills and a narrow dendritic form.

The remaining lakes listed in Table 3.4 have far smaller total and background extinction coefficients, even though some are considered eutrophic (e.g. Esthwaite Water and Blelham Tarn, Talling 1971). The distinctive feature of Mt. Bold Reservoir, apparent from these comparisons, is the combination of both depth and high background extinction. It has been demonstrated that the large ε_q values in Mt. Bold result mainly from absorption by dissolved colour, and scattering by suspended particulate matter. This will result in depletion of light available for photosynthesis, both through competitive absorption and reduction in the euphotic depth. However the final extent of light restriction to phytoplankton photosynthesis and growth is dependent on the mixing depth. As this is a function of the thermal regime of the water column, incoming solar radiation plays a significant role in its determination.

THERMAL REGIME

3.6 Introduction

It has been demonstrated (Fig. 3.4) that in Mt. Bold Reservoir the absorption of radiation in the 400-700ηm range is virtually

complete at a depth of c.2 metres. Wavelengths on either side of this range are more strongly attenuated and consequently the majority of the sun's radiation is absorbed by the upper two metres. The distribution of this heat load through the lake system, and the formation of the consequent thermal regime is of fundamental importance to physical, chemical and biological cycles.

Unlike many reservoirs in the northern hemisphere, Mt. Bold fills rapidly in the winter months but remains largely undisturbed by inflowing water during summer. Exceptions to this generalization occur in particularly dry years when large volumes of water may be pumped from the Murray River. The three year study period included examples of each of the major inflow regimes.

During the first year the catchment provided a minimal volume of water and large quantities were pumped from the Murray River, entering the reservoir continuously from July 1977 to March 1978 (Fig. 1.5(a)). Increased quantities of catchment water entered between June and September 1978, however as this was insufficient to meet requirements, low rate pumping of Murray River water commenced in December and continued until March 1979 (Fig. 1.5(b)). Inflow to the reservoir in the final season was due completely to catchment run-off. Considerable quantities of water entered during October 1979, but flow rapidly diminished and was negligible after November (Fig. 1.5(c)). Outflow disturbance of the near surface layers is minimized by the position of the offtake point at c.5m above maximum depth.

3.7 Seasonal Variations in Thermal Structure

Depth-time diagrams for isotherms (Fig. 3.14) illustrate the variation in thermal regime at the southern sampling site and site A which is situated near the confluence of the Onkaparinga River and Echunga Creek (Fig. 1.4).

Isothermal conditions prevailed during autumn and winter (March-August), water temperatures reaching a minimum of 9°C. Marked stratification of the water column occurred during September and October, and by November, in each year except 1977, an intense thermocline had formed. The lack of thermocline formation during late 1977 was attributed to turbulence resulting from the large inflow of water via the Onkaparinga River. Consequently site A showed virtually no stratification over the entire summer, while at the southern site weak, spasmodic thermocline formation occurred (Fig. 3.14(a)).

Intense thermoclines developed at both sites during November 1978, however these were weakened and forced to greater depths with the onset of inflow during December (Fig. 3.15). Both sites showed a brief recovery in early January due to a short period of particularly intense solar radiation (Fig. 3.19). In contrast thermoclines which formed in November 1979, persisted and intensified over the summer period (Fig. 3.16).

3.8 Heat Distribution in the Epilimnion

Distribution of the heat load through the lake is a function of

turbulence resulting from both wind action and water currents. In general the epilimnia of lakes are turbulent as a result of direct wind action.

The most notable feature of the wind regime influencing Mt. Bold was the lack of any marked seasonal variation in daily wind run (Fig. 3.17), for example during 1979-80 values oscillated around a mean of 247 km d^{-1} (η=165, S.E. of mean = 6.4). Westerlies predominate in winter while in summer easterlies prevail, although wind direction in this season is quite variable. The reservoir is most affected by winds moving parallel to the long east-west axis (Fig. 1.4), it being well protected by topography and minimal fetch from winds in other quarters. As a result directional variability of the summer wind regime acts to reduce potential wind mixing. This effect was observed in a time series of temperature profiles taken over a day during the height of the summer period (27 December 1979). A north-westerly wind prevailed during these temperature measurements, with a total wind run for the day close to the average value (Table 3.5). Temperature profiles taken during the early morning showed isothermal conditions in the epilimnion (Fig. 3.18). As the day progressed thermal stratification of the euphotic zone increased to a maximum in the mid-afternoon, when a very large temperature differential (4°C) was apparent over the top 40cm indicating a lack of vertical mixing. By early evening surface water temperatures had started to fall.

The lack of surface mixing suggests that the prevailing north-westerly was having an insignificant effect on the water column.

As these same conditions prevailed through the previous day (Table 3.5) it can be assumed that wind induced mixing had been minimal over 48 hours. Granted this interpretation, interest focuses on the overnight return of the epilimnion to an isothermal condition.

The rapid fall in surface temperature observed during the early evening indicated that thermal convection might be playing a significant role in epilimnion mixing. Support for this was provided by the large daily variation in air temperatures, minimum and maximum values frequently differing by 12°C (Fig. 3.19), and at times by as much as 22°C. As a result night air temperatures were often 8-10°C below average euphotic zone temperatures (Fig. 3.19). These data suggest that mixing of the epilimnion occurred overnight, even when wind induced turbulence was minimal.

3.9 Heat Distribution Below the Thermocline - Eddy Diffusivity

The lower section of the relatively well mixed epilimnion is delineated by the thermocline, which acts as a barrier isolating the epilimnion from hypolimnetic waters. Utilization of the vast reserve of nutrients present within the hypolimnion, and the recycling of nutrients removed from the euphotic zone by particulate flux, depends on rates of transfer across the metalimnion. As a result, the vertical transport of material is a fundamental consideration in thermally stratified lakes.

Eddy diffusion is generally regarded as the main mechanism of vertical flux within the metalimnion and hypolimnion (Mortimer, 1942; Hutchinson 1957). This is based on the assumption that at a given depth the mean vertical velocity due to turbulence is small when compared to the instantaneous vertical water velocity (Hutchinson 1957; Powell & Jassby 1974), an assumption supported by calculations of heat transport below the thermocline (Hutchinson 1957).

Vertical turbulent transport due to diffusive processes is described by the Fickian diffusion equation,

$$F_{sz} = - K_{sz} \frac{\partial s}{\partial z} \qquad (3.7a)$$

where F_{sz} is the mean flux of substance s in the vertical direction, K_{sz} the vertical eddy diffusivity ($cm^2 s^{-1}$), and $\frac{\partial s}{\partial z}$ the concentration gradient. Thermal energy flux (H_ω) can be described by an analogous equation,

$$H_\omega = - \rho c \, A_z \frac{\partial \theta}{\partial z} \qquad (3.7b)$$

where ρ is fluid density, c specific heat capacity, A_z vertical eddy conductivity and $\frac{\partial \theta}{\partial z}$ the temperature gradient. In general eddy conductivity and diffusivity are considered equivalent, (Hutchinson 1941, 1957; Lerman & Stiller 1969; Happey 1970a, b; Hickman 1974) and in the remainder of the discussion both are represented by the symbol A. The product (ρc) is taken as unity (Hutchinson 1957; Jassby & Powell 1975).

Although eddy diffusivities may be calculated directly from flux equations (Hutchinson 1941; Mortimer 1941-42; Jassby & Powell 1975), frequent use has been made of an indirect method developed by McEwen (1929, cited in Hutchinson 1941; Hutchinson 1941; Bachmann & Goldman 1965; Lerman & Stiller 1969; Happey 1970a; Hickman 1974). Experimental measurements (Hesslein & Quay 1973) and theoretical considerations (Powell & Jassby 1974) have cast doubt on the general validity of this indirect approach.

In an attempt to assess the role of eddy diffusivity in the vertical flux of nutrients in Mt. Bold Reservoir both approaches have been utilized and the results compared. Calculations are based on a series of temperature profiles taken at 1 or 2 weekly intervals through the heating periods of 1978 and 1979 (Fig. 3.20).

3.10 Eddy Diffusivities Calculated by the McEwen Method

Differentiation of equation (3.7b) with respect to depth produces a function relating eddy diffusivity to temperature change,

$$\frac{\partial \theta_z}{\partial t} = \frac{\partial A_z}{\partial z}\frac{\partial \theta_z}{\partial z} + A_z \frac{\partial^2 \theta_z}{\partial z^2} \qquad (3.8)$$

where $\frac{\partial \theta_z}{\partial t}$ is the rate of change of temperature with time at depth z, and $\frac{\partial^2 \theta_z}{\partial z^2}$ the second derivative of the temperature variation with depth at z. If a region of the water column is considered where A is constant, then the eddy diffusivity may be calculated

from,

$$A = \frac{\partial \theta_z}{\partial t} \cdot \frac{\partial z^2}{\partial^2 \theta_z} \qquad (3.9)$$

It is the estimation of $\frac{\partial \theta_z}{\partial t}$ and $\frac{\partial^2 \theta z}{\partial z^2}$ which forms the basis of this approach.

To obtain an average value of $\frac{\partial \theta_z}{\partial t}$ for each 1 metre depth, the data relating temperature to time were fitted by linear regression, even though it is evident (Fig. 3.20) that frequently temperature variation with time is markedly non-linear. However linear regression provides a reasonable estimate of the mean rate of change, as shown by r^2 values which were always >0.80 and in the majority of cases >0.90 (Table 3.6 & 3.7).

Analysis of $\frac{\partial \theta}{\partial t}$ for 1978 was restricted to the period 5/9/78 - 28/11/78 (Table 3.6) due to marked disruption of the temperature gradient by the influx of Murray River water early in December (Fig. 3.20). During 1979-1980, $\frac{\partial \theta}{\partial t}$ was calculated for each 1 metre depth over the period 12/9/79 - 9/1/80 (Table 3.7). An estimate of the average temperature of each 1 metre layer, at the mid-point of the heating period, was calculated from the linear regression equations (θ_H in Table 3.6 & 3.7).

The variation of the average $\frac{\partial \theta}{\partial t}$ values with depth is depicted in Fig. 3.21. In the epilimnion $\frac{\partial \theta}{\partial t}$ is constant, as expected from the well mixed conditions. Below this, $\frac{\partial \theta}{\partial t}$ falls exponentially with depth, the points forming a straight line on the semi-logarithmic graphs (Fig. 3.21). Hutchinson (1941) termed this

the clinolimnion, and considered it to be limited on its upper surface by the thermocline. The region below this, where $\frac{\partial\theta}{\partial t}$, is higher than would be expected from extrapolation of the exponential fall in the clinolimnion, was termed the bathylimnion.

The estimation of $\frac{d^2\theta}{dz^2}$ is based on an equation derived by McEwen (cited in Hutchinson 1941) describing the variation of hypolimnetic temperatures with depth,

$$(\theta - C) = C_1 e^{-az} \qquad (3.10)$$

where C, C_1 and a are constants. Differentiating with respect to depth,

$$\frac{d^2\theta}{dz^2} = C_1 a^2 e^{-az} \qquad (3.11)$$

$\frac{d^2\theta}{dz^2}$ can be estimated from this equation if C_1 and a are known. The methods used to estimate the constants in equations (3.10) and (3.11) followed those described by Hutchinson (1941). In essence it can be shown that if equation (3.10) describes hypolimnetic temperatures then,

$$\theta_z = C + \frac{\Delta\theta}{1-e^{-a}}$$

where $\Delta\theta$ is the difference in temperature between two consecutive depths, calculated in Table 3.6 & 3.7 as the difference between average layer temperatures mid-way through the heating period. C and a were calculated from this function by the linear regression of θ_H on $\Delta\theta$ (Table 3.8; Fig. 3.22), and the value of C_1 estimated

as,

$$C_1 = \frac{\Sigma\ (\theta_H - C)}{\Sigma\ e^{-az}} \quad ,$$

where Σ is the sum over the clinolimnion and bathylimnion, and $(\theta_H - C)$ the difference between the average layer temperature mid-way through the heating period, and C (Hutchinson 1941). Substitution of these values into equation (3.12), derived from equations (3.9) and (3.11),

$$A = \frac{\partial\theta}{\partial t} \frac{1}{C_1 a^2 e^{-az}} \qquad (3.12)$$

yields an estimate of A which is valid at depths where A is constant (cf. equations (3.8) and (3.9)). To select these depths Hutchinson (1941) compared semilogarithmic graphs of $\frac{d\theta}{dt}$ and $(\theta - C)$ against depth. It follows from equations (3.10) and (3.12) that

$$\ell n\ (\theta - C) = \ell n\ C_1 - az$$

and

$$\ell n \frac{d\theta}{dt} = \ell n\ (C_1 a^2 A) - az$$

Provided A is constant these two equations describe parallel straight lines, and Hutchinson considered obtaining such a result as the "criterion of validity". This criterion is generally offered to support the use of McEwen's method (Lerman & Stiller 1969; Happey 1970a; Hesslein & Quay 1973; Hickman 1974). Accepting this argument for the present time and applying the

technique to the Mt. Bold data the criterion was met over the depths 6-11m in 1978 (Fig. 3.21(a)) enabling the calculation of, eddy diffusivity values (Table 3.6). The 1979-80 data (Fig. 3.21(b)) although showing a reasonably parallel response over the range 8 - 16m contains a marked discontinuity at 13m. This resulted from the persistence of secondary thermoclines formed by windy weather early in the heating period (cf. Fig. 3.16, 18/9/79, 31/10/79, 14/11/79). The parallel response on either side of the discontinuity suggests that a mean value should provide a reasonable estimate of the vertical diffusivity (Table 3.7). Average diffusivity values for the clinolimnion in 1978-79 and 1979-80 were respectively 0.165 and 0.113 $cm^2\ s^{-1}$ which are higher than those calculated by Hutchinson (1941) for Lake Mendota and Linsley Pond, and by Hesslein & Quay (1973) for lake 227 in the Experimental Lakes area, but of a similar magnitude to those obtained from Abbot's Pool (Happey 1970a), Lake Tiberias (Lerman & Stiller 1969) and Lake Tahoe (Dillon et al 1975).

3.11 Eddy Diffusivities Calculated from Heat Flux and Thermal Gradients

Hesslein & Quay (1973) compared eddy diffusivities calculated from the McEwen method with *in situ* dye and radon dispersal measurements and found order of magnitude differences between estimates.

Hutchinson (1941, 1957) compared estimates from the McEwen method with those from heat flux calculations and, based on the "criterion of validity", rejected the heat flux values which tended to increase with depth rather than remain constant. He postulated

that lateral transport of heat in the bathylimnion caused heat flux estimates of diffusivity to increase with depth, and to appear anomalously high in the clinolimnion.

Powell & Jassby (1974) re-analyzed the McEwen approach without the assumption of constant A, and demonstrated that the straightness and parallelism "criterion of validity" did not necessarily imply that A remained constant. This is simply shown by taking the natural logarithm of equation (3.8) after substituting $\frac{d\theta}{dz}$ and $\frac{d^2\theta}{dz^2}$ calculated from equation (3.10)

$$\frac{d\theta_z}{dt} = -\frac{dA_z}{dz} C_1 a e^{-az} + A_z C_1 a^2 e^{-az}$$

$$\ell n \frac{d\theta_z}{dt} = \ell n[(-\frac{1}{a}\frac{\partial A_z}{\partial z} + A_z) C_1 a^2] - az$$

This function will be linear and parallel to $\ell n\ (\theta - C)$ vs z when

$$-\frac{1}{a}\frac{\partial A_z}{\partial z} + A_z = r_1$$

where r_1 is a constant. The solution to this equation (Powell & Jassby 1974)

$$A_z = r_1 + r_2 e^{az} \qquad (3.13)$$

contains an unknown constant r_2. When A_z is described by equation (3.13) Hutchinson's "criterion of validity" will be met but A will not be constant unless it is assumed that the unknown $r_2 = 0$. This assumption is implicit in the McEwen approach.

Powell & Jassby (1974) used the data of Hutchinson (1941) to demonstrate that the McEwen method may in cases lead to erroneous results.

Forelian heat budgets (Hutchinson 1957) were calculated for Mt. Bold Reservoir, providing estimates of the heat flux (H_ω) through unit area of depth planes over the heating periods used previously with the McEwen approach.

$$H_\omega = \frac{100\ \Sigma_B^z\ (\theta_o - \theta_t)}{t \times 86.4 \times 10^3}\ \text{cal. cm}^{-2}\ \text{s}^{-1} \qquad (3.14)$$

where z is the layer (below the thermocline) for which the eddy diffusivity is to be calculated, and B the depth of the reservoir bottom. θ_o is the initial temperature of each 1 metre layer and θ_t the temperature after time t days. The constant (100) converts temperature change to calories cm^{-2} in each 1 metre layer, and 86.4×10^3 is the number of seconds in a day. Average $\frac{d\theta}{dz}$ values were estimated for each depth by the mean for all sampling dates of the differences $(\theta_{z+1} - \theta_z)$ and $(\theta_z - \theta_{z-1})$ (Mortimer 1941-42) and eddy diffusivity calculated using equation (3.7b) (Table 3.9 & 3.10).

In calculating heat fluxes Jassby & Powell (1975) included a term for direct heating by solar radiation. The euphotic depth in Mt. Bold is c.2m while the thermocline is positioned at c.5-6m (Fig. 3.21), therefore direct heating of the clinolimnion and hypolimnion can be ignored. It is assumed that lateral transport of heat is negligible (cf. Hutchinson 1941, 1957).

The average clinolimnion diffusivities calculated from heat flux are 0.372 and 0.412 $cm^2\ s^{-1}$ respectively for the 1978 and 1979-1980 data (Table 3.9 & 3.10) representing a 2 - 4 fold increase over the values calculated from McEwen's method. Powell & Jassby (1974) suggested that such differences may be a result of assuming A_z constant when it actually varies. If this is the case then according to equation (3.13),

$$\ell n\ (A_z - r_1) = \ell n\ r_2 - az \qquad (3.15)$$

where r_1 is taken to be the estimate of diffusivity from McEwen's method, and A_z the estimate from heat flux calculations (Powell & Jassby 1974). The graphs of $\ell n\ (A_z - r_1)$ vs z do not satisfy the relationship (Fig. 3.23) and consequently the differences observed here cannot be attributed to this cause. In fact the data fall on approximately horizontal lines implying r_2 is close to zero, and that a relatively constant difference occurs between the two estimates in the clinolimnion.

At this juncture the choice of a representative eddy diffusivity coefficient cannot be objectively made, the evidence for both techniques appearing to be equally valid. However the energy flux data is more directly determined and has greater potential than McEwen's method in enabling diffusivities to be calculated for the entire hypolimnetic region (Table 3.9 & 3.10, Fig. 3.24). In the next section the validity of calculated eddy diffusivities is tested by comparison with the flux of a chemical compound. However, pre-empting the results of those calculations, the heat

flux diffusivities are used here to describe the variation of vertical eddy diffusivity with depth in the water column.

The zone displaying greatest thermal stratification (6 - 11m, Fig. 3.15 & 3.16) is marked by relatively low and constant values for the eddy diffusivity (Fig. 3.24). Below this region values steadily increase to 26 m peak suddenly at 28 - 30m, and then decrease towards the reservoir bottom.

The maximum values correspond closely to the depth of the reservoir outflow, which is positioned c.5m above maximum depth. The horizontal flow of water through these lower layers undoubtedly increases eddy diffusivities in the upper layers of the water column, aiding in the vertical transport of nutrients.

3.12 Eddy Diffusivities Calculated from Mass Flux and Concentration Gradients

Rarely do circumstances permit the use of naturally occurring chemical compounds in estimating eddy diffusivities by mass flux. However, during the 1979-1980 summer period in Mt. Bold Reservoir, a rather unique vertical distribution of NO_3-N enabled flux rates of this compound to be estimated and an eddy diffusivity calculated for comparison with thermal diffusivity. In mid-November 1979 (Fig 4. 3) rapid algal growth depleted the NO_3-N content of the epilimnion, as epitomized by the concentration at 0m, and this remained below detectable levels ($<10\mu g\ N\ell^{-1}$) through the rest of the summer. Removal of NO_3-N from the

second sampling depth at 10m was not obvious until the epilimnion concentration had fallen to <10μg ℓ^{-1}, NO_3-N was then removed rapidly from this depth until it too was reduced to levels below the detection limit. Similarly the NO_3-N concentration at 20m and below remained virtually constant, until the 10m concentration reached <10μg ℓ^{-1}, NO_3-N was then removed simultaneously from the 20 and 30m depths. This unexpected, simultaneous removal from depths separated by 10m can be explained by the increased turbulence due to water flow towards the reservoir outlet. The 20-30m zone is therefore well mixed relative to the vertical removal of NO_3-N. Below 30m the concentration remained at c.600 μg ℓ^{-1} (Fig. 4.3).

Estimates of mass flux variables were calculated for the 40 day period (9/1/80 - 18/2/80) during which NO_3-N was removed from the 20-30m zone (Fig. 4.3). The flux of NO_3-N through unit area of the 20m layer was estimated from the change in concentration (645 to 10 μg Nℓ^{-1}) in the 20-30m zone, yielding a value of 635 μg NO_3-N cm^{-2}. The average concentration gradient driving this flux was estimated as 28.3×10^{-5} μg cm^{-3} cm^{-1} from the difference in NO_3-N concentration at 10m (35 μg ℓ^{-1}) and 30m (600 μg ℓ^{-1}). The eddy diffusivity at 20m calculated from these values using equation (3.7a) was 0.65cm^2 s^{-1}.

Heat flux calculations over the same period (H_ω = 6841 cal. cm^{-2} in 40 days, average $\frac{d\theta}{dt} = 29 \times 10^{-4}$ °C cm^{-1}) gave an eddy diffusivity estimate of 0.683 cm^2 s^{-1} for the 20m depth. The similarity of these two estimates provides strong support for

the heat flux calculations as a means of estimating eddy diffusivity. The values are similar to the average diffusivity calculated from heat flux measurements (0.593 $cm^2\ s^{-1}$) over the 17 weeks prior to 9/1/80 (Table 3.10, 20m).

The large vertical separation between sampling depths for chemical analysis (10m), precluded the use of similar calculations for other nutrients, and other time periods. However, the frequently observed sequential decline of nutrients with depth during thermally stratified periods (Fig. 4.2 & 4.3 ; see Chp.4) suggests that quantitative data on the vertical transport of nutrients could readily be obtained by a carefully planned monitoring program.

3.13 Discussion

The seasonal thermal pattern in Mt. Bold Reservoir is classified as warm monomictic in the scheme proposed by Hutchinson and Löffler (1956), and is by far the most common pattern observed in Australian lakes and reservoirs (Williams & Wan 1972). Holomixis occurs once and takes place in winter at temperatures above 4°C (Fig.3.14(a)-(c)). The typical dimictic pattern of northern temperate lakes has never been observed in Australia (Williams & Wan 1972).

A distinct thermocline forms in summer separating the hypolimnion from the epilimnion, however turbulent mechanisms continue to govern the vertical movement of heat and chemicals even below the epilimnion. This is quantitatively illustrated

by the very large values obtained for eddy diffusivities (Table 3.9 & 3.10) compared with the molecular thermal conductivity of water (0.12×10^{-2} cm^2 s^{-1}). The importance of vertical turbulent transport to the chemical regime in the lake was dramatically illustrated by the removal of NO_3-N from the 20-30m zone. In 40 days 635 µg NO_3-N cm^2 were transported through the 20m layer by turbulent mechanisms providing a source of NO_3-N for the zones above. This will naturally be of great consequence to the biological cycles.

The magnitude of the vertical diffusivity estimates from the southern sampling site may not be representative of the reservoir generally. The effect of the outlet was evident in the eddy diffusivity profiles (Fig. 3.24) and the increased turbulence near the reservoir bottom quite likely increased diffusivities in the upper layers. Further upstream where the outlet effect is minimal, diffusivities are expected to be smaller.

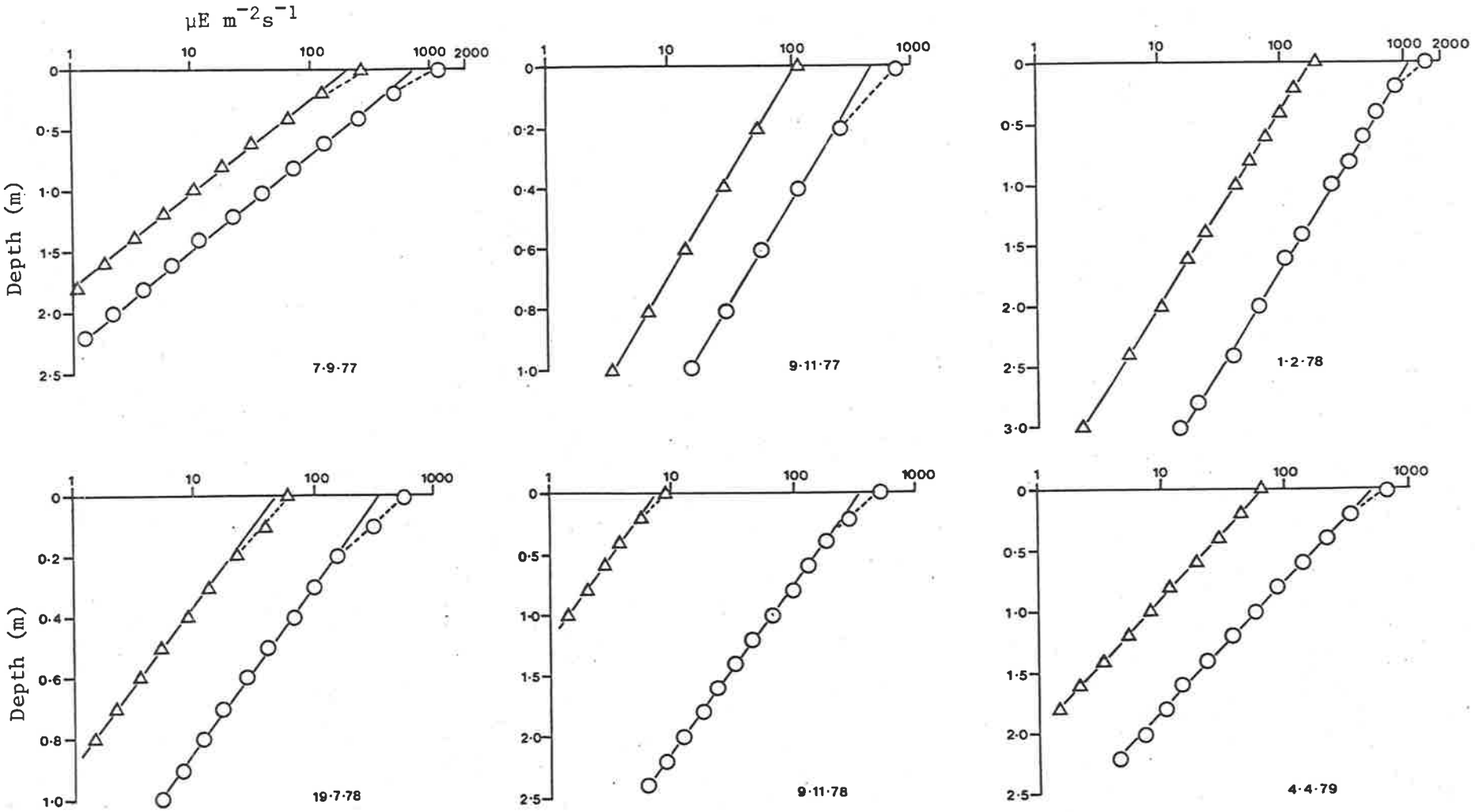

Fig. 3.1: Typical downwelling (o) and upwelling (Δ) irradiance measurements from Mt Bold Reservoir.

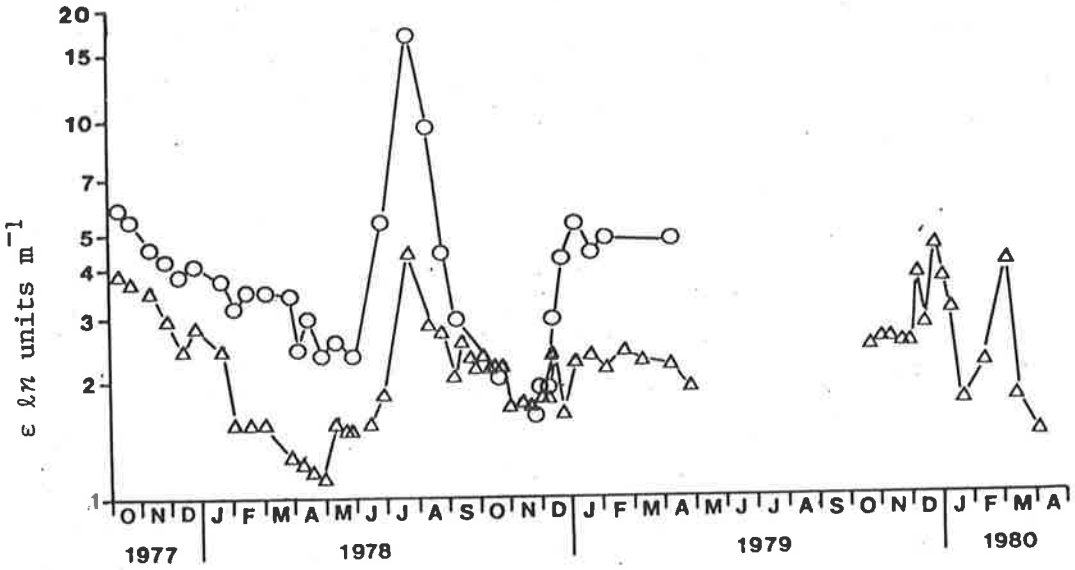

Fig. 3.2: Seasonal variation in vertical extinction coefficients (ε) for the north (o) and south (△) sampling sites.

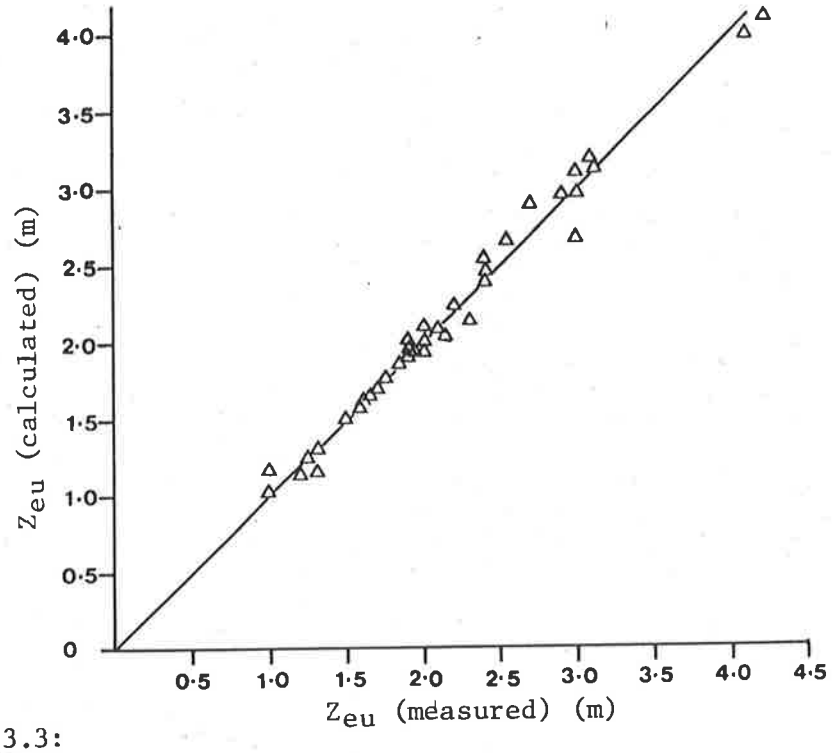

Fig. 3.3:

Comparison of measured and calculated values of the euphotic depth (Z_{eu}). Linear regression: Z_{eu} (calculated) = 0.08 + 0.98 Z_{eu} (measured), r^2 = 0.98.

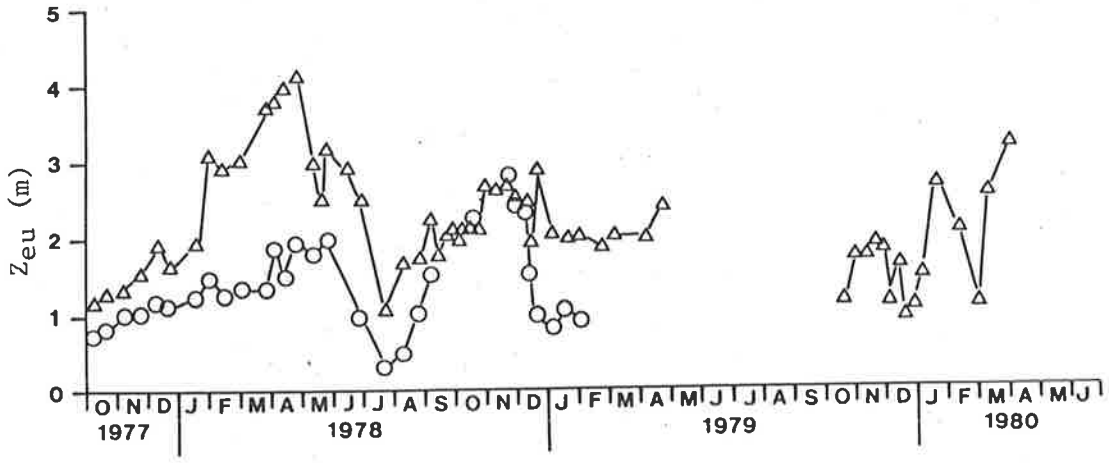

Fig. 3.4: Seasonal variation in depth of the euphotic zone (Z_{eu}) for the north (o) and south (△) sampling sites.

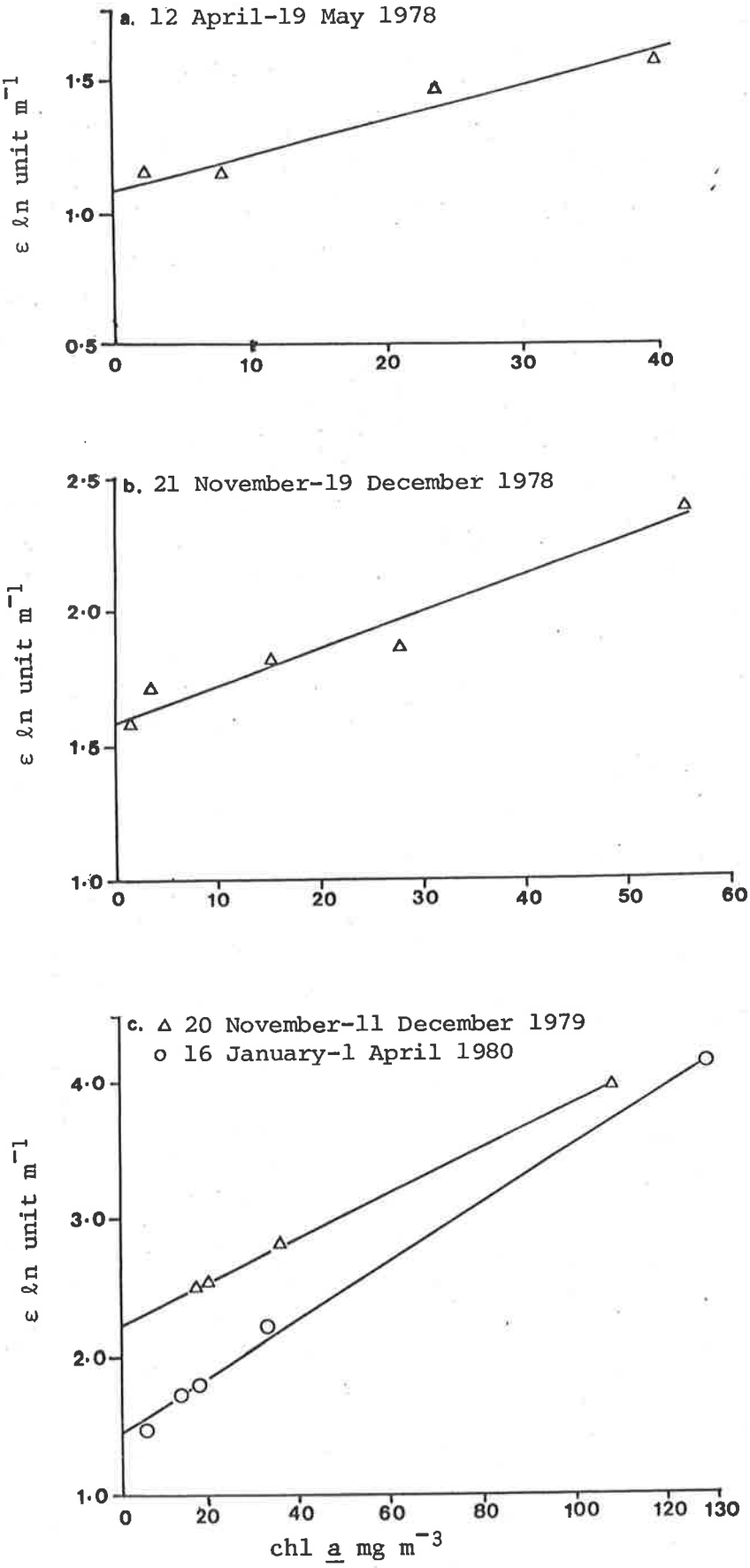

Fig. 3.5: The relationship between the vertical extinction coefficient (ε) and the concentration of chlorophyll a within the euphotic zone of Mt Bold Reservoir during four periods. See Table 3.1 for linear regression statistics.

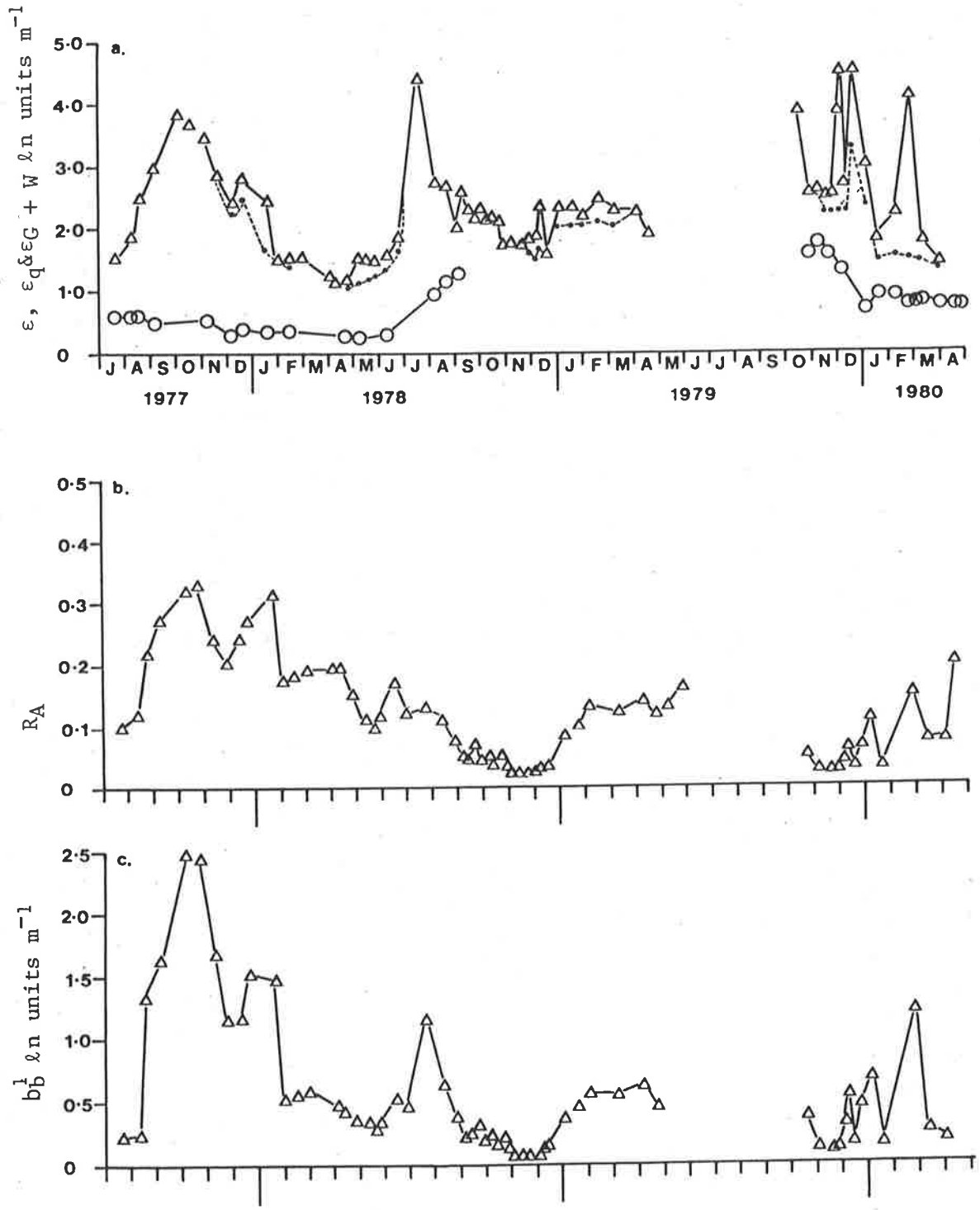

Fig. 3.6: a. Seasonal variation in vertical extinction coefficient (ε ▲—▲), background extinction coefficient (εq ●—●) and the extinction due to dissolved colour plus water, as determined on filtrates (ε_{G+W} o–o). All data for the south sampling site.

b. Seasonal variation in the asymptotic reflectance ratio (R_A) at the south sampling site.

c. Seasonal variation in the asymptotic backscattering coefficient (b_b^1) for the south sampling site.

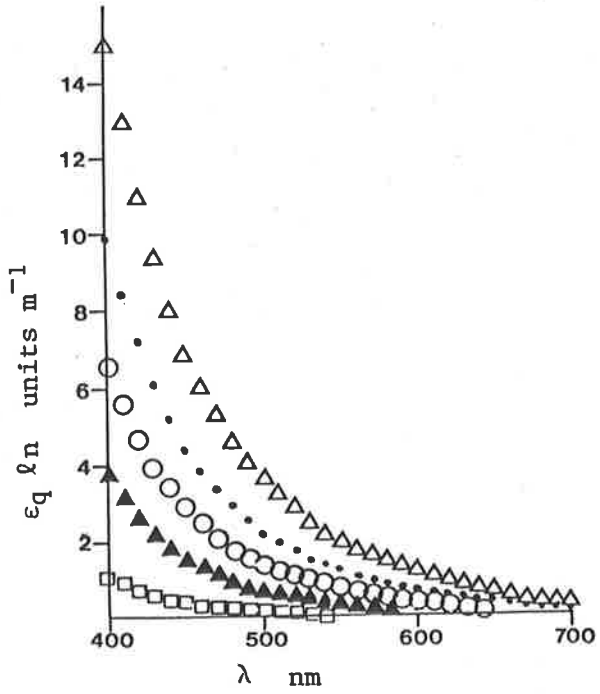

Fig. 3.7: Extinction coefficients due to dissolved colour (ε_q), at 10 nm wavelengths for selected dates during the study period.

Fig. 3.8: Percentage energy content in 10 nm intervals of incoming solar irradiance collected on a horizontal plane, for the wavelength 400 - 700 nm. Nomenclature for the different graphs enables location of the data source.

a. Judd *et al.* (1964, Table V)

□ correlated colour temperature 5500° K

▲ correlated colour temperature 6500° K

Henderson & Hodgkiss (1963, Table 1)

● E_2

△ E_3

b. Winch *et al.* (1966, Table 1)

△ E_1

○ E_5

▲ E_6

c. Taylor & Kerr (1941, Table 11)

▲ Overcast sky

△ Sun and sky

Thekaekara (1970)

○

d. Average percentage energy distribution (•) and average percentage quanta distribution (▲) derived from the above data.

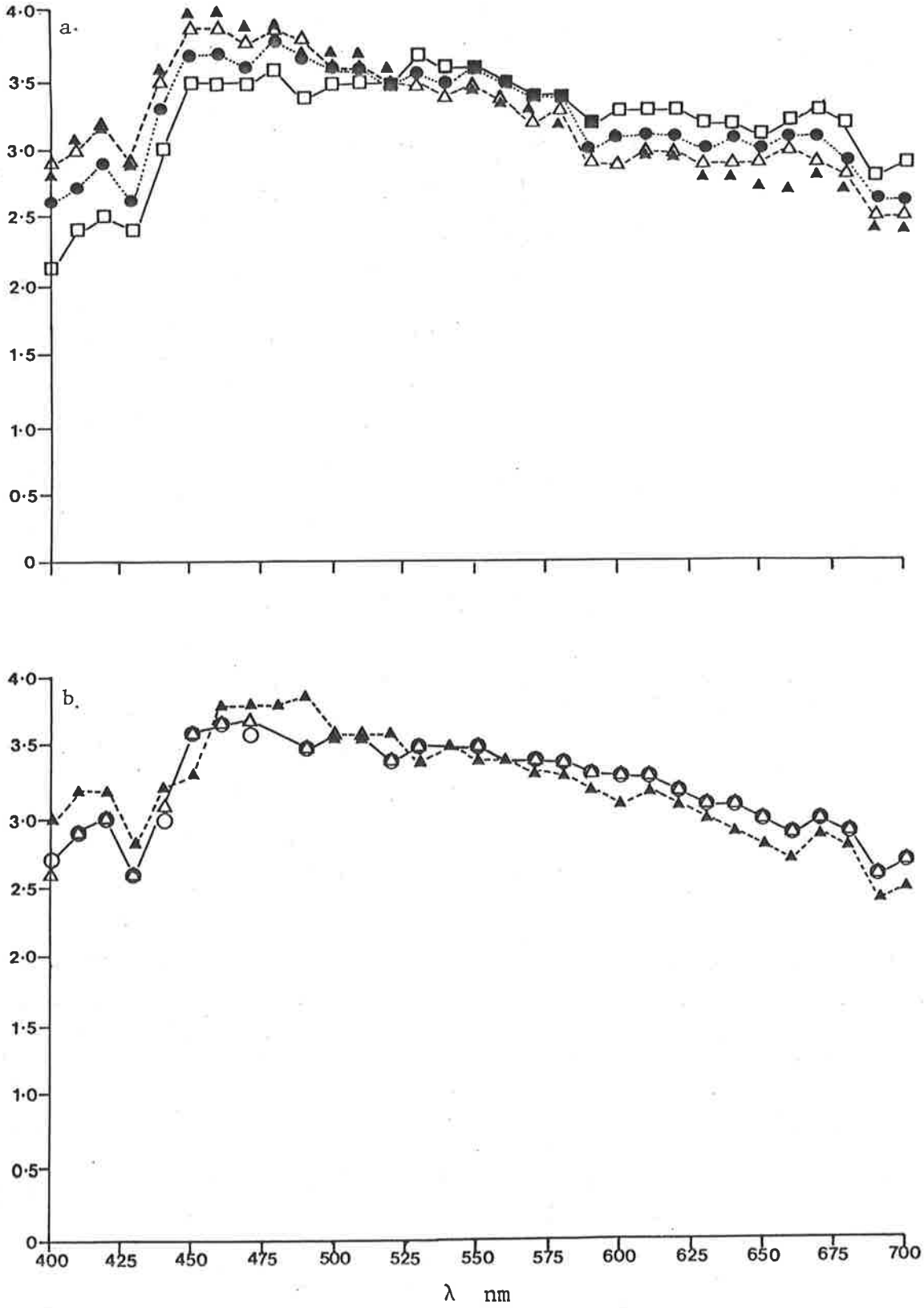
a.
b.
4·0
3·5
3·0
2·5
2·0
1·5
1·0
0·5
0
400
425
450
475
500
525
550
575
600
625
650
675
700
λ nm

Fig. 3.8

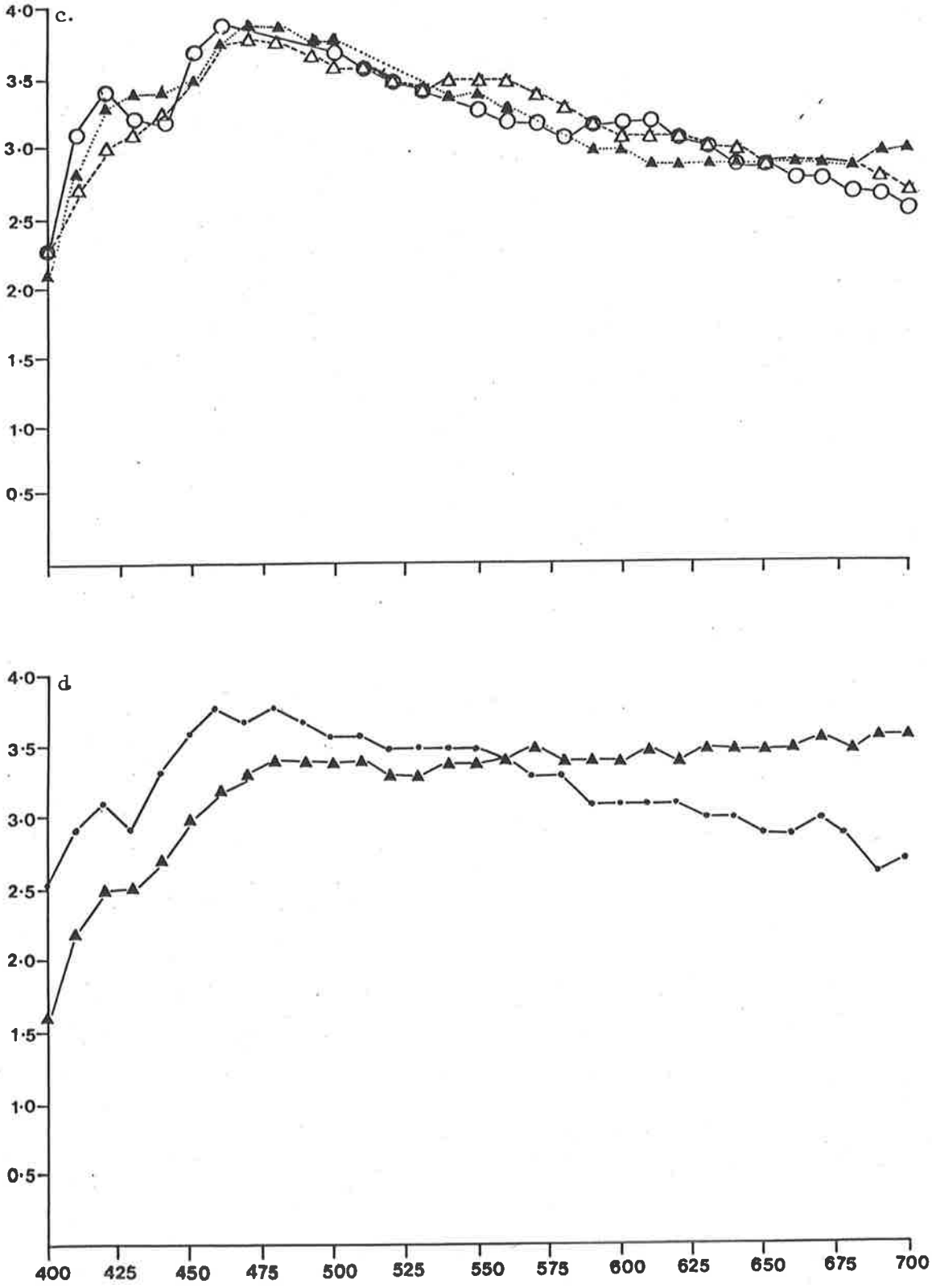
c.
4·0
3·5
3·0
2·5
2·0
1·5
1·0
0·5
d
4·0
3·5
3·0
2·5
2·0
1·5
1·0
0·5
400
425
450
475
500
525
550
575
600
625
650
675
700

Fig. 3.8 (cont.)

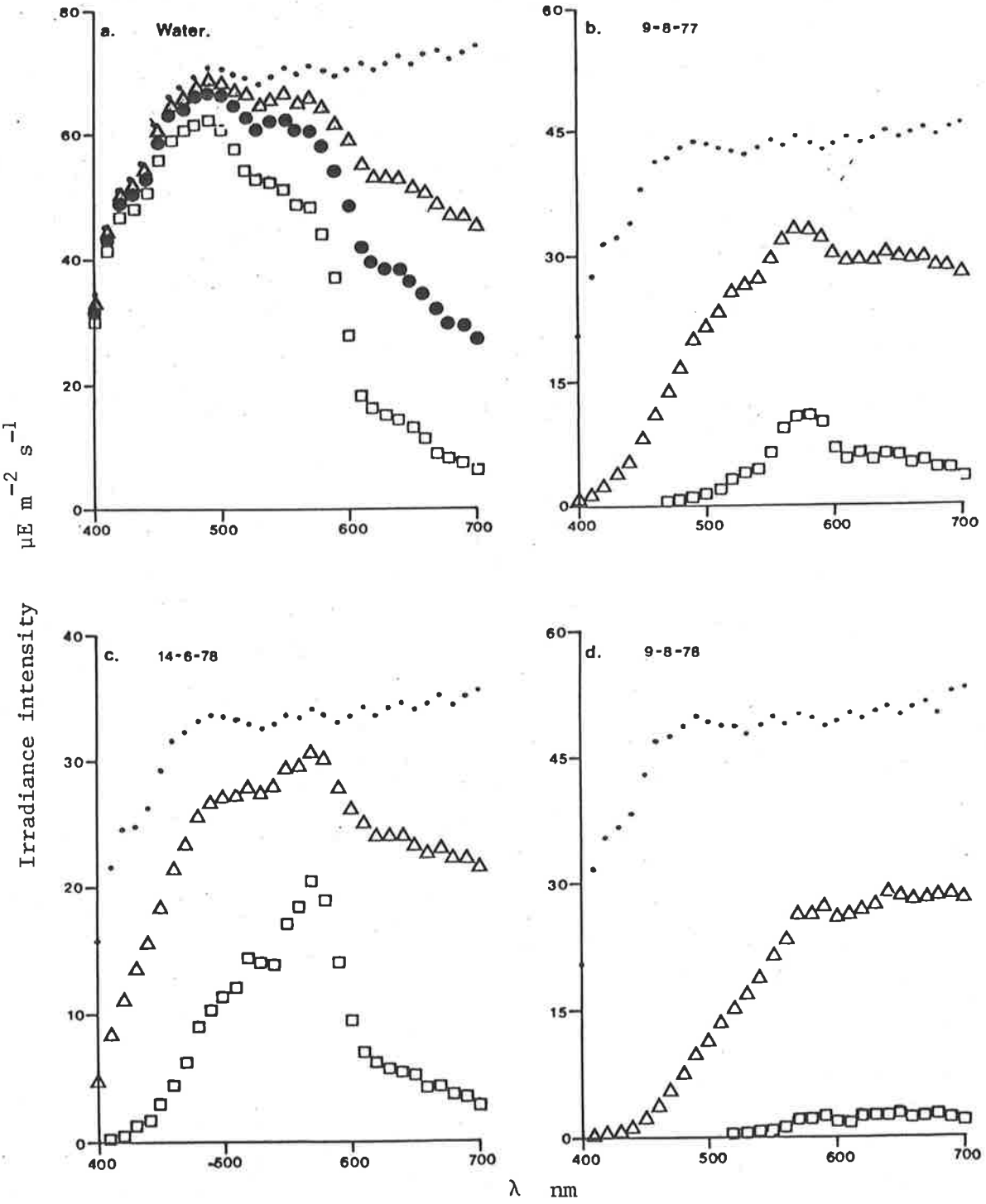

Fig. 3.9: Calculated spectral distribution of light at depths of 0.0 m (•), 1.0 m (△), 2.0 m (●) or 5.0 m (□) for
(a) clear natural water (Smith & Tyler 1967), and
(b-g) hypothetical columns of Mr Bold water containing only dissolved colour. (See text)

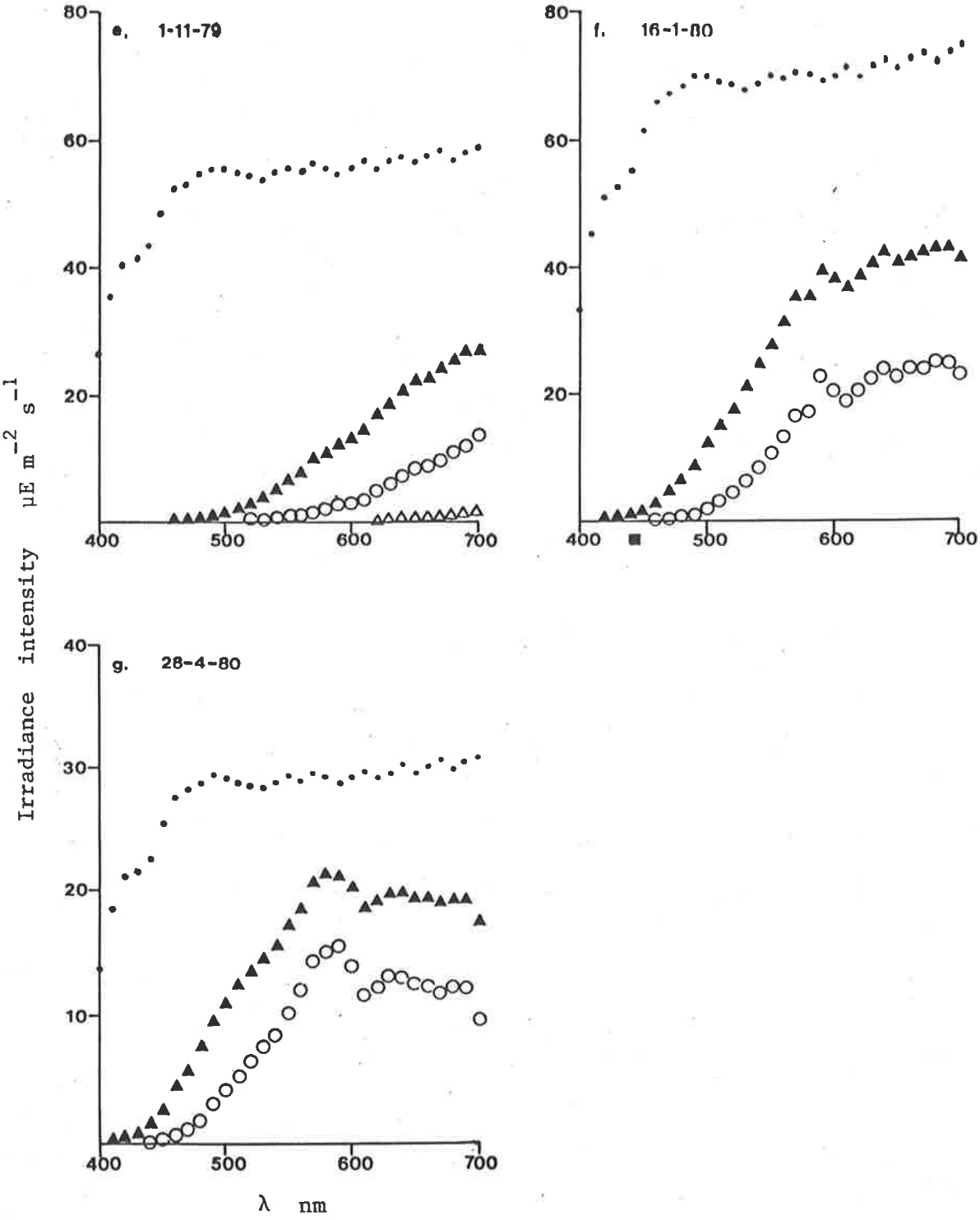
e. 1-11-79
f. 16-1-80
g. 28-4-80
Irradiance intensity μE m^{-2} s^{-1}
λ nm
80
60
40
20
30
10
400
500
600
700

Fig. 3.9 (cont.)

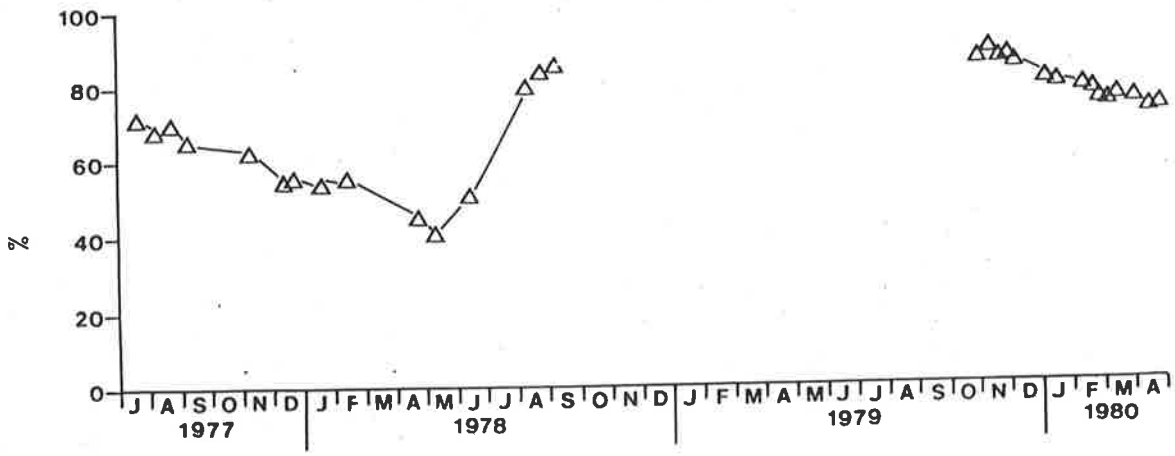

Fig. 3.10: Seasonal variation in percentage attenuation of irradiance due to dissolved colour (ε_G) for filtrates at Mt. Bold Reservoir water, where dissolved colour and water are the only absorbants ($\varepsilon_G + \omega$)

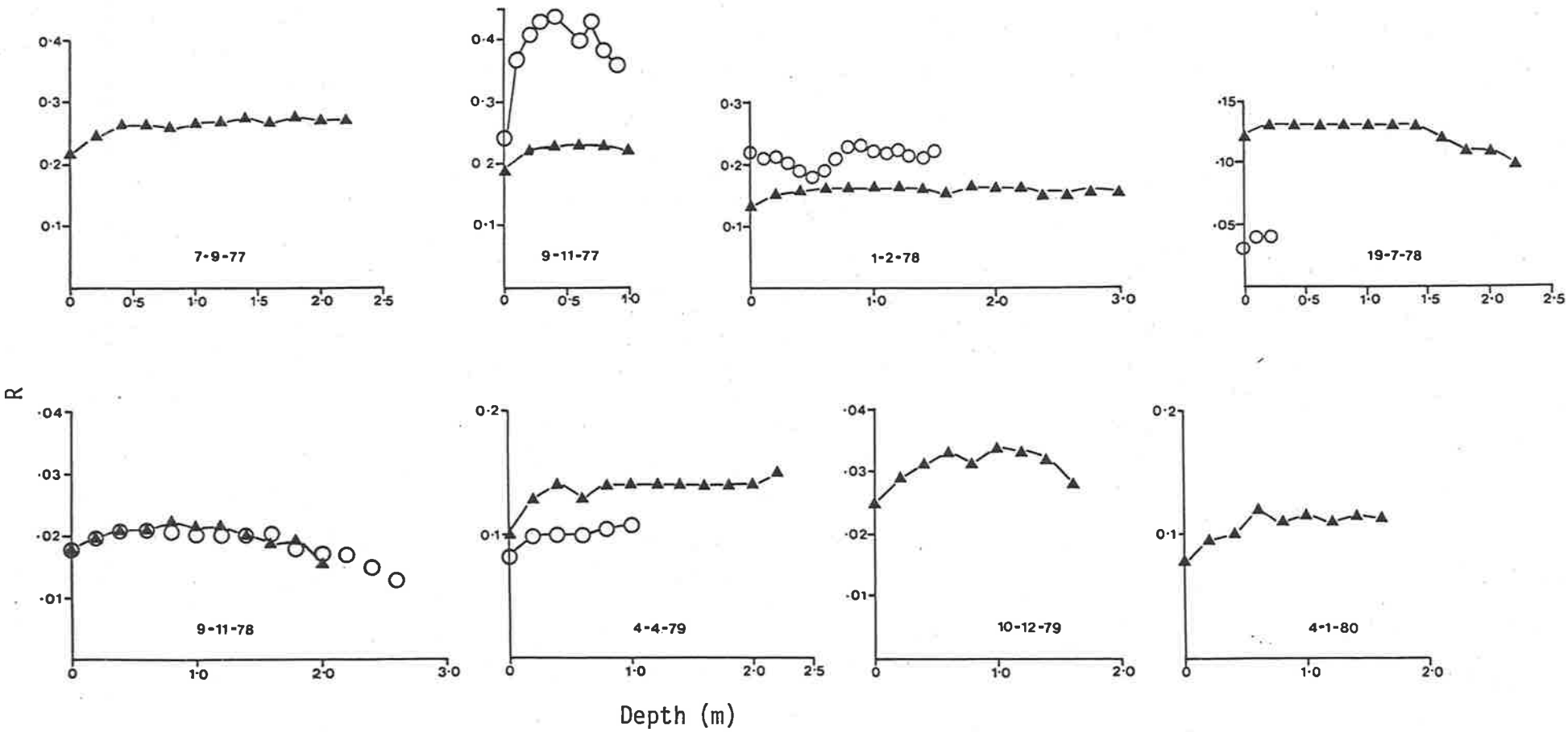

Fig. 3.11: Examples of the variation with depth of reflectance ratios (R) measured at the north (o) and south (▲) sampling sites.

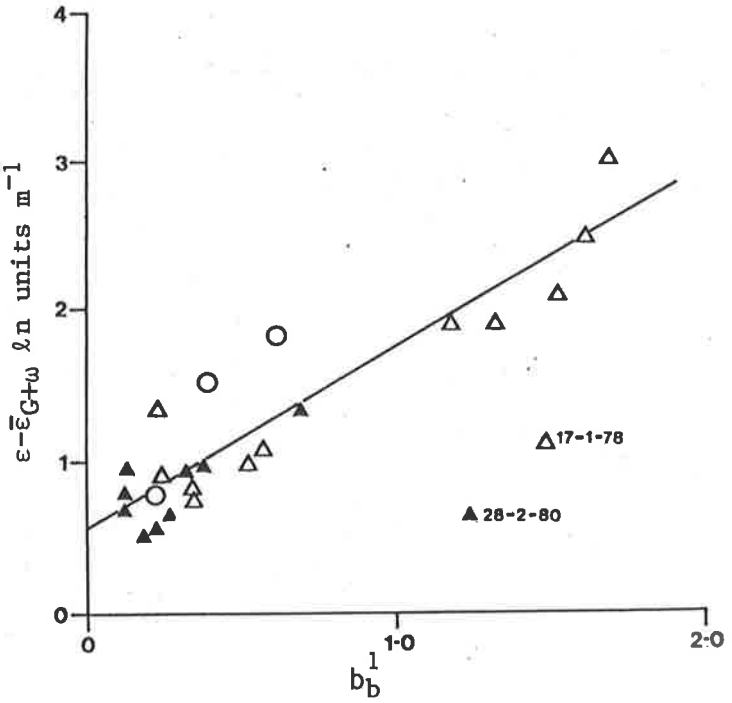

Fig. 3.12: The relationship between the asymptotic backscattering coefficient (b_b^1) and an estimate of the total scattering coefficient ($S=\varepsilon-\bar{\varepsilon}_{G+\omega}$, equation 3.6) for periods when $\bar{\varepsilon}_{G+\omega}$ was determined.

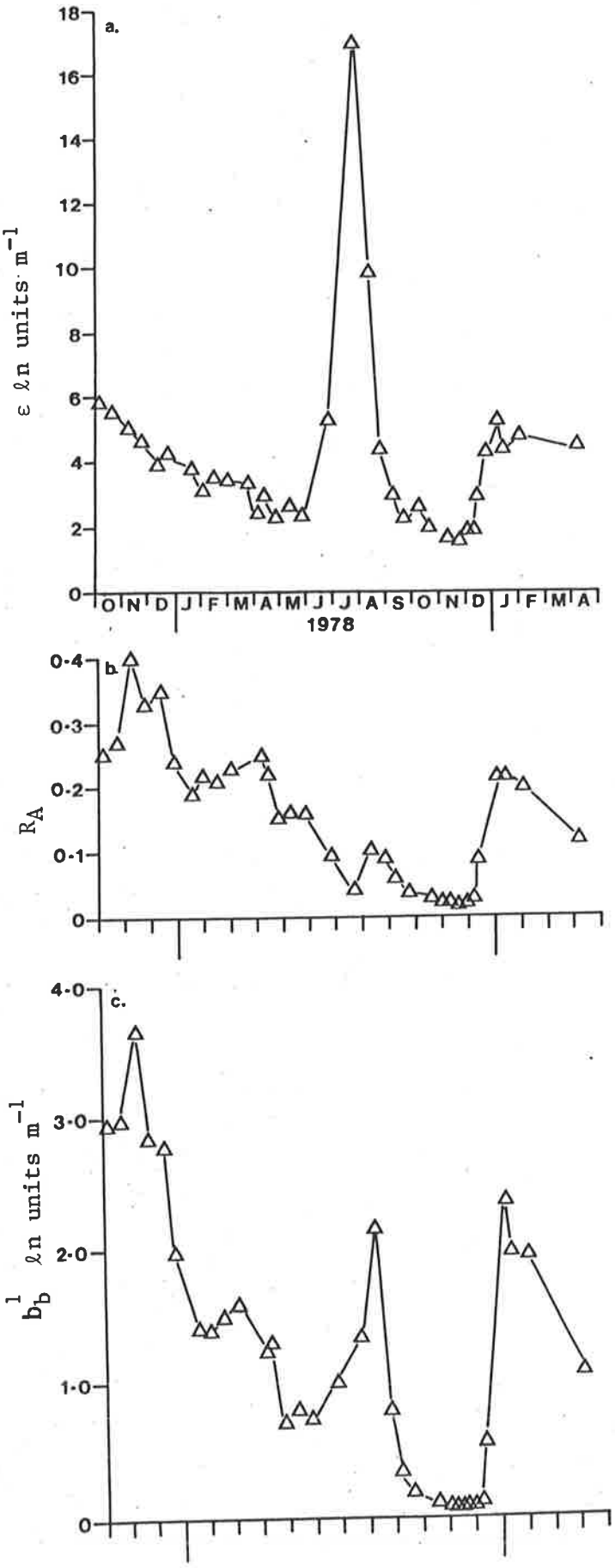

Fig. 3.13: Seasonal variation at the north sampling site of,

(a) Vertical extinction coefficient (ε),

(b) Asymptotic coefficient ratio (R_A).

(c) Asymptotic backscattering coefficient (b_b^1).

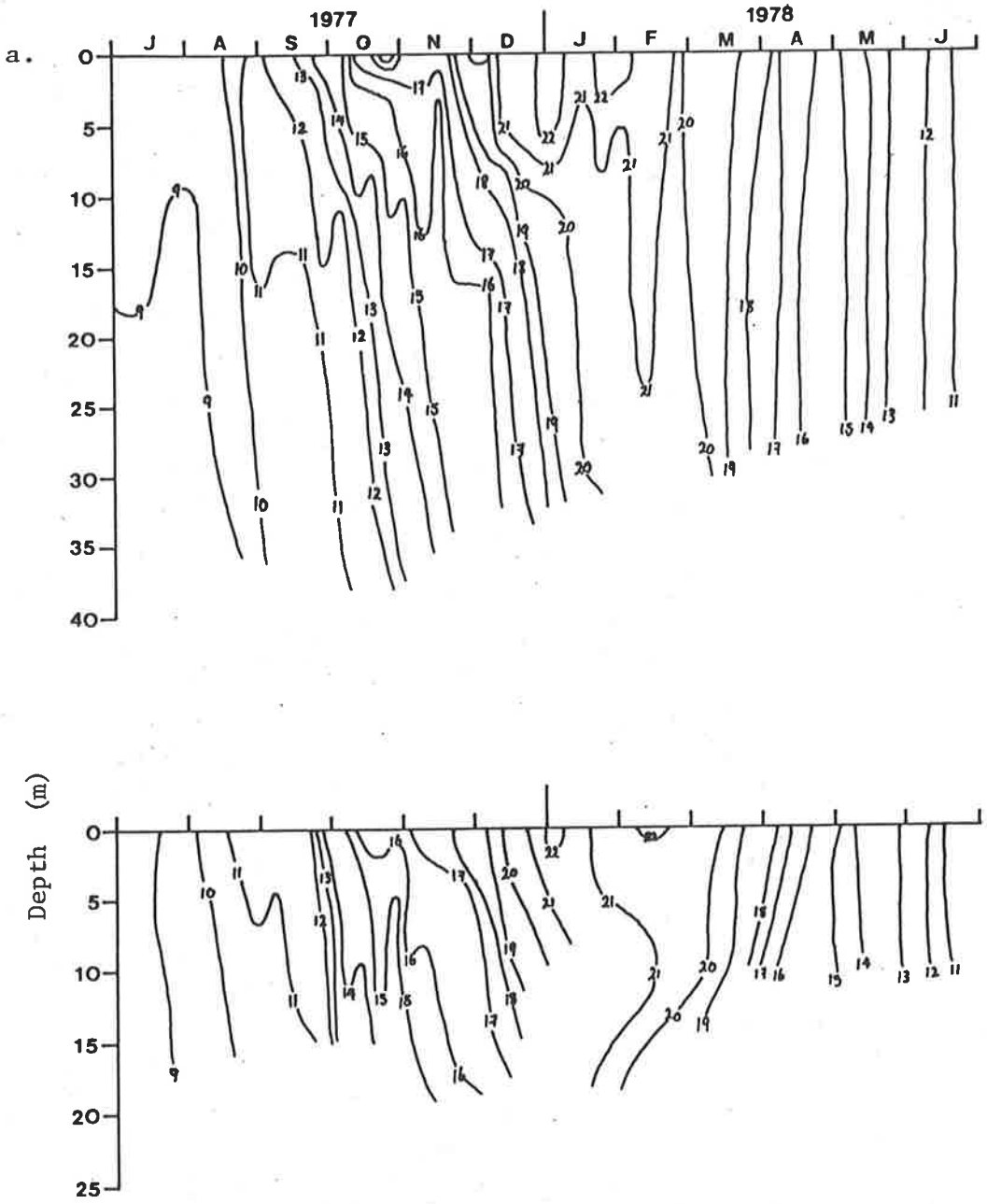

Fig. 3.14: Depth-time distribution of temperature at the south sampling site (upper) and site A (Fig.].4)(lower) for annual periods July-June,

(a) 1977-78

(b) 1978-79

(c) 1979-80

b.

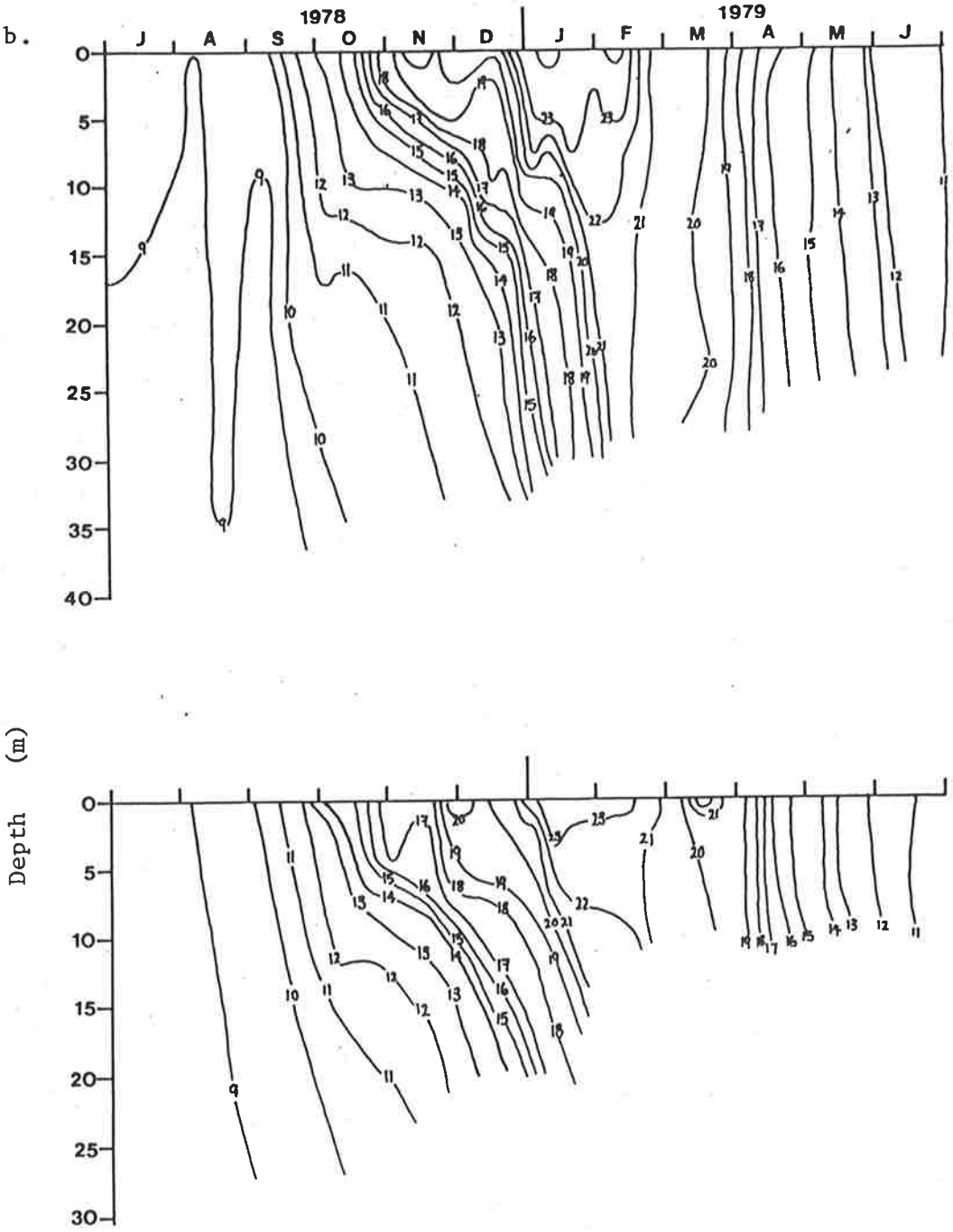

Fig. 3.14 (cont.)

c.

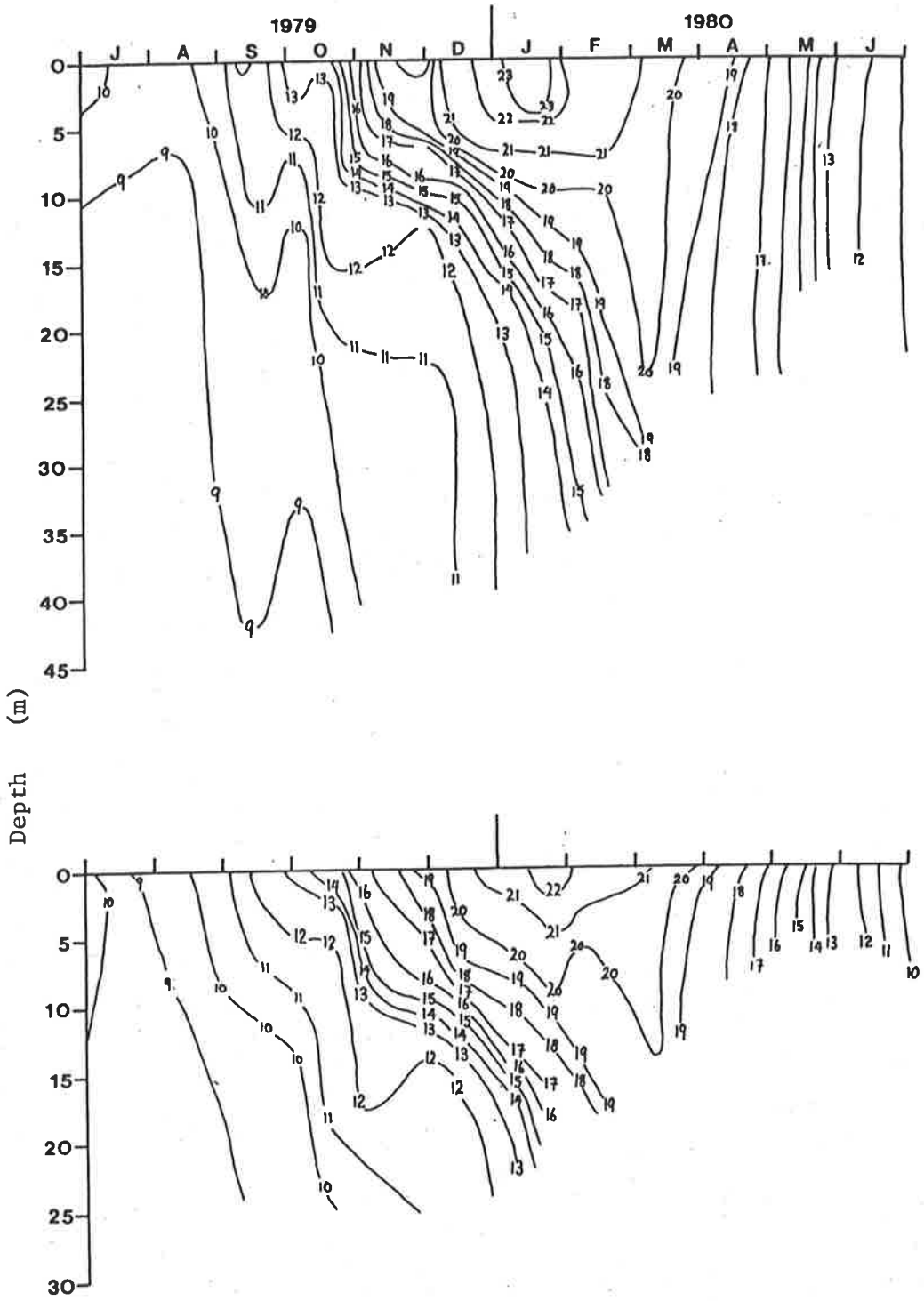

Fig. 3. 14 (cont.)

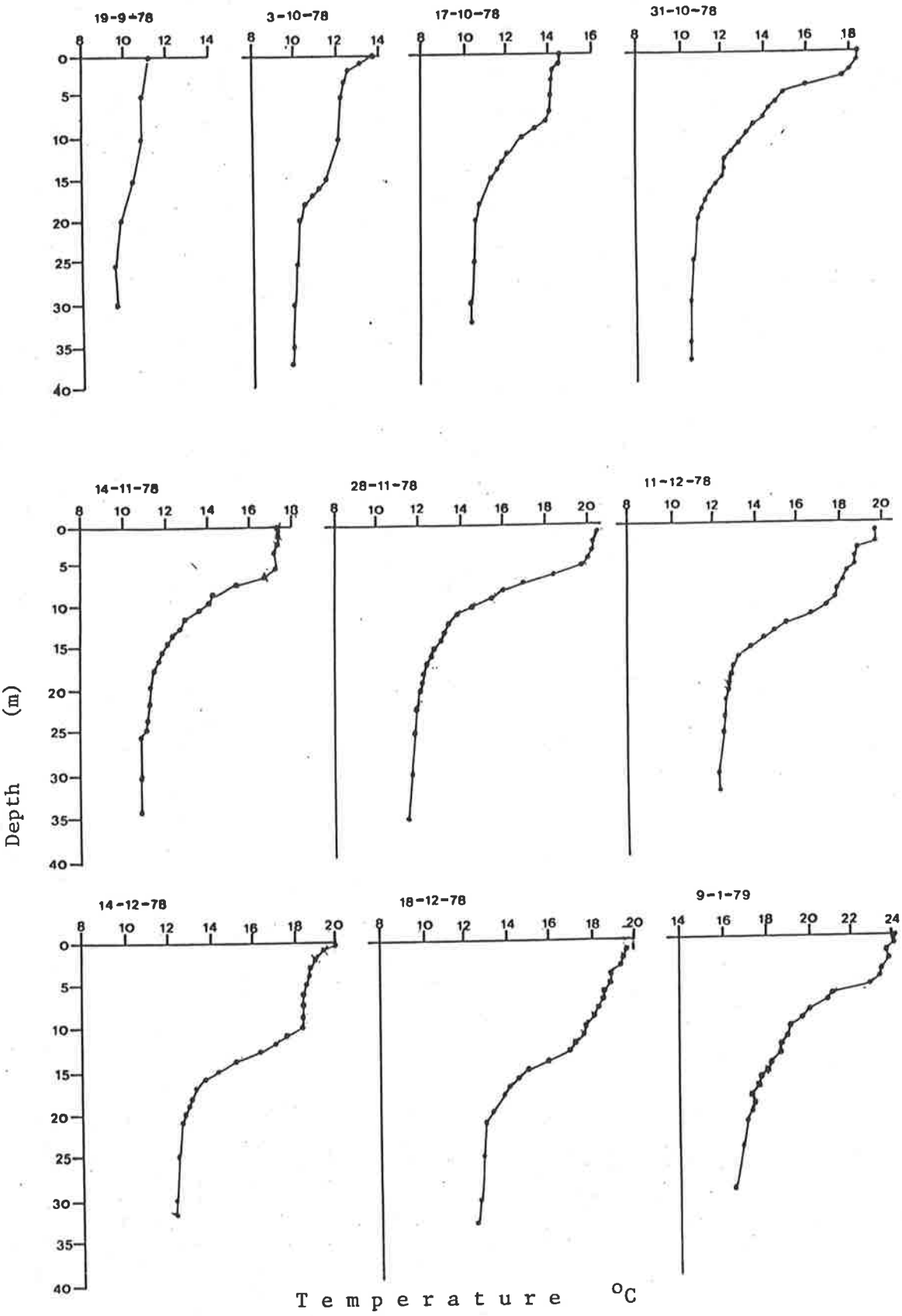

Fig. 3.15: Temperature profiles measured at the south sampling site during spring and summer 1978-79.

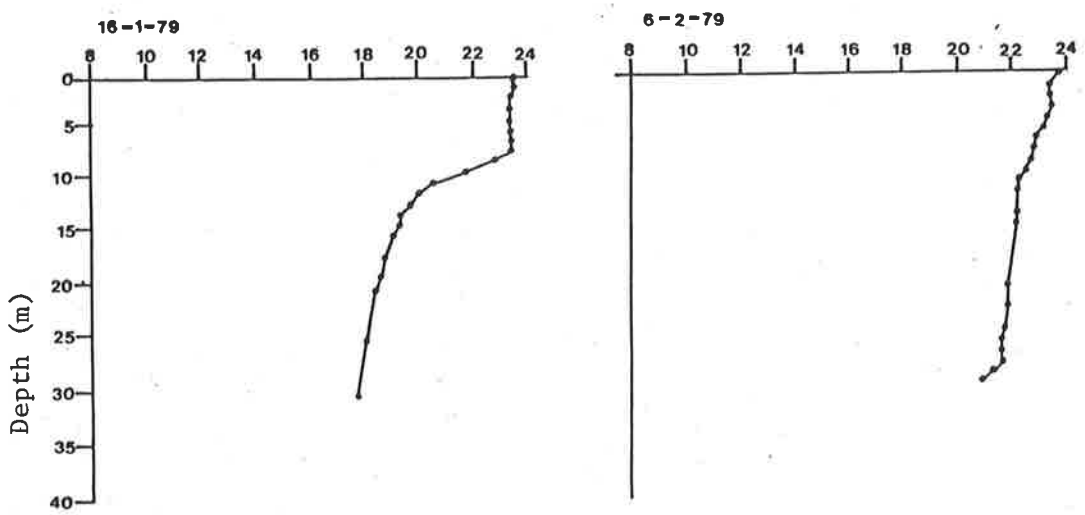

Fig. 3.15 (cont.)

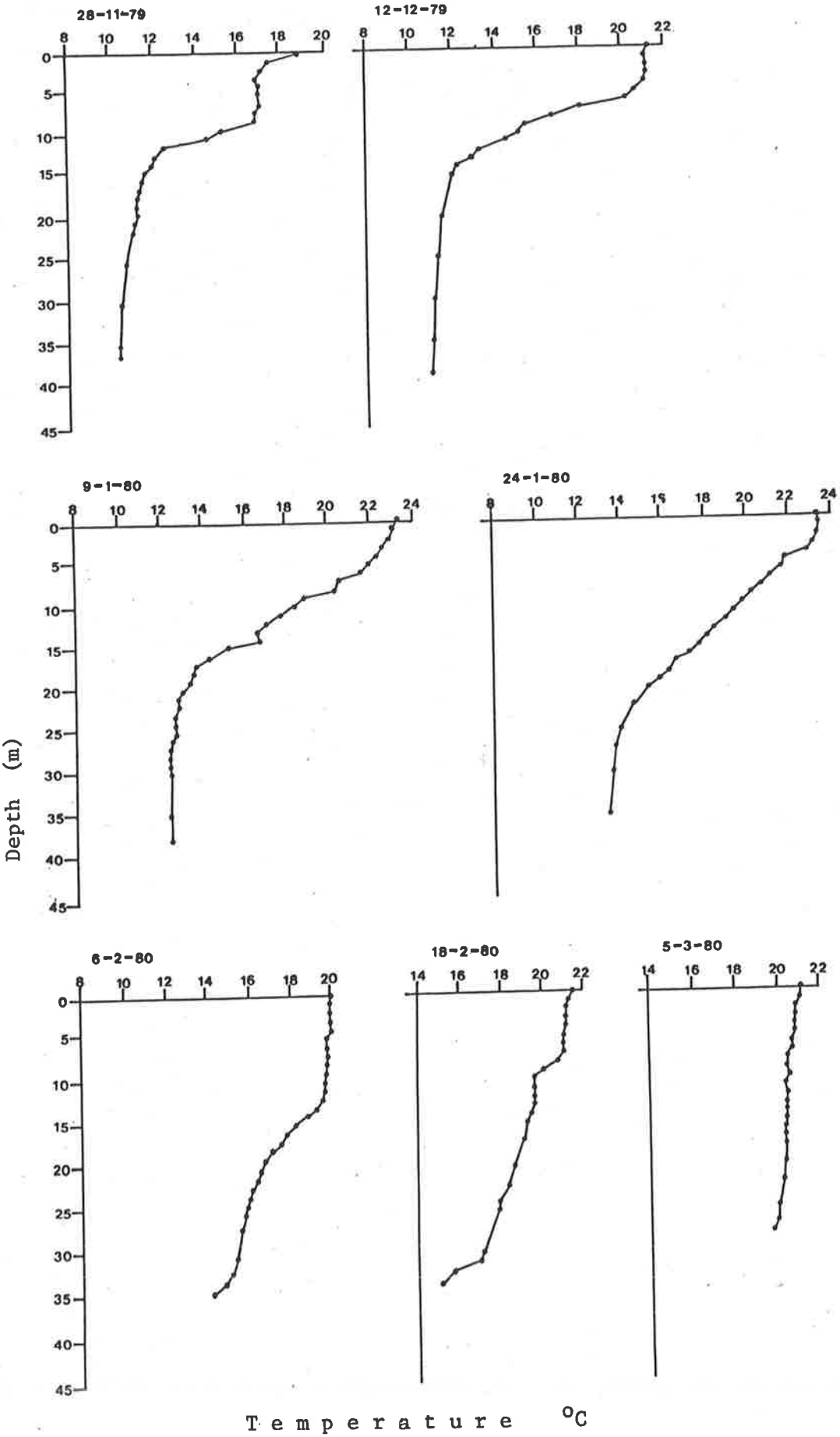
28-11-79
12-12-79
9-1-80
24-1-80
6-2-80
18-2-80
5-3-80
Depth (m)
Temperature °C

Fig. 3.16:(cont.)

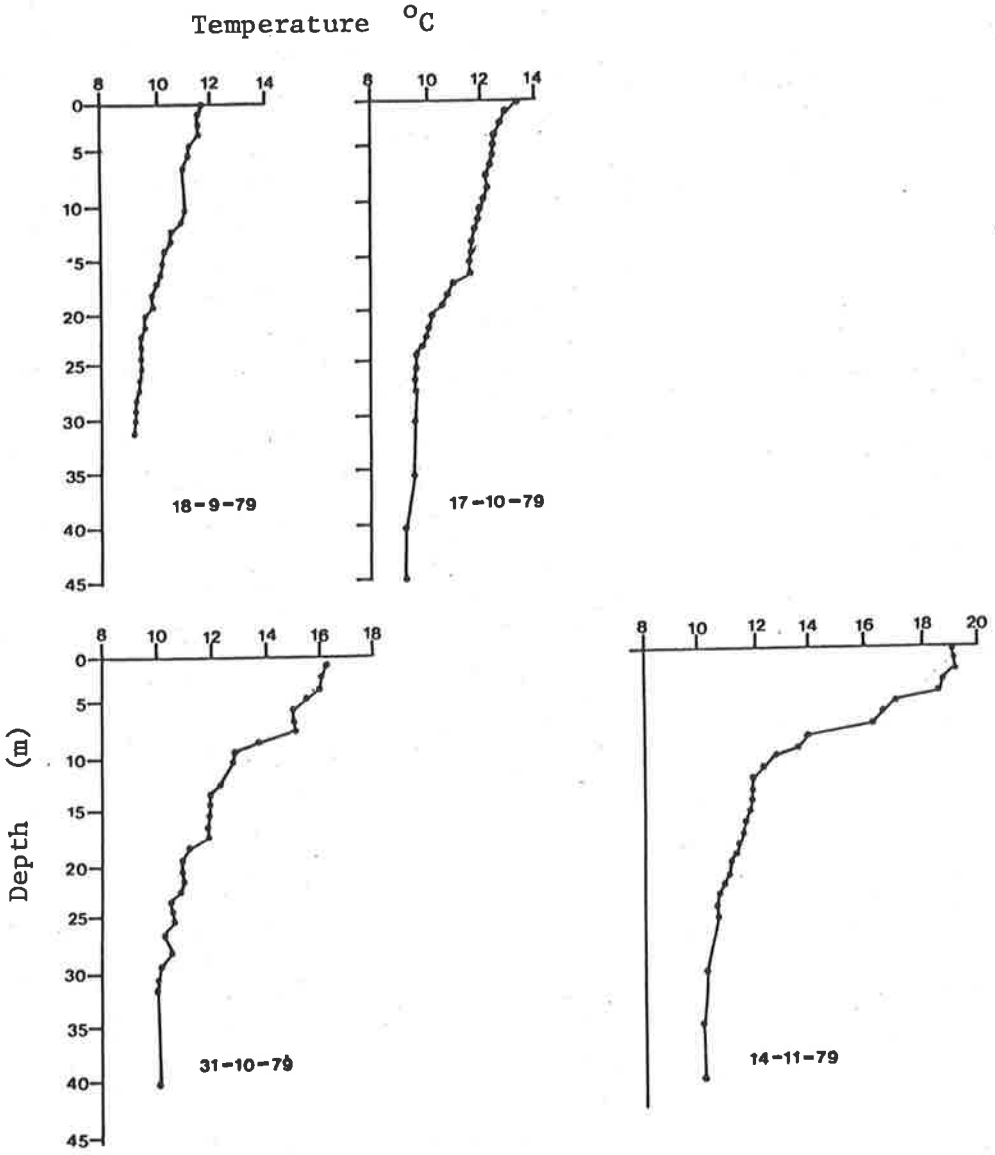

Fig. 3.16: Temperature profiles measured at the south sampling site during spring and summer 1979-80.

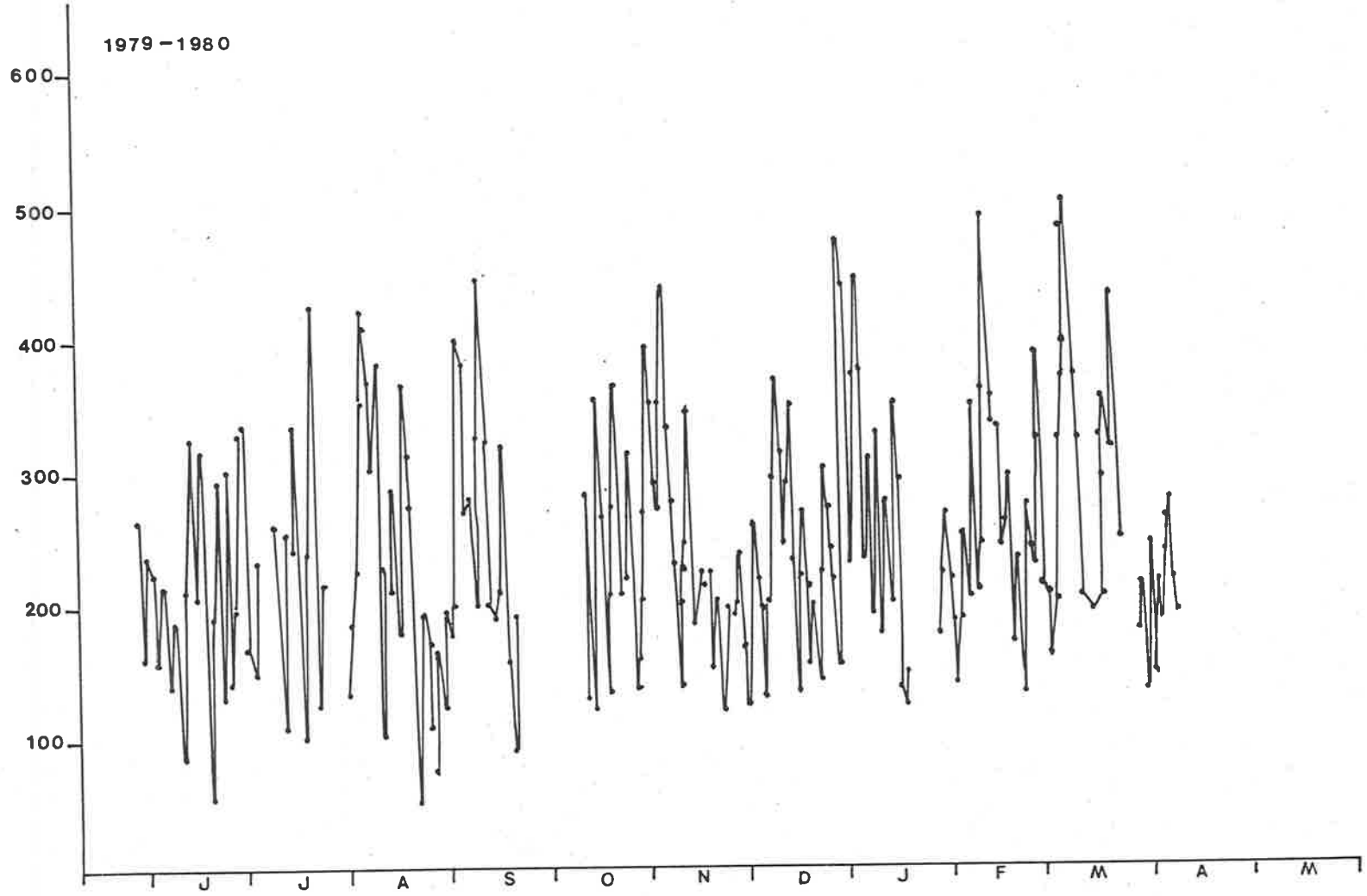

Fig. 3.17: Daily wind run at Mt Bold Reservoir, 1979-80, Km d^{-1}

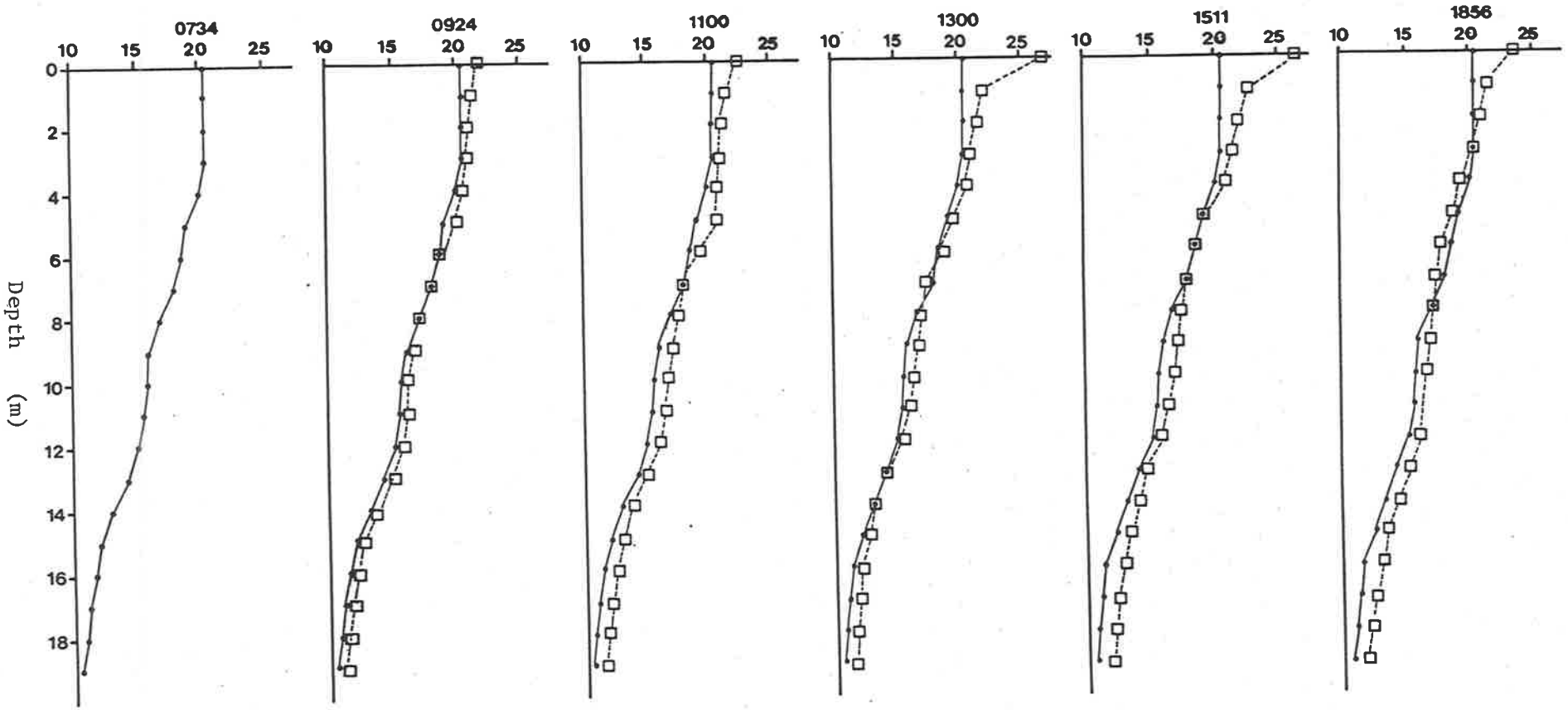

Fig. 3.18: Time series of temperature profiles for 27 December 1979, °C.

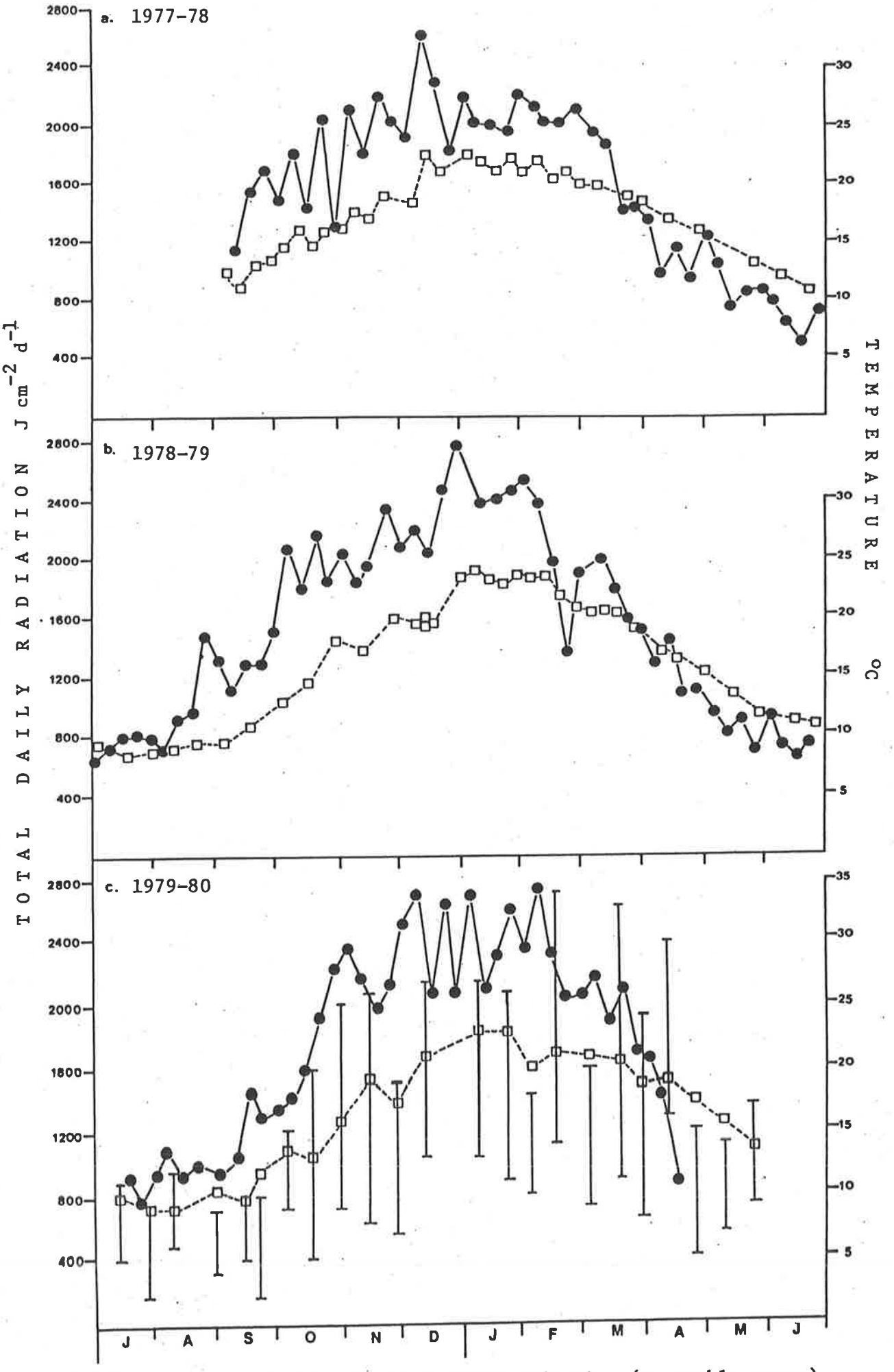

Fig. 3.19: Seasonal variation in total daily radiation (●, weekly means) and mean temperature of the euphotic zone (□) at the south sampling site. Vertical lines in (c) represent max/min air temps.

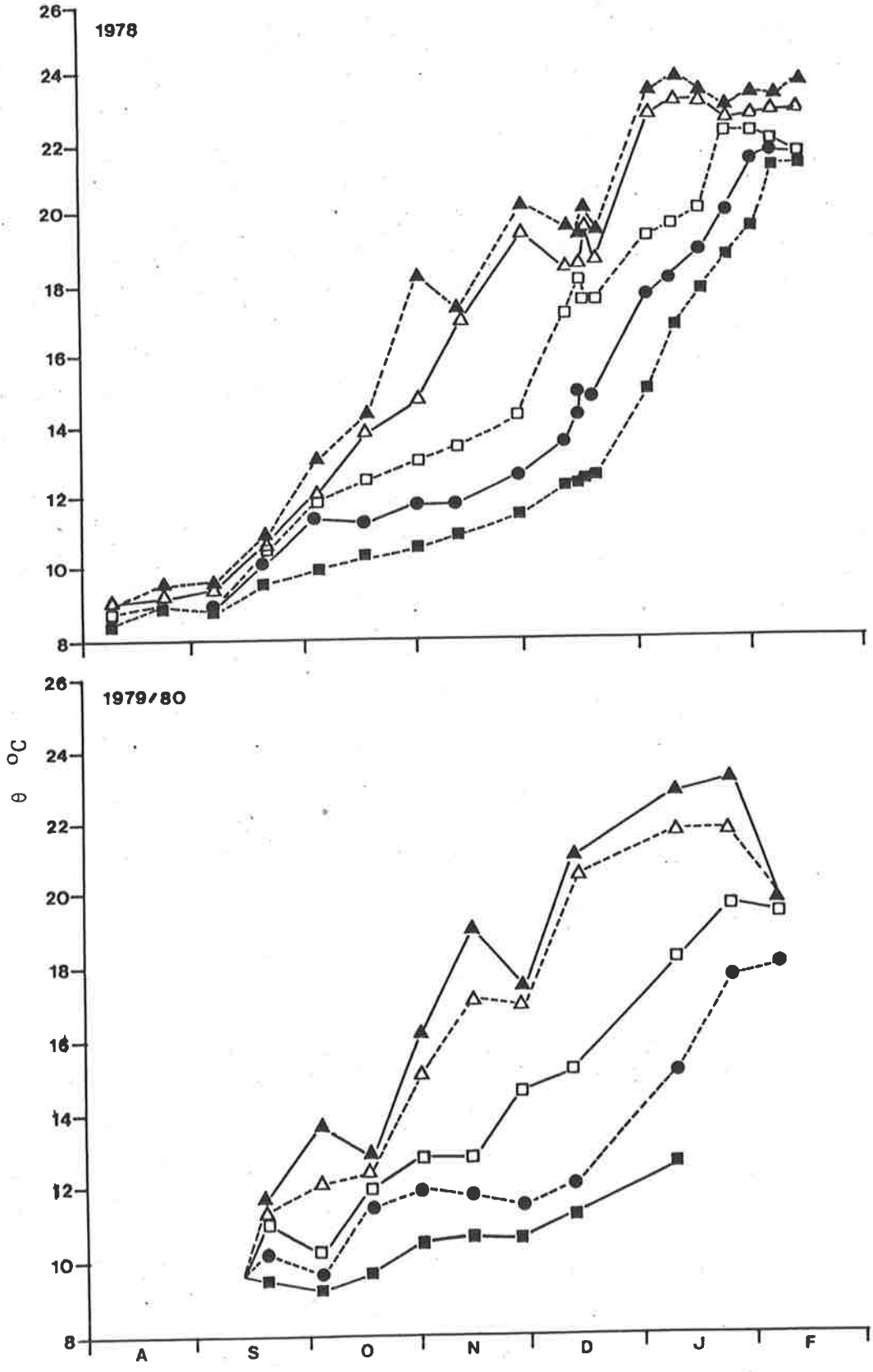

Fig. 3. 20: Increase in temperature (θ) at selected depths during spring and summer of 1978 and 1979-80.

▲ 1.0 m, △ 5.0 m, □ 10.0 m, ● 15.0 m, ■ 25.0 m.

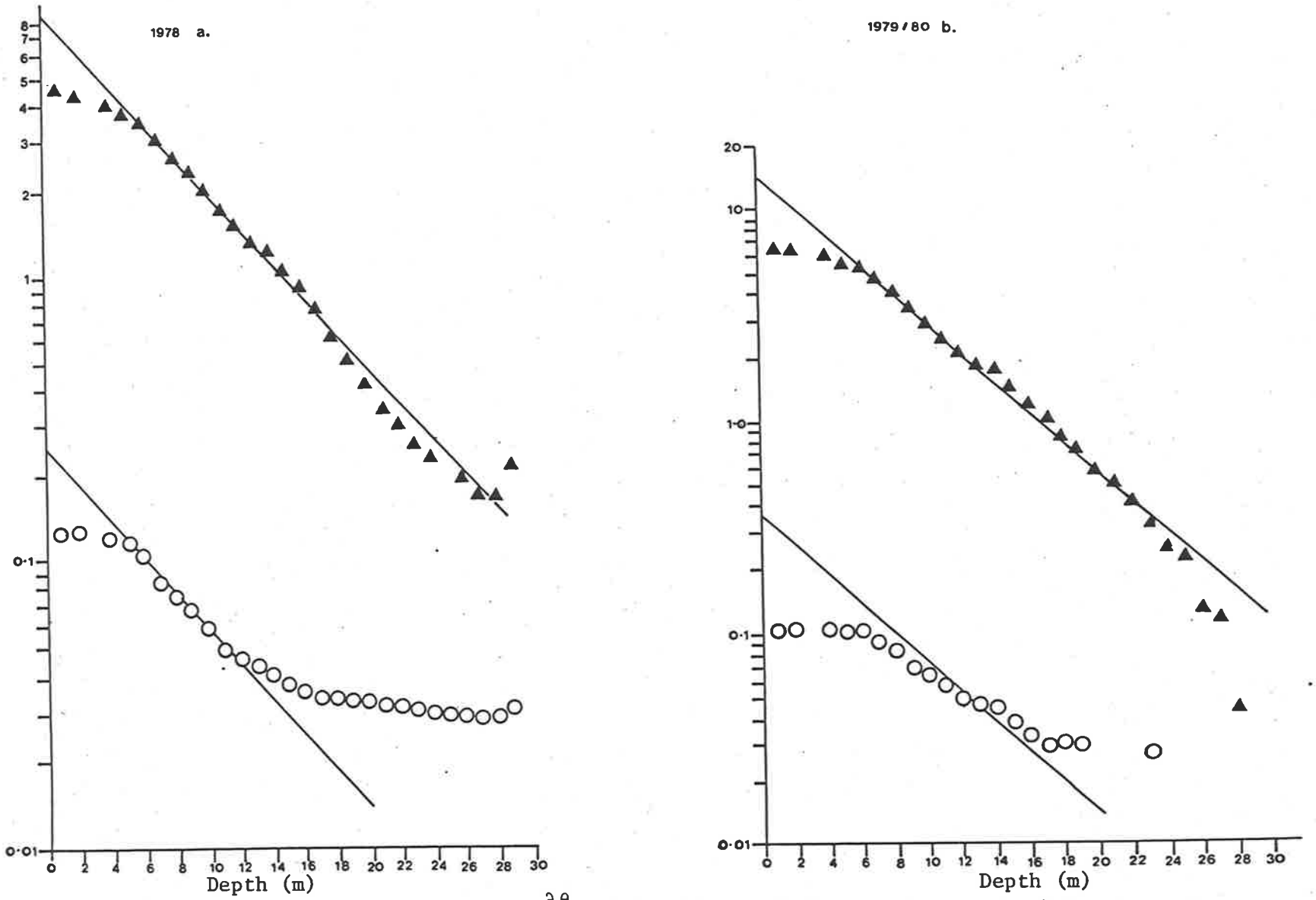

Fig. 3.21: Semi-logarithmic plot of depth variation in $\frac{\partial \theta}{\partial t}$ values (o) and (θ-C)(▲, equation 3.10)for the spring-summer heating period of (a) 1978 and (b) 1979-80.

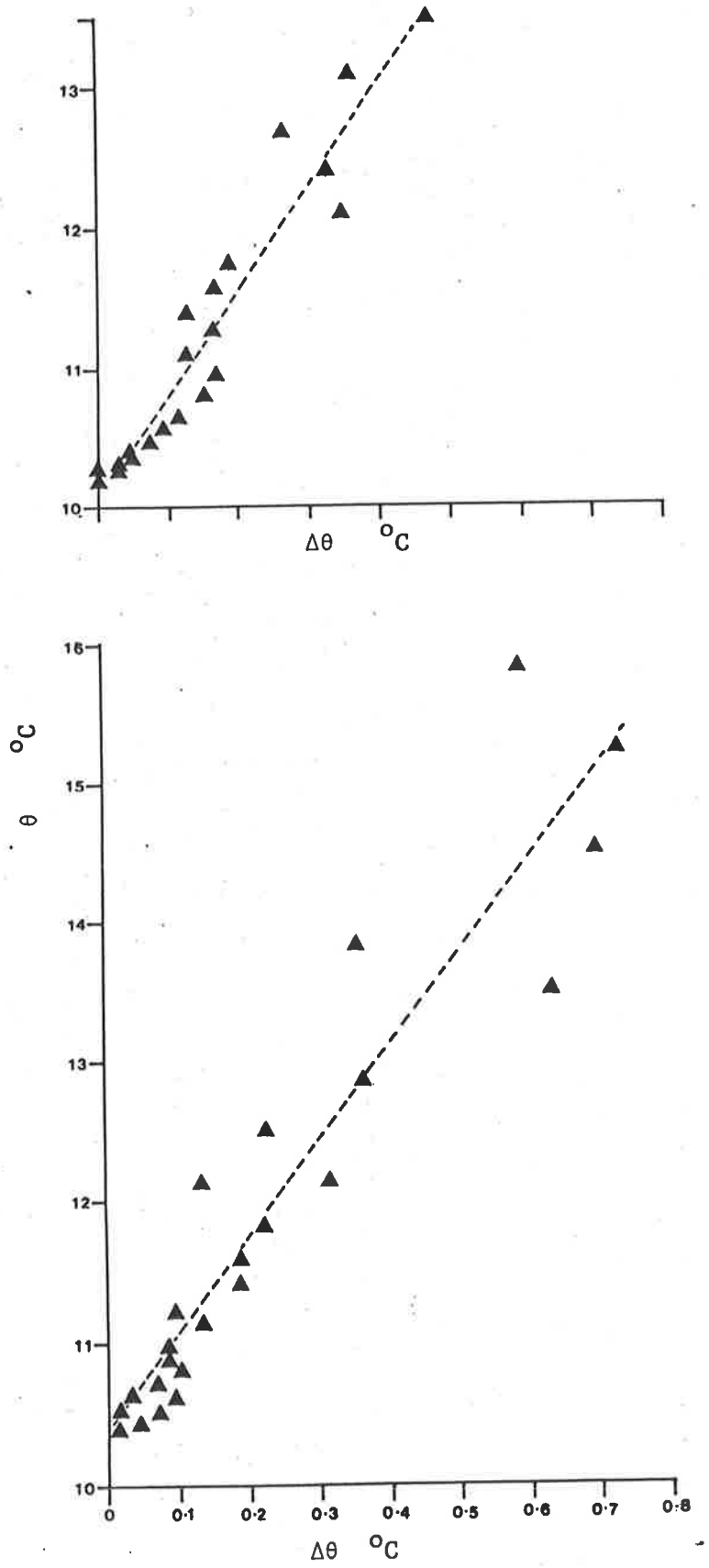

Fig. 3.22: Linear regression of θ_H (average temperature of 1 metre layers half way through the heating period) and $\Delta\theta$ (average temperature difference across the 1.0 m layer) for 1978 (upper) and 1979-80 (lower) (statistics in Table 3.8).

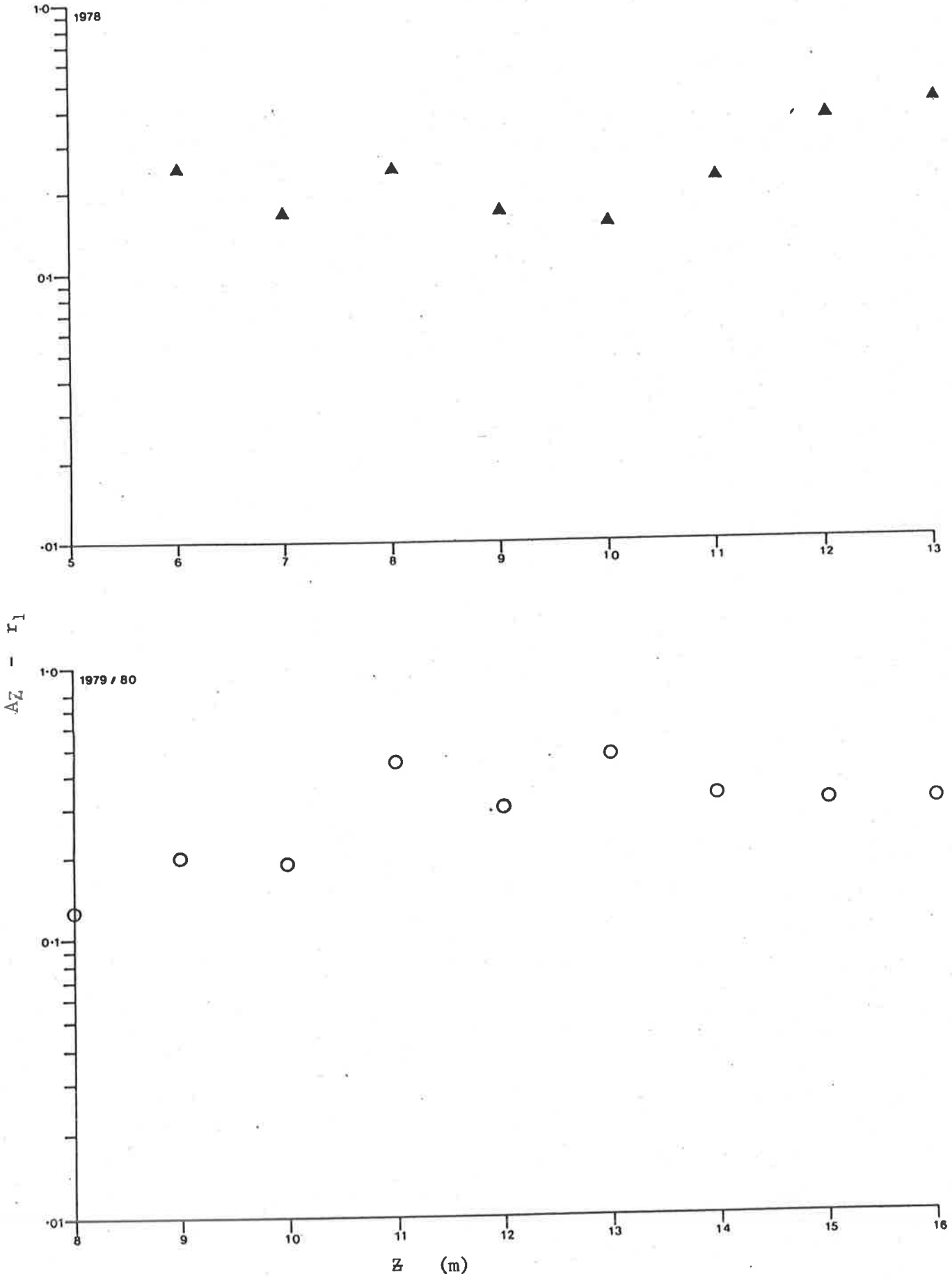

Fig. 3.23: Semilogarithmic plot of $(A_Z - r_1)$ versus depth (Z) (see equation 3.15)

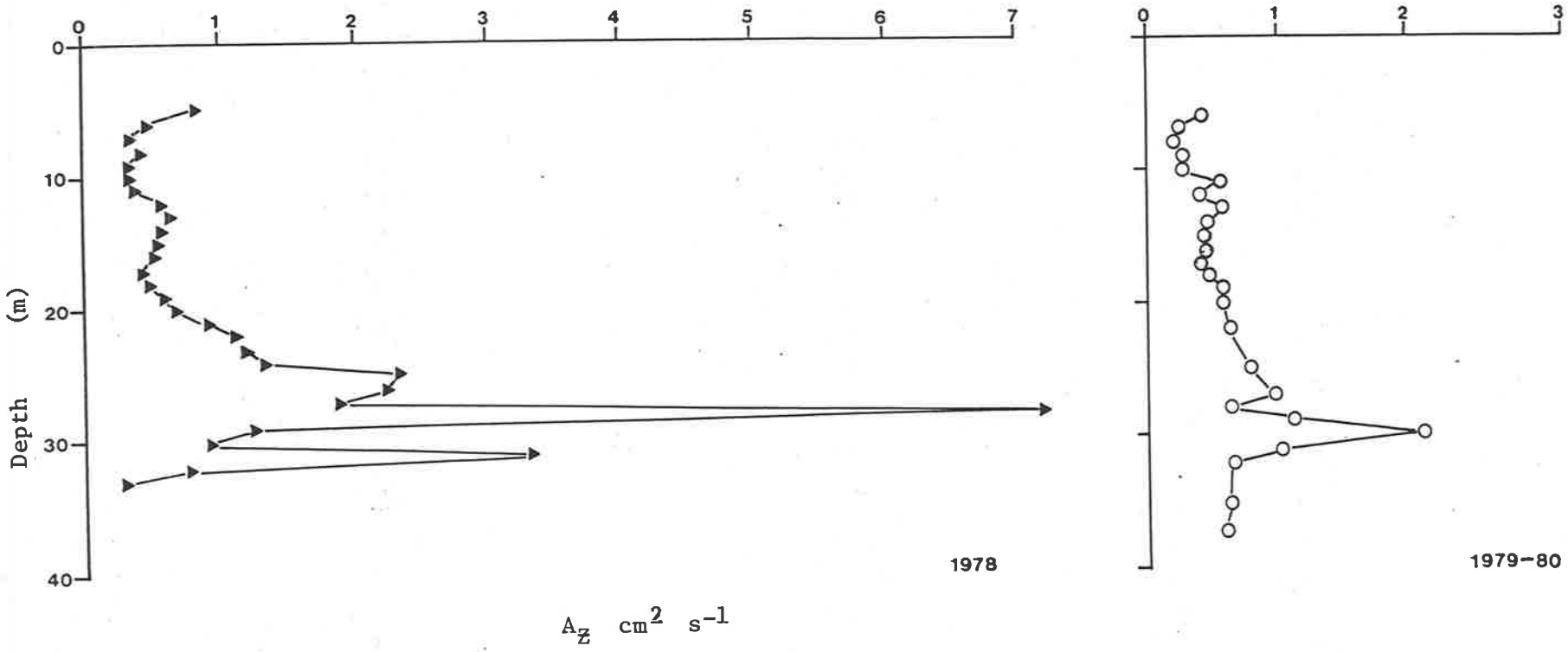

Fig. 3.24: Variation in eddy diffusivity (A_z) with depth during 1978 and 1979-80.

TABLE 3.1

Period	Figure	εq	ε_s	r^2	Sy.x	S_c	S_s	n	Chlorophyll a concentration for 50% light attenuation (mg m^{-3})
12/4 - 17/5/78	3.5A	1.095	0.0122	0.93	0.070	0.057	0.0024	4	90
21/11 - 19/12/78	3.5B	1.590	0.0133	0.95	0.075	0.050	0.0017	5	120
20/11 - 11/12/79	3.5C	2.209	0.016	0.99	0.006	0.005	0.0001	4	138
16/1 - 1/4/80	3.5C	1.440	0.021	0.99	0.081	0.048	0.0008	5	69

Specific extinction coefficient per unit chlorophyll *a* (ε_s, m^2 mgchl *a*) and background extinction (εq, ℓn units m^{-1}) estimated from the linear regression of the extinction coefficient (ε) on chlorophyll *a* concentration (mg m^{-3}). The chlorophyll *a* concentration resulting in 50% light absorption is shown. Regression statistics: Correlation coefficient (r^2), standard deviation (Sy.x), standard error for εq (S_c) and ε_s (S_s), number of samples (n).

TABLE 3.2

Wavelength nm	400	410	420	430	440	450	460	470	480	490	500	510	520	530	540
Quanta %	1.6	2.2	2.5	2.5	2.7	3	3.2	3.3	3.4	3.4	3.4	3.4	3.3	3.3	3.4
Energy %	2.2	2.9	3.2	3.2	3.3	3.6	3.8	3.8	3.8	3.8	3.7	3.6	3.5	3.4	3.4

Wavelength nm	550	560	570	580	590	600	610	620	630	640	650	660	670	680	690
Quanta %	3.4	3.4	3.5	3.4	3.4	3.4	3.5	3.4	3.5	3.5	3.5	3.5	3.6	3.5	3.6
Energy %	3.4	3.3	3.3	3.2	3.1	3.1	3.1	3.0	3.0	3.0	2.9	2.9	2.9	2.8	2.8

Wavelength nm	700
Quanta %	3.6
Energy %	2.8

Mean percentage distribution of quanta and energy for global radiation (400-700 nm) incident on a horizontal plane.

TABLE 3.3

Date	chla	$\varepsilon_s b$	ε	εq	$\varepsilon_{G+\omega}$	$\frac{\varepsilon_G}{\varepsilon_{G+\omega}}$	$\varepsilon q - \varepsilon_{G+\omega}$	R_A	b_b'
19/7/77			1.53		0.61	70	0.92	0.1	0.234
9/8/77			1.94		0.58	67	1.36	0.12	0.233
17/8/77			2.52		0.62	69	1.90	0.21	1.33
7/9/77			3.0		0.51	63	2.49	0.27	1.63
5/10/77	2.6		3.89		-	-	-	0.32	2.49
19/10/77	1.9		3.7		-	-	-	0.33	2.44
9/11/77	3.9		3.5		0.46	61	3.04	0.24	1.68
23/11/77	4.2		2.89		-	-	-	0.20	1.16
13/12/77	10	0.15	2.43	2.28	0.37	53	1.91	0.24	1.17
20/12/77	24	0.36	2.84	2.48	0.39	55	2.09	0.27	1.53
17/1/78	54	0.95	2.41	1.68	0.36	52	1.11	0.31	1.49
1/2/78	0.9		1.48		-	-	-	0.17	0.5
15/2/78	5	0.09	1.55	1.46	0.38	54	1.08	0.18	0.56
1/3/78			1.54		-	-	-	0.19	0.59
5/4/78			1.22		-	-	-	0.19	0.46
12/4/78	2.4		1.15		-	-	-	0.19	0.44
26/4/78	8	0.1	1.13	1.03	0.29	43	0.74	0.15	0.34
10/5/78	39.5	0.48	1.55	1.07	0.26	39	0.81	0.11	0.34
17/5/78	23.6	0.29	1.45	1.16	-	-	-	0.10	0.29
24/5/78	14.4	0.18	1.45	1.27	-	-	-	0.12	0.35
14/6/78	16	0.24	1.57	1.33	0.32	49	1.01	0.17	0.53
28/6/78	13	0.16	1.84	1.68	-	-	-	0.12	0.44
18/7/78	1		4.45		-	-	-	0.13	1.16
9/8/78	0.4		2.77		0.93	78	1.84	0.11	0.61
23/8/78	0.3		2.69		1.15	81	1.54	0.072	0.39
6/9/78	0.5		2.04		1.24	83	0.8	0.051	0.21
12/9/78	0.4		2.60					0.05	0.26
19/9/78	0.9		2.28					0.07	0.32
26/9/78	1.9		2.19					0.04	0.18
3/10/78	1.9		2.31					0.051	0.24
10/10/78	2.4		2.12					0.036	0.15
17/10/78	2.3		2.18					0.05	0.22
24/10/78	6		2.13					0.03	0.13
31/10/78	5		1.72					0.025	0.086
9/11/78	3.4		1.75					0.021	0.074
21/11/78	3.8		1.71					0.021	0.07
30/11/78	15.5	0.21	1.81	1.60				0.024	0.087
6/12/78	27.6	0.37	1.86	1.49				0.035	0.13
12/12/78	55.2	0.73	2.37	1.64				0.032	0.15
3/1/79	16	0.21	2.29	2.08				0.084	0.38
17/1/79	16	0.21	2.29	2.08				0.1	0.46
1/2/79	5.4		2.15					0.13	0.56
21/2/79	15.9	0.34	2.44	2.1				-	-
7/3/79	20	0.27	2.27	2.0				0.12	0.54
4/4/79	4.2		2.22					0.14	0.62
18/4/79	3.2		1.91					0.12	0.46

.../Continued

Table 3.3 (Continued)

Date	chla	$\varepsilon_s b$	ε	εq	$\varepsilon_{G+\omega}$	$\frac{\varepsilon_G}{\varepsilon_{G+\omega}}$	$\varepsilon q - \varepsilon_{G+\omega}$	R_A	b_b'
17/10/79	2.2		3.9					0.05	0.39
1/11/79	3.5	0.06	2.59	2.53	1.55	86	0.98	0.025	0.13
12/11/79	7.7	0.12	2.6	2.48	1.73	88	0.75	-	-
20/11/79	17	0.27	2.48	2.21	1.53	86	0.68	0.022	0.11
24/11/79	18	0.29	2.5	2.21	1.41	84	0.80	0.024	0.12
4/12/79	106.7	1.71	3.93	2.22	1.29	83	0.93	0.04	0.31
7/12/79			4.57	-				0.06	0.55
11/12/79	34.7	0.56	2.78	2.22				0.035	0.19
18/12/79	79.7	1.28	4.57	3.29				0.05	0.46
4/1/80	43.2	0.69	3.04	2.35	1.01	78	1.34	0.11	0.67
16/1/80	12.5	0.26	1.72	1.46	0.96	78	0.5	0.034	0.17
13/2/80	31.7	0.67	2.2	1.53	0.54	76	0.99	0.083	0.365
28/2/80	127.9	2.69	4.13	1.44	0.79	73	0.65	0.15	1.24
11/3/80	15.5	0.33	1.78	1.45	0.80	74	0.65	0.073	0.26
1/4/80	5.5	0.12	1.44	1.32	0.76	73	0.56	0.072	0.21

Legend - Table 3.3

Seasonal variation in measured and derived parameters describing the light regime at the southern sampling site.

(a) Extinction coefficients (ℓn units m^{-1}) resulting from,

- ε, total extinction coefficient
- $\varepsilon_s b$, chlorophyll attenuation
- εq, background attenuation. Appearance of numbers in this column indicates that chlorophyll attenuation has been considered (equation 3.3) whereas blanks indicate $\varepsilon q \simeq \varepsilon$.
- $\varepsilon_{G+\omega}$, attenuation due to water and gelbstoff alone, determined spectrophotometrically on filtrates.
- b_b', asymptotic backscattering coefficient
- $\varepsilon q - \varepsilon_{G+\omega}$ estimate of the volume scattering function (see equation 3.6)

(b) Dimensionless ratios,

- $\frac{\varepsilon_G}{\varepsilon_{G+\omega}}$ Percentage of $\varepsilon_{G+\omega}$ due to gelbstoff
- R_A Asymptotic reflectance.

(c) chla concentration mg m^{-3}

Lake	Spectral range (nm)	ε	εq	a	Source
Mt Bold Reservoir	PAR	1.13-4.6	1.0-4.5	-	This chapter
Lake George, Uganda	535-685	3-19	2.4	1.33	Ganf 1974
Lake Kinneret, Israel	PAR	0.2 -3.3	0.49	-	Dubinsky & Berman 1979
Loch Leven, Scotland	590	0.8 -3.0	0.49	1.33	Bindloss 1976
Lake Minnetonka, USA	PAR	0.7 -2.8	0.68	-	Megard *et al.* 1979
Lough Neagh, Ireland	630	1.3 -2.0	1.1	1.15	Jewson 1977
Lake Erken, Sweden	PAR	1.02	-	-	Rodhe 1965
Lake Croispol, Scotland	PAR	0.55-0.57	-	-	Spence *et al.* 1971
Lake Ontaria, Canada	PAR	0.15-0.58	-	-	Stadelmann *et al.* 1974, calculated by Dubinsky & Berman 1979
Esthwaite Water, England	530	0.46-0.71	0.4	1.33	Talling 1957a, 1971
Windermere, England	530	0.3 -0.5	0.32	1.33	Talling 1960, 1971
Blelham Tarn, England	530	0.5,0.63,0.88	-	1.33	Talling 1957a, 1969
Ennerdale Water, England	530	0.13	-	1.33	Talling 1957a, 1971
Crater Lake, USA	PAR	0.017-0.037	-	-	Smith *et al.* 1973, Smith & Tyler 1967

Table 3.4: The range of vertical extinction coefficients (ε, *ln* units m^{-1}) and background extinction coefficients (εq, *ln* units m^{-1}) observed in a number of lakes. εq values have been estimated from the linear regression of ε on chlorophyll *a* concentration, or from periods when chlorophyll concentration was negligible. In cases where the extinction of a particular wavelength was measured, the factor (a) suggested by the authors to correct the results to extinction of PAR, is given ($a\varepsilon_{\lambda} = \varepsilon_{PAR}$).

TABLE 3.5

Date	I_o	Wind run km d^{-1}	Daily wind run distribution (km/6h) 0200-0800h	0900-1400h	1400-2000h	2000-0200h
26/12/79	2793	297	92	62	83	60
27/12/79	2793	267	87	43	71	66

Total incident radiation (I_o, joules cm^{-2} d^{-1}) and total and 6 hourly wind runs, for a 2 day period. Wind was consistently from the north-west.

TABLE 3.6

Depth	a	b	r^2	Θ_H	$\Delta\Theta$	Θ_H-C	e^{-az}	A $\frac{m^2}{d}$	$\frac{cm^2}{s}$
1	9.32	0.1276	0.96	14.673	0.2424	4.63	-	-	-
2	9.09	0.1270	-	14.430		4.39			
4	8.99	0.1204		14.051	0.1949	4.01			
5	9.01	0.1153	0.98	13.856	0.3136	3.82			
6	9.21	0.1031		13.540	0.4681	3.50	0.427	1.439	0.167
7	9.48	0.0855	0.98	13.072	0.3615	3.03	0.371	1.375	0.159
8	9.54	0.0755		12.710	0.2645	2.67	0.322	1.400	0.162
9	9.56	0.0686		12.446	0.3335	2.41	0.279	1.466	0.170
10	9.63	0.0592		12.112	0.3470	2.07	0.242	1.457	0.169
11	9.66	0.0497	0.88	11.765	0.1834	1.73	0.210	1.411	0.163
12	9.58	0.0475		11.581	0.1673	1.54	0.182	1.551	0.179
13	9.59	0.0434	0.85	11.414	0.1262	1.38	0.158	1.634	0.189
14	9.56	0.0411		11.288	0.1679	1.25	0.137		
15	9.54	0.0375		11.120	0.1267	1.08	0.119		
16	9.49	0.0357		10.993	0.1692	0.95	0.103		
17	9.42	0.0334		10.824	0.1580	0.79	0.090		
18	9.24	0.0339		10.666	0.113	0.63	0.078		
19	9.18	0.0327		10.553	0.514	0.095	0.068		
20	9.07	0.0330		10.459	0.075	0.420	0.059		
21	9.08	0.0311		10.383	0.042	0.344	0.051		
22	9.02	0.0316		10.341	0.044	0.302	0.044		
23	9.02	0.0304		10.297	0.029	0.258	0.038		
24	9.03	0.0294		10.268	0.032	0.229	0.033		
25	9.01	0.0293		10.236	0.002	0.197	0.029		
26	9.00	0.0293		10.235	0.028	0.196	0.025		
27	9.02	0.0283		10.207	0.004	0.168	0.022		
28	9.01	0.0285		10.203	-	0.164	0.019		
29	8.93	0.0316		10.254	0.084	0.215	0.016		
30	8.99	0.0281	0.96	10.171		0.132	0.014		

Results from the linear regression of temperature (Θ°C) on time (t days) for each 1.0 metre layer, over the period 5/9/78 - 28/11/78 at the southern sampling site;

$$\Theta = a + b\ t$$

The range of the regression coefficient (r^2) is shown for selected depths. The average temperature for each 1 metre layer, mid-way through the heating period (Θ_H), was estimated from the linear relationships, and the average temperature difference between layers ($\Delta\Theta$) calculated. The constants C and a were estimated as described in the text and shown in Table 3.8 and Fig. 3.22a. The constant $C_1 = 8.34$ was calculated from

$$\frac{\Sigma_{Z_1}^{Z_2} (\Theta - C)}{\Sigma_{Z_1}^{Z_2} e^{-aZ}}$$ where $Z_1 = 6$m and $Z_2 = 29$m.

Eddy diffusivities (A) for the clinolimnion are given as both $m^2 d^{-1}$ and $cm^2 s^{-1}$

TABLE 3.7

Depth m	a	b	r^2	Θ_H	$\Delta\Theta$	Θ-C	e^{-aZ}	A $\frac{m^2}{d}$	$\frac{cm^2}{s}$
1	10.47	0.1079	0.94	16.941		6.54			
2	10.42	0.1069		16.829		6.535			
4	9.92	0.1083		16.418		6.423			
5	9.82	0.1043	0.96	16.075	0.2393	6.012			
6	9.73	0.1018		15.835	0.5869	5.669	0.449	0.632	0.073
7	9.75	0.917		15.248	0.7245	5.429	0.382	0.726	0.084
8	9.51	0.0837		14.524	0.6976	4.842	0.326	0.822	0.095
9	9.59	0.0707	0.96	13.826	0.3297	4.118	0.277	0.822	0.095
10	9.58	0.0653		13.497	0.6295	3.420	0.236	0.815	0.094
11	9.40	0.0578	0.87	12.867	0.3642	3.091	0.201	0.884	0.102
12	9.49	0.0502	0.84	12.503	0.2225	2.097	0.146	0.937	0.108
13	9.45	0.0472	0.83	12.280	0.1352	1.874	0.124	1.036	0.120
14	9.36	0.0464		12.145	0.319	1.739	0.106	1.192	0.138
15	9.53	0.0383	0.80	11.825	0.2210	1.419	0.090	1.158	0.134
16	9.64	0.0328	0.80	11.605	0.1875	1.199	0.077	1.159	0.134
17	9.58	0.0306		11.417	0.1918	1.011	0.066	1.26	0.146
18	9.40	0.0304		11.225	0.0995	0.819	0.056		
19	9.34	0.0298		11.126	0.1362	0.720	0.048		
20	9.27	0.0287	0.93	10.990	0.0841	0.584	0.041		
21	9.22	0.0282		10.906	0.0833	0.500	0.035		
22	9.16	0.0277		10.822	0.1003	0.416	0.029		
23	9.09	0.0273		10.722	0.0675	0.316	0.025		
24	9.03	0.0270		10.655	0.0244	0.249	0.021		
25	9.00	0.0272	0.92	10.630	0.0948	0.224	0.018		
26	8.93	0.0267		10.535	0.0164	0.129	0.015		
27	8.94	0.0263		10.519	0.0696	0.113	0.013		
28	8.86	0.0265		10.449	0.0422	0.043	0.011		
29	8.81	0.0266	0.92	10.407	0.0188	0.001	0.010		
30	8.78	0.0270		10.395	0.0121	-	-		

$\Sigma_6^{30}(\Theta\text{-C}) = 42.48 \quad \Sigma_6^{30} e^{-aZ} = 2.973 \quad C_1 = 14.289$

Results from the linear regression of temperature (Θ°C) on time (t days) for each 1 metre layer over the period 12/9/79 - 9/1/80, at the southern sampling site;

$$\Theta = a + b\ t$$

The range of the correlation coefficient (r^2) is shown for selected depths.

The average temperature for each 1 metre layer, mid-way through the heating period (Θ_H), was estimated from the linear relationships, and the average temperature difference between layers ($\Delta\Theta$) calculated.

The constants C and a were estimated as described in the text and shown in Fig. 3.22b and Table 3.8. The constant $C_1 = 14.289$ was calculated from

$$\frac{\Sigma_{Z_1}^{Z_2}(\Theta\text{-C})}{\Sigma_{Z_1}^{Z_2} e^{-aZ}}$$ where $Z_1 = 6$m and $Z_2 = 30$m.

Eddy diffusivities (A) for the clinolimnion are given as both m^2d^{-1} and cm^2s^{-1}

TABLE 3.8

Period	C	Slope	r^2	a
1978	10.039	7.565	0.92	0.142
1979/80	10.406	6.75	0.88	0.160

Results from the linear regression of Θ_H on $\Delta\Theta(°C)$, and calculated constants C and a for equation (3.10).

TABLE 3.9

Depth	$(\Theta_o-\Theta_t)$	$100\ \Sigma_B^Z\ (\Theta_o-\Theta_t)$	Ave $\frac{d\Theta}{dZ}$	A
5	10	12210	19.3×10^{-4}	0.861
6	8.8	11210	33.6 "	0.454
7	7.5	10330	42.9	0.328
8	6.9	9580	32.1	0.406
9	6.3	8890	35.8	0.338
10	5.5	8260	35	0.321
11	4.7	7710	27.1	0.387
12	4.5	7240	17.9	0.551
13	4.3	6790	15.0	0.616
14	4.1	6360	15.7	0.552
15	3.8	5950	15.0	0.540
	3.6	5570	15.0	0.506
	3.4	5210	16.4	0.433
	3.3	4870	13.6	0.488
	3.2	4540	10.4	0.594
20	3.1	4220	8.6	0.668
	3	3910	5.9	0.902
	3	3610	4.4	1.12
	2.9	3310	3.8	1.19
	2.8	3020	3.1	1.32
25	2.8	2740	1.6	2.33
	2.8	2460	1.5	2.23
	2.7	2180	1.6	1.86
	2.7	1910	$\simeq$0.36	7.2
	3.1	1640	1.8	1.24
30	2.7	1330	2.0	0.905
	2.7	1060	0.43	3.35
	2.7	790	1.4	0.768
	2.6	520	2.4	0.295
34	2.6	260		

Forelian Heat Budget 1978

The change in temperature (°C) between 5/9/78 (Θ_o) and 28/11/78 (Θ_t) for each 1 metre depth interval, and the consequent change in heat content ($100\ \Sigma_B^Z\ (\Theta_o-\Theta_t)$, calories cm^{-2}, equation 3.14) between the bottom of the reservoir and each 1 metre level. The average change in temperature with depth ($\frac{d\Theta}{dZ}$, °C cm^{-1}) was determined as described in the text, and eddy diffusivity (A, cm^2s^{-1}) calculated using equation 3.7b.

TABLE 3.10

Depth	$(\Theta_o-\Theta_t)$	$100\Sigma_B^Z (\Theta_o-\Theta_t)$	Ave $\frac{d\Theta}{dZ}$	A
6	11.79	06734	36.3	0.444
7	10.82	15555	63.5	0.236
8	10.54	14473	62.9	0.222
9	9.07	13419	44.2	0.293
10	8.58	12512	42.9	0.281
11	8.08	11654	20.5	0.548
12	7.35	10846	25.7	0.407
13	7.05	10111	16.3	0.598
14	7.25	9406	19.3	0.470
15	5.74	8681	21.7	0.447
16	4.79	8107	17.4	0.449
17	4.28	7628	18.1	0.406
18	4.15	7200	14.2	0.489
19	3.94	6785	11.1	0.590
20	3.6	6391	10.39	0.593
22	3.41	5682	8.83	0.621
25	3.32	4678	5.83	0.774
27	3.21	4022	5.83	0.774
28	3.24	3701	5.7	0.626
29	3.31	3377	2.9	1.12
30	3.34	3046	1.38×10^{-4}	2.12
31		2712	2.5×10^{-4}	1.05
32	3.47	2376	3.6×10^{-4}	0.637
35	3.35	1337	2.1×10^{-4}	0.614
36	3.34	-		
37	3.34	668	1.1×10^{-4}	0.585
38	3.34	334		

Forelian Heat Budget 1979-80

The change in temperature (°C) between 12/9/79 (Θ_o) and 9/1/80 (Θ_t) for each 1 metre depth interval, and the consequent change in heat content ($100\Sigma_B^Z (\Theta_o-\Theta_t)$, calories cm^{-2}, equation 3.14) between the bottom of the reservoir and each 1 metre level. The average change in temperature with depth ($\frac{d\Theta}{dZ}$, °C cm^{-1}) was determined as described in the text, and eddy diffusivity (A cm^2 s^{-1}) calculated using equation 3.7b.

THE CHEMICAL ENVIRONMENT

GENERAL DESCRIPTION

4.0 Introduction

The nutrient composition of lake water, and its variation with time, can be a fundamental determinant of standing crop (Sakamoto 1966; Dillon & Rigler 1974; Smith 19-), rate of biomass development (Schindler & Fee 1975; Golterman 1975 p.255) and species succession (Soeder et al 1971; Titman 1976; Kilham 1978). Techniques measuring nutrient variation range from direct-chemical analysis, to biological assays. Typically each approach has drawbacks which complicate interpretation, particularly when utilized in field measurements, and greatest insight is obtained by contrasting results from several approaches.

Unpublished chemical data, collected by the Engineering and Water Supply Department for purposes of water quality monitoring (methods in Chp 2), were made available for analysis. The large vertical spacing of water samples (10m) precluded use of standard depth-time diagrams to illustrate seasonal variation, instead the temporal sequence was depicted individually for each depth. Large breaks in sampling sequences at 30 and 40m resulted from decreases in reservoir depth.

Discussion concentrates on the southern sampling site although data from site A (Fig. 1.4) are occasionally referenced.

Patterns at both positions were similar and the description of the chemical regime for the southern site holds equally well for site A (Fig. 4.5, 4.6).

Euphotic zone chlorophyll a concentrations were used to illustrate variations in phytoplankton biomass (Fig. 4.1) in relation to major nutrient fluctuations. A full discussion of phytoplankton dynamics follows in Chp 5.

As described in the introduction (Chp 1), each of the three seasons investigated during the study period was typified by a different inflow regime. During the 1977/78 season large volumes of water were pumped from the Murray River, resulting in a continuous inflow from July 1977 to April 1978 (Fig. 1.5a). Although an increased proportion of water was received from the catchment during 1978/79 supplies were boosted by summer pumping of Murray River water (Fig. 1.5b). In 1979/80 catchment runoff accounted for the total inflow of water to the reservoir, and the summer period was marked by a complete lack of inflow (Fig. 1.5c).

The following discussion is divided into these three periods to illustrate the variations in nutrient conditions which resulted from the different inflow patterns.

4.1 Continuous High Inflow Season (1977/78)

Total phosphorus and orthophosphate-P (soluble reactive phosphorus) remained at relatively high levels throughout the summer period

(Fig. 4.2). The maintenance of these levels was directly related to inflow of Murray River water (Fig. 1.5a), both components increasing soon after the commencement of pumping (27/7/77) and decreasing rapidly in April/May 1978 after inflow diminished. It is noteworthy that the chlorophyll a maximum which occurred in January (Fig. 4.1) had very little effect on either total phosphorus or orthophosphate while the second maximum which occurred following cessation of pumping decreased orthophosphate to $<10 \mu gP\ell^{-1}$ at all depths.

In contrast NO_3-N (Fig. 4.3) which increased with inflow to 800 $\mu gN\ell^{-1}$, was depleted to levels of c. 20 $\mu gN\ell^{-1}$ by the first algal maximum. Treatment with $CuSO_4$ removed phytoplankton from the water column on 25/1/78 (Fig. 4.1) and within three weeks nitrate levels had increased to c. 200 $\mu gN\ell^{-1}$ remaining at this level for the following 11 weeks. A similar response was evident at site A (Fig. 4.6) suggesting that NO_3-N concentrations of inflowing water had decreased dramatically over the pumping period. The second biomass maxima again reduced NO_3-N to levels below the limits of detection.

Concentrations of NH_3-N varied little throughout the season remaining at 50-100 $\mu gN\ell^{-1}$ (Fig. 4.4). Silicon concentrations (SiO_2, $mg\ell^{-1}$) followed a pattern comparable to orthophosphate (Fig. 4.4), rising to a maximum level of 15 $mg\ell^{-1}$ with the influx of Murray water, maintaining this value until pumping ceased, and then rapidly decreasing to 2 $mg\ell^{-1}$ in association with the diatom dominated biomass peak of May.

4.2 Winter Catchment Inflow Augmented by Summer Pumping (1978/79)

Inflow from the catchment area began in June, (Fig. 1.5b) and resulted in increased nutrient concentrations in the reservoir. Total and orthophosphate phosphorus reached similar levels to the previous season (Fig. 4.2) while NO_3-N (Fig. 4.3) attained a peak concentration double that observed in 1977.

Concentrations of both NO_3-N and orthophosphate were expected to rise with increased water contribution from the catchment, due to the multiple land usage (Fig. 1.2) and excess store of nutrient material which had not been fully mobilized in previous dry years (Buckney 1979). However the increase in NO_3-N without a concomitant increase in orthophosphate-phosphorus was surprising, perhaps suggesting an increased sewage input.

Inflow had virtually ceased by October when marked increases in chlorophyll *a* (Fig. 4.1) and associated decreases in NO_3-N, orthophosphate and silicon were first evident. Silicon depletion (Fig. 4.4) was minimal compared with the previous mid-year diatom maximum, reflecting the smaller diatom component of the 1978/79 spring biomass increase.

The depletion rate of NO_3-N (Fig. 4.3) was similar at all depths until mid-October when thermocline formation diminished the removal rate from lower layers. By late November surface concentrations had fallen to 500 $\mu g NO_3\text{-}N \ell^{-1}$ and increased

removal from 10 and 20m was evident (Fig. 4.3). The sequence was interrupted by commencement of pumping in early December, and $CuSO_4$ treatment of the algal bloom in mid-December.

Following $CuSO_4$ treatment chlorophyll concentrations rapidly returned to levels of c. 15$\mu g \ell^{-1}$, further decreasing the NO_3-N concentration of surface waters, and resulting in continued removal from all depths below until the return of isothermal conditions in February (Fig. 3.14b). The minimum NO_3-N concentration of c. 200 $\mu gN \ell^{-1}$, observed following autumnal overturn, was far in excess of the minimum observed in January and May 1978.

Orthophosphate concentrations followed a markedly different pattern from the previous season (Fig. 4.2). Rapid depletion from the surface layers reduced concentrations to minimal values (10 μgPO_4-$P \ell^{-1}$) by early December, with subsequent reductions occurring down through the water column. Pumping did not noticeably vary concentrations at either sampling site (Fig. 4.2, 4.5) even though the volume of water which entered over the three months was approximately equivalent to the volume held within the reservoir.

4.3 Total Inflow from Catchment during Winter 1979/80

As with previous years concentrations of monitored nutrients increased with inflow. Orthophosphate concentrations (Fig. 4.2) peaked during October correlating with the final large influx of

water. Maximum concentrations were virtually identical to those observed in the previous two seasons.

NO_3-N concentrations (Fig. 4.3) reached maximum values in August, and decreased during the periods of maximum inflow (September and October, Fig. 1.5c). Peak concentrations were lower than those observed in the previous season, and of similar magnitude to concentrations measured in 1977/78 when the inflow source was the Murray River.

Silicon concentrations (Fig. 4.4) showed a brief maximum in July, particularly within the surface layer, but after the major inflow of water, concentrations were only slightly above those of late summer.

A persistent thermocline formed rapidly at the end of October (Fig. 3.14c) by which time inflow had virtually ceased. Increased algal growth, in response to curtailment of mixing depth, decreased surface concentrations of silicon, orthophosphate and NO_3-N, while concentrations at lower depths declined progressively (Fig. 4.4, 4.2, 4.3). The sequential reduction with depth of NO_3-N, to levels below the limit of detection was utilized in Chapter 3 to calculate eddy diffusivity (Section 3.12).

Orthophosphate showed a similar sequential decline to 20m, but at 30m the concentration increased dramatically in mid-February, presumably due to the proximity of anoxic sediments (Mortimer 1941/42). The sequential reduction of nutrient concentrations with depth in the 1978/79 and 1979/80 seasons

illustrates the resistance of thermal stratification and thermocline formation to vertical transport. In the 1977/78 season when the thermal regime was continually disturbed by high level pumping, nutrient decreases occurred simultaneously at all depths. This was also evident in May 1978 when isothermal conditions indicated complete circulation.

Two possible causes can be suggested for difference in vernal NO_3-N concentrations (Fig. 4.3) between 1978/79 and 1979/80; either a diminished total load, or the dilution of an equivalent load by the greater inflow volume of the latter period. As in both seasons the reservoir was reduced to similar levels prior to filling (Fig. 1.6), the effect on NO_3-N concentrations of inflow of equivalent water volumes can be readily assessed.

In 1978 peak NO_3-N concentrations were observed in mid-September when the reservoir depth had increased to 37.5m (Fig. 1.6). In 1979 this depth was attained by early September. A comparison of these two periods (Fig. 4.3) demonstrated that the NO_3-N load of 1979 was far less than that of 1978 adding support to the earlier suggestion that nutrients accumulate within the catchment during dry years. However the consistent value of the soluble phosphorus concentration (Fig. 4.2) appears anomalous.

Buckney (1979), investigated the seasonal variation in chemical concentrations at six sites along the Onkaparinga River, upstream from Mt. Bold Reservoir. During periods of peak

river flow concentrations of NO_3-N were low and orthophosphate-P concentrations maximal, a pattern observed in the reservoir during filling in 1979/80.

It was also noted that orthophosphate-P concentrations diminished as water moved downstream. At the site closest to Mt. Bold oscillations in concentration were small, and absolute concentrations less than those of upstream stations. It was suggested that either orthophosphate-P was rapidly absorbed from the water, or it was significantly diluted in the rivers middle reaches. The consistent vernal orthophosphate concentration of the reservoir suggests a significant phosphate buffering capacity within the system.

This brief description of seasonal N, P and Si patterns clearly illustrates the complexity of the nutrient regime in the reservoir. Variations in nutrient load resulted not only from differences between the two major water sources, but also to marked changes within each of these sources. Thus nutrient input from the catchment was dependent on the climatic conditions of previous seasons, while the nutrient load from the River Murray appeared to vary temporally through a season. Loads carried by River Murray water also vary seasonally, depending on climatic conditions within its catchment.

4.4 Oxygen Regime

Decomposition of organic material in the hypolimnion of

thermally stratified lakes consumes significant amounts of oxygen. The degree of oxygen depletion depends on the quantity of organic material sedimented, the thickness of the hypolimnion and hypolimnetic temperatures (Stewart 1976; Cornett & Rigler 1979). The hypolimnion of Mt. Bold is endowed with high temperatures (up to 20°C, Fig. 3.14), significant input of both allochthonous and autochthonous organic material (Kinnear unpubl. thesis) and is 20-30m thick.

Anaerobic conditions in the hypolimnion can lead to nutrient release from the sediments, with the possibility of these nutrients being available for biological incorporation (Mortimer 1941/42; Hutchinson 1957).

The oxygen structure of the reservoir varied significantly between the three years (Fig. 4.7) as might be expected from the difference in thermal regimes (Fig. 3.14 (a) - (c)).

Turbulence, which minimized the thermal stratification of the water column in 1977/78 (Fig. 3.14a) acted against the formation of oxygen depleted zones (Fig. 4.7a), and only briefly within the vicinity of the sediments, did oxygen concentrations fall below 4 mg ℓ^{-1} (Fig. 4.7a).

Increased oxygen stratification was evident in 1978/79 (Fig. 4.7b) in accord with the presence of a persistent thermocline (Fig. 3.14b). Oxygen concentrations in the hypolimnion decreased following

thermocline formation, until early January when oxygen isopleths in the upper layers of the hypolimnion were forced to deeper depths. This occurrence coincided with a decrease in the temperature stratification of the hypolimnion (Fig. 3.14b) and was attributed to increased turbulence due to the initial inflow of Murray River water. Following this perturbation oxygen concentrations were again reduced throughout the hypolimnion until autumnal overturn in February. Although hypolimnetic oxygen concentrations fell to lower levels than in the previous year, most of the water column contained concentrations greater than 2 mg ℓ^{-1} and only in the vicinity of the sediments were zero oxygen levels approached.

The undisturbed thermal regime of 1979/80 resulted in extreme oxygen depletion of the hypolimnion (Fig. 4.7c). Oxygen concentrations decreased following thermocline formation in October to a minimum in late January when all depths below 11m contained less than 0.5 mg $O_2 \ell^{-1}$. The pungent odour of H_2S was noticeable in samples from lower depths and could be smelt for several hundreds of metres around the hypolimnetic outlet, while rocks in the splash zone of the outlet were coated with yellow sulphides. Under these conditions the concentration of orthophosphate directly above the sediments (30m, Fig. 4.2) increased three-fold to 240 µg PO_4-P ℓ^{-1}.

Mortimer (1941/42) demonstrated that phosphorus was released from the sediments due to reduction of ferric complexes. Hutchinson (1957) suggested that in the presence of sulphides,

reoxygenation which occurred as the chemicals were moved up through the hypolimnion by turbulence, might result in precipitation of ferric sulphides as well as phosphate complexes. Depending on the stoichiometry, this could release phosphate for biological use.

Despite the presence of H_2S in concentrations sufficient to form insoluble complexes on reoxygenation of the water (viz. at the outlet) there was no noticeable increase in orthophosphate concentrations in the upper levels of the hypolimnion (Fig. 4.2). However this does not negate the possibility of increased supply as the flux of phosphate through hypolimnetic layers, and changing water volume with depth acts against a simple concentration increase.

NUTRIENT BUDGET MODELS

4.5 Introduction

Recognition of the controlling influence of phosphorus on phytoplankton yields in many northern hemisphere lakes (Sakamoto 1966; Vollenweider 1968; Dillon & Rigler 1974; Smith 1979) has provided a conceptually and mathematically simple basis for predicting average summer biomass levels and mean photosynthetic rates (Smith 1979) from average phosphorus concentrations. However the confidence limits for such predictions are extremely broad. This is in part a result of applying phosphorus based models to lakes in which the ratio of average total

nitrogen and total phosphorus for the growing season suggests nitrogen may be limiting ($\overline{TN}:\overline{TP}<C.21$) (Smith 1979, 19-). Incorporation of the $\overline{TN}:\overline{TP}$ ratio in a variable yield chlorophyll-phosphorus model (Smith 19-) decreased prediction errors for north temperate lakes and confirmed that the chlorophyll yield resulting from a given $\overline{TP}$ concentration was highly sensitive to variations in $\overline{TN}:\overline{TP}$.

Although the available data from Mt. Bold spans only 3 years, the value of nutrient budget models in assessing phytoplankton biomass levels, warrants attempts to illustrate this potential in the hope of stimulating further interest. The lack of published data on nutrient and chlorophyll regimes in Australian lakes and reservoirs forestalls analyses similar to those utilized for north temperate lakes, yet the required data is quite likely held by state water authorities. Mt. Bold, with its widely varying nutrient regime, provides an excellent opportunity to model a single, turbid reservoir.

Growing season (typically October - February) averages of total nitrogen, total phosphorus, orthophosphate-P ($\overline{OP}$) and particulate phosphorus ($\overline{PP}$) were calculated from concentrations in surface samples (see methods, Chp 2) collected at one or two weekly intervals (Fig. 4.2, 4.3). The particulate phosphorus concentration for each sampling date was estimated as the difference between total phosphorus and orthophosphate-P, and consequently soluble, organically bound phosphorus (i.e., requiring digestion for analysis) was included in the particulate fraction.

The low $\overline{TN}:\overline{TP}$ ratios observed in Mt. Bold (Table 4.1) necessitated the use of Smith's variable yield model.

4.6 Variable Yield Chlorophyll-Phosphorus Model

Weiss (1979, referenced in Smith 19-) analyzed 213 North Carolina lakes and reservoirs for the relationship between mean growing season total dissolved phosphorus ($\overline{TDP}$) and the $\overline{TN}:\overline{TP}$ ratio (Fig. 4.8a). It was found that as the ratio decreased, and nitrogen became limiting, the residual phosphate levels measured as $\overline{TDP}$, increased. As a result $\overline{TP}$ no longer approximated the phosphorus available for incorporation into particulate form ($\overline{PP}$), and the relationship between $\overline{TP}$ and average growing season chlorophyll concentration ($\overline{b}$) showed increased variation. Weiss illustrated that $\overline{TDP}$ was highly correlated with $\overline{TN}:\overline{TP}$,

$$\log \overline{TDP} = -1.65 \log \overline{TN}:\overline{TP} + 3.18 \qquad r^2 = 0.94 \qquad (4.1)$$

and that the ratio of particulate-P to total-P decreased consistently as the $\overline{TN}:\overline{TP}$ ratio declined (Fig. 4.8b),

$$\overline{PP}:\overline{TP} = 0.0204\ \overline{TN}:\overline{TP} + 0.334 \qquad r^2 = 0.66 \qquad (4.2)$$

Strictly the value of $\overline{PP}$ obtained from Mt. Bold is not comparable with the $\overline{PP}$ of Weiss, as it contains an unknown contribution from the soluble organic-P fraction and so is an over-estimate. Similarly the orthophosphate-P measurement from Mt. Bold is not

comparable with the $\overline{TDP}$ of Weiss which includes both orthophosphate and soluble organic-P. To determine the extent of the difference, the relationship between $\overline{OP}$ and $\overline{TN}:\overline{TP}$ for each season in Mt. Bold (Table 4.1) was plotted on Weiss' graph of $\overline{TDP}$ vs $\overline{TN}:\overline{TP}$ (Fig. 4.8a), while the points $\overline{PP}:\overline{TP}$ versus $\overline{TN}:\overline{TP}$ (Table 4.1) were plotted on Weiss' similarly labelled graph (Fig. 4.8b). In both cases the values from Mt. Bold fell surprisingly close to the relationships depicted for the North Carolina lakes. However, transformation of the Mt. Bold values to those of Weiss, by correcting for soluble organic-P would increase the disparity between the two data sets.

Buckney (1979) found average total dissolved phosphorus levels in the Onkaparinga River to be approximately twice orthophosphate values. Consequently correction of the Mt. Bold values would result in substantially different relationships than found for the North Carolina lakes.

Equations similar to equations 4.1 and 4.2 were derived for Mt. Bold from the three seasonal points. Although statistically questionable, the equations are likely to be a substantial improvement over the direct application of the relationships presented by Weiss. $\overline{PP}$ in these equations is as determined for Mt. Bold.

$$\log \overline{OP} = - 0.838 \log \overline{TN}:\overline{TP} + 2.65 \qquad r^2 = 0.99 \qquad (4.3)$$

$$\overline{PP}:\overline{TP} = 0.0128\ \overline{TN}:\overline{TP} + 0.34 \qquad r^2 = 0.93 \qquad (4.4)$$

Smith (19-) extrapolated equation (4.2) to $\overline{PP}:\overline{TP} = 1.0$, which suggested that total phosphorus estimated particulate phosphorus only when $\overline{TN}:\overline{TP} > 32.6$. Analyzing 21 north latitude lakes which met this criterion a close logarithmic relationship was found between $\overline{b}$ and $\overline{TP}$,

$$\log \overline{b} = 1.55 \log \overline{TP} - 1.25 \qquad r^2 = 0.97 \qquad (4.5)$$

Note that in this situation $\overline{TP}$ and $\overline{PP}$ are interchangeable. Smith (19-) assumed that for all lakes this single relationship existed between chlorophyll concentration and particulate phosphorus, independent of $\overline{TN}:\overline{TP}$, and that a single relationship, as given by equation (4.2), connected the ratio $\overline{PP}:\overline{TP}$ to $\overline{TN}:\overline{TP}$. On these assumptions equation (4.5) can be rewritten in terms of $\overline{TP}$ for any level of $\overline{PP}:\overline{TP}$,

$$\log \overline{b} = 1.55 \log \frac{\overline{TP}}{\overline{TP}:\overline{PP}} - 1.25$$

If $\log \overline{b}$ is plotted against $\log \overline{TP}$, the x-axis intercept occurs when $\overline{b}=1.0$, and substituting equation (4.2)

$$\overline{TP} = \frac{6.404}{\overline{PP}:\overline{TP}} = \frac{6.404}{0.0204\ \overline{TN}:\overline{TP} + 0.334}$$

Therefore the general equation for the family of parallel lines depicting the relationship between $\log \overline{b}$ and $\log \overline{TP}$ for a variable $\overline{TN}:\overline{TP}$ ratio is,

$$\log \overline{b} = 1.55 \left[\log \overline{TP} - \log \frac{6.404}{0.0204\ \overline{TN}:\overline{TP} + 0.334}\right] \qquad (4.6)$$

The above equation incorporates the $\overline{PP}:\overline{TP}$ vs $\overline{TN}:\overline{TP}$ relationship obtained by Weiss (equation (4.2)). If this is replaced with the estimate from Mt. Bold (equation (4.4)) then,

$$\log \overline{b} = 1.55 \left[\log \overline{TP} - \log \frac{6.404}{0.0128\ \overline{TN}:\overline{TP} + 0.34}\right] \qquad (4.7)$$

It is implicitly assumed in this equation that for Mt. Bold the relationship between chlorophyll concentration and average growing season particulate phosphorus is equivalent to that suggested by Smith (19-) (equation (4.5)).

The only season for which average summer chlorophyll concentration could be reasonably calculated was 1979/80 when Mt. Bold was not influenced by $CuSO_4$ treatment. The calculation covers the period October 1979 to 1st April 1980 (Fig. 4.1) during which the average chlorophyll concentration of the euphotic zone was 33 mg chl a m^{-3} (Table 4.1). Application of equation 4.7 using the data in Table 4.1 provided an estimate of 33.7 mg chl a m^{-3}, the remarkable accuracy of which was probably somewhat fortuitous.

In 1977/78 and 1978/79 equation 4.7 over-estimated the average summer chlorophyll concentration by a factor of c. 2.5 (Table 4.1) presumably as a result of $CuSO_4$ dosing, although variation in mixing regime may have contributed.

The successful prediction of the 1979/80 average chlorophyll concentration suggests that equation 4.4 describes the relationship between the ratios $\overline{PP}:\overline{TP}$ and $\overline{TN}:\overline{TP}$ reasonably well for Mt. Bold. As discussed earlier the $\overline{PP}$ calculated for the reservoir is an over-estimate compared to $\overline{PP}$ calculated by Weiss. Consequently if equation 4.4 was corrected for this difference it would deviate even further from the relationship found by Weiss (equation 4.2), implying that for a given $\overline{TN}:\overline{TP}$ ratio there is a larger incorporation of phosphorus into particulate phosphorus in the North Carolina lakes. The associated larger residual phosphorus concentration for a given $\overline{TN}:\overline{TP}$ ratio in Mt. Bold (Fig. 4.8a) could be the result of a further limiting factor.

It has been suggested that phytoplankton biomass levels in Australian inland waters tend to be lower than expected from northern hemisphere experience, due to light restriction caused by high turbidity (Williams 1973, 1976; Ganf 1976). However the difference in $\overline{PP}:\overline{TP}$ ratios may equally well result from differences in the distribution of $\overline{TN}$ or $\overline{TP}$ between nutrient compartments. The unravelling of these relationships could provide valuable insight to the variation observed between lakes in the average summer chlorophyll to total phosphorus relationship (Smith 19- ; Nicholls & Dillon 1978).

Although mass nutrient models simplify the complexity of nutrient regimes and provide valuable information on average total biomass yields, they give no information on factors determining

the rate at which standing crop is attained (Schindler & Fee 1975; Golterman 1975 p.255). The rate limiting factors may well be nutrients other than those recognized by nutrient budget models as determining yield. Furthermore, as the relative abundance of species comprising the biomass will be determined by factors limiting net growth rates, these are of particular interest in consideration of phytoplankton seasonal succession.

DETERMINATION OF NUTRIENT AVAILABILITY FROM ALGAL BIOASSAYS

4.7 Introduction

Investigation of nutrient limitation in aquatic environments has been based largely on enrichment experiments, in which nutrients are supplied either to a test algal species growing in filtered water, or to the natural phytoplankton. The outcome of many such experiments has confirmed the particular importance of nitrogen and phosphorus in limiting growth, however silicon (Lund 1950; Hamilton 1969), vitamins (Droop 1970), trace elements (Goldman 1972) and other micronutrients (Smayda 1974) have at times been implicated.

Enrichment techniques range from whole lake experiments (Schindler 1971) to small volume batch cultures (Smayda 1974). Of the various techniques the batch culture method utilizing natural phytoplankton assemblages (Schelske et al 1978) provides the simplest means of obtaining information on short term variations in limiting nutrients. Use of the natural population avoids

the problem of selecting a "representative" test organism (Goldman 1978) and provides an innoculum conditioned to, and integrating the nutrient regime of the preceeding period (Schelske 1978; Goldman 1978). This is particularly significant in light of the well documented luxury consumption of nutrients by algae (Stewart et al 1978; Tilman & Kilham 1976; Lund et al 1975). Comparison of batch culture techniques with whole pond enrichment (O'Brien & de Noyelles 1976) has provided support for this method, although reliability of bioassays to identify specific limiting nutrients has not always been confirmed (Reynolds & Butterwick 1979).

The summer cycle of nutrient availability at the southern sampling site of Mt. Bold Reservoir, was investigated using batch culture bioassays with the natural phytoplankton assemblage. Attention was focused on the role of nitrogen and phosphorus, as previous experimental work (Ganf 1980, In press) had shown a lack of response to enrichment by other nutrients.

Water samples from selected depths were enriched with phosphorus (+P), nitrogen (+N) and both nitrogen and phosphorus (N+P) and incubated as described in Chapter 2. Phytoplankton growth was monitored daily using *in vivo* chlorophyll fluorescence and compared with growth in control flasks containing unenriched water samples. Fluorometric measurements described typical growth curves (Fig. 4.9) and average growth rates K (doublings day $^{-1}$) were calculated from,

$$\log F_t = \log F_o + Kt \log 2 \qquad (4.8)$$

where F_o was initial fluorescence and F_t fluorescence at time t (day). Only data points from the end of lag-phase and at the time of maximum fluorescence were used in calculations. Average growth rates for each date and depth are given in Appendix 1, and shown graphically in Fig. 4.11.

4.8 Depth Distribution of Growth Potential

Variation of growth potential within the water column was evident from results of control flasks (Fig. 4.10b). Nutrient depletion reduced the growth potential of surface layers to zero in early December with concomitant decreases down to 10m. The zone of zero growth potential deepened progressively through December in a manner similar to that described for 1978/79 (Fig. 4.10a) (Ganf 1980). However, in mid-January the zone was disrupted and surface waters showed increased potential for supporting phytoplankton growth. The zero growth zone reformed in February and eventually extended down to 15m (Fig. 4.10b), only to be destroyed by autumnal mixing in March (Fig. 3.14c).

The period of increased growth potential observed in the surface waters during late-January and early-February was preceded by a decline in chlorophyll *a* concentration (Fig. 4.1) and a slight increase in surface concentrations of orthophosphate-phosphorus (Fig. 4.2), NO_3-N (Fig. 4.3) and silicon (Fig. 4.4). Mixing depth increased from 5m on 24/1/80, to 13m on 6/2/80, but then decreased to 9m by 18/2/80 (Fig. 3.16).

Although 81mm of rain fell on January 11th, previous measurements indicated that this was unlikely to provide a source of nutrients. For example 109mm of rain on 12 December caused no increase in growth potential of water samples collected on 27 December, and similarly 163mm, which fell over the period 28-30 December, had not stimulated growth in samples collected on 4 January.

Consequently it appeared that the increased mixing depth had entrained nutrients from the hypolimnion. It is evident from Fig. 4.7c that mixing reached the oxygen depleted zone, and possibly reoxygenation and precipitation of ferric sulphides released phosphorus for biological incorporation.

4.9 Nutrient Limitation

The addition of both nitrogen and phosphorus (N+P) to bioassay samples increased growth compared to control flasks, indicating the presence of other essential nutrients in sufficient concentrations to sustain between 2 and 5 doublings of the innocula (Fig. 4.11). The variation in growth potential of (N+P) enriched flasks was presumably a result of changing concentrations in these other nutrients. Minimum growth stimulation by the addition of (N+P) occurred in mid-March, and maximum stimulation in late April when the water was highly coloured and turbid following heavy rains.

The relative importance of nitrogen and phosphorus to the increased growth resulting from (N+P) enrichment was ascertained from single additions of N or P. As might be expected in a stratified water

column, the depth variation of growth response to single enrichment was complicated (Fig. 4.11). In the following discussion events at the surface are followed and compared with results from other depths.

Bioassay measurements began in early December, by which time surface growth potential was negligible. While the addition of both nitrogen and phosphorus (N+P) increased the growth potential, the single addition of either nutrient was ineffective, suggesting that both nutrients were "equally" limiting.

Unenriched samples from 2.5m supported phytoplankton growth, however the addition of (N+P) stimulated the growth response whereas single additions did not, again indicating a balanced limitation.

At 5 and 10m, NO_3-N addition stimulated growth to the same level as (N+P) enrichment, demonstrating that phosphorus was present in sufficient concentrations to support growth but that nitrogen concentrations were restrictive.

During January phosphorus additions stimulated growth in surface samples while nitrogen caused no increase over control levels, indicating the presence of a nitrogen source and the limiting function of phosphorus. At depths of 2.5, 5 and 10m, N and P were equally limiting by mid-January, while at 15m and below nitrogen remained the limiting nutrient, virtually restoring growth rate to levels obtained from (N+P) enrichment. In summation these results indicated phosphorus sufficiency at depths below 15m,

a balanced limitation with N up to 2.5m and phosphorus deficiency in the surface layers. This situation was dramatically altered during the last few days of January when addition of phosphorus ceased to stimulate growth at any depth, whereas the addition of nitrogen stimulated growth to the same level as (N+P) enrichment. This change correlated with the observed increase in growth potential of control flasks (Fig. 4.10b) and suggested an influx of available phosphorus to depths above 15m. The specific source of phosphorus could not be determined from the available data, however the intense oxygen depletion of the hypolimnion, which reached a maximum coincident with the period (Fig. 4.7c) offered the possibility of an increased phosphorus flux from the deeper water layers.

During February the epilimnion (0-5m) reverted through a balance position, where N and P were equally limiting, to phosphorus limitation, a situation maintained throughout the rest of the season.

The variations which occurred at depths of 10m and below during this latter period will not be considered in any detail. In general phosphorus was limiting at 10 and 15m after February, while both N and P were equally limiting at 20 and 30m (Fig. 4.11).

CHEMICAL AND PHYSIOLOGICAL INDICATORS OF NUTRIENT LIMITATION

4.10 N:P Ratios

(Measured variables and calculated ratios are presented in Appendices 2 and 3).

In determining the relative importance of nitrogen and phosphorus to growth limitation, frequent use has been made of critical N:P ratios based on stoichiometry (Redfield 1958), and the assumption that the demand for nutrients will be in proportion to the relative concentration in the algal cells (Ryther & Dunstan 1971; Sakshaug & Myklestad 1973). Although this approach tends to ignore recycling (Schindler & Fee 1975) and the often observed lack of relationship between growth and measurable levels of nutrients in the medium (Caperon & Meyer 1972; Droop 1974; Stewart et al. 1978) it has been successfully applied in a number of cases (Forsberg et al. 1978; Rinne & Tarkiainen 1978). Critical values of the N:P ratio are generally in the range 5-17 (Redfield 1958; Ryther & Dunstan 1971; Healey 1975; Forsberg et al. 1978).

The ratio of inorganic N ($NH_4^+ + NO_3^+ + NO_2^-$):orthophosphate-P for Mt. Bold during the 1979/80 season is shown in Fig. 4.12a. Significant algal growth occurred during October - March (Fig. 4.1), and the N:P ratio remained between c. 5-17 for most of this period indicating that either, or both, phosphorus or nitrogen could be limiting.

Rinne & Tarkiainen (1978) used the ratio of total nitrogen to total phosphorus and suggested that when TN:TP was greater than 7 phosphorus was limiting while values lower than 7 indicated nitrogen limitation.

Forsberg et al. (1978) investigated the TN:TP ratio in a number of Swedish lakes and set the critical level for nitrogen limitation as TN:TP <10 and for phosphorus limitation as TN:TP >17. In the region TN:TP = 10-17 both or either nutrients could be limiting. This range of values is identical to that derived by Sakamoto (1966) for a series of Japanese lakes.

In Mt. Bold the TN:TP ratio remained between c. 10-17 for most of the 1979/80 growth season, again indicating nitrogen and/or phosphorus limitation (Fig. 4.12b). Rinne & Tarkiainen (1978) argued that the ratio of inorganic N (N_s) to inorganic P (orthophosphate P=OP) could be used as an index of the nutrients immediately available for algal growth, and that when this ratio was higher than TN:TP, phosphorus was the limiting factor while if N_s:OP was less than TN:TP, nitrogen would be limiting. Their scheme can be summarized as,

$$N_s:OP < TN:TP < (\text{ca. } 7) < TN:TP < N_s:OP$$

N limiting P limiting

The two ratios, as found in Mt. Bold, are plotted together (Fig. 4.12a) for ease of comparison. Throughout the growth season N_s:OP<TN:TP, suggesting continual nitrogen limitation, a

result not supported by bioassay measurements.

Average growing season $\overline{TN}$ and $\overline{TP}$ concentrations have been successfully used to predict average chlorophyll yield in a large number of lakes (Sakamoto 1966; Dillon & Rigler 1974; Smith 19- ; Section 4.6). Introduction of the variable yield model by Smith (19- , Section 4.6) has highlighted the significance of the $\overline{TN}:\overline{TP}$ ratio in influencing chlorophyll yield. This ratio in Mt. Bold varied from 8.3 in 1977/78 (Table 4.1) indicating possible nitrogen limitation, to 18.6 in 1978/79 which indicated possible phosphorus limitation. In 1979/80 $\overline{TN}:\overline{TP}$ = 12.4 which like the other nutrient ratios discussed indicated either N and/or P limitation.

Physiological indicators of nutrient limitation, assessed from fluctuations in cellular composition, have a number of attributes which make them preferable to both bioassay enrichment studies and water chemistry analyses. The most obvious feature is that they provide a direct measure of the nutrient limitation to which the population has been subjected, unlike the other methods which test the ability of the sampled water to maintain growth. Measurements of cellular composition can be rapidly completed, minimizing the chance of artifact due to enclosure, and enabling analysis of a large number of samples.

Healey (1975, 1978) reviewed the literature on cellular composition and suggested critical, quantitative values depicting nutrient limitation. However a distinct handicap to application of

compositional indicators in the field is the difficulty of measuring phytoplankton cellular attributes when algae comprise only a fraction of the seston. This is a particularly difficult problem in the turbid waters of Mt. Bold Reservoir, where not only will zooplankton, bacteria and detritus interfere with analysis but also suspended, allochthonous organic material.

4.11 Cellular N:P Ratio

Cellular contents of nitrogen and phosphorus were estimated as organic nitrogen (Total Kjeldahl nitrogen - (NH_3-N)) and organic phosphorus (Total phosphorus - orthophosphate phosphorus). Healey (1975) suggested a critical N:P level of 10 for cellular composition, with ratios above 10 indicating P limitation. The ratio in the euphotic zone of Mt. Bold was always greater than 10 (Fig. 4.12c), however the magnitude held little significance as contributions from allochthonous material were unknown, neither parameter showing a close relationship with chlorophyll a concentration or cell volume.

A different approach to the use of this ratio is based on a number of assumptions which were generally met in Mt. Bold during the 1979/80 season. If it was assumed that inflow of particulate material was negligible, that either nitrogen or phosphorus was limiting and that at any moment loss of N and P due to sedimentation was in the same ratio as it occurred, then variations in the ratio could be attributed to differences in relative uptake of the two nutrients. Under such conditions

the ratio would be expected to increase when P was less available and decrease when N was limiting.

A comparison of bioassay results from surface layers (Fig. 4.11) with directional changes in the N:P ratio (Fig. 4.12c) provided support for the analysis.

In late November and early December the ratio changed from a decreasing to an increasing function. During this changeover a balance point was expected where both N and P would appear equally limiting. The surface bioassay of early December showed such a response.

Through December and into mid-January the ratio increased and as would be predicted, bioassay results showed P limitation. In late-January the ratio fell rapidly, the rate of fall decreasing in February, and reversing in mid-February, suggesting nitrogen limitation followed by a balanced response and then P limitation. Bioassay results agreed in essence showing definite N limitation in late January, a balance position in early February and P limitation through late February and into March.

The ratio predicted either slight N limitation or a balance point in late March, followed by phosphorus limitation until the inflow from heavy rains in mid-April. Again the bioassay results supported the predictions showing a balance point at the end of March and phosphorus limitation thereafter.

The success of the organic N: organic P ratio in predicting the limiting nutrient within the euphotic zone of 1979/80 resulted largely from the lack of inflow during this period, and the stable thermal regime. These attributes enabled the required assumptions to be closely approximated. The ratio may not have been so successful in 1977/78 or 1978/79 when inflow of Murray River water complicated the thermal structure and contributed organic material to the euphotic zone. The ability of the ratio to describe variations in nutrient limitation easily and rapidly from routine measurements taken for water quality monitoring warrants it further research.

4.12 Cellular Chlorophyll Content

The chlorophyll content of phytoplankton is altered not only by nutrient limitation, but also by temperature and light intensity (Healey 1975; Falkowski & Owens 1980), however very low values are largely associated with extreme N or P depletion (Healey 1975, 1978). Chlorophyll *a* concentration and total phytoplankton cell volume were measured in euphotic samples from Mt. Bold Reservoir as described in Chp. 2. The ratio (Fig. 4.13a) varied widely over the growth season, from a maximum of 12 to a minimum of 2.5 µg chla. mm^{-3} cell volume.

The critical range of 7-10µg chla/mg dry wt (Healey 1975, 1978) was converted to a cell volume basis by assuming a specific gravity of 1.0 and a wet weight to dry weight ratio of 4:1 (Healey 1975), giving a range of 1.75 - 2.5µg chla mm^{-3}cell

volume. The observed ratio reached the upper limits of the critical range (Fig. 4.13a) but never fell below it. As similar values can be induced in culture by factors other than nutrient limitation (eg. high light intensity) the lowest observed chlorophyll contents do not unequivocally indicate nutrient depletion.

It is interesting to note the marked increase in cellular chlorophyll content during the latter half of January, coincident with the period of hypothesized phosphorus influx, and followed by the period of nitrogen depletion.

4.13 Cellular Protein and Carbohydrate Content

Cellular proportions of protein and carbohydrate, the two major components of algal cells, have been found to vary widely in response to nutrient limitation (Antia et al. 1963; Haug, Myklestad and Sakshaug 1973; Healey 1975; Myklestad 1977; Stone 1981 unpublished thesis), with carbohydrate content increasing and protein content decreasing. Healey (1975) found that with relatively few exceptions, protein values greater than 0.4 mg/mg dry wt and carbohydrate values less than 0.3 mg/mg dry wt indicated nutrient sufficiency, while protein below 0.3 and carbohydrate above 0.4 indicated nutrient deficiency. Based on a wet weight to dry weight ratio of 4:1, the critical range converted to 0.075-0.1 mg carbohydrate or protein per mm^3 cell volume.

Data on the protein and carbohydrate concentrations (methods in Chp. 2) of euphotic zone water from Mt. Bold Reservoir (Stone 1981 unpublished thesis) were made available for analysis.

Protein:cell volume ratios were always greater than the critical level (Fig. 4.13b), indicating nutrient sufficiency. However, carbohydrate/cell volume ratios were also generally greater than the critical value (Fig. 4.13c) indicating nutrient deficiency. These opposing predictions on nutrient status restricted any general statement on the growth conditions of the populations. Closer analysis did however, provide information on the nutrient regime. In December, carbohydrate content increased and protein decreased, a typical response of cells undergoing nutrient limitation (Healey 1975; Stone 1981 unpubl. thesis), and the result expected from increased phosphorus limitation depicted by bioassay analysis (Fig. 4.11).

A small decrease of cellular carbohydrate in early January, followed by a large increase in cell protein, coincided with the observed increase in orthophosphate P and NO_3-N of the surface layer (Fig. 4.2, 4.3). This effect was short lived and in mid-January carbohydrate again increased, while protein content decreased.

Interpretation of the large decline in both cellular carbohydrate and protein from late January to mid-February was made increasingly difficult by the sparseness of data points. As a result it was not known whether carbohydrate content decreased

prior to protein. Under the proposed nutrient pattern of a phosphorus influx followed by nitrogen limitation, it might be expected that cellular carbohydrate reserves would fall rapidly, followed by a decrease in protein content.

Carbohydrate content increased during the remainder of February indicating nutrient limitation, which bioassay results demonstrated was phosphorus.

A decrease in carbohydrate, and increase in protein during early March indicated nutrient availability, possibly as a result of autumnal overturn. The reverse trend in late March suggested the return of nutrient limitation. Throughout this period bioassays indicated phosphorus limitation.

4.14 Protein:Carbohydrate Ratio

The fact that nutrient deficiency has opposite effects on protein and carbohydrate contents of algae has led to the use of the protein/carbohydrate ratio (P/C) as an indicator of nutrient deficiency. Healey (1975) found the P/C ratio to be a far more reliable indicator than protein or carbohydrate alone and set a critical range of 0.8 - 1.2, with values lower than this indicating nutrient deficiency. Following extensive culture measurements on diatoms, Myklestad (1977) set a similar critical value of 1.0.

In Mt. Bold the ratio decreased to critical levels for the two

periods (Fig. 4.13d), late December to early January and mid February to early March. Although these corresponded to periods of nutrient limitation as illustrated from bioassays, the majority of the results suggested no nutrient limitation, a result at odds with the bioassay data (Fig. 4.11).

Analysis of the directional change in the ratio led to a description of variation in the nutrient regime similar to that obtained from the organic N:organic P ratio and the bioassay results. In general these all depicted nutrient depletion through December and early January, an increased nutrient availability in mid January with a return to depletion in February, and a further brief increase in nutrient availability in early March followed by continued nutrient limitation. The similarity of these results suggested that the compositional indicators were responding to fluctuations in the nutrient regime in the expected manner, but that the critical levels determined on cultured, laboratory populations were not indicating the true significance of these changes. In cases where large background interference was likely eg. organic N/organic P ratio, this result was anticipated. However in the case of chlorophyll *a* concentration and cell volume where interference was expected to be minimal, critical values still appeared unreasonable (Fig. 4.13a).

The linear relationship between chlorophyll *a* and protein concentration (Fig. 4.14a) and cell volume and carbohydrate (Fig. 4.14b) demonstrated that phytoplankton were the major source of these compounds. Yet despite minimal interference

critical levels for carbohydrate and protein provided the most inconsistent interpretation of the nutrient regime, protein results predicting nutrient sufficiency and carbohydrate nutrient deficiency.

As these inconsistencies resulted from the application of laboratory measured critical levels, an attempt was made to assess critical levels directly for the field situation.

4.15 Field Determination of Critical Levels for Compositional Indicators

Laboratory efforts to determine the switch-over point from limitation by one nutrient to limitation by another have frequently utilized the idea of a balance point, ie. the ratio between two nutrients when they are present in concentrations where neither is limiting relative to the other, when all other nutrients are in excess (Droop 1974; Myklestad 1977). It is assumed that in such conditions the phytoplankton take up a "preferred" chemical composition.

The surface bioassay results from Mt. Bold contained three balance points. On these occasions the addition of (N+P) stimulated growth, implying adequate concentrations of other nutrient requirements. The single addition of N or P resulted either in no growth at all (10th December, Fig. 4.11) or a similar, small growth response for both nutrients (6th February and 1st April, Fig. 4.11) suggesting, in these latter cases particularly, that neither N or P were limiting. If it is considered that on these

dates phytoplankton composition was in the "preferred" state, then measured or interpolated values for compositional variables may be used to estimate critical field levels.

Except for the TN:TP and organic N:organic P ratios, (Fig. 4.12b&c) the critical field levels for each compositional indicator were similar on dates when balanced limitation was observed (Fig. 4.13). This was not as surprising as it first appeared, in that *Microcystis* dominated the population from mid December onwards (Chapter 5). The similarity of the values in fact provided some support for the concept of the balance point.

Critical field values were substantially higher than critical values suggested from culture work (Table 4.2), and indicated periods of marked nutrient depletion (Fig. 4.13) which inter-correlated between the various compositional indicators, and coincided with bioassay results.

4.16 Discussion

The large seasonal variation in nutrient input from the catchment area and Murray River, represents a significant problem to efforts aimed at controlling phytoplankton biomass levels by manipulation of nutrient loads. The concept of a single nutrient being the prime determinant of phytoplankton yield appears untenable in the light of the data from Mt. Bold Reservoir.

In general the ratios of average growing season total nitrogen ($\overline{TN}$)

to total phosphorus ($\overline{TP}$) concentration, implied that either or both nutrients could be significant in determining average growing season chlorophyll *a* concentrations, $\overline{b}$ (Table 4.1).

The successful prediction of the 1979/80 mean growing season chlorophyll *a* concentration from a variable yield chlorophyll-phosphorus model based on that of Smith (19-) suggested that variation in $\overline{TN}$:$\overline{TP}$ ratio could be accounted for successfully. With further substantiation such a model might provide a foundation for predicting the effect of changing nutrient loads on chlorophyll *a* concentrations. However as the model was based on average growing season values of surface samples, the problem remains of relating these to changes in loadings. The seasonal variability in the mixing regime of the reservoir (Chp. 3) may cause this to be a difficult problem.

Bioassay results for 1979/80 demonstrated a change in limiting nutrient both in time, and vertically within the stratified water column. The occurrence of a phosphorus deficiency in surface layers, but a sufficiency at progressively deeper depths through the season, suggests that the vertical movement of nutrients by water turbulence (Chp. 3) may become particularly important during the thermally stratified period.

The significance of a slight increase in surface mixing was dramatically illustrated by a change from phosphorus limitation to nitrogen limitation. Following re-establishment of a shallow epilimnion, phosphorus limitation returned as chlorophyll *a* increased

in response to the nutrient spiking.

Once critical values had been set for compositional indicators in the field they predicted nutrient fluctuations which corresponded with bioassay results. Although the successful compositional indicators provided no insight to the identity of the limiting nutrient, they illustrated when nutrient conditions had improved. Such indicators may provide a useful numerical measure of nutrient supply.

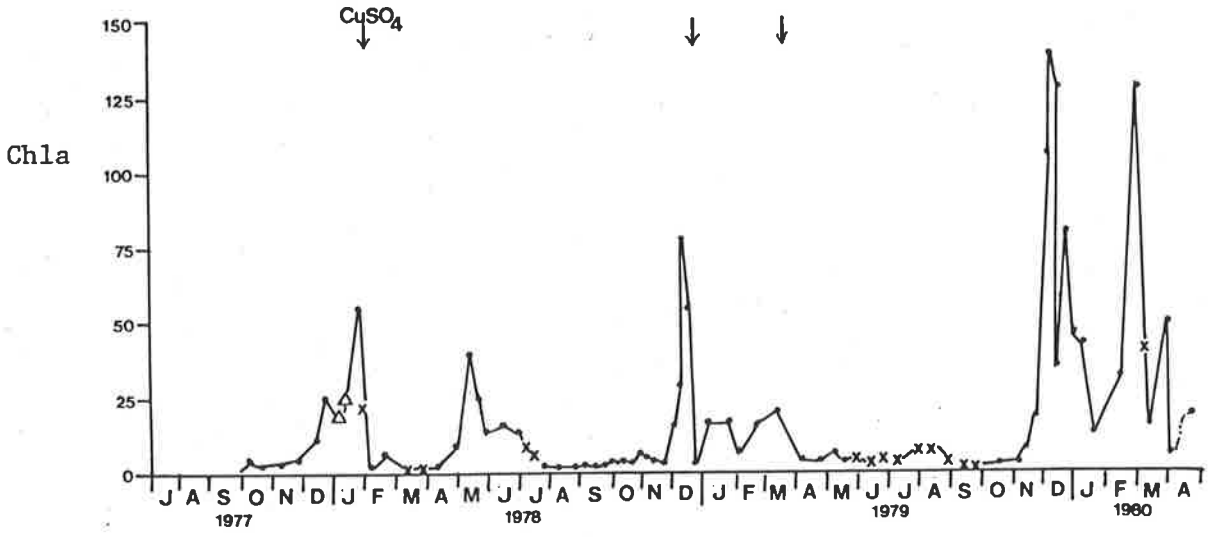

Fig. 4.1: Seasonal variation in chlorophyll a concentration at the southern sampling site.

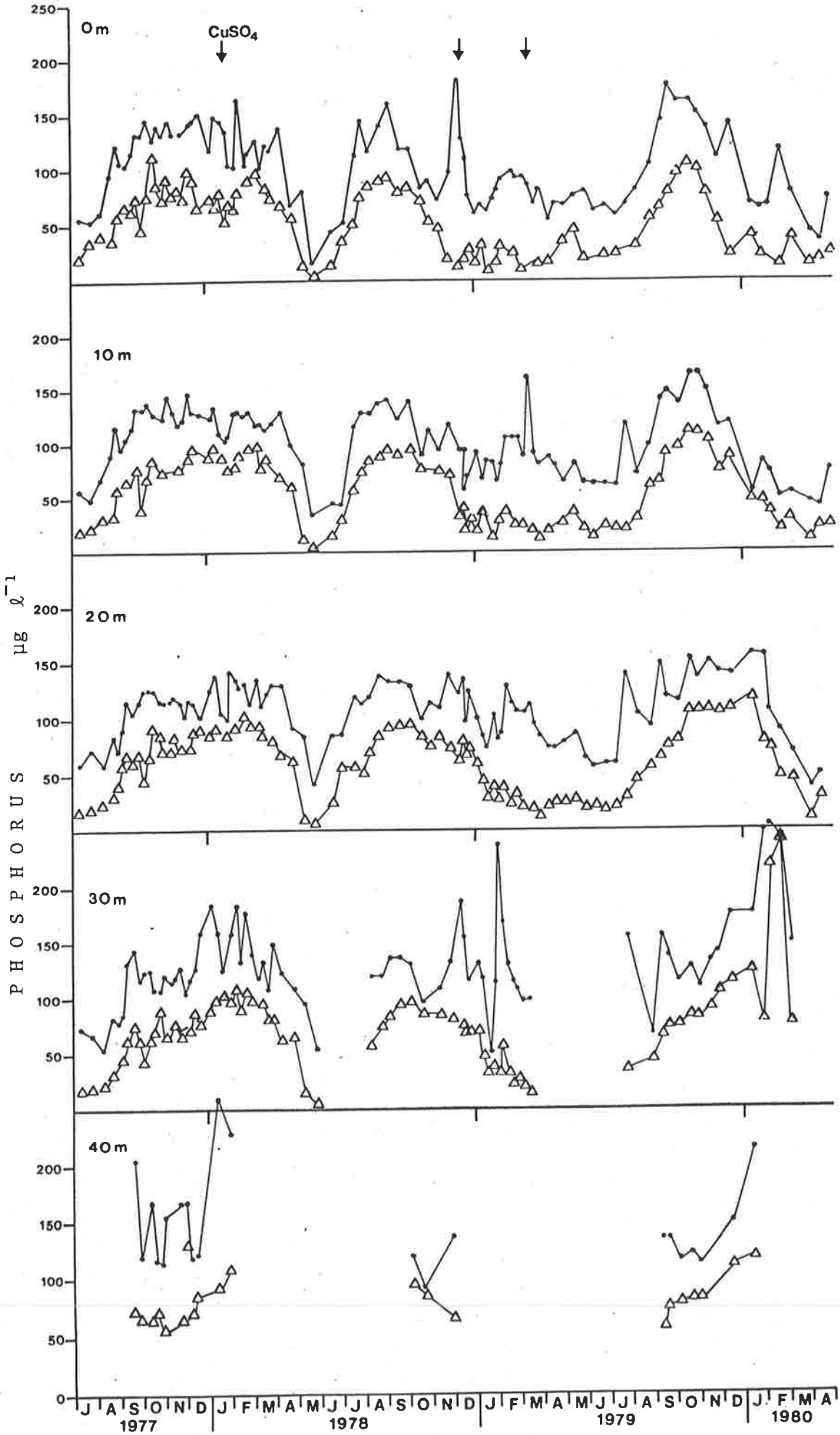

Fig. 4.2: Seasonal variation in concentration of total phosphorus (•) and orthophosphate phosphorus (△) at the south sampling site at 0, 10, 20, 30 and 40 m.

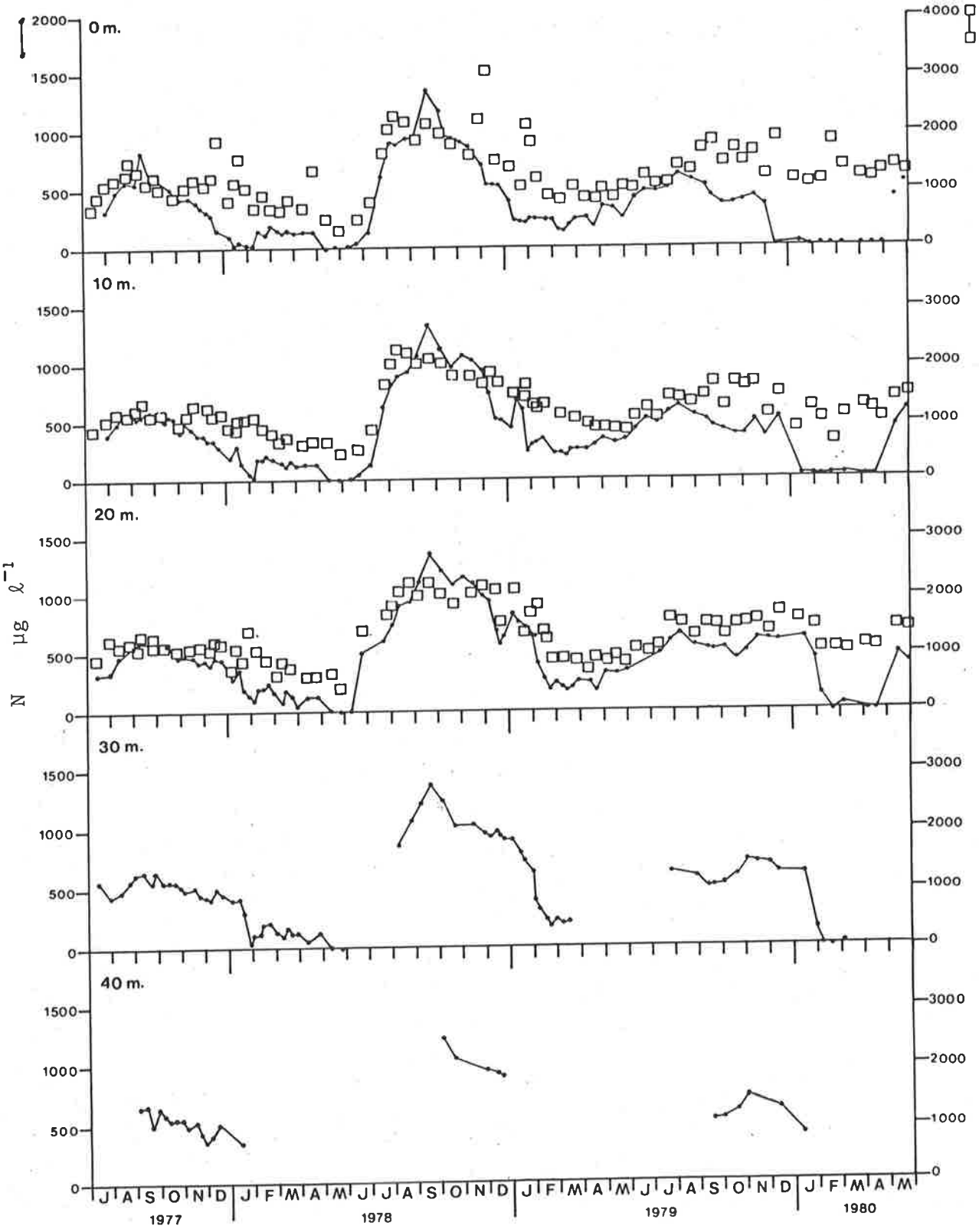

Fig. 4.3: Seasonal variation in Total nitrogen (□) and nitrate nitrogen (•) at the south sampling site for depths 0, 10, 20, 30 and 40 m.

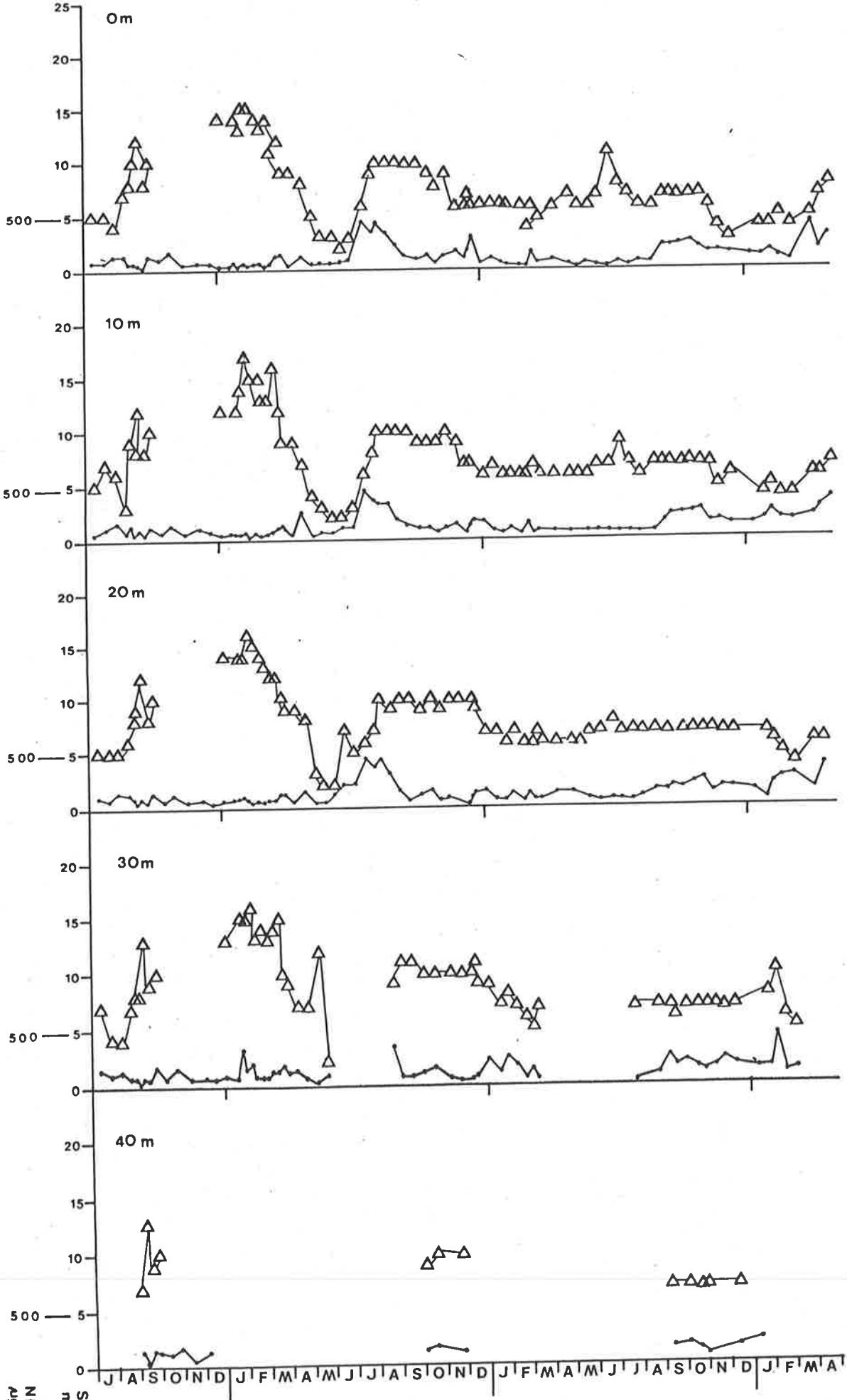

Fig. 4.4: Seasonal variation in ammonia nitrogen (•) and silicon dioxide (△) concentrations at the south sampling site at 0, 10, 20, 30 and 40 m.

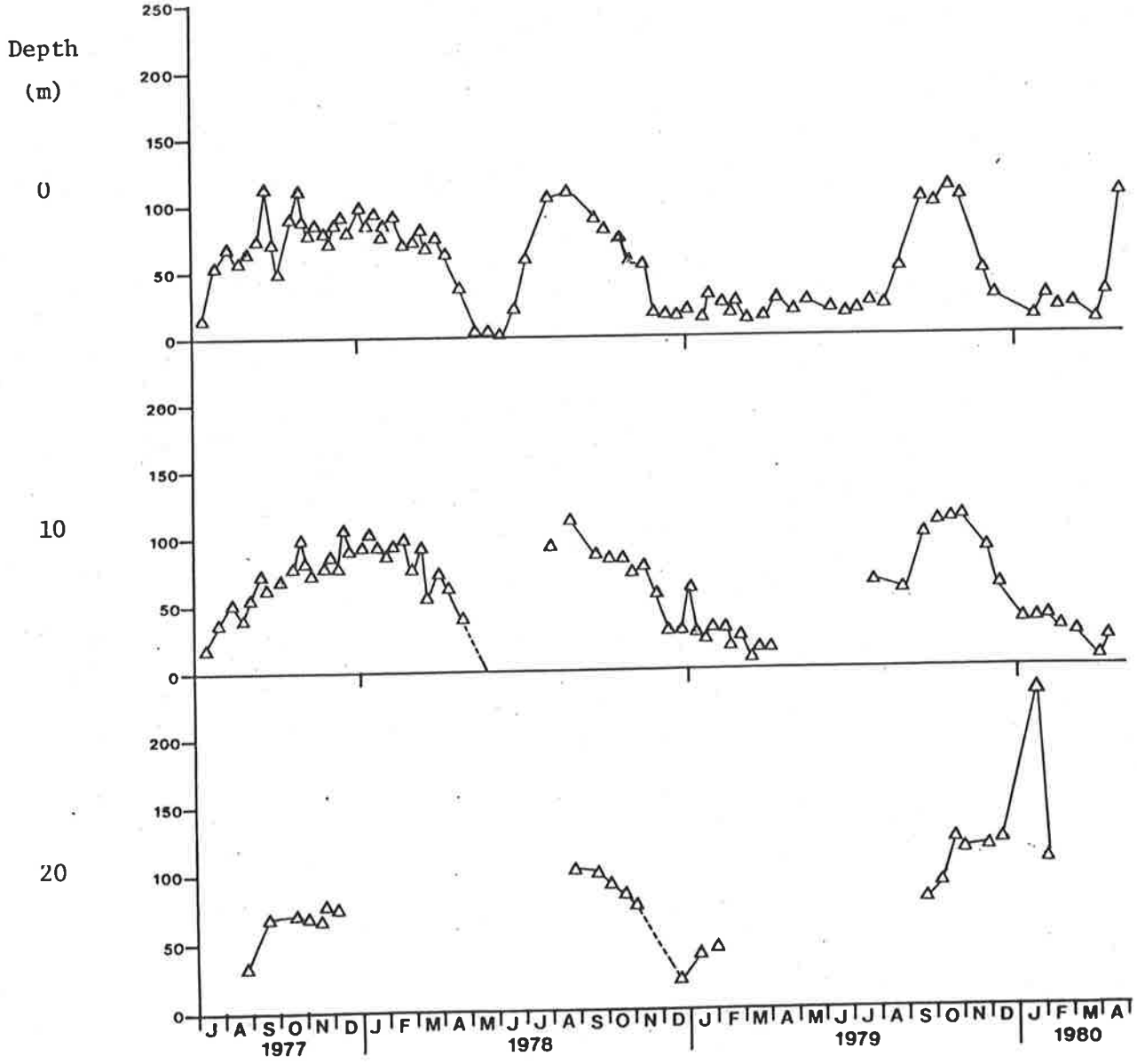

Fig. 4.5: Seasonal variation in concentration of orthophosphate phosphorus at sampling site A for depths 0, 10 and 20 m.

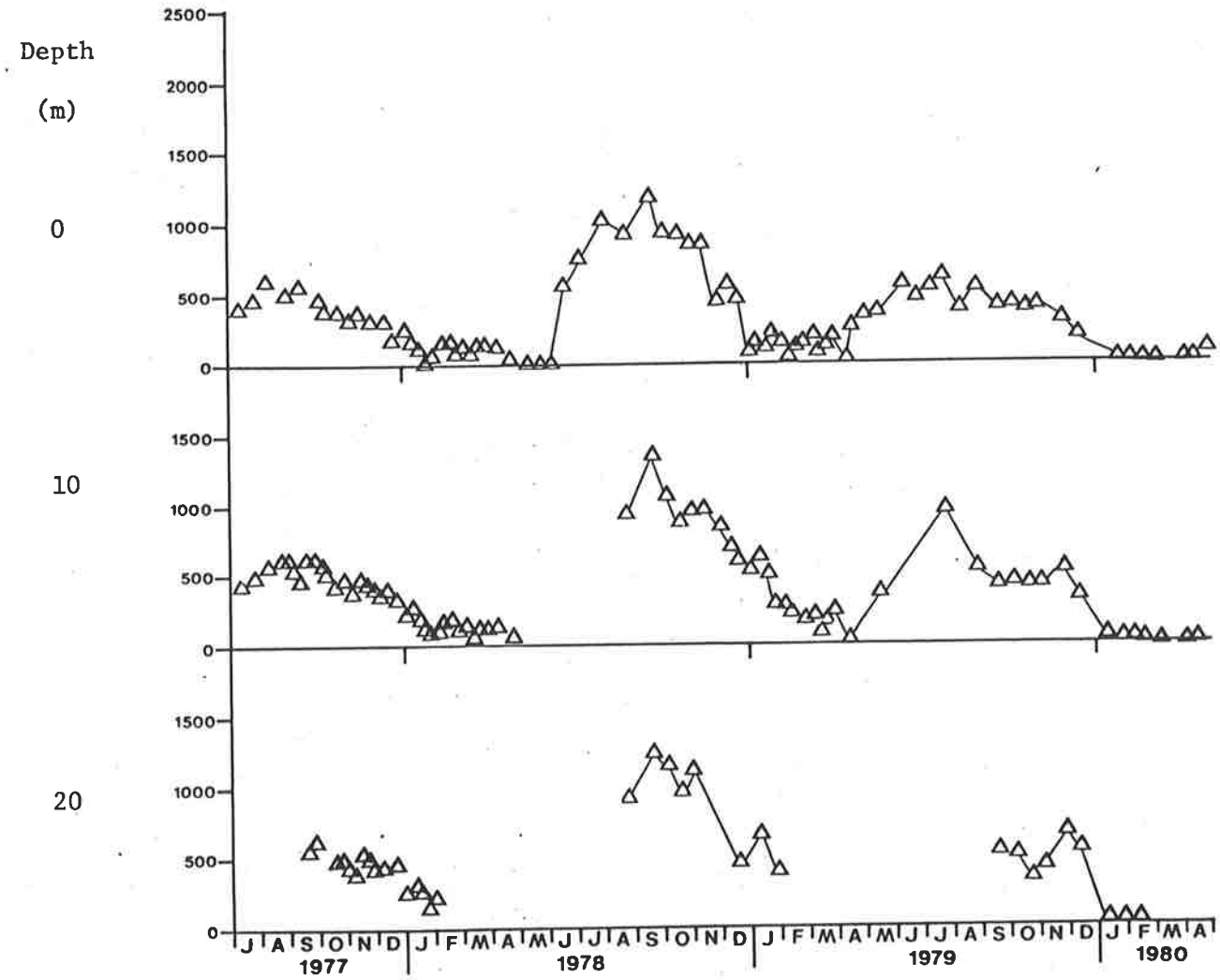

Fig. 4.6: Seasonal variation in nitrate nitrogen concentration at sampling site A for depths 0, 10 and 20 m.

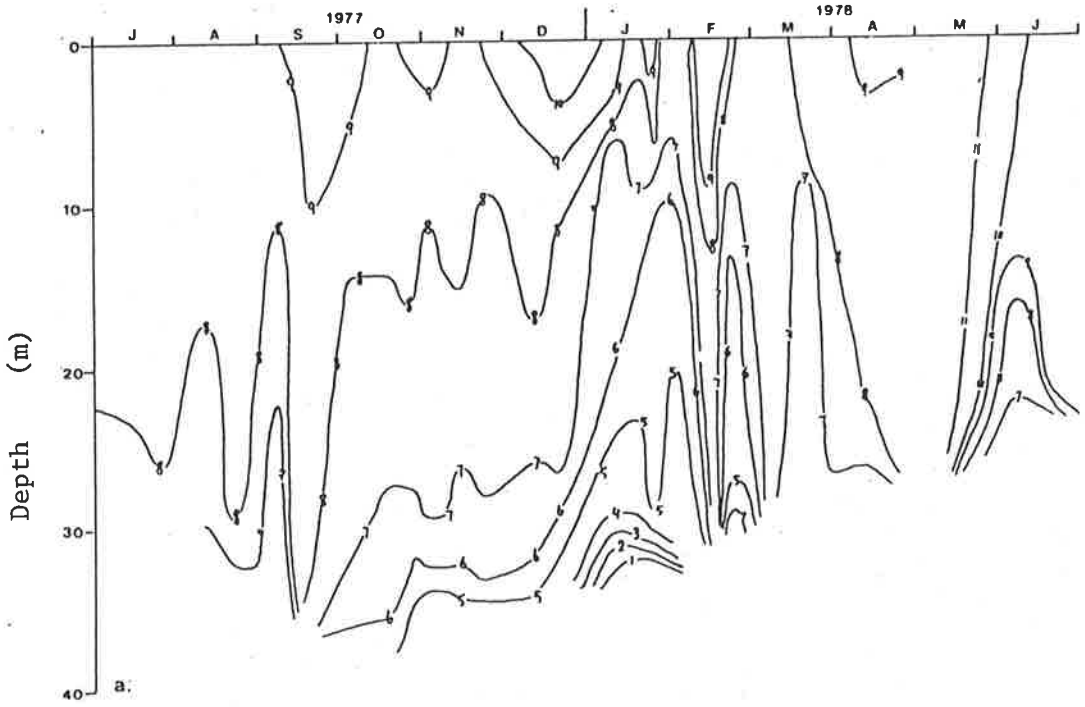

Fig. 4.7: Depth-time diagrams of oxygen concentration for the south sampling site,

a. 1977-78

b. 1978-79

c. 1979-80

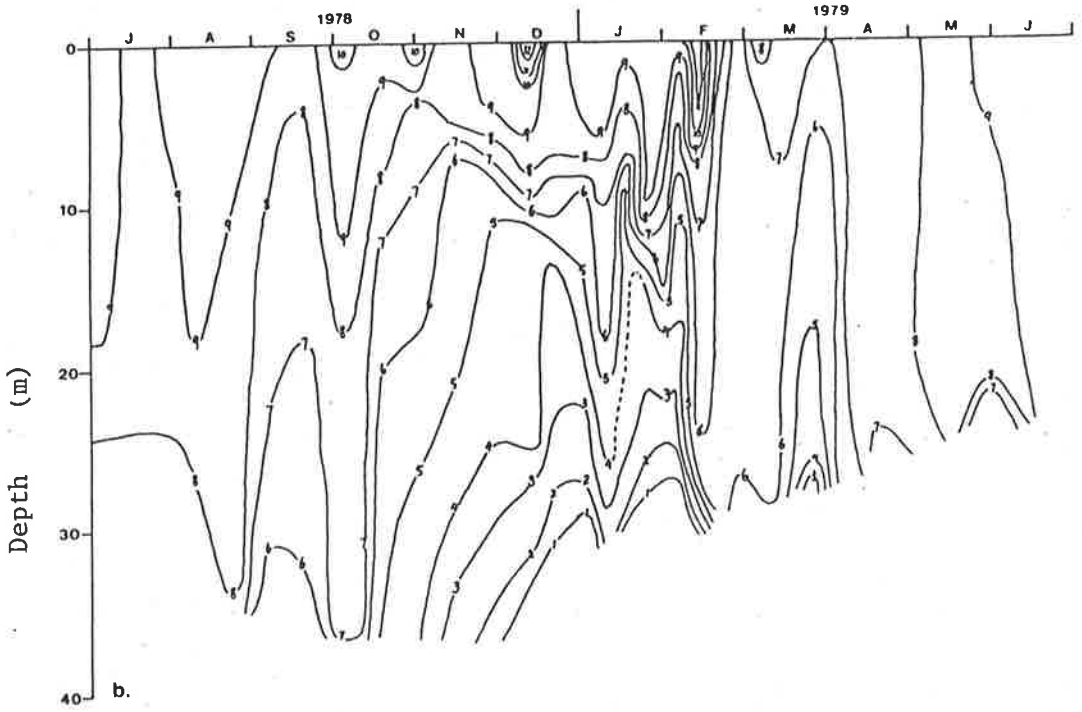
1978
1979
J
A
S
O
N
D
J
F
M
A
M
J
0
10
20
30
40
Depth (m)
b.

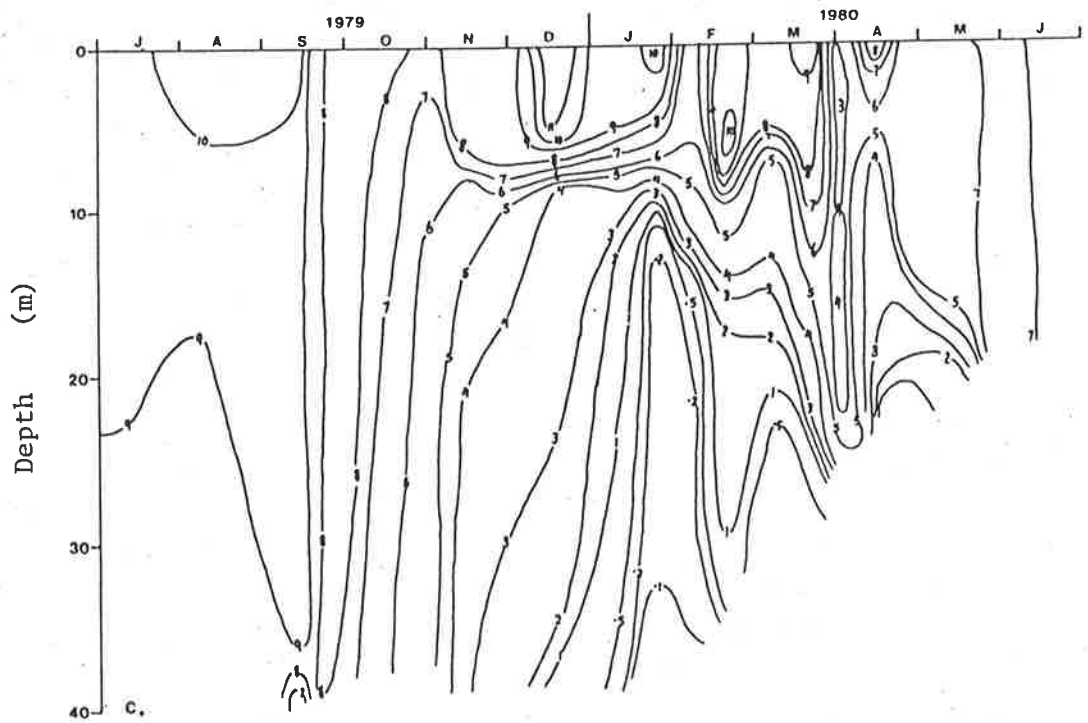
1979
1980
J
A
S
O
N
D
J
F
M
A
M
J
0
10
20
30
40
Depth (m)
c.

Fig. 4.7 (cont).

Fig. 4.8: a. Correlation between average total dissolved phosphorus ($\overline{TDP}$) and the $\overline{TN}$: $\overline{TP}$ ratio in 213 North Carolina lakes and reservoirs (●)(from Smith, unpublished), compared with the relationship between orthophosphate-P ($\overline{OP}$) and $\overline{TN}$: $\overline{TP}$ ratio for Mt Bold Reservoir (▲).

b. Correlation between the ratio of mean particulate-P to mean total-P ($\overline{PP}$: $\overline{TP}$) and the $\overline{TN}$: $\overline{TP}$ ratio in 213 North Carolina lakes and reservoirs compared with the relationship between $\overline{PP}$: $\overline{TP}$ and $\overline{TN}$: $\overline{TP}$ as calculated for Mt Bold Reservoir (▲).

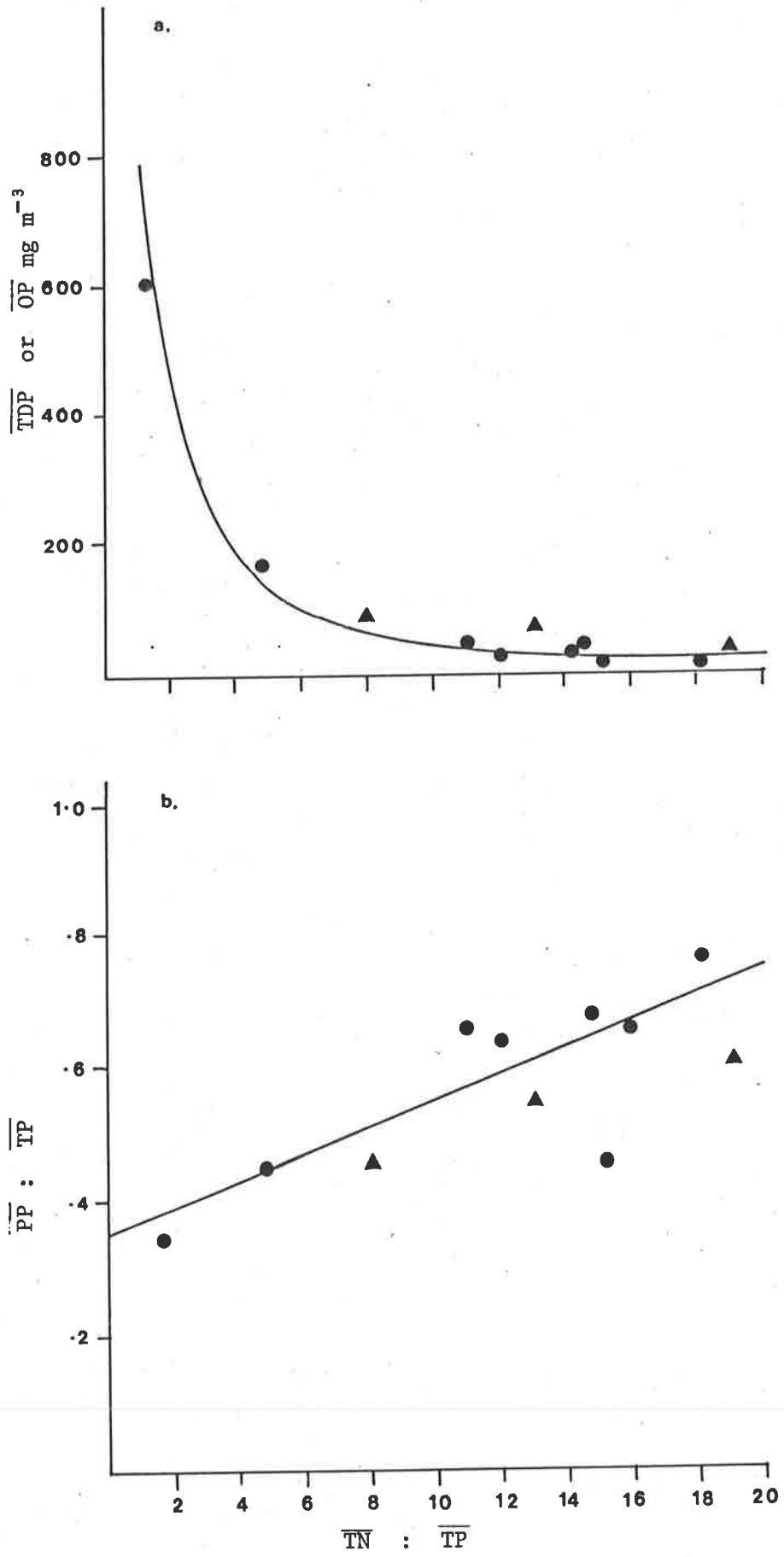
a.
800
600
400
200
$\overline{TDP}$ or $\overline{OP}$ mg m^{-3}
b.
1·0
·8
·6
·4
·2
$\overline{PP}$: $\overline{TP}$
2
4
6
8
10
12
14
16
18
20
$\overline{TN}$: $\overline{TP}$

Fig. 4.8:

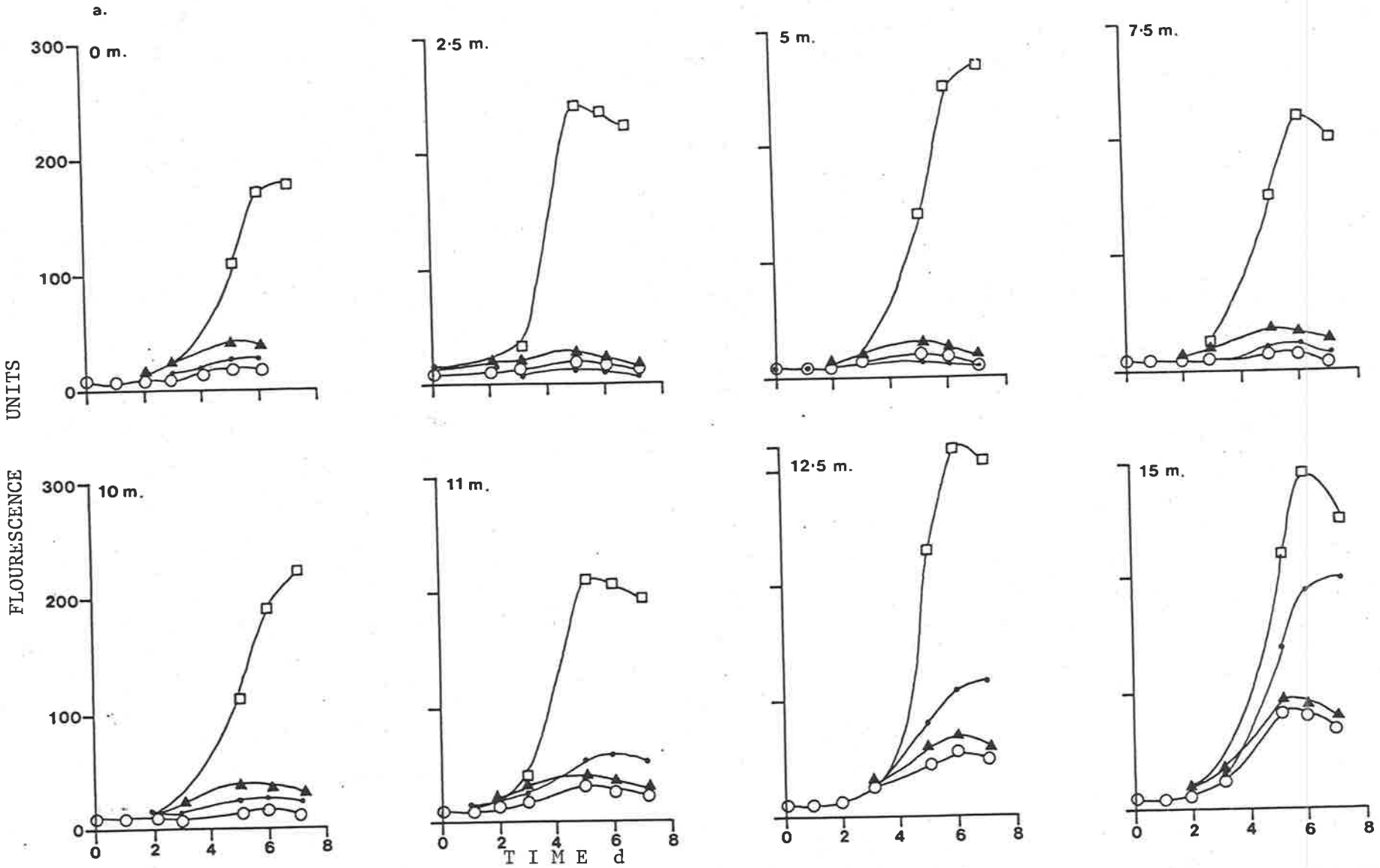

Fig. 4.9: Results of two bioassay experiments illustrating the variation in flourescence with time over the incubation period for control (0), +N (•), +P (▲) and N+P (□) flasks. (a) 16.1.80, (b) 18.6.80.

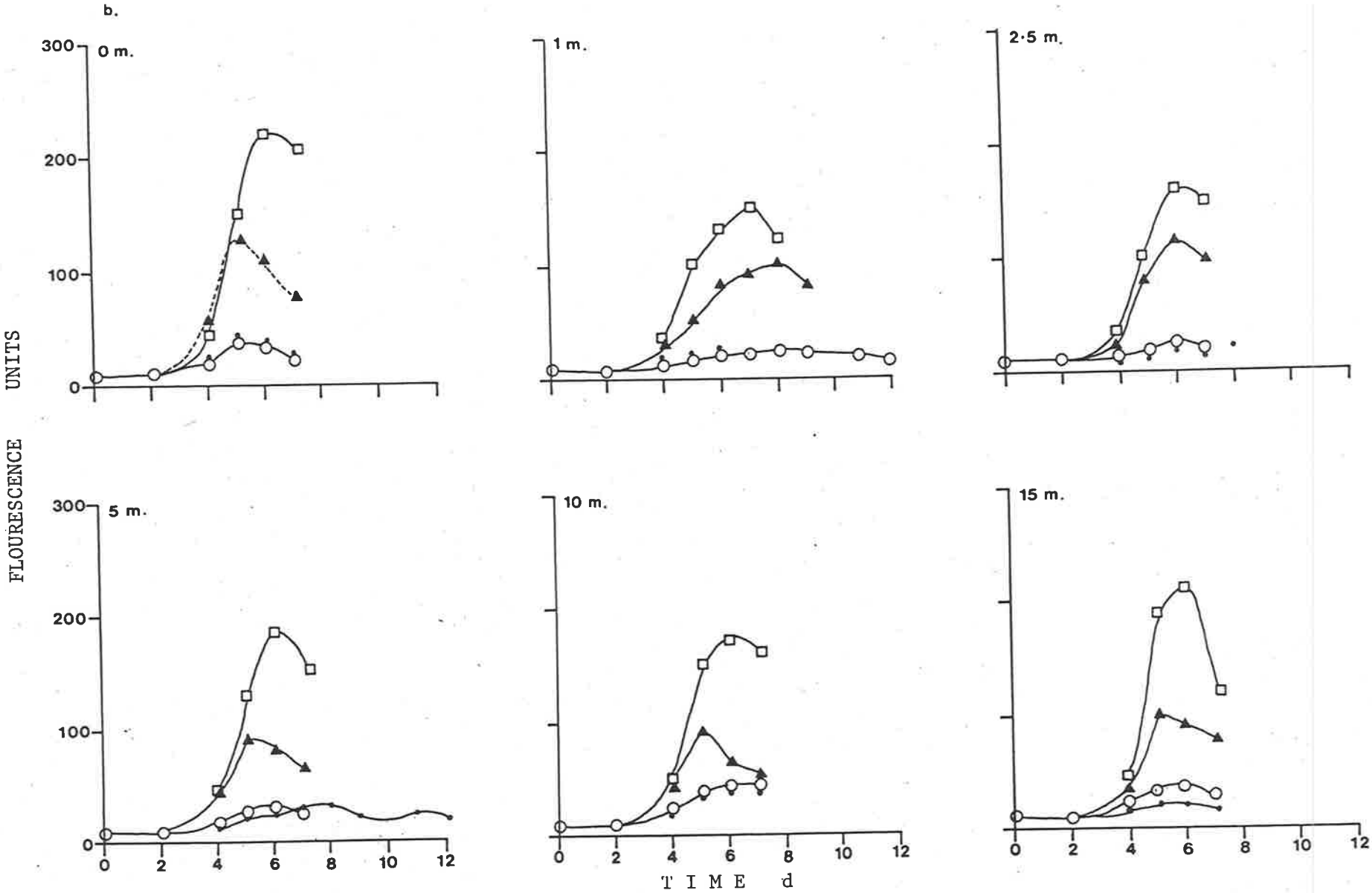
b.
0 m.
1 m.
2·5 m.
5 m.
10 m.
15 m.
300
200
100
0
UNITS
FLOURESCENCE
0
2
4
6
8
10
12
T I M E d

Fig. 4.9 (cont.)

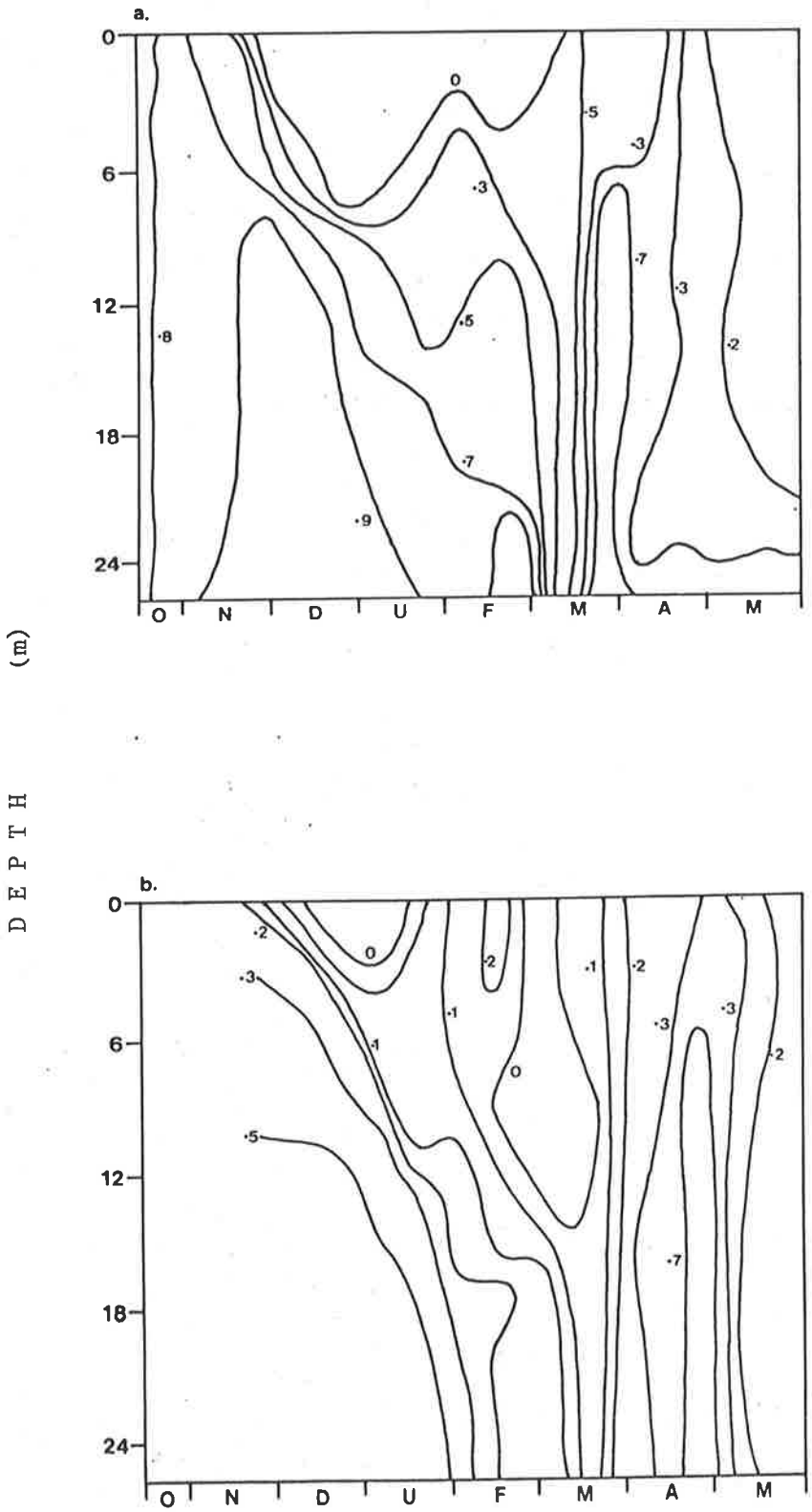

Fig. 4.10: Depth distribution of growth potential at the south sampling site as determined from bioassays.

(a) 1978-79

(b) 1979-80

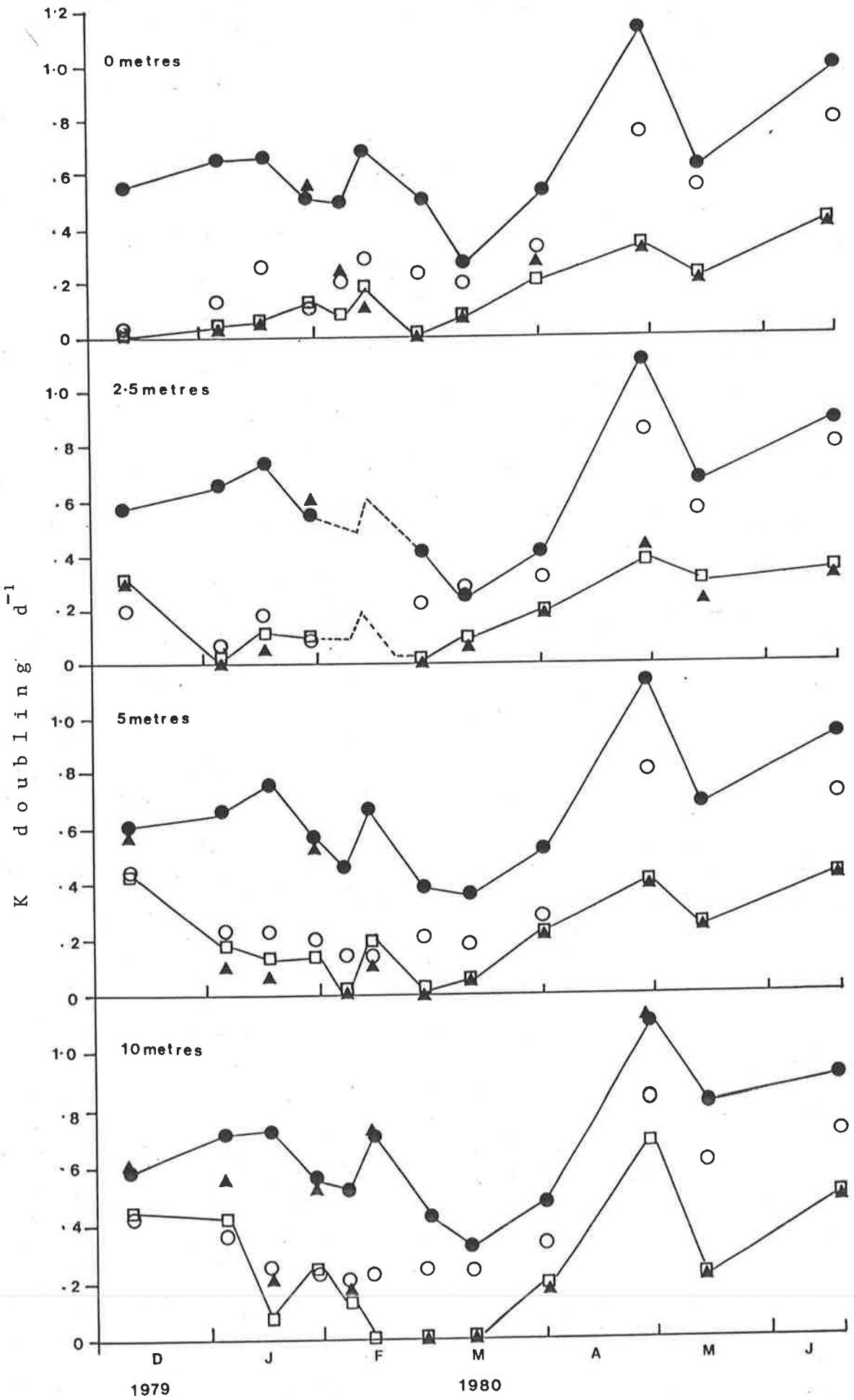

Fig. 4.11: Average growth rate (k) observed in bioassays for sample depths of 0, 2.5, 5, 10, 15, 20, 25 and 30 m; ● N+P, ○ +P, ▲ +N, □ control.

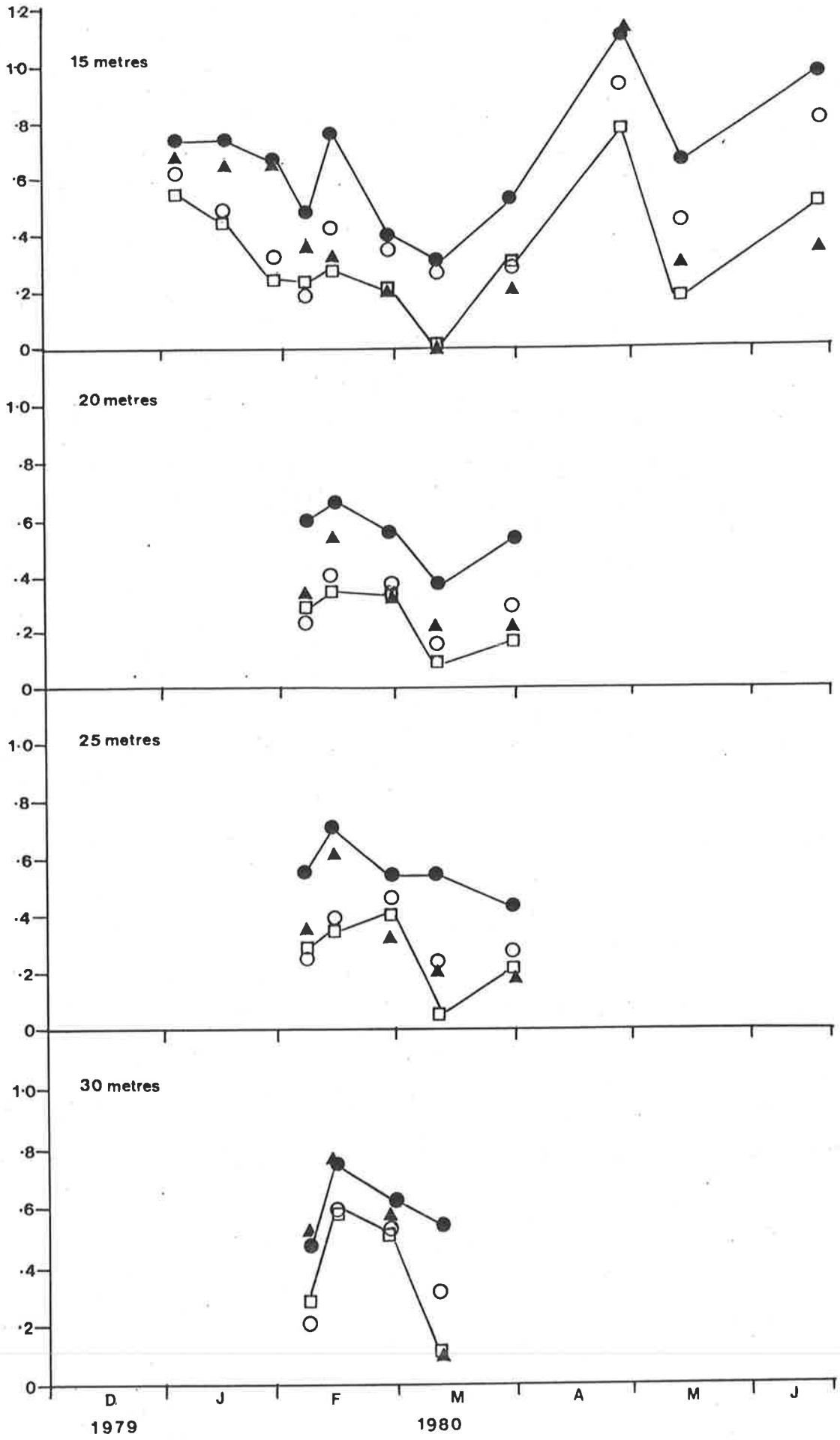
15 metres
20 metres
25 metres
30 metres
1·2
1·0
·8
·6
·4
·2
0
D
J
F
M
A
M
J
1979
1980

Fig. 4.11: (cont.)

Fig. 4.12: Seasonal variation in

a. ratio of inorganic-N to orthophosphate P (Δ) and total-N to total-P (■).

b. ratio of total-N to total-P (Δ) showing values when N and P appeared equally limiting in bioassays (●).

c. ratio of inorganic nitrogen to organic phosphorus (Δ , calculation described in text) showing values when N and P appeared equally limiting in bioassays. The critical level defined by Healey (1975) is shown (----).

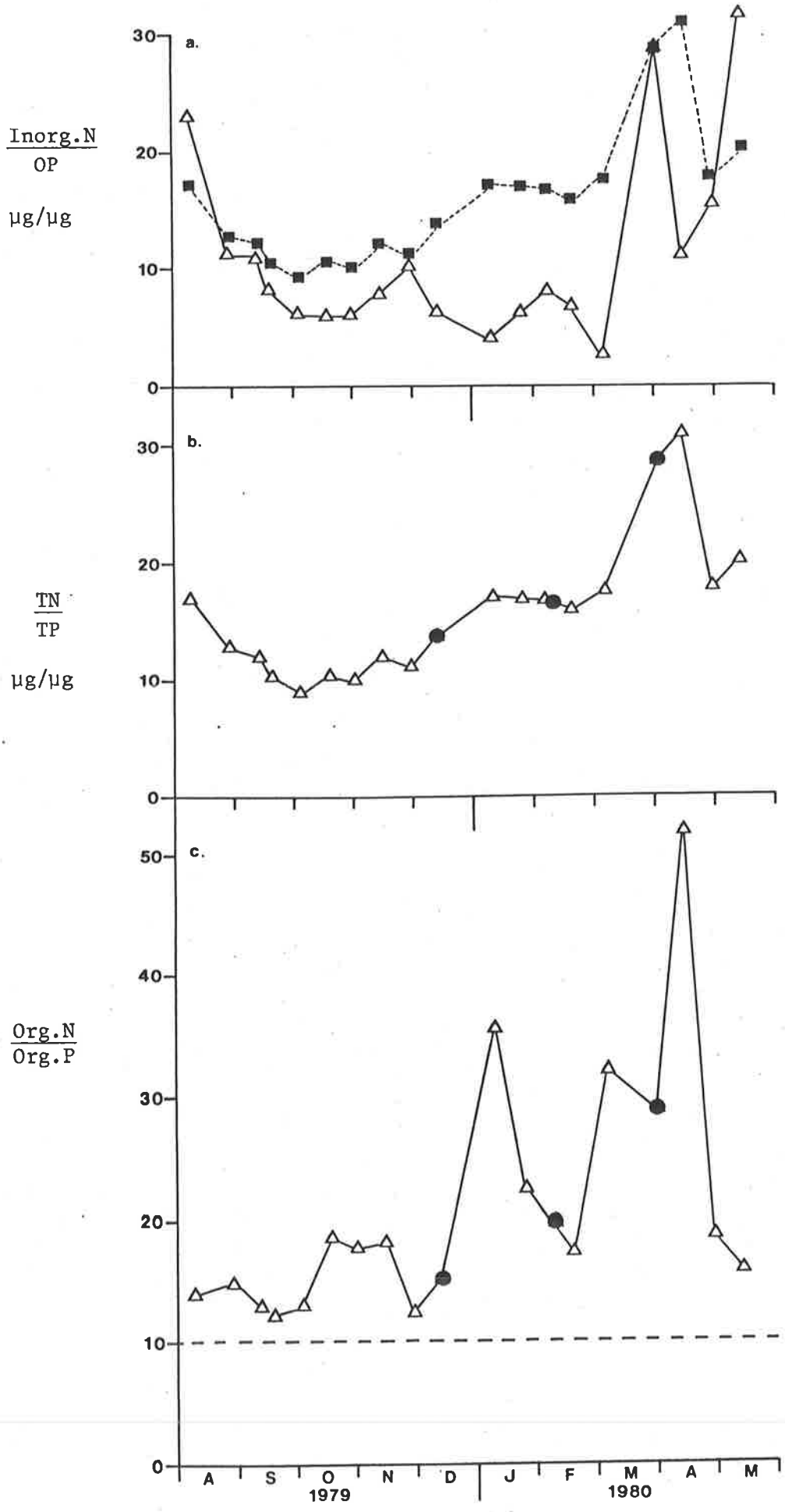
a.
Inorg.N
OP
µg/µg
30
20
10
0
b.
TN
TP
µg/µg
30
20
10
0
c.
Org.N
Org.P
50
40
30
20
10
0
A
S
O
N
D
J
F
M
A
M
1979
1980

Fig. 4.12:

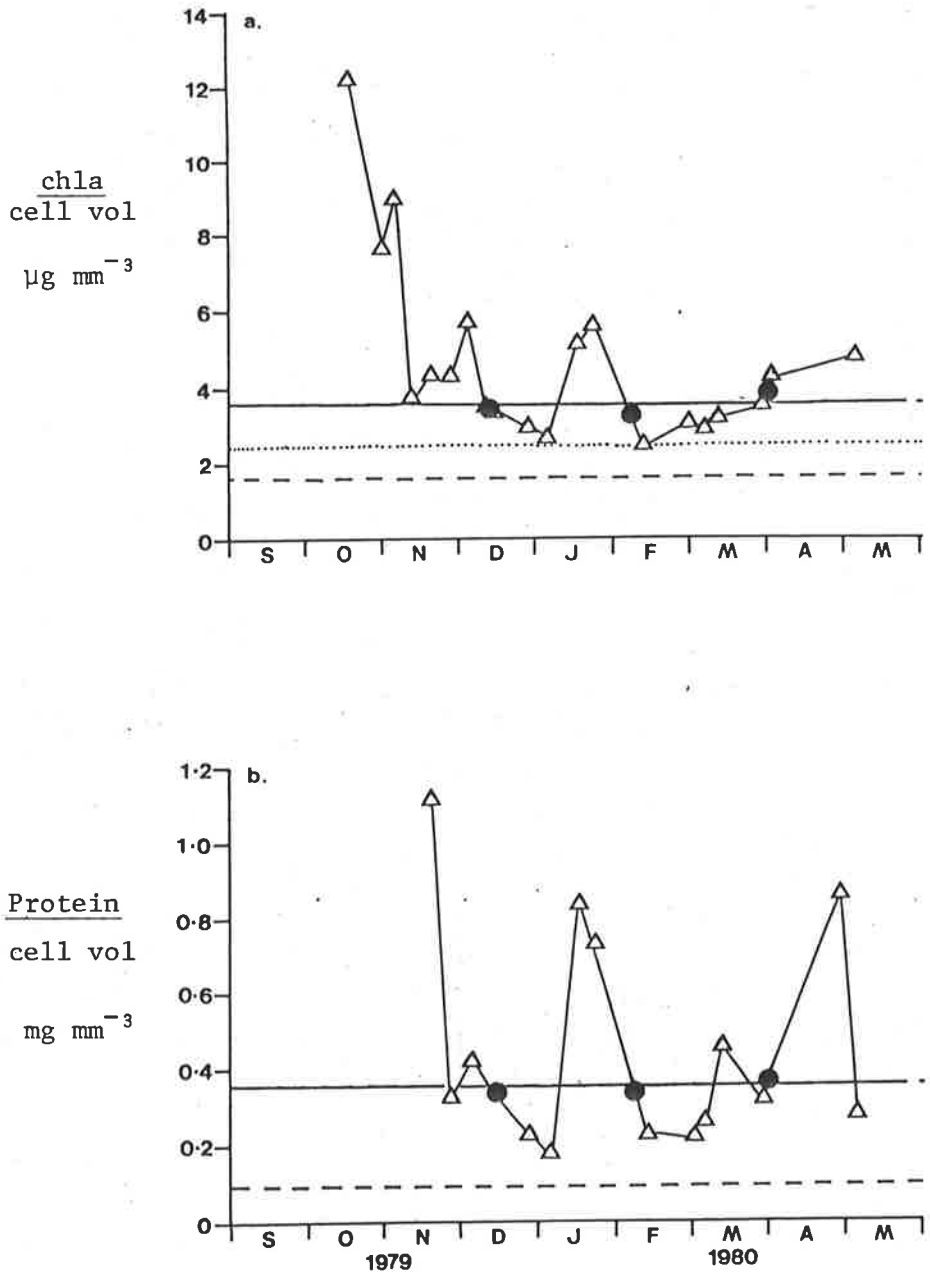

Fig. 4.13: Seasonal variation in

a. chlorophyll a to cell volume ratio (Δ) showing values when N and P appeared equally limiting (●) and the critical ratio suggested by these values (——). Critical ratios determined from Healey (1975, 1978) also are depicted (----,····).

b. protein to cell volume ratio (Δ). Other symbols as described in a. with a single critical level from Healey (1975)(----).

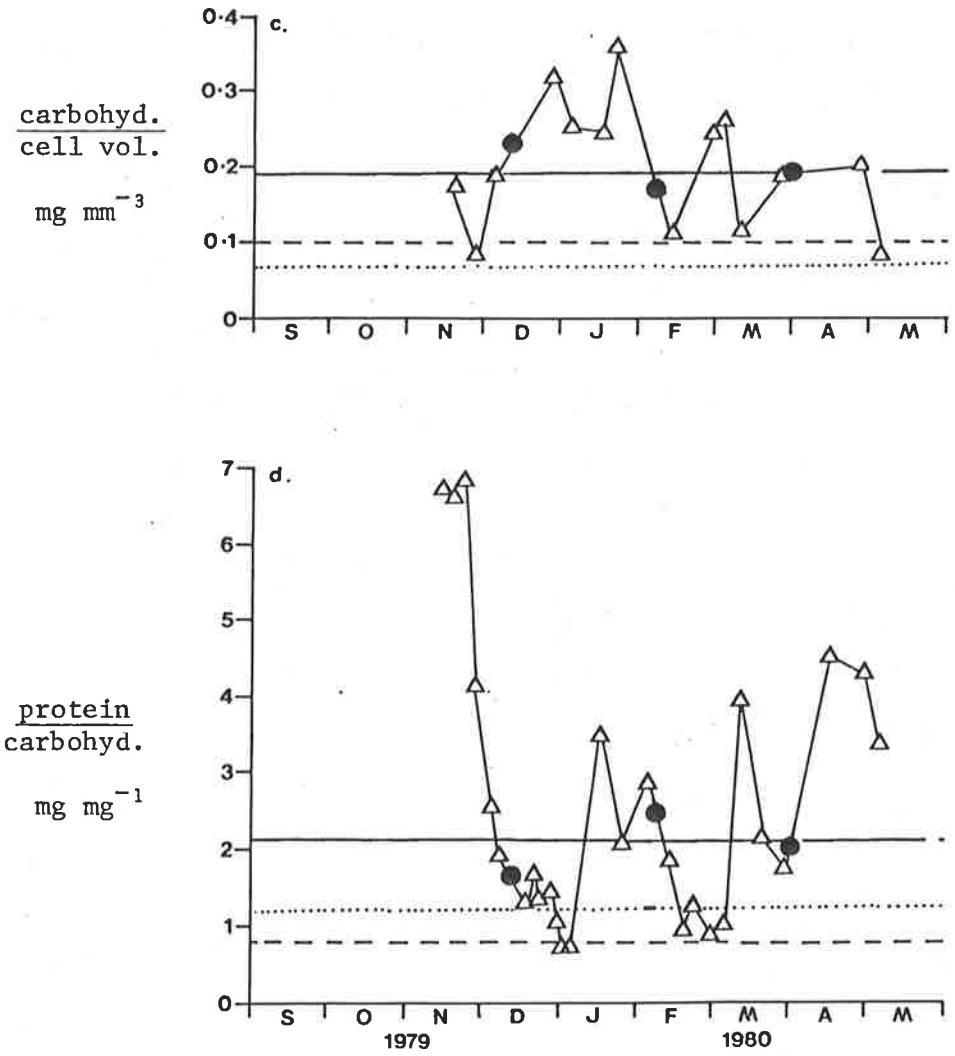

Fig. 4.13: (cont.)

c. carbohydrate to cell volume (Δ). Other symbols as described in a.

d. protein to carbohydrate (Δ). Other symbols as described in a.

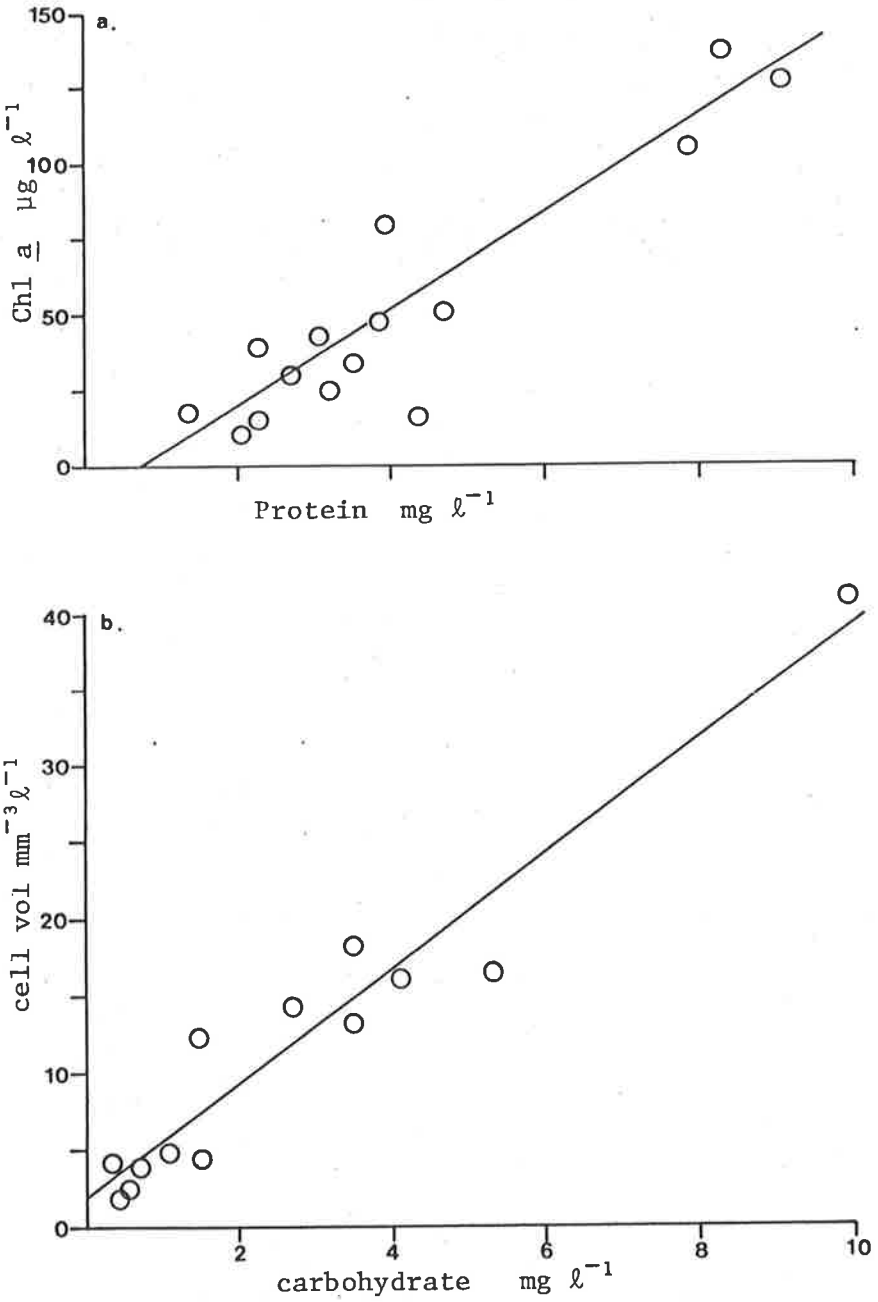

Fig. 4.14:

a. Correlation between the concentration of chlorophyll a and protein in integrated euphotic zone samples.

[Chl a]=16.22 Protein-12.32 r^2=0.91, n=15, intercept not significantly different from zero (P>0.05).

b. Correlation between total cell volume and carbohydrate concentration of integrated euphotic zone samples.
Cell volume= 3.71 carbohydrate + 2.14 r^2=0.92 n=15, intercept not significantly different from zero (P>0.05).

TABLE 4.1

Period	$\overline{PP}$	$\overline{OP}$	$\overline{TN}$	$\overline{TP}$	$\overline{PP}$:$\overline{TP}$	$\overline{TN}$:$\overline{TP}$	$\overline{b}$	Predicted $\overline{b}$ Smith 19-	Predicted $\overline{b}$ Equation (4.7)
1977-78	58.9	76.7	1132.3	135.7	0.43	8.3	12	39.3	32.6
1978-79	51.4	39.1	1678.8	90.5	0.57	18.6	10.8	35.9	25.9
1979-80	64.7	52.0	1539.0	124.1	0.52	12.4	33	43.3	33.7

Average Growing Season Concentrations ($\mu g\ \ell^{-1}$) of particulate phosphorus ($\overline{PP}$), orthophosphate phosphorus ($\overline{OP}$), total nitrogen ($\overline{TN}$), total phosphorus ($\overline{TP}$) and chlorophyll a ($\overline{b}$). Ratios are those used to calculate predicted $\overline{b}$, either from the equation of Smith (19-) (equation 4.6), or the modified equation for Mt. Bold Reservoir (equation 4.7).

TABLE 4.2

		Critical field value	Critical value from Healey (1975)
$\frac{\text{Chlorophyll a}}{\text{cell volume}}$	$(\frac{\mu g}{mm^3})$	3.6	2.5
$\frac{\text{Protein}}{\text{cell volume}}$	$(\frac{mg}{mm^3})$	0.36	0.1
$\frac{\text{Carbohydrate}}{\text{cell volume}}$	$(\frac{mg}{mm^3})$	0.19	0.075 - 0.1
$\frac{\text{Protein}}{\text{carbohydrate}}$	$(\frac{mg}{mg})$	2.2	0.8 - 1.2

A comparison of critical values for compositional indicators determined from culture work (Healey 1975) and directly in the field at Mt. Bold Reservoir. Healey's original values were converted from dry weight to cell volume basis assuming a specific gravity of 1.0 and wet wt:dry wt = 4.1 (Healey 1975).

PHYTOPLANKTON BIOMASS FLUCTUATIONS AND SEASONAL SUCCESSION

SEASONAL VARIATION IN PHYTOPLANKTON BIOMASS

5.0 Introduction

Large phytoplankton biomass fluctuations are commonly associated with major changes in the physical structure of the water column, which alter the average irradiance per cell and the nutrient regime (Riley 1942; Talling 1971; Round 1971; Lewis 1978*a*; Reynolds 1973*b*, 1980; Harris & Piccinin 1980). Despite the acknowledged importance of these physical events, little quantitative data is available to directly assess the relative significance of the various factors involved.

The water column of Mt Bold Reservoir annually undergoes large changes in both its physical and chemical nature (Chp. 3 & 4), providing an environment where the influence of these changes on phytoplankton biomass may be assessed.

5.1 General Patterns

Chlorophyll *a* concentration and total cell volume (Chp. 2) of integrated euphotic zone samples from 1978-79 and 1979-80 were significantly correlated within each season (Fig. 5.1 & 5.2), linear functions explaining over 90% of the variation. This allowed comparison of seasonal biomass patterns from changes in chlorophyll *a* concentration. However, slopes of the linear relationships varied significantly between seasons (Fig. 5.1 & 5.2, slopes significantly different $P < 0.001$; y-axis intercepts not significantly different $P > 0.05$) and precluded the use of chlorophyll *a* concentrations for biomass comparisons. Dersotová (1981) found similar between season and between lake variations.

Seasonal fluctuations in euphotic zone chlorophyll *a* concentrations did not follow a distinct recurring sequence (Fig. 4.1). This was partially the result of $CuSO_4$ treatment during 1977-78 and 1978-79, but was also a function of the marked physical and chemical variations typical of the reservoir, as demonstrated by the different biomass patterns of 1975-76 (Ganf 1980) and 1979-80 (Fig. 5.3 & 4.1) when $CuSO_4$ was not used. Despite differences between seasons common features were evident.

The simplest pattern occurred in 1975-76 (Fig. 5.3) and was similar to the classic pattern of temperate lakes (Round 1971; Kalff & Knoechel 1978) except with the spring biomass maximum shifted to early summer.

In general, low winter chlorophyll *a* concentrations ($< 5\mu g\ \ell^{-1}$) were followed by increasing concentrations throughout spring (Fig. 4.1). Initiation of the spring increase occurred in October of 1977 and 1979 (Fig. 5.4 and 5.6) but in early September of 1975 and 1978 (Fig. 5.3 & 5.5), coinciding precisely with reduction in mixing depth resulting from stratification of the water column (Fig. 3.14). This suggested that improved light conditions might be a major factor stimulating biomass accumulation. Similar observations for optically deep lakes and marine environments were made by Riley (1942), Pechlaner (1970), Talling (1971), Hitchcock and Smayda (1977), Paasche & Ostergren (1980).

Biomass typically reached a maximum in December (Fig. 5.3, 5.5 & 5.6), although during 1977-78 the maximum occurred notably later (Fig. 5.4). This was probably a result of increased turbulence as Murray River water entered the reservoir (Chp. 3).

In all years biomass declined during mid-summer. In 1977-78 and 1978-79 this was enhanced by $CuSO_4$ treatment shortly after the initial decrease in chlorophyll *a* concentration (Fig. 5.4 & 5.5).

In autumn chlorophyll *a* maximum generally occurred in March and April, concomitant with autumnal overturn. For example overturn occurred in late February of 1979 (Fig. 3.14b) resulting in an earlier autumn peak than 1980 when isothermal conditions were not attained until March (Fig. 3.14c).

5.2 The vernal biomass increase

The suggested correlation between initiation of the spring phytoplankton increase and improving irradiance was investigated using the average irradiance within the mixed zone as a measure of the mean irradiance received by a cell ($\bar{I}$). Riley (1957) suggested that $\bar{I}$ ($MJm^{-2}\ d^{-1}$) could be estimated from,

$$\bar{I} = \frac{I_o\ (1 - e^{-\varepsilon z_m})}{\varepsilon z_m} \qquad 5.1$$

where I_o is the average daily incoming irradiance for the week prior to the experimental data ($MJm^{-2}\ d^{-1}$), z_m the mixed depth (m) and ε the vertical extinction coefficient (ℓn units m^{-1}, see Chp. 3).

Realistic estimates of mixed depth could not be obtained for 1977 (see Chp. 3) and analysis was restricted to 1978 and 1979 .

Estimates of the variables in equation 5.1 for the periods 23/8/78 to 12/12/78 and 18/9/79 to 11/12/79 are given in Table 5.1 along with the calculated mean irradiance of the mixed layer ($\bar{I}$), and chlorophyll *a* concentrations. The increase in $\bar{I}$ over these periods resulted mainly from reduction in the mixed depth enhanced by increases

in incidence irradiance (Table 5.1).

In 1978 $\bar{I}$ increased exponentially from 0.109 to 1.573 $MJm^{-2}\,d^{-1}$, concomitant with an exponential increase in chlorophyll *a* concentration (Fig. 5.7*a*, Table 5.1). Fig. 5.8*a* shows that $\bar{I}$ and chlorophyll *a* concentration were linearly related up to an $\bar{I}$ value of 1.57 $MJm^{-2}\,d^{-1}$.

The rate of biomass accumulation was calculated by linear regression, using the logarithmic form of the exponential growth equation,

$$\ell n\, x_t = \ell n\, x_o + kt \qquad 5.2$$

where x_t is the chlorophyll *a* concentration at time t day, x_o the initial chlorophyll *a* concentration and k the specific rate of increase. As expected from the linear relationship between chlorophyll *a* concentration and $\bar{I}$ (Fig. 5.8*a*), the rate of biomass increase ($k = 0.047d^{-1}$, $r^2 = 0.90$) was statistically indistinguishable from the rate of increase in $\bar{I}$ ($k = 0.046d^{-1}$, $r^2 = 0.96$) calculated by replacing x_t and x_o in equation 5.2 with $\bar{I}_t$ and $\bar{I}_o$.

Due to inclement weather in 1979, persistent thermal stratification of the water column did not occur until late October (Fig. 3.14). Stratification then set in rapidly, accompanied by a marked increase in incident solar irradiance (Fig. 3.19). Consequently the mean irradiance of the mixed zone increased over a week from values less than 0.42 to 1.38MJ $m^{-2}\,d^{-1}$ (Fig. 5.7b; Table 5.1).

Prior to this increase chlorophyll *a* concentrations had fluctuated directly with $\bar{I}$ (Fig. 5.8b), but during the rapid change chlorophyll *a* accumulation lagged behind the mean light intensity. However, by the following week it had returned to expected levels (Fig. 5.8b).

The exponential rate of biomass accumulation (equation 5.2) between 17/10/79 and 12/11/79 was 0.06 d^{-1} (r^2 = 0.89, Fig. 5.9) while a similar calculation gave a value of 0.07 d^{-1} for the rate of $\bar{I}$ increase. Statistical analysis showed there was no significant difference between these values (slopes not significantly different, $P > 0.1$).

5.3. Midsummer biomass minimum

To assess the effect of epilimnetic nutrient depletion on mid-summer biomass minima, bioassays of water samples from selected depths were used to determine the growth potential of the water column. The techniques and results were discussed in Chapters 2 and 4.

The midsummer biomass decrease during 1979-80, and prior to $CuSO_4$ treatment in 1978-79, coincided with a reduction of growth potential in the euphotic zone (Fig. 4.10). The increased growth response from bioassay flasks spiked with nitrogen and phosphorus suggested that nutrient limitation, through its effect on growth rate, was a major determinant of the midsummer minima.

Further support for the role of nutrient limitation was afforded by the biomass variations of 1979-80. During this season the characteristics of early summer and autumn maxima were evident (Fig. 4.1), however an extra biomass peak was observed in February, and followed the period of increased nutrient availability demonstrated by bioassays and compositional indicators (Chp. 4). This response to a natural spiking of epilimnetic waters illustrated the significance of nutrient limitation.

The biomass decrease during late February and early March again coincided with decreased growth potential of the water column (Fig. 4.10).

5.4 Autumn biomass peak

Increased mixing during autumnal overturn resupplied nutrients to the euphotic zone as evidenced by increased growth in bioassay control flasks (Fig. 4.11). However extension of the mixed depth simultaneously resulted in a decline in the mean irradiance of the mixed zone ($\bar{I}$) (equation 5.1). The occurrence of the autumn maxima therefore appeared dependent on the relative significance of increased nutrient supply and reduced light availability.

PHYTOPLANKTON SEASONAL SUCCESSION

5.5 Introduction

The species which comprise the major proportion of the phytoplankton biomass of a lake are relatively few in number, and frequently appear in an annually recurring pattern (Round 1971; Reynolds 1980). This sequential change in dominant species is termed seasonal succession.

Lewis (1978*a*) devised an hypothetical time tract for the succession of major algal groups in tropical Lake Lanao. Unlike temperature lakes where the abrupt changes which initiate successional sequences usually relate to seasonal weather changes, in Lake Lanao frequent successional episodes were initiated during an annual cycle. At the class or division level the algal sequence within a complete episode was similar to the sequence frequently observed in temperate lakes, and qualitatively described some time ago (Pearsall 1932).

Reynolds (1980) resolved the periodicity of phytoplankton assemblages in several English lakes on the basis of two major variables, nutrient availability and column stability, though recognizing the possible action of other factors such as grazing. A qualitative "probability matrix" was constructed, which predicted the dominant algal group under varying conditions of the two variables. The marked similarity between this scheme and that for Lake Lanao (Lewis 1978*a*), suggests that successional sequences may well be subject to a relatively small number of controlling variables. The recognition of these driving factors will be facilitated by the comparison of similarities between lake systems. Mt Bold in the southern hemisphere offers such a comparison, partly on geographical grounds and partly because of its turbid nature.

The successional sequences in Mt Bold Reservoir during 1978-79 and 1979-80, were determined from the proportional contribution of species to total cell volume (Fig. 5.10 and 5.11, Table 5.2). As the specific taxonomic position of many of the algae is tentative, the discussion of seasonal periodicity is based in part on the class or division level. Since the major proportion of biomass is composed of a relatively few species at any one time, arguments based on one level of organization should be readily applicable to the other. Indeed it is at the higher levels of classification that similarities between successional sequences have been recognized (Lewis 1978*a*; Reynolds 1980).

5.6. General description of seasonal succession

To facilitate comparison between the two seasons, and to assist in following the verbal description, dominant and co-dominant species have been listed in order of occurrence (Table 5.3).

Two cryptonomad species dominated the initial biomass increase of 1978-79 (Fig. 5.10; Table 5.3). In mid-October these species were supplanted by *Ceratium hirundinella* (O.F. Muell) Dujardin, and *Cyclotella meneghiniana* Kuetzing, which co-dominated briefly before being replaced by *Melosira* sp.

This large diatom occurred in only one sample (Fig. 5.10) despite weekly collecting, demonstrating the rapidity with which species succession may occur. It is evident that where possible samples should be obtained more frequently, particularly in the early stages of a succesional sequence.

Trachelomonas spp. immediately succeeded the diatom (Fig. 5.10) while co-dominance by *Ceratium* and *Microcystis aeruginosa* Kuetzing followed in November, with *Anabaena spiroides* Klebahn. becoming a third co-dominant in early December (Table 5.3).

The mid-December application of $CuSO_4$ removed all species from the euphotic zone, but within two weeks *Microcystis* biomass levels had surpassed those prior to dosing, and except for a brief *Ceratium* peak during early February, dominated until autumnal overturn.

Trachelomonas spp. dominated the overturn period with *Melosira varians* C. Agardh as co-dominant.

Two green algae which formed only small components of the total biomass but were at times relatively numerous (Fig. 5.5), were *Dictyosphaerium pulchellum* Wood which appeared in late November and *Oocystis parva* West & West, which comprised 25% of total volume shortly after $CuSO_4$ treatment (Fig. 5.10).

The desmid, *Closterium* sp. occurred in low numbers early in the sequence (< 4 cells ml^{-1}) and in late August, prior to biomass increases, made up almost 100% of the cell volume. This was considered dominance by default rather than active growth and precluded from the sequence.

At the start of the 1979-80 vernal biomass increase *Cryptomonas* spp. and *Trachelomonas* spp. co-dominated (Fig. 5.11; Table 5.3). These species were followed by *Ceratium hirundinella*, which then co-dominated successively with *Cyclotella meneghiniana* and *Melosira varians*. In early December *Microcystis aeruginosa* and *Anabaena spiroides* briefly formed co-dominants with *Ceratium*, but by January *Microcystis* accounted for > 90% of the total biomass and continued to do so until May.

A decrease in *Microcystis* cell numbers during January (Fig. 5.6), concomitant with nutrient limitation (Fig. 4.10b) increased the percentage contribution of *Anabaena* to total cell volume (Fig. 5.11) although cell numbers of *Anabaena* did not alter (Fig. 5.6).

Following the influx of nutrients in late January (Cht. 4), *Microcystis* cell concentrations increased to the maximum observed value, but then declined again during early March, when bioassay results indicated further nutrient depletion of the epilomnion (Fig. 4.10b).

The brief increase in *Microcystis* biomass which occurred at autumnal overturn was not followed by the rapid population decline observed in 1978-89 (Fig. 5.5 & 5.6). Instead the population persisted until May, then decreased rapidly resulting in dominance by *Trachelomonas* sp.

5.7. Succession rate

The sequential listing of dominant species (Table 5.3) illustrated the direction of the successional sequence, but provided no quantitative data on the succession rate. Furthermore the selection of "representative" examples of species shifts was subjective.

Lewis (1978*b*) formulated an index of succession rate based on the changes in abundance of individual species. The variable was termed the summed difference (SD) index, and estimated over a short time interval as;

$$SD = \frac{\Sigma_i \left| [b_i(t_1)/B(t_i)] - [b_i(t_2)/B(t_1)] \right|}{t_2 - t_1} \qquad 5.3$$

where $b_i(t)$ is the abundance of the ith species, and B(t) the community size at time t. The index provides a measure of relative community stability, and can be used to identify critical periods of structural change (Reynolds 1980).

Cell volume measurements were used to estimate abundance of the major species in Mt Bold Reservoir over the two seasons 1978-79 and 1979-80, and the summed difference index calculated for each sampling interval (Table 5.4, Fig. 5.12). Periods of rapid change in community structure appeared as peaks (Fig. 5.12), usually exceeding 0.1 d^{-1}. Following the precedent of Reynolds (1980) this level is taken as indicative of a significant change in species composition and the occurrence of such peaks used to objectively partition the successional sequence.

The major shifts in population composition recognized by this approach may be compared with the sequential listings (Table 5.3) which have been numbered in accordance with the numerical notation used in Fig. 5.12. The correspondence between sequences was very close with only two major disparities. In 1978-79 the SD index indicated that a change from 87% Trachelomonads, 7% *Ceratium* (Group 4 Table 5.3) to 49% Trachelomonads, 29% *Ceratium*, 17% cryptomonads was significant whereas this had not been included in the sequential listing. However the more important disparity was in the succeeding change to 53% *Microcystis*, 18% *Ceratium*, 11% Cryptomonads. This obvious species shift was included in the sequential listing (Table 5.3, Group Z), but did not appear significant by the SD index (Table 5.4, 31/10-21/11/78, SD = 0.067, Fig. 5.12a). The cause of this discrepancy was the three week period between the two samples which resulted in an incorrect measure of succession rate (Reynolds 1980).

Similarly the rapid change in percentage contribution of *Anabaena* in January 1980 (Fig. 5.12b, Table 5.4, 4/1-16/1/80) might well have yielded a significant SD value if the sampling period had been less than twelve days.

5.8. Environmental change and succession rate

As succession is a response to environmental change, rate of succession should be related statistically to rate of environmental change (Jassby & Goldman 1974; Lewis 1978*b*).

The controlling environmental factors may be divided into mechanisms affecting growth or loss rate (Kalff & Knoechel 1978), the balance of these determining a species success, and population composition.

Preceding sections have demonstrated the particular importance of two growth control factors. The mean irradiance of the mixed zone ($\bar{I}$) which determined the increase of biomass during the initial onset of thermal stratification (Fig. 5.7; 5.8) and nutrient availability which bioassay results suggested controlled growth throughout the stratified period (Chp. 4).

In the following analysis attrition rates were not considered separately, and consequently those independent of the variation in growth control factors were assumed to have a small effect on the rate of biomass change. Accepting this simplifying assumption, succession rate should be related to the rate of change of resource supply, either irradiance when it is the controlling variable, or nutrient concentration.

The mean irradiance of the mixed zone, $\bar{I}$ [equation (5.1)] was used to quantify the light regime, and for the period when irradiance was a major determinant of net growth rate (12/9/78-24/10/78, Table 5.5 Fig. 5.7), $\bar{I}$ was significantly correlated with the SD measure of succession rate (Fig. 5.13*a*). Unfortunately few data points were available for the period of rapid increase in $\bar{I}$ during 1979-80, and its effect on succession rate could not be quantitatively assessed.

In Chapter 4 it was shown that during the stratified period of 1979-80, compositional indicators varied in response to changes in the nutrient regime. Of the compositional measures used (Fig. 4.13) protein and carbohydrate related most directly to the phytoplankton (Fig. 4.14) and were least subjective (cf. ratios on cell volume

basis), and provides an estimate of the growth potential of the population (Stone, unpublished thesis). These attributes suggest that the ratio may be a useful index of nutrient supply.

During the period when bioassays indicated nutrient limitation (7/12/79-5/3/80, Fig. 4.10*b*), succession rate and the protein - carbohydrate ratio were significantly correlated (Table 5.6; Fig. 5.13*b*). The data point for 22/1-13/2/80 (Table 5.6) were precluded from the correlation due to the particularly long period between samples.

5.9. Discussion

Attempts to assess the significance of the improving vernal light regime to the onset of biomass increase, have focussed largely on the relationship between photosynthesis, incident irradiance, respiration and mixing depth (Talling 1971; Steel 1973). Although theoretically sound, technical problems in the application of these models have resulted in disparity between predicted and observed periods of growth (Jewson 1976; Jones 1977*c*; Ganf 1980; Chapter 6).

In contrast only limited attention has been paid to direct relationships between the effective light regime and net observed growth.

Riley (1957, 1967) demonstrated that initiation of spring diatom blooms in coastal estuaries was dependent on a critical level of the mean irradiance for the mixed zone ($\bar{I}$) of ca. 1.7 MJ $m^{-2}d^{-1}$ (40 gcal. $cm^{-2}d^{-1}$). Similar critical values have subsequently been reported from various marine locations (Barlow 1958; Gieskes & Kraay 1975; Hitchcock & Smayda 1977).

The data for Mt Bold Reservoir demonstrated that initiation of the vernal biomass increase resulted from a continued improvement in the mean irradiance of the mixed zone ($\bar{I}$, Fig. 5.7 & 5.8). Chlorophyll *a* concentration was directly dependent on mean irradiance up to a value of ca. 1.6 MJ $m^{-2}d^{-1}$, and the rapidity with which this value was achieved determined the initial rate of chlorophyll *a* increase. Once $\bar{I}$ had attained 1.6 MJ $m^{-2}d^{-1}$ variations in chlorophyll *a* concentration were independent of further increases in $\bar{I}$ (Table 5.1, Fig. 5.7), indicating that the value represented a critical mean irradiance at which light ceased to limit biomass accumulation. This suggestion initially appears contentious. Such a critical irradiance value would imply that with an increase in chlorophyll *a* concentration, the irradiance available per unit chlorophyll *a* would decrease, assuming Z_m and I_o remained constant (equation 5.1). Under these conditions it seems unlikely that changes in biomass could be independent of the mean irradiance. However it is shown later (Chp. 6, Discussion) that equation 5.1 is closely allied to the equation calculating the mean irradiance absorbed per unit chlorophyll *a* (equation 6.19a), and that under certain conditions changes in $\bar{I}$ will be proportional to changes in the mean chlorophyll absorption. The critical value can therefore be interpreted as a critical level of light absorption per unit chlorophyll *a*.

Following attainment of the critical $\bar{I}$ value in 1979, chlorophyll *a* concentrations immediately increased above those expected from the spring relationship between chlorophyll *a* and $\bar{I}$ (Fig. 5.7b). However in 1978, chlorophyll *a* concentration fell following the attainment of the critical $\bar{I}$ value and did not increase for several

weeks (Fig. 5.7*a*). It may be postulated that this delay in biomass increase, despite the sufficient light conditions, resulted from a further restriction on the population. Nutrients were not particularly limiting at this time, as demonstrated by bioassay data (Fig. 4.10*a*) and although alternative factors may be suggested grazing pressure would explain the delay. Unfortunately data are not available to assess this hypothesis.

The critical value of 1.6 MJ $m^{-2}d^{-1}$ suggested from the present data is similar to that found necessary by Riley (1967) and Hitchcock & Smayda (1977) to initiate diatom blooms. Persistent increase in diatom biomass, particularly *Cyclotella meneghiniana,* was only observed in Mt Bold Reservoir when the mean irradiance of the mixed zone approached the critical value (Fig. 5.5 & 5.6).

Reynolds (1972, 1973*b*) estimated the effective light regime from the product of daylength and the fraction of the isothermal volume illuminated. Over several seasons increases in *Asterionella formosa* and *Fragillaria crotonensis* coincided with attainment of a 6.4h day^{-1} mean exposure period. The value of 1.6 MJ $m^{-2}d^{-1}$ from Mt Bold Reservoir represents a mean exposure of ca. 4.4 h day^{-1}, however without knowledge of the incident irradiance for the lakes studied by Reynolds, the values cannot be directly compared.

The biomass peak which followed the initiation of spring growth in 1979-80 (Fig. 4.1) reduced the mean irradiance of the mixed zone, $\bar{I}$ to 0.919 MJ $m^{-2}d^{-1}$. Accepting 1.6 MJ $m^{-2}d^{-1}$ as the critical value determining the onset of light limitation, the oscillations in biomass following this peak (Fig. 4.1) were related to accompanying variations in the mean irradiance (Table 5.1). However, the large mid-summer biomass

decline occurred despite $\bar{I}$ values in excess of the critical level (e.g. 16/1/80 $\bar{I}$ = 2.43) implying the action of a further limiting factor, which bioassay results suggested was nutrients.

The critical value of $\bar{I}$ was used to predict the autumn mixing depth resulting in light limitation. An average incoming irradiance (I_o) of 18 MJ $m^{-2}d^{-1}$ (Fig. 3.19), and an average extinction coefficient (ε) of 2.0 ℓn units m^{-1} (Fig. 3.4) were assumed for the autumn period. Substitution of these values into equation 5.1 indicated that a mixing depth of ca. 6m would result in light limitation.

Despite this requirement of a relatively shallow mixing zone, biomass peaks of *Microcystis* appeared in March and May of 1980 although autumnal overturn had occurred in early March (Fig. 3.16). Two factors apparently contributed to this anomalous situation, the reappearance of small temperature gradients in surface layers during the day, even though the reservoir as a whole was cooling, and the buoyancy of *Microcystis* cells. The stable surface layers enabled the buoyant *Microcystis* to remain in the upper layers of the water column, minimizing the decrease in the mean irradiance encountered by the cells. This situation contrasted with the autumn of 1979 when the water column remained completely isothermal following overturn, and the *Microcystis* population declined immediately (Fig. 5.5).

As a result of the rapid increase in $\bar{I}$ during 1979-80, all major species commenced growth within a two week period (Fig. 5.6). Net growth rates, calculated from changes in cell number during the initial increase in early November [equation (5.2)] were not

significantly different ($P > 0.05$, Table 5.7). The mean doubling rate for all species was ca. 0.3 day^{-1}. The similarity of growth rates suggested that final dominance by blue-green algae was most likely a result of decreased attrition rates (Knoechel & Kalff 1975), a view supported by the rapid decline in some of the competing species e.g. *Cyclotella meneghiniana* (Fig. 5.6).

Similarities between species sequences of 1978-89 and 1979-80 were evident from the sequential listings (Table 5.3). In both seasons cryptomonads played a dominant role in the initial biomass increase, a position analogous to that observed by Lewis (1978*a*) and Reynolds (1980).

The early appearance of the dinoflagellate *Ceratium hirundinella* as a dominant, contrasted sharply with the successional sequences depicted by Lewis (1978) and Reynolds (1980). More in accord with these schemes was the occurrence late in the 1979 sequence of a *Ceratium* peak coincident with a decrease in *Microcystis* biomass (Fig. 5.10). The general successional pattern which followed the cryptomonad - *Ceratium* suite was similar in both seasons, moving from diatoms to blue-greens to trachelomonads. The positions occupied by diatoms and blue-green algae were similar to those described by Lewis (1978*a*) and Reynolds (1980).

A noticeable absence from the successional sequence was a period of dominance by green algae (Lewis 1978*a*). Members of this group were generally observed in the period overlapping, or following diatom dominance (Table 5.3, Fig. 5.5), however only *Dictyosphaerium pulchellum* attained any degree of significance during this period (Table 5.3).

Lewis (1978*b*) investigated the rate of succession in Lake Lanao, and used the absolute change in biomass and primary production as bioassays of the rate of change of resource supply to the phytoplankton community. Both parameters were significantly correlated with the SD index of succession rate, and their relative contributions to variation in succession rate determined by multiple linear regression.

To provide insight into the effect of specific mechanisms on succession rate, analysis must deal with specific measures of resource supply, rather than parameters describing the summed result from the interplay of several factors. The difficulty is the intractability of numerically assessing variables determining growth and loss rates.

The mean irradiance of the mixed zone ($\bar{I}$) provided a measure of the effective light regime which correlated with biomass increases up to a crifical value of 1.6 MJ $m^{-2}d^{-1}$. During the period when $\bar{I}$ appeared as the major determinant of biomass fluctuations (12/9/78-24/10/78, Table 5.5) it was significantly correlated with the SD index of succession rate (Fig. 5.13*a*). The relationship indicated that succession rate increased as the light regime improved.

Following the establishment of thermal stratification nutrients were progressively depleted from the epilimnion, resulting in a decrease in the protein-carbohydrate ratio (Chp. 4, Fig. 4.13). During the period when bioassays indicated a degree of nutrient limitation (7/12/79-5/3/80) (Fig. 4.11) the SD index was significantly correlated with the protein to carbohydrate ratio (Fig. 5.13*b*).

The relationship indicated that succession rate was high when the protein-carbohydrate ratio was high, but decreased when the nutrient supply became less suitable and caused a decline in the protein - carbohydrate ratio.

Although attention has centred on factors controlling growth, a similar analysis may be applied if loss mechanisms can be numerically assessed. Lewis (1978*b*) estimated the significance of grazing simply from grazer biomass. Although somewhat unrealistic a significant correlation with the SD index of succession rate was obtained.

A second major loss factor of particular significance following increased thermal stratification of the water column, is sedimentation (Knoechel & Kalff 1975; Smayda 1980). Although sinking is dependent on water turbulence, cellular density and size may provide a sufficient index of relative sinking rates to assess the significance of this loss to species succession. Further discussion of this aspect will be continued in Chapter 8 where a technique for measuring cellular density is described.

It appeared from the present analysis that variations in available light and nutrients could explain a large proportion of the change in succession rate.

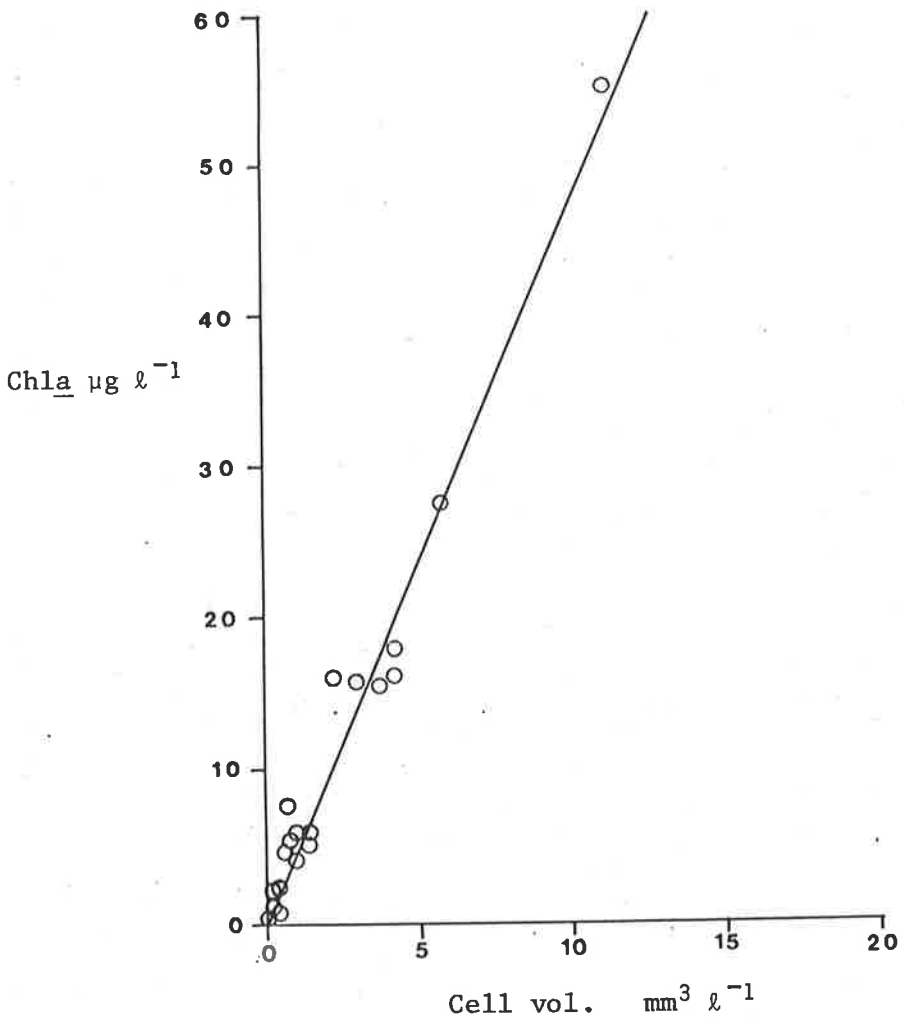

Fig. 5.1: Correlation between chlorophyll a concentration and cell volume for integrated euphotic zone samples from 1978-79. [chla] = 1.069+4.66 [cell volume], r^2=0.97, n=19.

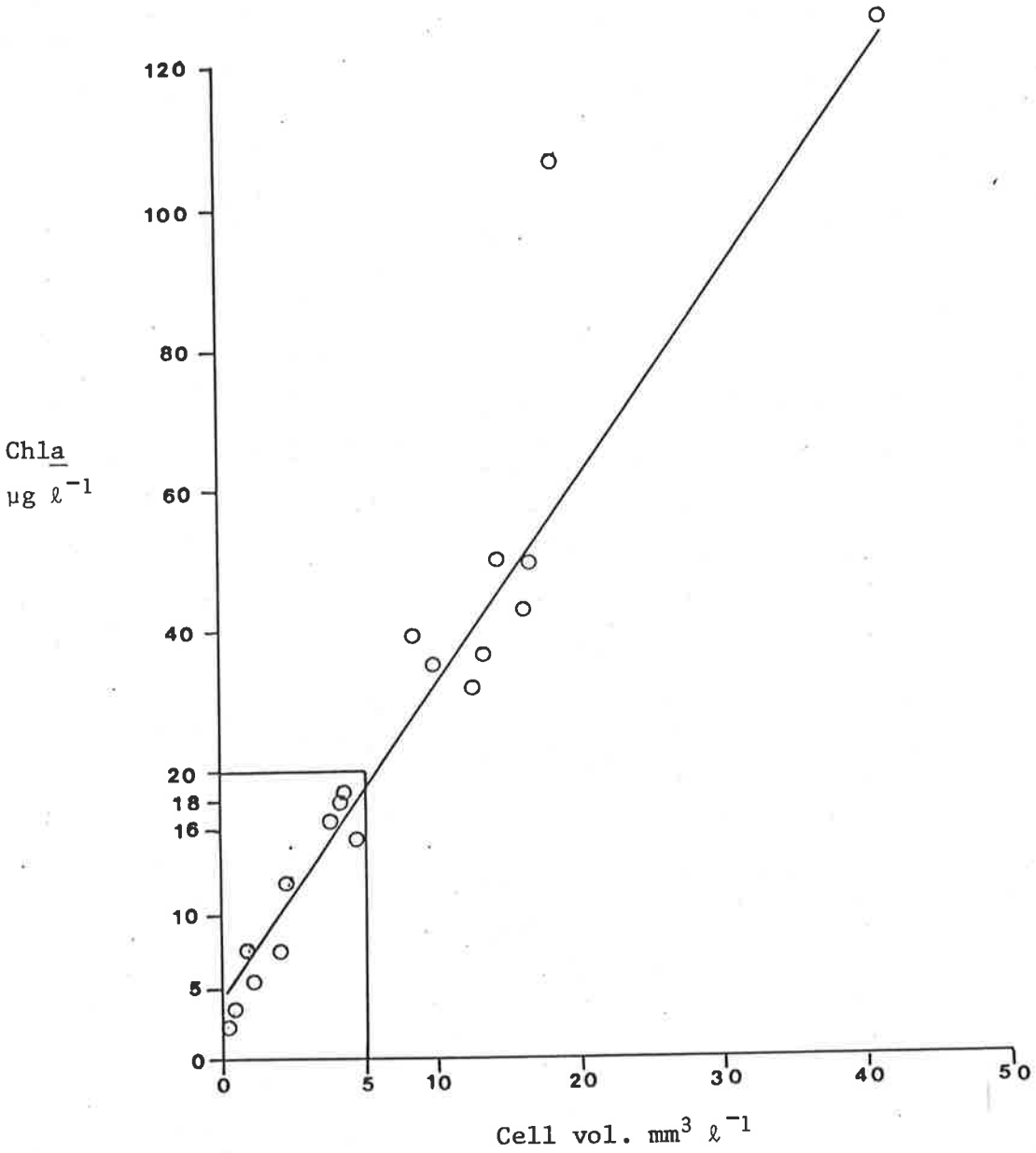

Fig. 5.2: Correlation between chlorophyll a concentration and cell volume for integrated euphotic zone samples from 1979-80. [chla] = 3.43+2.95 [cell volume], r^2=0.98, n=18.

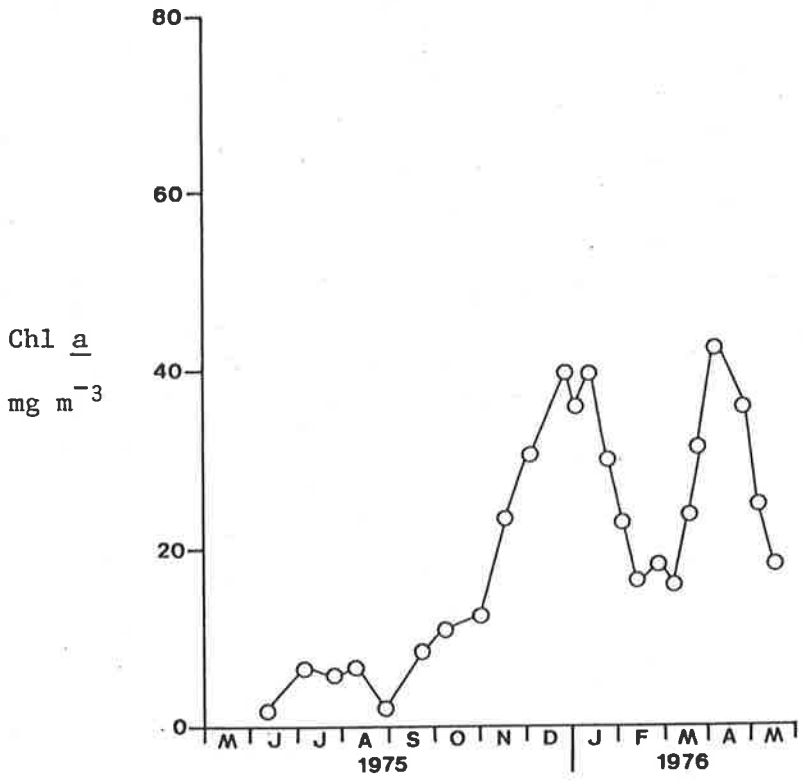

Fig. 5.3: Seasonal variation in chlorophyll a concentration at the south sampling site 1975-76.

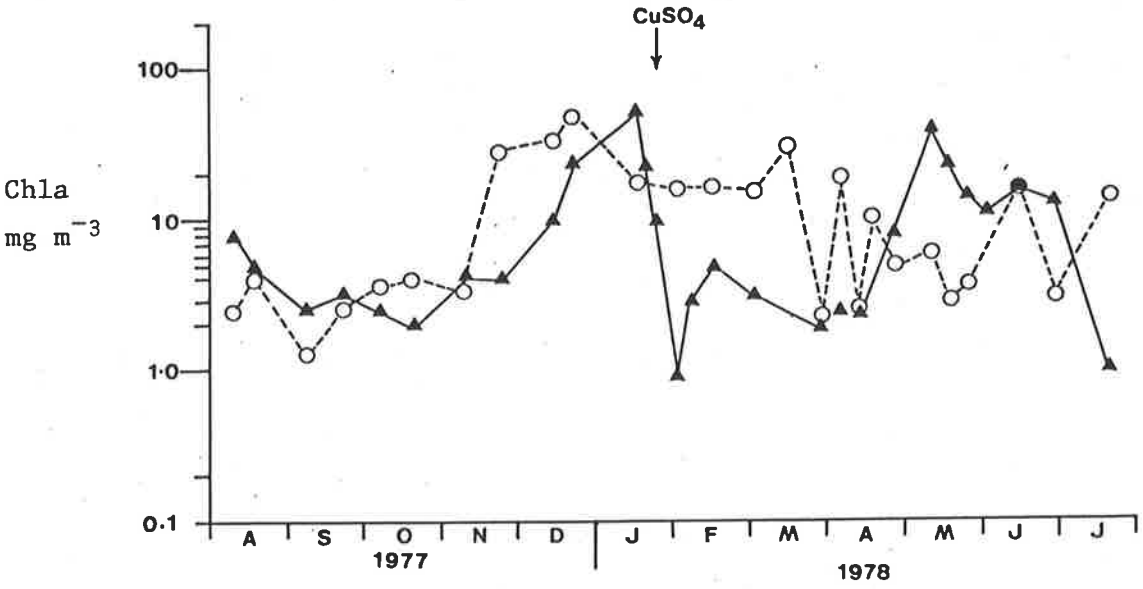

Fig. 5.4: Semi-logarithmic plot of the seasonal variation in chlorophyll a concentration for 1977-78 at the south (▲) and north (o) sampling sites. Arrow denotes $CuSO_4$ treatment of reservoir.

Fig. 5.5: Semi logarithmic plots of the seasonal variation in

a. chlorophyll a concentration at the south (△) and north (○) sampling sites.

b. cell numbers at the south sampling site, of *Cyclotella* (■), *Trachelomonas* (●), *Anabaena* (□), *Microcystis* (○), and *Dictyosphaerium* (▲).

c. cell numbers at the south sampling site, of Cryptomonads (□,▲), *Closterium* (■), *Oocystis* (●), unknown flagellate (○), *Ceratium* (◆).

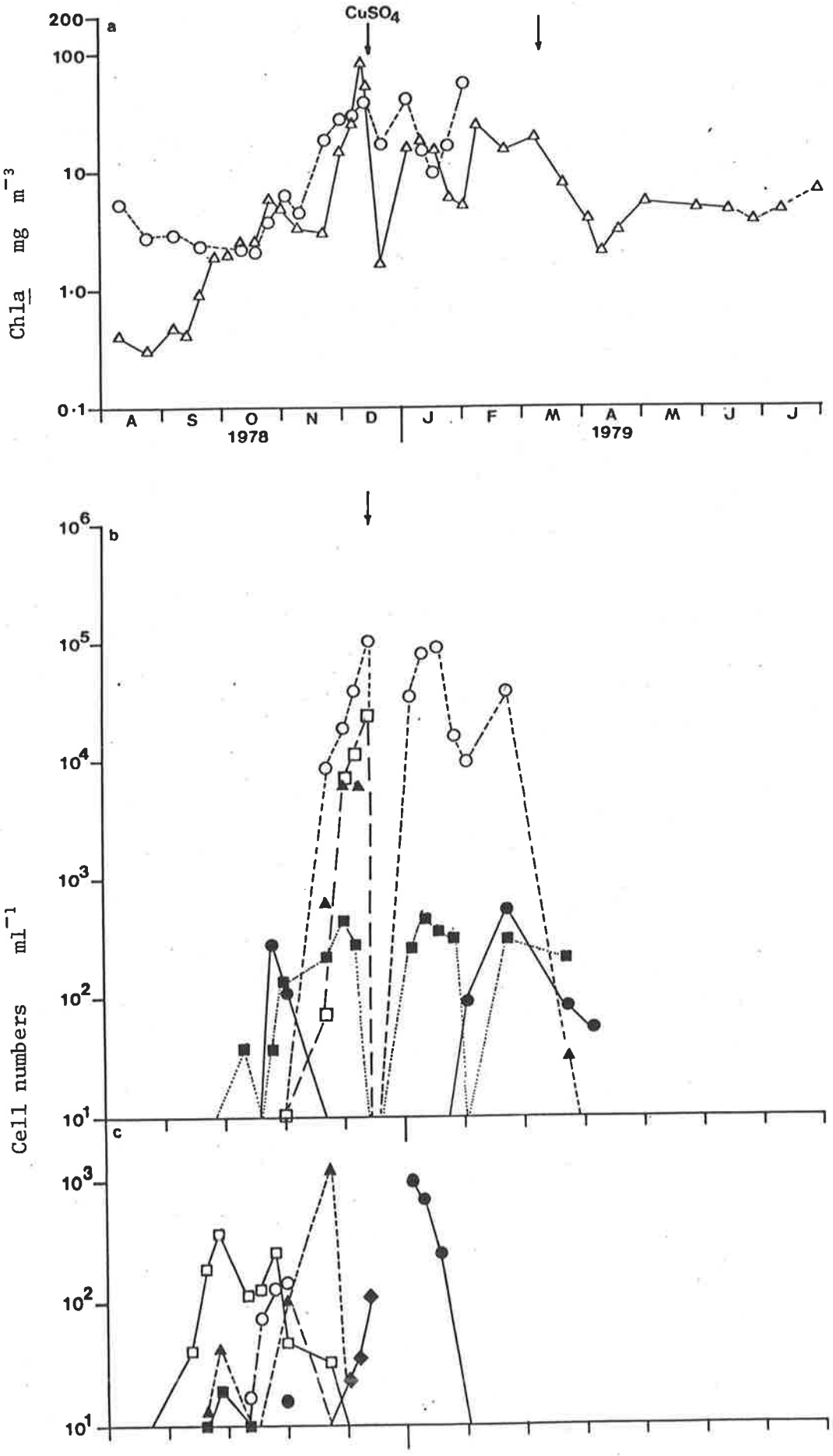
CuSO4
a
200
100
10
1·0
0·1
Chla mg m-3
A
S
O
N
D
J
F
M
A
M
J
J
1978
1979
b
10^6
10^5
10^4
10^3
10^2
10^1
Cell numbers ml-1
c
10^3
10^2
10^1

Fig. 5.5:

Fig. 5.6: Semi-logarithmic plots of seasonal variation at the south sampling site of

a. chlorophyll a concentration,

b. cell numbers of *Melosira* (○), *Cyclotella* (◆), *Microcystis* (▲), *Anabaena* (□), *Sphaerocystis* (●).

c. cell numbers of *Ceratium* (○), cryptomonads (■,▲), trachelomonads (□), *Closterium* (●).

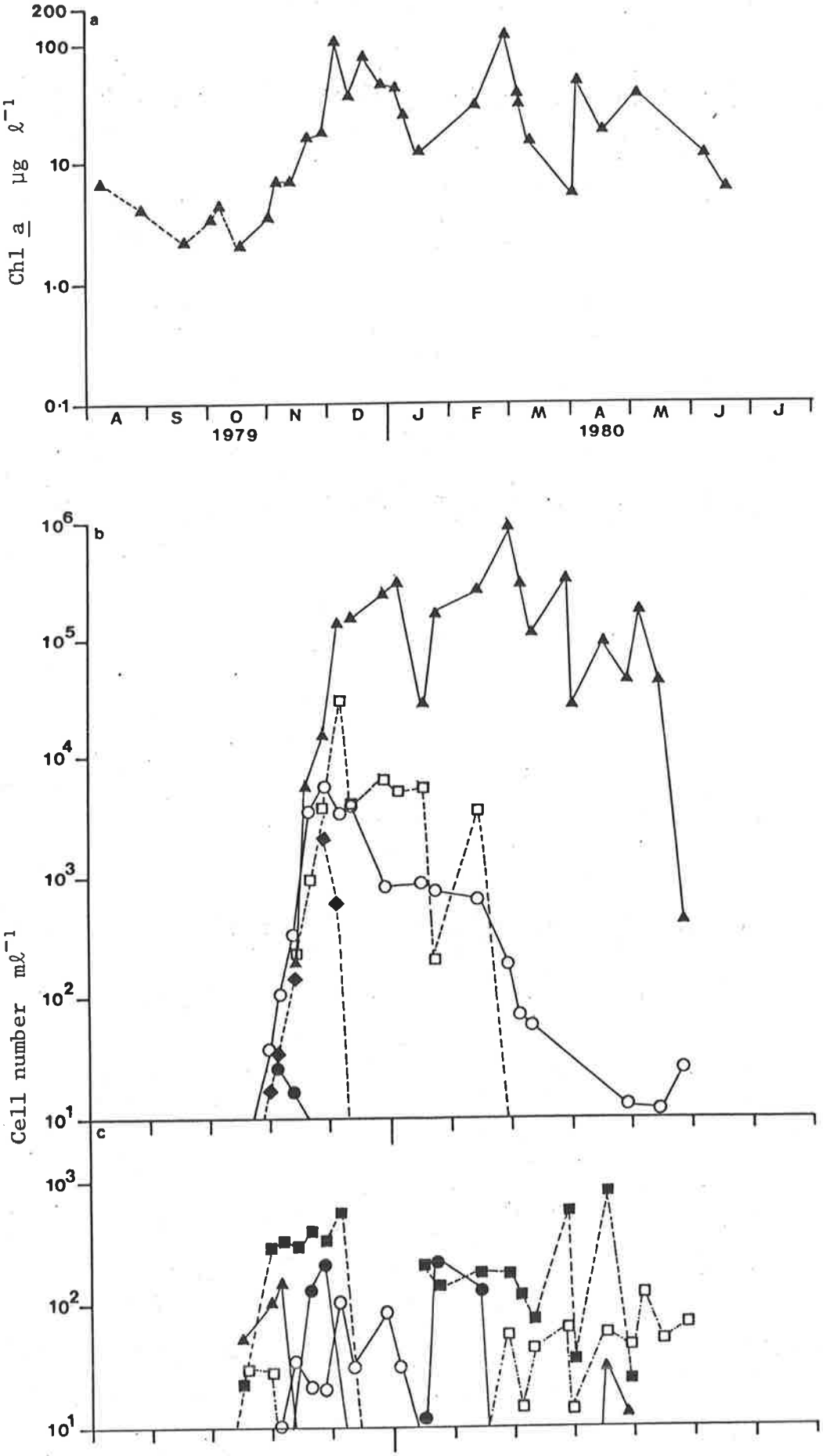
a
200
100
10
1·0
0·1
Chl a µg ℓ⁻¹
A
S
O
N
D
J
F
M
A
M
J
J
1979
1980
b
10⁶
10⁵
10⁴
10³
10²
10¹
Cell number mℓ⁻¹
c
10³
10²
10¹

Fig. 5.6:

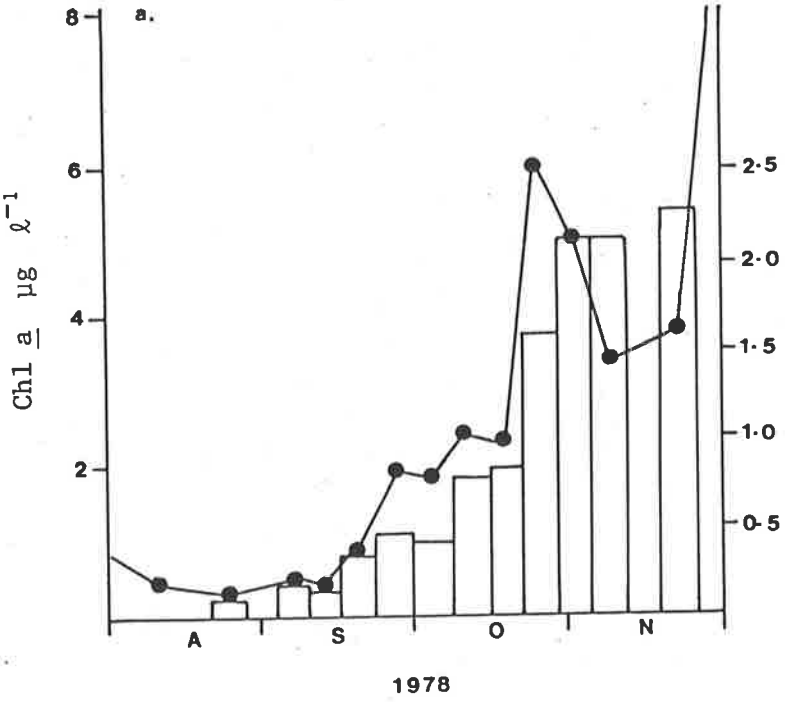

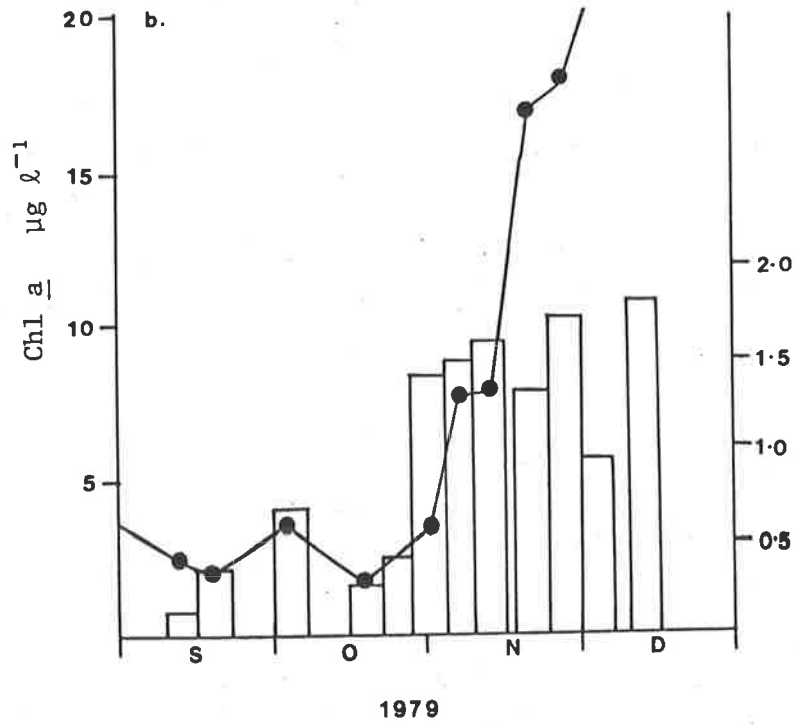

Fig. 5.7: Increase in the mean irradiance of the mixed zone ($\bar{I}$) and the chlorophyll a concentration during initiation of the spring biomass increase in (a) 1978 and (b) 1979.

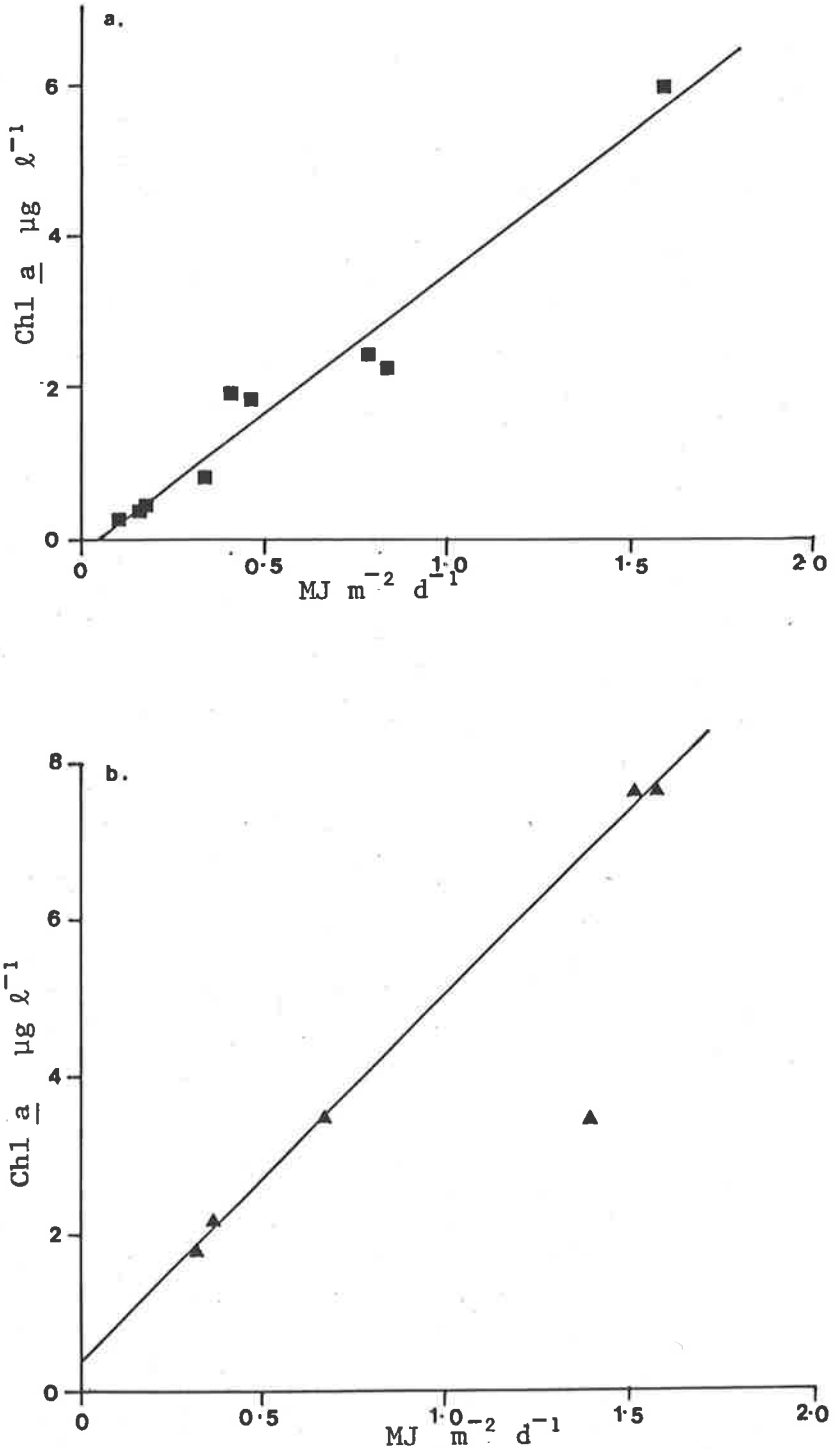

Fig. 5.8: Correlation between the mean irradiance of the mixed zone ($\bar{I}$) and chlorophyll a concentration during initiation of the spring biomass increase in

a. 1978 [chla]=-0.15+3.71 $\bar{I}$ r^2=0.96, n=9

b. 1979 (not including the disparate point - see text)
[chla]= 0.390+4.742 $\bar{I}$ r^2=0.99, n=5.

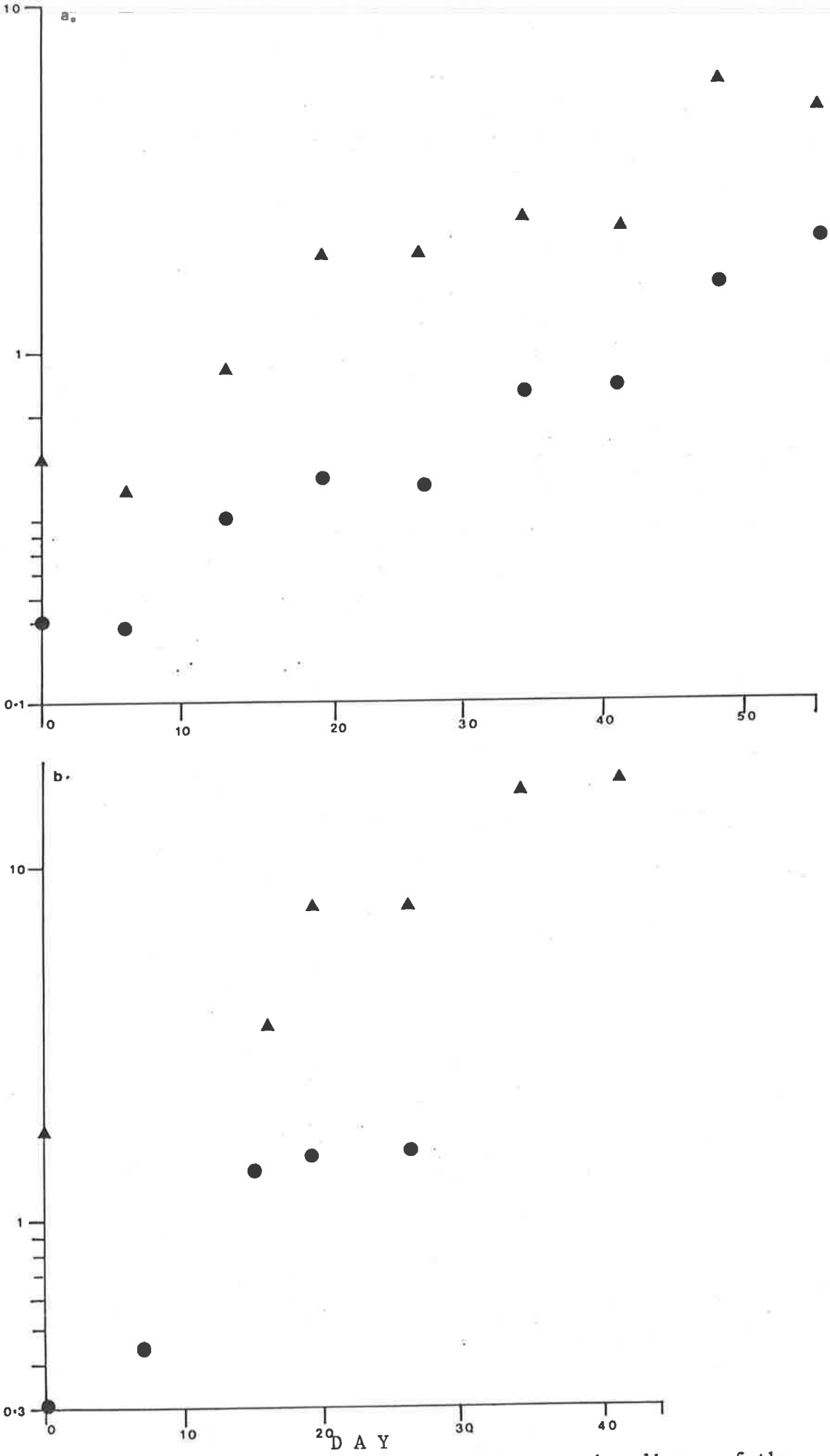

Fig. 5.9: Semi-logarithmic plot of the variation in mean irradiance of the mixed zone ($\bar{I}$) and chlorophyll a concentration during the initiation of the spring biomass increase in a) 1978 and b) 1979. $\bar{I}$ (○), chl a (▲).

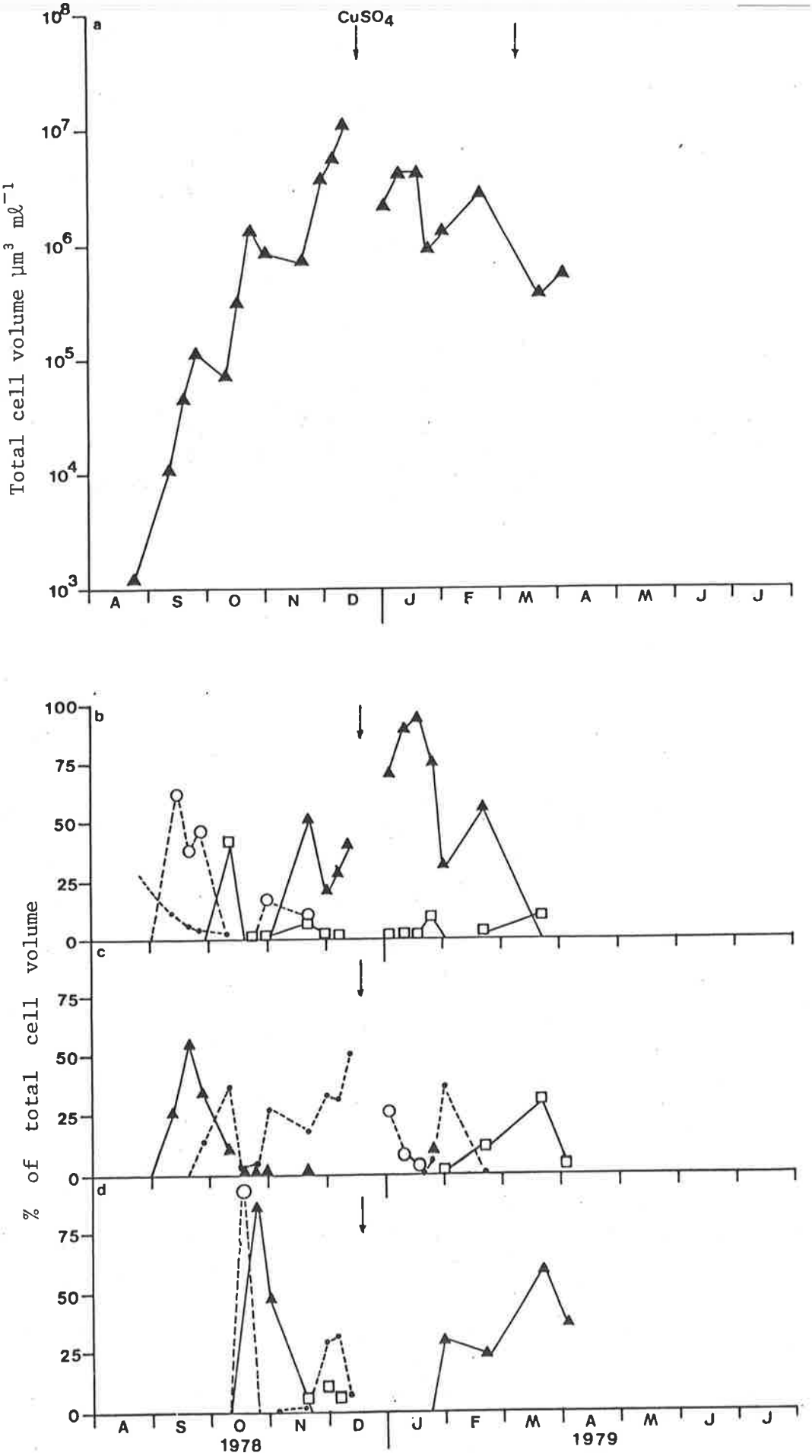

Fig. 5.10: a.Semi-logarithmic plot of the change in total cell volume over the 1978-79 growth season, and percentage of total cell volume due to:
b. *Cryptomonas* (○), *Cyclotella* (□), *Microcystis* (▲),
c. *Cryptomonas* (▲) *Ceratium* (•), *Oocystis* (○), *Melosira varians* (□),
d. *Melosira*sp. (○), *Trachelomonas* (▲), *Dictyosphaerium* (□).

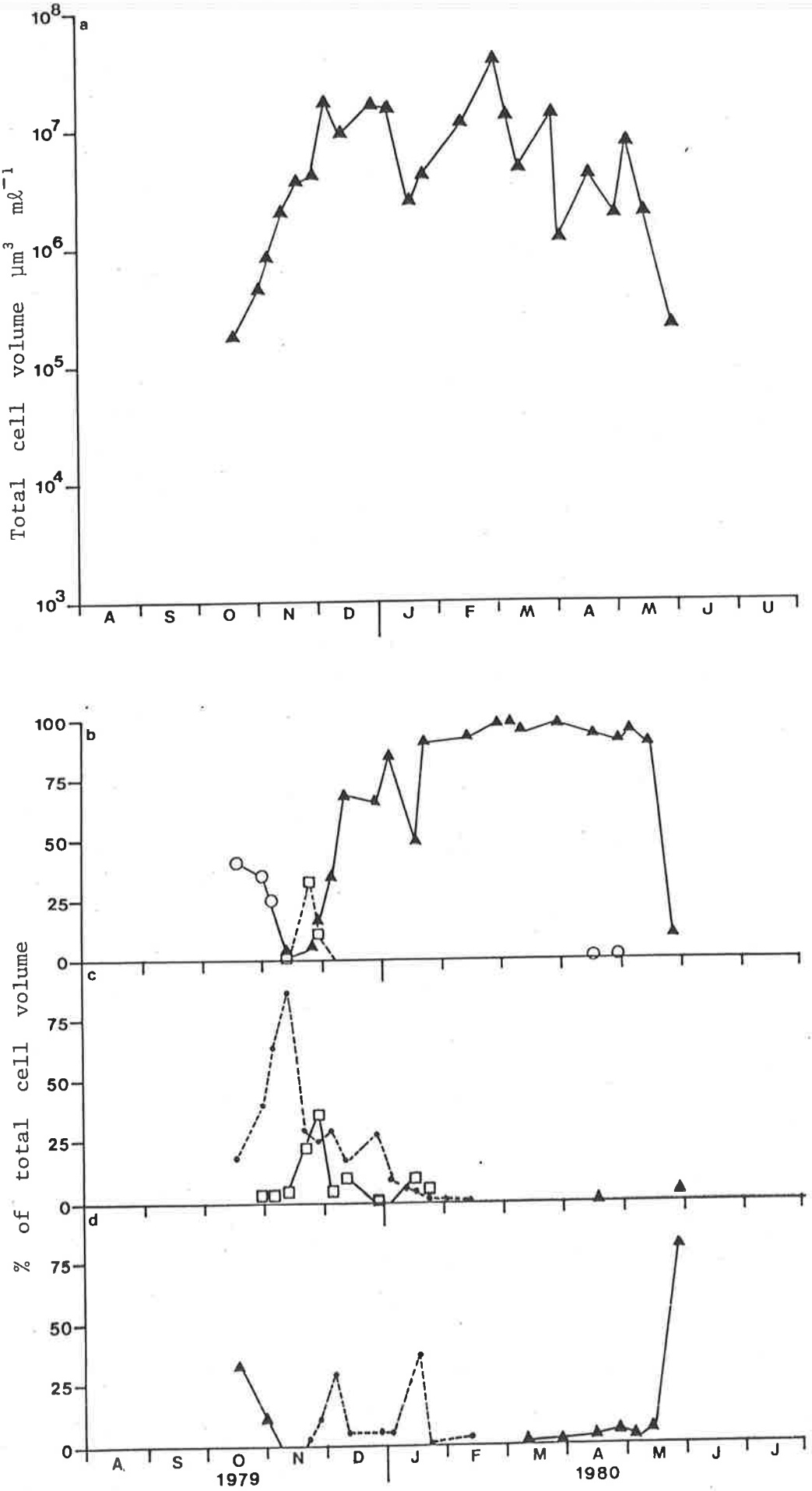

Fig. 5.11: a. Semi-logarithmic plot of the change in total cell volume over the 1979-80 growth season and percentage of the total cell volume due to (b) *Cryptomonas* (○), *Microcystis* (▲), *Cyclotella* (□), (c) *Ceratium* (•), *Melosira varians* (□), *Crytomonas* (▲), (d) *Trachelomonas* (▲), *Anabaena* (•).

Fig. 5.12: Seasonal variation in the summed difference index (SD) and species composition (denoted numerically) for

a. 1978-79

1. Cryptomonads
2. *Cyclotella* and *Ceratium*
3. *Melosira* sp.
4. Trachelomonads
5. Trachelomonads, *Ceratium*
6. *Ceratium*, *Anabaena*, *Microcystis*
7. *Ceratium*, *Microcystis*
8. *Microcystis*
9. *Microcystis*, *Ceratium*, Trachelomonads

b. 1979-80

Same associations as above, plus

10. *Ceratium* (& Cryptomonads)
11. *Melosira varians*

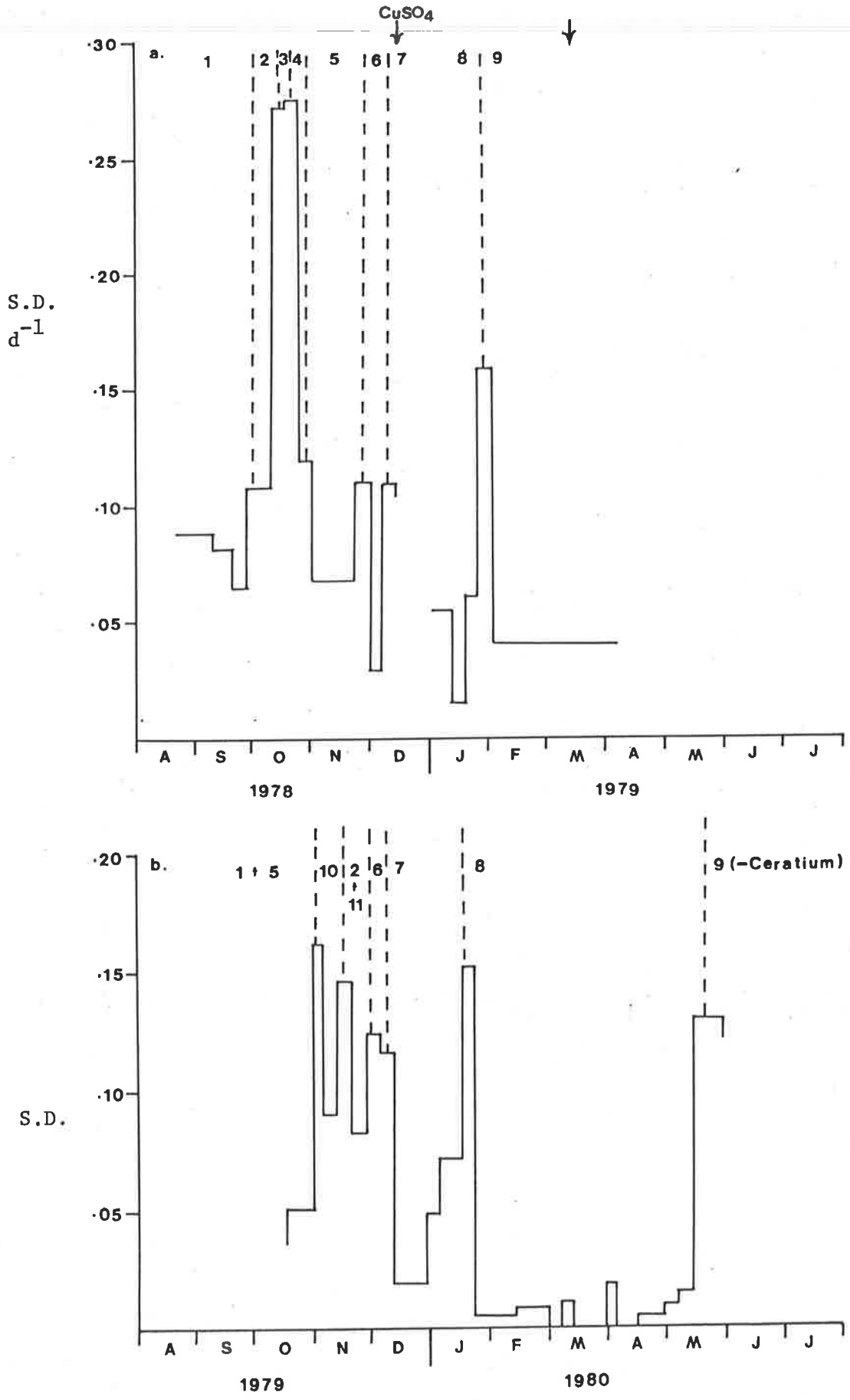
CuSO4
a.
1
2
3
4
5
6
7
8
9
·30
·25
·20
·15
·10
·05
S.D.
d-1
A
S
O
N
D
J
F
M
A
M
J
J
1978
1979
b.
1 + 5
10
2
11
6
7
8
9 (-Ceratium)
·20
·15
·10
·05
S.D.
A
S
O
N
D
J
F
M
A
M
J
J
1979
1980

Fig. 5.12:

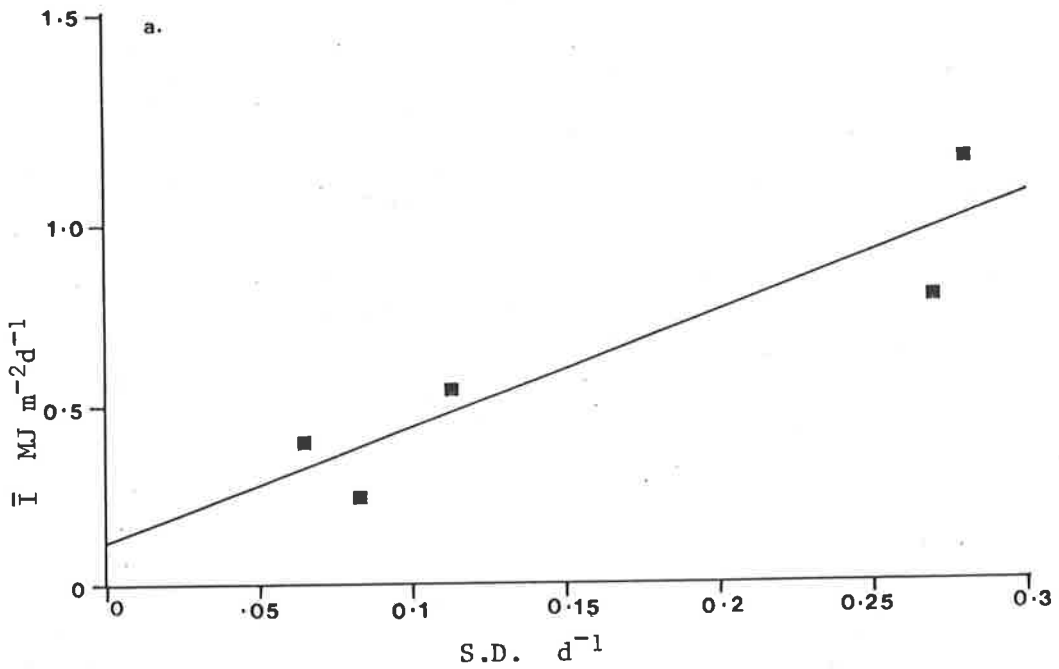

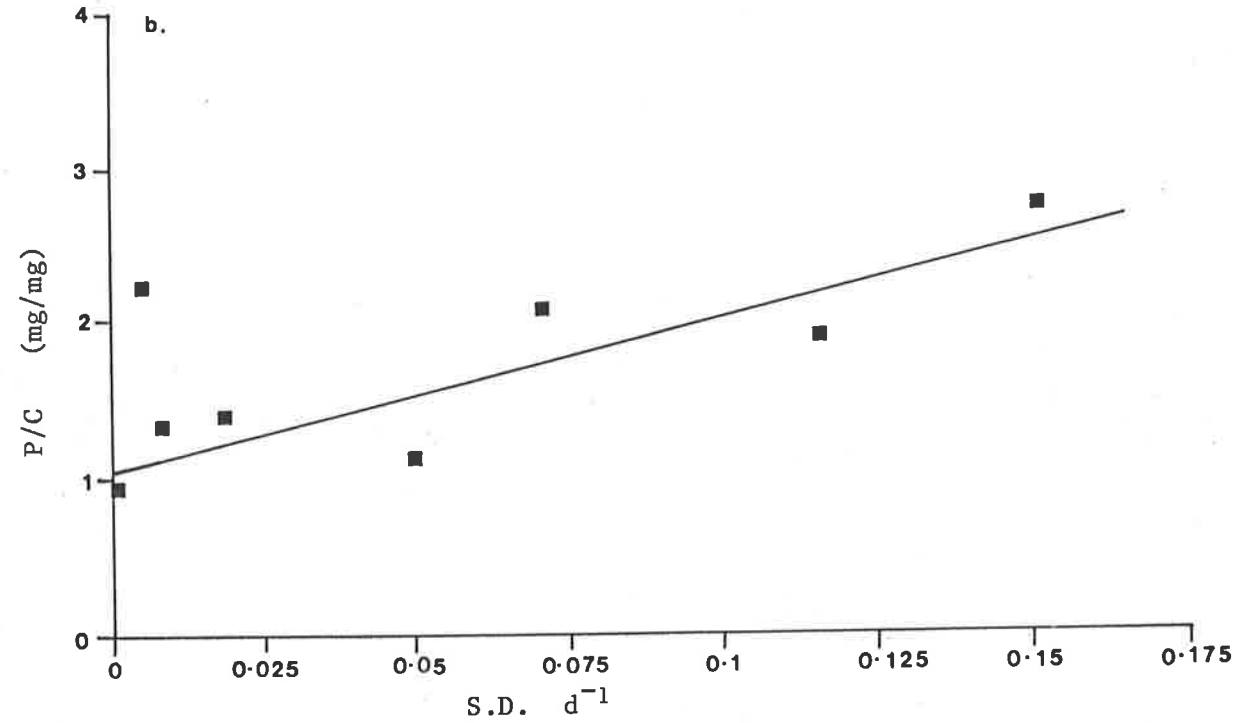

Fig. 5.13: a. Correlation between mean irradiance of the mixed zone ($\bar{I}$) and the summed difference index of succession rate (SD)
$\bar{I}$ = 0.102 + 3.245 SD, r^2=0.83.

b. Correlation between the protein/carbohydrate ratio and the summed difference index of succession rate (SD)
$\frac{\text{Protein}}{\text{Carbohydr.}}$ = 1.067+9.786 SD, r^2=0.75.

TABLE 5.1

Date	b	I_o	ε	Z_m	$\bar{I}$ MJ $m^{-2}d^{-1}$
23/8/78	0.3	10.166	2.69	35	0.109
6/9/78	0.5	12.348	2.10	34	0.172
12/9/78	0.4	10.993	2.6	26	0.164
19/9/78	0.9	11.446	2.28	15	0.336
26/9/78	1.9	12.801	2.19	13	0.449
3/10/78	1.9	14.681	2.31	15	0.420
10/10/78	2.4	20.933	2.12	12.5	0.789
17/10/78	2.3	17.920	2.18	10	0.822
24/10/78	6	21.759	2.13	6.5	1.573
31/10/78	5	18.445	1.72	5	2.144
9/11/78	3.4	18.373	1.75	5	2.098
21/11/78	3.8	19.427	1.71	5	2.266
30/11/78	15.5	22.137	1.81	5.5	2.224
6/12/78	27.6	19.124	1.86	7.5	1.385
12/12/78	55.2	22.062	2.37	9.5	0.979
10/9/79	2.5	10.238	4.0	23	0.113
18/9/79	2.2	14.232	4.0	10	0.357
3/10/79	3.5	13.326	4.0	5	0.667
17/10/79	1.8	16.036	3.9	13	0.315
24/10/79	-	20.027	3.2	14	0.445
1/11/79	3.5	21.386	2.6	6	1.385
5/11/79	7.7	23.488	2.6	6	1.506
12/11/79	7.7	22.511	2.6	5.5	1.573
20/11/79	17	19.578	2.5	6	1.313
27/11/79	18	21.231	2.5	5	1.695
4/12/79	106.7	25.221	3.9	7	0.919
11/12/79	34.7	27.407	2.8	5.5	1.792
18/12/79	79.7	20.769	4.6	5	0.909
27/12/79	48.8	27.705	3.7	5	1.500

Chlorophyll a concentration (b, mg chla m^{-3}), average incident total irradiance over 7 days prior to sampling date (I_o, MJ m^{-2} d^{-1}), vertical extinction coefficient (ε, ℓn units m^{-1}) and mixed depth (Z_m, m) for dates during the onset of thermal stratification of 1978/79 and 1979/80. The mean irradiance of the mixed zone ($\bar{I}$, MJ m^{-2} d^{-1}) was calculated using equation 5.1.

	Cell volume μm^3
Cyanophyta	
Anabaena spiroides Klebahn	155
Microcystis aeruginosa Kuetzing	44
Euglenophyta	
Trachelomonas sp. 1	1771
Trachelomonas sp. 2	4190
Chlorophyta	
Chlamydomonas globosa Snow	126
Staurastrum gracile Ralfs.	-
Sphaerocystis shroeteri Chodat.	62
Closterium sp.	300
Dictyosphaerium pulchellum Wood	65
Oocystis parva West & West	178
Eudorina elegans Ehrenberg	650
Bacillariophyceae	
Cyclotella meneghiniana Kuetzing	234
Melosira varians Agardh.	266
Melosira sp.	10150
Dinophyceae	
Ceratium hirundinella (O.F.M.)Dujardin	50588
Cryptophyceae	
Cryptomonas ovata Ehrenberg	444
Cryptomonas erosa Ehrenberg	70

Table 5.2: Major phytoplankton species of Mt. Bold Reservoir and estimates of cell volume.

TABLE 5.3

1978-79

1	2	3	4	Z	6
Cryptomonads(.89) →	Cyclotella(0.43) Ceratium(0.37) →	Melosira(0.94) →	Trachelomonads(0.87) Ceratium(0.07) →	Microcystis(0.53) Ceratium(0.18) Cryptomonad(0.11) →	Anabaena(0.32) Ceratium(0.31) Microcystis(0.29) Dictyosphaerium(.10)

8	9	
→ Microcystis(0.9) →	Ceratium(0.38) Microcystis(0.31) Trachelomonas(0.28) →	Trachelomonad(0.59) Melosira(0.32)

1979-80

1+5	10	2+11	11+6+2	6	7
Cryptomonads(0.41) Trachelomonad(0.26) Ceratium(0.17) →	Ceratium(0.86) →	Cyclotella(.34) Ceratium(0.29) Melosira(0.24) →	Melosira(0.36) Ceratium(0.25) Microcystis(0.15) Cyclotella(0.11) Anabaena(0.11) →	Microcystis(0.34) Anabaena(0.29) Ceratium(0.28) →	Microcystis(0.65) Ceratium(0.27)

8	9(-Ceratium)
→ Microcystis(>0.9) →	Trachelomonad(0.83) Microcystis(0.09)

Species sequence and percentage contribution to total cell volume for the 1978/79 and 1979/80 growth seasons.

1978 - 79		1979 - 80	
Period	SD	Period	SD
12.09 - 19.09.78	$\frac{0.58}{7} = 0.083$	17.10 - 01.11.79	$\frac{.771}{15} = 0.051$
19.09 - 26.09.78	$\frac{0.457}{7} = 0.0652$	01.11 - 05.11.79	$\frac{0.650}{4} = 0.163$
26.09 - 10.10.78	$\frac{1.503}{14} = 0.107$	05.11 - 12.11.79	$\frac{0.6135}{7} = 0.088$
10.10 - 17.10.78	$\frac{1.91}{7} = 0.272$	12.11 - 20.11.79	$\frac{1.17}{8} = 0.146$
17.10 - 24.10.78	$\frac{1.923}{7} = 0.275$	20.11 - 27.11.79	$\frac{.575}{7} = 0.082$
24.10 - 31.10.78	$\frac{.820}{7} = 0.117$	27.11 - 04.12.79	$\frac{.866}{7} = 0.124$
31.10 - 21.11.78	$\frac{1.417}{21} = 0.067$	04.12 - 11.12.79	$\frac{0.81}{7} = 0.116$
21.11 - 30.11.78	$\frac{.992}{9} = 0.110$	11.12 - 27.12.79	$\frac{.251}{14} = 0.018$
30.11 - 06.12.78	$\frac{.173}{6} = 0.029$	27.12 - 04. 1.80	$\frac{.393}{8} = 0.049$
06.12 - 12.12.78	$\frac{.646}{6} = 0.108$	04.01 - 16. 1.80	$\frac{.857}{12} = 0.071$
03.01 - 10. 1.79	$\frac{.380}{7} = 0.054$	16.01 - 22. 1.80	$\frac{.908}{6} = 0.151$
10.01 - 17.01.79	$\frac{.108}{7} = 0.015$	22.01 - 13.02.80	$\frac{.115}{22} = .005$
17.01 - 24.01.79	$\frac{.425}{7} = 0.061$	13.02 - 28.02.80	$\frac{.117}{15} = .008$
24.01 - 01.02.79	$\frac{1.258}{8} = 0.157$	28.02 - 05.03.80	-
01.02 - 21.02.79	$\frac{.834}{20} = 0.042$	05.03 - 11.03.80	$\frac{.069}{6} = .012$
21.02 - 21.03.79	$\frac{1.209}{28} = 0.043$	11.03 - 28.03.80	$\frac{.023}{17} = .001$
21.03 - 04.04.79	$\frac{.584}{14} = 0.042$	28.03 - 01.04.80	$\frac{.072}{4} = .018$
		01.04 - 16.04.80	$\frac{.015}{15} = .001$
		16.04 - 28.04.80	$\frac{.06}{12} = .005$
		28.04 - 05.05.80	$\frac{.072}{8} = .009$
		05.05 - 13.05.80	$\frac{.116}{8} = .015$
		13.05 - 26.05.80	$\frac{1.659}{13} = .128$

Table 5.4: Calculation of the summed difference index (SD d^{-1}, equation 5.3) for the 1978-79 and 1979-80 growth seasons. The individual values of the calculation and the index are shown in the column SD.

Date	SD d^{-1}	$\bar{I}$ $MJm^{-2}d^{-1}$
12.09-19.09.78	0.083	0.21
19.09-26.09.78	0.065	0.39
26.09-10.10.78	0.107	0.55
10.10-17.10.78	0.270	0.81
17.10-24.10.78	0.280	1.17

Table 5.5: Values of the summed difference index (SD d^{-1}, equation 5.3) and the mean irradiance of the mixed zone ($\bar{I}$ $MJm^{-2}d^{-1}$, equation 5.1) during initiation of the vernal biomass increase of 1978.

Date	SD	Protein / Carbohydrate	
27.11-04.12.79	0.124	3.3	
7.12	0.116	1.9	
11.12-27.12.79	0.018	1.4	
27.12-04.01.80	0.049	1.01	
04.01-16.01.80	0.071	2.1	
16.01-22.01.80	0.151	2.76	
22.01-13.02.80	0.005	2.2	
13.02-22.02.80	0.008	1.39	
28.02-05.03.80	0	0.95	AUTUMNAL OVERTURN
05.03-11.03.80	0.012	2.48	
11.03-20.03.80	0.001	3	

Table 5.6: Values of the summed difference index (SD d^{-1}, equation 5.3) and the protein to carbohydrate ratio (mg/mg) during the summer and autumn of 1979-80.

Species	n	μ	r^2	d
Melosira varians	6	0.180	0.98	0.26
Cyclotella	4	0.302	0.94	0.44
Microcystis	4	0.188	0.94	0.27
Anabaena	4	0.226	0.97	0.33
Cryptomonas sp.		ca.0.171		ca.0.25

Table 5.7: Net specific growth rate (μd^{-1}) and doubling rate (d-doubling d^{-1}) calculated from cell numbers, for the period of rapid spring growth in November 1979. The number of samples (n) used in each linear regression (equation 5.2) and the correlation coefficient (r^2) also are given. Slopes of regression lines (μ) were not significantly different ($P>0.05$) except for *Melosira* and *Cyclotella* ($0.02<P<0.05$).

PHYTOPLANKTON PHOTOSYNTHESIS AND ITS DETERMINANTS

6.1 Introduction

Photosynthesis is the primary pathway of carbon fixation in phytoplankton and its quantitative description central to a functional understanding of population dynamics. The relationship between photosynthesis and light intensity has been extensively studied and a number of mathematical equations developed to assist data interpretation (Talling 1957a, b; Steele 1962; Vollenweider 1965; Fee 1973; Bannister 1974; Jassby & Platt 1976). The variables identified by these models enable a quantitative comparison between different aquatic environments. For example, the relatively simple model of Talling (1957a, b) has been used to compare experimental data derived from a wide ecological range (Talling 1965; Rodhe 1965; Bindloss 1974; Ganf 1975; Jewson 1976; Jones 1977b; Harris et al. 1980).

Australian inland waters are generally very turbid compared with North American and European freshwaters (Kirk 1977; Ganf 1980; Chp. 3) and it is of interest to see if the relative importance of model parameters is maintained or whether significant differences occur in the unusual underwater light climate. To date the limited published results on phytoplankton photosynthesis in Australian waters do not permit this (Walker 1973; Croome & Tyler 1975; Bowles et al. 1979; Ganf 1980).

6.2 Theory

The model proposed by Talling (1957a, b) to integrate instantaneous photosynthesis depth profiles, was based on the relationship between photosynthesis and irradiance described by Smith (1936).

The semi-empirical expression suggests a suite of variables which determine the depth integral,

$$\Sigma P = \frac{bP_m}{\varepsilon} \ell n \left(\frac{I_o'}{0.5I_k}\right) \qquad 6.1$$

where ΣP is the integral photosynthetic rate (mg C m^{-2} h^{-1}), b the phytoplankton biomass (mg chl a m^{-3}), P_m the maximum specific photosynthetic rate (mg C mg chl a^{-1} h^{-1}), I_o' the photosynthetically active incident solar irradiance (PAR, 400-700 nm in μ Einstein m^{-2} s^{-1}) corrected for surface reflection (Chp. 2), I_k the light intensity characterizing the onset of light saturation (μ Einstein m^{-2} s^{-1}), and ε the diffuse extinction coefficient calculated from the exponential decrease of photosynthetically active radiation with depth (ℓn units m^{-1}) (Chp. 3).

In the original model (Talling 1957b) the vertical extinction coefficient ε was represented by (a ε min) where ε min was the vertical extinction coefficient for the most penetrating wavelength and a an empirical correction factor. Talling (1957b) estimated a to be 1.33, however the value varies with the underwater spectral distribution (Jewson 1977). The use of quantum sensors (eg. Lambda Inst.) which measure the waveband (400-700 nm) of photosynthetically active

radiation enables direct computation of an average extinction coefficient (Chp. 3).

Talling (1957a) defined I_k as the light intensity at which extrapolations of the initial linear region and the light saturated region of the photosynthesis-irradiance curve intersect. If the slope of the linear region is α (mg C mg $chla^{-1}h^{-1}(\mu$ Einstein m^{-2} $s^{-1})^{-1}$) then,

$$\alpha = \frac{Pm}{I_k} \qquad 6.2$$

The initial slope is a function of the photochemical reactions of photosynthesis while the maximum rate is limited by the dark reactions (Yentsch & Lee 1966; Steeman-Nielsen 1974; Jones 1978). Variation in these variables has been associated with light intensity adaptation by phytoplankton (Jorgensen & Steeman-Nielsen 1966; Vollenweider 1970; Steeman-Nielsen 1974; Jones 1978). However Pm is also affected by temperature (Talling 1957a; Bindloss 1974; Jewson 1976) nutrient conditions (Eppley & Renger 1974; Senft 1978) and population density effects (Wright 1960; Ganf 1972; Talling et al. 1973; Bindloss 1974).

When considering long term population dynamics, estimates of daily integral photosynthesis are more useful than hourly integral rates. However the necessity for minimizing incubation periods (Vollenweider & Nanwerck 1961) means that daily rates can only be directly measured from a series of short term experiments over a day. The general impracticality of this approach has resulted in attempts to estimate daily rates from single short term experiments. Various

solutions have been applied to this problem, ranging from simple irradiance ratios (Vollenweider 1969; Megard 1972; Lewis 1974; Idso & Foster 1975; Eppley & Sharp 1976) to more complex approaches estimating the photosynthetically active radiation received through the day (Fee 1973a, b; Talling 1957b, 1971).

Talling (1957b) extended his short term integral model to daily estimates by assuming that b, Pm, ε and I_k (equation 6.1) did not show significant diurnal variation. Substitution of the daily average incident irradiance ($\bar{I}_o'$) in the light function enabled calculation of the average hourly rate of integral photosynthesis, which when multiplied by the daylength (Δ,h) provided an estimate of the daily integral (ΣΣP, mgC m^{-2} d^{-1}),

$$\Sigma\Sigma P = \frac{bPm}{\varepsilon} \ln \left(\frac{\bar{I}_o'}{0.5I_k}\right) \Delta\ 0.9 \qquad 6.3$$

where 0.9 is an empirical factor (Talling 1957b) which corrects for the overestimate obtained from using $\bar{I}_o'$. Jewson (1975) confirmed the applicability of this expression when variables other than light intensity remained relatively constant.

The form of equation (6.3) described by Talling (1957b), contained the logarithmic light function in terms of optical depth,

$$\Sigma\Sigma P = \frac{bPm}{\varepsilon} \ln 2 \left(\frac{\ln \left(\frac{\bar{I}_o'}{0.5I_k}\right)}{\ln 2}\right) \Delta\ 0.9 \qquad 6.4$$

where the term

$$\left(\frac{\ln \left(\frac{\bar{I}_o'}{0.5I_k}\right)}{\ln 2}\right) \Delta\ 0.9 = [\text{L.D.H.}]^{\text{day}} \qquad 6.5$$

represented light-division-hours calculated using $\bar{I}_o'$, the daily average incident irradiance. Utilizing this notation equation (6.3) becomes

$$\Sigma\Sigma P = \frac{bPm}{\varepsilon} \ell n\ 2\ [L.D.H]^{day} \qquad 6.6$$

When experimental techniques measure gross photosynthesis equation (6.3) or (6.6) may be used to assess daily gross integral photosynthesis under unit surface area. The estimation of net integral photosynthesis then requires a measure of respiratory losses. These depend on both respiratory rates and the ratio of the euphotic depth to the mixing depth (Talling 1957b; Steel 1973; Ganf 1976).

Talling (1957b, 1971) defined the column compensation point as the mixing depth for which daily integral photosynthesis and respiration rate ($\Sigma\Sigma R$) were equal, resulting in zero net photosynthesis for the circulating population. On the assumption that a single mean respiration rate adequately describes phytoplankton respiratory losses the daily respiration integral may be estimated as,

$$\Sigma\Sigma R = b\ P_m\ r\ Z_m\ .24 \qquad 6.7$$

where r is the ratio of specific respiration rate to photosynthetic capacity (P_m) (mg C (or O_2) mg $chla^{-1}$ h^{-1}), and Z_m(m) is the mixed depth of the water column. The ratio of daily integral photosynthesis to respiration can then be described (Talling 1957b, 1971) using equations (6.6) and (6.7) as,

$$\frac{[L.D.H]^{day}\ \ell n\ 2}{\varepsilon\ Z_m\ 24r} = q_c \qquad 6.8$$

At column compensation point the critical value of the ratio q_c=1.0, and

$$\frac{[L.D.H]^{day}\ \ell n\ 2}{\varepsilon\ Z_m} = 24r \qquad 6.9$$

This relation differs slightly from Talling (1971) and Jewson (1976) in using ε rather than ε min.

When daily column photosynthesis is greater than column respiration then q_c>1 and biomass will accumulate provided other loss factors are negligible.

RESULTS

6.3 Comparison of O_2 and ^{14}C Estimates of Photosynthesis

Controversy regarding the interpretation of ^{14}C uptake data has existed since the technique was developed. It is clear that initially ^{14}C uptake will be closely related to gross photosynthesis (GP) but will diverge from this if the fixed carbon is affected by processes of respiration or excretion (Lewis 1974). If this occurs the measured uptake rate will be less than GP but greater than net photosynthesis (NP), and will approach NP with time as the cellular compartments become uniformly labelled. The effect of incubation time on measured photosynthetic rates was clearly demonstrated by Vollenweider & Nauwerck (1961).

Harris and Piccinin (1977) compared short term oxygen and ^{14}C measurements and found that on average carbon uptake was measuring gross photosynthesis. Ganf & Horne (1975) reported that in Lake George uptake of ^{14}C agreed best with gross photosynthesis. However Lewis (1974), assuming a photosynthetic quotient (P.Q=$\frac{O_2}{CO_2}$ molar) of 1.2, concluded that the ^{14}C technique was measuring net photosynthesis in Lake Lanao.

To assess the present ^{14}C technique with its associated correction factors (Chp. 2), parallel 4h, ^{14}C and O_2 incubations were compared over a range of environmental conditions typical of Mt. Bold Reservoir. Gross photosynthesis was estimated from the difference in final oxygen concentration between light and dark bottles (Chp. 2), and the mean value for each depth plotted against the corresponding average ^{14}C estimate (Fig. 6.1(a)-(c)). The relationships appeared linear and were evaluated using regression equations. Linear functions accounted for >93% of the variation between the variables (Fig. 6.1(a)-(c)), with all slopes significantly different from zero ($P<0.001$).

If the ^{14}C technique measures net photosynthesis, then when plotted against a measure of gross photosynthesis (Fig. 6.1), respiration should appear as a negative y-axis intercept. Despite the occurrence of large respiration rates (Table 6.1), y-axis intercepts were not significantly different from zero ($P>0.05$) except for 5/4/78 (Fig. 6.1b) when the intercept was different at $P=0.05$ but not at $P=0.02$. In this case the respiration rate estimated from the y-axis intercept was <25% of the measured dark respiration rate.

These results indicated that the ^{14}C technique was closely approximating gross photosynthesis as determined from O_2 exchange measurements. The reduced incubation time (ca. 2h) used for regular ^{14}C determinations would further increase the probability of this result.

It follows from the close relationship between gross photosynthesis and ^{14}C uptake that extracellular release of labelled carbon was minimal over the incubation periods, a conclusion supported by the results of Lewis (1974) and Harris & Piccinin (1977). Extracellular products were undetectable on occasions when direct measurement was attempted.

Photosynthetic quotients calculated from slopes of linear regression equations varied between 0.9 and 1.93 (Table 6.1). A regression on all data points, including five dates when ^{14}C and O_2 results were compared at only a single depth, (η=41; P(mgC.mg chla^{-1}h^{-1}) = -0.34+0.345 GP (mgO_2 mgchla^{-1}h^{-1}) r^2 = 0.95, S.E. of y on x = 0.72, S.E. of constant = 0.16, S.E. of slope = 0.013), yielded an average P.Q. of 1.09, agreeing closely with the value of 1.13 obtained by Harris & Piccinin (1977) for a large number of determinations on natural populations. Strickland (1960) suggested a similar average value of 1.2.

Specific rates of respiration and gross maximum photosynthesis (mgO_2 mg chla^{-1} h^{-1}), calculated from oxygen measurements, exhibited a wide range of values (Table 6.1), with respiration varying from indetectable levels to 90% of P_m. The particularly high respiration

rates per unit chlorophyll-a suggested a large non-algal component. Ganf (1980) reported similar high levels from this reservoir.

6.4 Depth Distribution of Photosynthesis

Seasonal variation in the depth distribution of photosynthesis was assessed from ^{14}C incubations (Fig. 6.2). The photosynthesis-depth curves were typical in shape (Talling 1957a, b; Lewis 1974; Bindloss 1974; Ganf 1975; Jewson 1976; Jones 1977b) with surface inhibition evident in virtually all profiles, a resulting sub-surface maximum photosynthetic rate, and an approximately exponential decline with low light intensities. Planimetric integration of these curves provided a measure of the areal rate of carbon fixation (mgC m^{-2} h^{-1}), which varied between 0.5 - 500mg C $m^{-2}h^{-1}$, maximum values generally occurring in summer and minimum values in winter (Fig. 6.3a).

The decrease in integral photosynthesis resulting from surface inhibition was determined planimetrically. Based on the assumption that P_m would continue unabated to the surface in non-inhibited profiles, the reduction in integral photosynthesis ranged between 0-8% with a mean of 2.9%. Values of similar magnitude have been found elsewhere (Ilmavirta 1974; Jewson 1976; Jones 1978).

6.5 Determinants of Hourly Integral Photosynthesis

Transformation of photosynthesis-depth profiles into photosynthesis-irradiance relationships was achieved through the Beer-Lambert law (Chp. 3, equation 3.1) using the average incident PAR for the incubation

period (I_o'), and the vertical extinction coefficient (ε, Chp. 3).

In the majority of experiments α, the initial slope of the photosynthesis-irradiance curve was determined by linear regression. Duplicate samples from the lowest light intensities were sequentially incorporated into the regression analysis and the slope calculated. The set of points giving the greatest slope provided the estimate of α. In general three or four duplicate samples below a light intensity of ca. 100 $\mu E\ m^{-2}\ s^{-1}$ were utilized and in all cases resulted in a correlation coefficient $r^2 > 0.95$.

The value of I_k was estimated from the ratio of P_m to α (equation 6.2), P_m being determined directly from the photosynthesis-irradiance curve. In a number of experiments the initial slope could not be reasonably estimated and I_k was determined graphically as the light intensity at 0.7 P_m, on the assumption that the photosynthesis-irradiance curve was adequately described by the equation of Smith (1936)(Talling 1957a, 1960; Jewson 1976; Jassby & Platt 1976).

Vollenweider (1965) demonstrated that Talling's integral (equation 6.1) was a specialized case of the general depth integral of Smith's equation,

$$\Sigma P = \frac{bPm}{\varepsilon} \left[\ell n\left(\frac{I_o'}{I_k} + \sqrt{1 + \left(\frac{I_o'}{I_k}\right)^2}\right) \right] \qquad 6.10$$

and only applied when $I_o' >> I_k$. The ratio I_o'/I_k for the data from Mt. Bold Reservoir ranged between 1.44-18.7 with a mean value of 6.6 (S.E. of mean - 0.4, η=88). The application of Talling's integral

with an I_o'/I_k ratio of 2.0 underestimates the correct integral by <4%. The minimum observed ratio of 1.44 was the only value less than 2.0, and underestimated the integral by <10%.

The validity of Talling's expression (equation 6.1) was tested by comparing calculated and planimetrically determined integrals. As the mathematical model does not consider surface inhibition this was neglected in the planimetric measurements by assuming sub-surface maximum photosynthetic rate continued to the surface. The calculated and measured integrals were closely correlated (Fig. 6.4) and yielded linear regression equation,

$$\Sigma P_{calculated} = -1.23 + 1.01\ \Sigma P_{planimetric} \qquad r^2 = 0.99$$

with the negative y-intercept not significantly different from zero ($P>0.05$). Similar results have been obtained from a range of aquatic environments (Talling 1965; Rodhe 1965; Bindloss 1974; Ganf 1975; Jewson 1976; Jones 1977b; Harris et al. 1980).

Seasonal variation in the determinants of integral photosynthesis recognized by Talling's model are illustrated in Fig. 6.3(a)-(c).

I_k varied between ca. 100-500 μE m^{-2} s^{-1} but did not follow a fixed seasonal pattern (Fig. 6.3c). During 1977/78 it increased from October through to late January and then declined to a minimum in May. The following season I_k increased from October to early September but then oscillated around a mean of ca. 275-300 μE $m^{-2}s^{-1}$ until finally declining in April. When photosynthesis measurements recommenced in

November 1979, I_k was ca. 300 μE m^{-2} s^{-1}, but declined to a minimum in late December, then increased again, finally returning to 300 μE m^{-2} s^{-1} in early March.

P_m and α, the components of I_k (equation 6.2), each showed seasonally varying patterns (Fig. 6.3b), however a general correspondence was evident between the two variables which acted to minimize changes in I_k. Thus increases or decreases in one generally coincided with a similar directional change in the other.

Values of the logarithmic light function, $\ell n \left(\frac{I_o'}{0.5I_k}\right)$ varied between 1.0 and 3.5 (Fig. 6.3c) with similar mean values for the southern (2.38, S.E. of mean - 0.08, η=48) and northern sampling sites, (2.33, S.E. of mean = 0.085, η=21). The constancy of the ratio suggested that $\frac{bPm}{\varepsilon}$ (equation 6.1) accounted for most of the variability in ΣP (Fig. 6.3a). This was substantiated by the linear relationship between them (Fig. 6.5a).

Analysis of seasonal data groups yielded significantly different slopes ($P<0.05$) of 2.29, 2.04 and 2.89 between years (Fig. 6.5b-d). No significant difference was observed between the north and south sampling site within a season. A similar range of values (1.75-2.47) was obtained by Harris et al. (1980). Earlier measurements (Talling 1965; Bindloss 1974; Jewson 1976; Jones 1977b) fell within the range of 1.9-2.6, but were obtained from the relationship between ΣP and $\frac{bPm}{\varepsilon min}$ and so could not be directly compared with the present results.

The maximum volumetric rate of photosynthesis (bPm, mgC m^{-3} h^{-1}) ranged from negligible (0.4) to 655 mgC $m^{-3}h^{-1}$(Fig. 6.3b), and accounted for a significant proportion of the variation in $\frac{bPm}{\epsilon}$ and consequently in integral photosynthesis (Fig. 6.6a). The correlation between bPm and chlorophyll concentration (Fig. 6.6b) suggested that major changes in integral photosynthesis were a function of chlorophyll concentration. This was substantiated by the correlation between ΣP and b (Fig. 6.7) (Figures 6.6 and 6.7 shown on log:log graphs for convenience. Statistics calculated on original data.).

The photosynthetic capacity P_m ranged between 1.0 and 14.6 mgC mgchla^{-1} h^{-1} (Fig. 6.3b), however 90% of values did not exceed 7 mgC mg chla^{-1} h^{-1}. This range is similar to values observed in northern temperate lakes, and overlaps lower values observed in tropical lakes (Table 6.2).

The temperature dependence of P_m has previously been demonstrated to have a Q_{10} of ca. 2 (Talling 1957a (2.3); Bindloss 1974 (2.2); Jewson 1976 (2.1); Jones 1977b (1.6); Hickman 1979 (2.2)). Pooled data for incubations at the southern sampling site suggested a Q_{10} of 2.4 although regression analysis indicated a large proportion of unexplained variation (Fig. 6.8a).

On a seasonal basis only the 1977/78 and 1978/79 data showed significant correlations with temperature giving Q_{10} values of 2.6 and 2.5 respectively, which were not significantly different from each other or the cumulative slope ($P>0.05$)(Fig. 6.8b-d). The large variation suggests that factors other than temperature were also

affecting photosynthetic capacity.

In 1979/80 measurements commenced after the initial warming period and only covered a temperature range of 16-23°C, therefore the lack of relationship between P_m and temperature was probably not significant.

The light intensity characterizing the onset of light saturation, I_k, is related by P_m by the initial slope (α) of the photosynthesis-irradiance curve (equation 6.2). At times of relatively constant α, I_k is expected to show the same response to temperature as P_m (Talling 1957a). I_k values from 1977/78 were significantly correlated with temperature (Fig. 6.9) giving a Q_{10} of 2.76, which was not significantly different from the Q_{10} for P_m (Fig. 6.8) over the same season ($P>0.05$). However no significant correlation was evident between I_k and temperature during 1978/79 or 1979/80 (Fig. 6.9b, c).

6.6 Daily Integral Photosynthesis

To demonstrate the validity of estimating daily rates from extrapolations of short term incubations, the daily integral photosynthesis for 27th December 1979 was estimated from six, one hour incubations carried out at staggered intervals using integrated euphotic samples. At this time the water column was strongly stratified (Fig. 6.10a) with the metalimnion extending from ca. 5-12m (Fig. 3.16). Algal growth had depleted nutrients from the upper layers of the water column, and the potential of the water to support growth, as determined from bioassay experiments, was negligible to a depth of 7.5m (Fig. 4.10b).

The dominant alga was *Microcystis aeruginosa* Kuetzing with *Ceratium hirundinella* (O.F. Muell.) Dujardin. and *Anabaena spiroides* Klebahn. making up most of the remaining biomass (Fig. 5.11).

In the early morning the epilimnion was typically isothermal (Chp. 3) to a depth of ca. 5m, however these layers became strongly stratified during the day (Fig. 6.10a). Large temperature variations were observed in the euphotic zone (1.2m), surface temperatures exceeding 26°C for a 2 h period following solar noon (Fig. 6.10a & 6.11a).

Chlorophyll-a profiles were measured fluorometrically to a depth of 12m using a Turner fluorometer and submersible pump as described in Chp. 2. Frequent water samples were taken from the fluorometer outlet to calibrate fluorescence readings with spectrophotometrically determined chlorophyll-a concentrations. The chlorophyll profiles demonstrated the marked effect of temperature stratification on phytoplankton distribution (Fig. 6.10b).

During the early morning chlorophyll a was evenly distributed throughout the 5m epilimnion, but decreased rapidly with depth in the hypolimnion. With the onset of thermal stratification in the euphotic zone at ca. 1000h, chlorophyll concentrations in the upper 2 metres of the water column decreased and a subsurface maxima developed between 2 and 3m which persisted for several hours (Fig. 6.10b).

Late in the afternoon the chlorophyll maxima dispersed as the surface water layers cooled, and by sunset (ca. 1930h Fig. 6.11a) maximum chlorophyll concentrations occurred in the euphotic zone.

Hourly integral rates of photosynthesis were estimated planimetrically and calculated using equation (6.1) (Talling 1957b) for each of the six incubation periods (Table 6.3). Talling's model successfully estimated hourly rates for each period except the last, where light intensity was too low to saturate photosynthesis.

Integral photosynthesis for periods between incubations was estimated by interpolation, and a total daily integral determined planimetrically from the resulting smooth curve (Fig. 6.11b).

The extended form of Talling's model (equation 6.6) was used to estimate daily integrals from each of the short term incubations (Table 6.4) and despite variations in parameters other than I_o', provided reasonable approximations.

Photosynthetic capacity displayed a diel variation with the maximum occurring near mid-day (Fig. 6.11c), a similar result to that obtained by MacCaull & Platt (1977) with natural populations and by Harding et al. (1981) for cultured marine diatoms.

Surface rates of photosynthesis were maximal prior to 0900h and decreased over the day (Fig. 6.11c), at other depths rates were symmetrically distributed around a solar mid-day maximum.

Theoretically, with all variables but light intensity constant, integral photosynthesis is expected to vary logarithmically with incident irradiance, a result of light saturation and the exponential decline of light intensity with depth (Talling 1957b). The diel variation in

P_m, combined with parallel changes in I_k, acted against this logarithmic dependence. The variation was sufficient for integral photosynthesis to be virtually proportional to incident irradiance (Table 6.3) as found by Goldman (1960), Tilzer (1973) and Lewis (1974). Consequently daily integral photosynthesis could be estimated from the fraction of daily irradiance received during the incubation period (Table 6.4). However, as integral photosynthesis does not always relate directly to incident irradiance (Talling 1971, Jewson 1975) daily rates were estimated using the extended version of Talling's equation. The close agreement between daily integral photosynthesis, and estimates calculated from experiments between ca. 1000-1400h provided support for the use of this period in regular photosynthesis measurements (Vollenweider 1965). The seasonal variation in daily integral rates estimated from short term incubations ranged from negligible (0.004) to 4.7 gC m^{-2} d^{-1} (Fig. 6.12).

Annual integral photosynthesis was measured planimetrically from curves joining daily integral estimates. Only data from 1979/80 provided an estimate unaffected by $CuSO_4$ treatment, and between October and May a value of 300 gC m^{-2} was obtained. As most photosynthesis occurs during this period (Fig. 6.12) the value closely approximates the annual integral.

6.7 Underwater Light-Climate and Respiration

Previous measurements of respiration in Mt. Bold Reservoir have generally yielded high rates per unit chlorophyll *a* (Ganf 1980), suggesting a large non-algal component. This, combined with low

biomass levels early in the season when variations in the light regime are most important (Chp. 5), has confounded attempts to assess periods of light sufficiency from the factor interaction described in equation (6.9).

In a manner analogous to that of Talling (1971) and Jewson (1976) the interaction of mixing depth, light regime and respiration described by equation 6.9 was depicted graphically by plotting $\frac{\varepsilon Z_m}{\ell n 2}$ against $[LDH]^{day}$ (Fig. 6.13).

The mixing depth, Z_m(m) (Fig. 6.14) was estimated from the extent of the isothermal epilimnion below a depth of ca. 2-5m. In this way superficial thermal gradients were excluded. The daylength, Δ was obtained from tables.

Although Fig. 6.13 illustrated the interaction of mixing depth and light regime, the relationship to actual relative respiration rates was unknown due to the difficulties of measuring phytoplankton respiration. To provide perspective, lines were included indicating the critical value of the ratio q_c, resulting in column compensation point (q_c=1.0, equation 6.8) for typical values of the relative respiration rate obtained from the literature (r=0.05, r=0.1; Talling 1971; Jewson 1976). The position of these lines was calculated from equation 6.9.

6.8 Integral Photosynthesis and Mean Irradiance of the Mixed Zone.

It was demonstrated in Chapter 5 that phytoplankton biomass levels were

correlated with the mean irradiance of the mixed zone ($\overline{I}$) up to a value of 1.6 MJ m^{-2} d^{-1}. During the spring increase of 1978, hourly rates of integral photosynthesis were also significantly correlated with $\overline{I}$ over the same range (Fig. 6.15, Table 6.5).

In 1979 only a few measurements of photosynthesis were made during the period of rapid vernal increase, however these showed a similar response to $\overline{I}$ and were included in Fig. 6.15 (Table 6.5).

For values of $\overline{I}$ above 1.6 MJ m^{-2} d^{-1} increases in integral photosynthesis appeared independent of further increases in $\overline{I}$ as observed for chlorophyll a concentration in Chapter 5.

DISCUSSION

6.9 Integral Photosynthesis

The direct comparison between lakes of integral rates of photosynthesis was complicated by variations in experimental design and calculation. It was evident from the data compiled in Table 6.6 however, that hourly integral rates for Mt. Bold Reservoir were generally lower than values observed in tropical lakes (L.Kilotes, L.Victoria, L.George) but of similar magnitude to rates observed in temperate lakes of the northern hemisphere. The most notable difference in comparison with the listed temperate lakes (Table 6.6) was the low minimum integral rate, which was similar to rates measured in oligotrophic lakes (eg. Toom Lake, Table 6.6). The low values were a function of the optically deep mixing conditions which prevailed in winter, a result

of the large attenuation of light by dissolved colour and suspended organic and inorganic material (Chp. 3). This resulted in low mean irradiances in the mixed zone and consequently low rates of integral photosynthesis (Fig. 6.15).

Minimum values shown for L.Minnetonka and Hamilton Harbour refer to ice-free periods, and winter minima are probably negligible (Megard 1972; Harris et al. 1980).

The annual gross photosynthesis of 300 gC m^{-2} estimated for Mt. Bold Reservoir was substantially lower than corresponding values for tropical and northern temperate lakes listed in Table 6.7, a consequence of the low winter rates of photosynthesis.

A further consequence of the large background attenuation of light was the close correlation between integral photosynthesis and chlorophyll a concentration (Fig. 6.7). As described in Chp. 3 the extinction coefficient ε may be partitioned into the extinction due to phytoplankton ($\varepsilon_s b$) and that due to background components (εq) where,

$$\varepsilon = \varepsilon_s b + \varepsilon q \qquad 6.11$$

The constancy of the logarithmic light function ($\ell n \left(\frac{I_o'}{0.5 I_k}\right)$) within a season, implied that most of the variation in integral photosynthesis resulted from variation in $\frac{bPm}{\varepsilon}$ (Fig. 6.5b-d). This term may be rewritten using equation 6.11 as, $\frac{bPm}{\varepsilon_s b + \varepsilon q}$, from which it is evident that when the extinction due to phytoplankton ($\varepsilon_s b$), is small compared to a constant background extinction (εq), integral photosynthesis will

change proportionately with bPm, the maximum volumetric rate of photosynthesis (Fig. 6.6a). As εq was consistently high in Mt. Bold Reservoir, and changes in P_m relatively small compared with changes in the chlorophyll *a* concentration b, integral photosynthesis correlated significantly with biomass (Fig. 6.7). Consequently both biomass and integral photosynthesis showed a similar dependence on the mean irradiance of the mixed zone ($\bar{I}$) for values below 1.6 MJ m^{-2} d^{-1}, and a similar independence of $\bar{I}$ above this value.

If the euphotic zone is taken as the depth to which 1% of the surface light penetrates (Chp. 3) then,

$$Z_{eu} = \frac{\ell n\ 100}{\varepsilon} = \frac{4.605}{\varepsilon_s b + \varepsilon q} \qquad 6.12$$

The large εq values attained in Mt. Bold Reservoir dampened variations in the depth of the euphotic zone expected from oscillations in biomass. As a result photosynthesis-depth profiles showed a marked degree of uniformity with respect to vertical extent (ca. 2-4m) and position of maximum photosynthetic rate (ca. 0.1-0.5m) (Fig. 6.2a-c).

The areal biomass within the euphotic zone Σb (mg chla m^{-2}) may be calculated from the product of the euphotic depth and the chlorophyll *a* concentration

$$\Sigma b = Z_{eu}.b = \frac{b\ \ 4.605}{\varepsilon_s b + \varepsilon q} \qquad 6.13$$

Applying similar arguments to those above, areal biomass will be largely proportional to biomass concentration when $\varepsilon_s b << \varepsilon q$.

The proportion of light attenuated by phytoplankton increases with biomass concentration (equation 6.11). In the limit when all light is absorbed by algae and $\varepsilon_s b >> \varepsilon q$, the population is completely self-shading and further increases in biomass reduce the depth of the euphotic zone proportionately. At this point the term $\frac{b}{\varepsilon_s b + \varepsilon q}$ (equation 6.13) maximizes at $\frac{1}{\varepsilon_s}$ and consequently areal biomass in the euphotic zone maximizes at $\frac{4.605}{\varepsilon_s}$, representing an important boundary condition to biomass levels. Similarly the component of integral photosynthesis, bPm/ε (equation 6.1) maximizes at P_m/ε_s, representing an upper theoretical limit to integral photosynthesis.

The extent to which natural populations attained the theoretical, maximum areal biomass was ascertained by comparison of experimentally determined values of b/ε, with the theoretical maximum of $1/\varepsilon_s$. In Mt. Bold Reservoir measures of ε_s obtained on four occasions (Fig. 3.5, Section 3.2) ranged from 0.016 to 0.021. A comparison of theoretical maxima with observed ratios of b/ε (Fig. 6.16) indicated that the populations never became completely self-shading. The maximum b/ε ratio, measured at the point of greatest chlorophyll concentration for the three seasons (Fig. 6.3a), accounted for only 65% of the theoretical maximum, while other values accounted for <50%.

Although these results imply that potentially there was light available within the euphotic zone to support an increased biomass level and rate of integral photosynthesis, the capability of the phytoplankton to utilize this potential depends on respiratory rates and mixing depth. Steel (1973, 1980) derived equations to estimate the maximum sustainable biomass and rate of integral photosynthesis however, the

difficulty of measuring *in situ* respiration rates in Mt. Bold Reservoir prevented application of these functions.

6.10 Integral Photosynthesis, Mean Irradiance of the Mixed Zone and Respiration.

The graphical illustration of the interplay between mixing depth and light regime (Fig. 6.13), included critical lines indicating zero net photosynthesis for typical values of the relative respiration rate. The data for 1978/79 indicated that on many of the sampling dates autotrophic growth would be predicted not to occur if "typical" relative respiration rates were assumed. However the points labelled 1-8 (Fig. 6.13a) correspond to the period of vernal increase in the mean irradiance of the mixed depth ($\overline{I}$), chlorophyll a concentration and integral photosynthesis. During this period (6/9/78 - 24/10/78) increases in chlorophyll a concentration (Chp. 5, Fig. 5.7 & 5.8) and integral photosynthesis (Fig. 6.15) were linearly related to $\overline{I}$. As growth was occurring, the relative respiration rate resulting in column compensation point for each date, provided a measure of the upper limit of the daily average relative respiration rate. Maximum relative respiration rates were calculated for data points 1-8 (Fig. 6.13) by substituting the relevant values of $\frac{\varepsilon Z_m}{\ell n 2}$ and $[LDH]^{day}$ into equation 6.9. These calculations indicated that initial spring growth occurred when relative respiration rates were less than 0.01. As the maximum specific rate of photosynthesis was ca. 2 mgC mg $chla^{-1}$ h^{-1}, the occurrence of growth implied an average respiration rate of less than ca. 0.02 mgC mg $chla^{-1}$ h^{-1}, suggesting a remarkable degree of adaptation to the low light environment.

The phytoplankton population during the vernal biomass increase was composed largely of flagellated species (Chp. 5, *Cryptomonas* spp, *Trachelomonas* spp and *Ceratium hirundinella*). The motility of these phytoplankton suggested that an alternative hypothesis to the apparently low respiration rates, might be the occurrence of a "biological mixing depth" substantially smaller than the mixing depth obtained from temperature profiles. Unfortunately insufficient data was available to assess this alternative.

6.11 Components of Integral Photosynthesis

It has been demonstrated that apart from temperature, nutrient availability may affect photosynthetic capacity (Glooschenko et al. 1974; Eppley & Renger 1974; Senft 1978). During the period December-February 1978/79 bioassay results indicated a lack of nutrients within the surface layers (Chp. 4, Fig. 4.10a), however P_m values were consistently among the highest observed (Fig. 6.3b).

Evidence for nutrient limitation during periods of the 1979/80 season came from both bioassay results and cellular compositional indicators (Chp. 4, Fig. 4.10a, Fig. 4.13). Variation in P_m (Fig. 6.3b) was similar to the general pattern observed in compositional indicators (Fig. 4.13), and over the nutrient depleted period (December-March, Fig. 4.10b) P_m and the protein-carbohydrate ratio were statistically correlated (Fig. 6.17). However the relationship was strongly influenced by a single large P_m value (9.9 mgC mg chla^{-1} h^{-1}), which in conjunction with the small number of data points, weakened the validity of the correlation.

Variations in photosynthetic capacity (P_m), and photosynthetic efficiency (α) have been considered potential mechanisms for adaptation to changing irradiance levels (Yentsch & Lee 1966; Talling 1966; Jorgensen & Steeman-Nielsen 1966; Vollenweider 1970; Jewson 1976; Jones 1978; Harris et al. 1980; Harris, 1978).

Vollenweider (1970) illustrated theoretically the significance to integral photosynthesis of adaptations in P_m, α and consequently their ratio I_k (equation 6.2), following a decrease in irradiance. Jones (1978) demonstrated the occurrence of the two mechanisms in Lough Neagh. He found that when diatoms predominated α remained relatively constant so that P_m, which altered in response to temperature, determined the variation in I_k. However, when blue-green algae were dominant, adaptation to variation in irradiance was principally determined by changes in photosynthetic efficiency (α).

Analysis of relationships between these variables for Mt. Bold Reservoir indicated seasonal differences in their relative importance.

During 1977/78 changes in I_k were closely correlated with P_m (Fig. 6.18a) but not with α (Fig 6.18b) which varied over a relatively narrow range. Consequently P_m and α were independent (Fig. 6.18c). Photosynthetic capacity was temperature dependent showing a Q_{10} of 2.6 which was not significantly different from the Q_{10} of 2.76 determined for I_k (Fig. 6.8b & 6.9a). These results were similar to relationships described by Jones (1978) for diatom dominated populations, however the data from Mt. Bold Reservoir covered a period initially dominated by *Microcystis aeruginosa* (23/11/77 - 15/2/78) and

then by *Cyclotella meneghiniana* (12/4/78 - 28/6/78) (M. Burch, personal communication).

In 1978/79, neither photosynthetic capacity (P_m) nor photosynthetic efficiency (α) were correlated with I_k, which showed reduced variation (Fig. 6.19a & b) compared with the previous season. P_m and α were strongly correlated suggesting that both were changing in unison (Fig. 6.19c), and consequently I_k did not increase with temperature in parallel to photosynthetic capacity (Fig. 6.8c & 6.9b). The period covered by this data included populations dominated by *Cyclotella meneghiniana* and *Ceratium hirundinella*, *Trachelomonas* spp, *Microcystis aeruginosa*, and *Melosira* sp (Fig. 5.10, Table 5.3).

Estimates of I_k from 1979/80 showed a significant correlation with photosynthetic efficiency (α) but not with photosynthetic capacity (P_m) (Fig. 6.20a & b) although P_m and α were significantly correlated (Fig. 6.20c). Jones (1978) found a similar lack of correlation between I_k and P_m during periods of blue-green algal dominance, when both I_k and α were correlated with the average light intensity over the preceeding five days. The values from Mt. Bold Reservoir showed no statistically significant correlation with light intensity although the population was for the most part dominated by *Microcystis aeruginosa* (Fig. 5.11, 1/11/79 - 1/4/80).

The data of Jones (1978) related to measurements taken in the well mixed but shallow Kinnego Bay (Maximum depth = 3.5m, Jones 1977a), where it might be expected that mean irradiance of the mixed column was closely related to variation in incident irradiance. It was

postulated that the lack of relationship between incident irradiance and α or I_k in Mt. Bold Reservoir, resulted from variations in mixing depth. To account for such variations the mean irradiance of the mixed zone ($\bar{I}$) calculated from equation (5.1) was used to assess the light regime during 1978/79 and 1979/80. However no statistically significant relationship was found between the mean irradiance of the mixed zone and α, I_k or P_m (Fig. 6.21a-c). Even when analysis was restricted to periods of light limitation ($\bar{I} < 1.6$ MJ m^{-2} d^{-1}) statistically valid relationships were not obtained.

Thus mechanisms for modifying photosynthesis irradiance relationships apparently occurred within Mt. Bold Reservoir, either singly or in unison, but they showed no clear cut relationship with either species composition, incident irradiance or mean irradiance of the mixed zone.

Harris et al. (1980) emphasized the important effect which changes in the ratio of euphotic to mixed depth has on photosynthesis. The appearance in Mt. Bold Reservoir of a particular strategy within a season, suggested that an over-riding influence of this nature might be affecting the photosynthetic variables. Although mixing regime varied between the three seasons (Chp. 3) the simultaneous influence on light and nutrient availability complicated any attempts at analysis.

A COMPARISON OF ABSORBED AND INCIDENT IRRADIANCE AS DETERMINANTS OF PHOTOSYNTHESIS.

6.12 Introduction

Empirical models describing photosynthesis-irradiance relationships (Smith 1936; Vollenweider 1965; Platt et al. 1980) and photosynthesis-depth integrals (Talling 1957b; Fee 1973) provide a basis for the comparison of data obtained through time and space. Variables contained within the models are used to assess both the physiological condition of the phytoplankton (Yentsch & Lee 1966; Jones 1978; Platt et al. 1980) and the importance of factors determining areal photosynthesis (Talling et al. 1973; Bindloss 1974; Jewson 1976; Section 6.0 - 6.11). As the models are constructed in terms of incident irradiance, comparisons between experiments are based on an implicit assumption of constant potential absorption per unit biomass.

The absorption of light by phytoplankton depends on pigment composition and cell architecture (Kirk 1975a; Platt & Jassby 1976), as well as the influence of the suspending medium on incident irradiance (Morel 1978; Atlas & Bannister 1980). Measurement of *in situ* phytoplankton extinction coefficients is difficult, and of the available data most refer to phytoplankton absorption of narrow wavebands (Talling 1960; Ganf 1974; Bindloss 1974) rather than photosynthetically active radiation (Scott 1978; Megard et al. 1979). The data does however demonstrate a threefold range in extinction coefficients.

Alternative attempts to estimate the average *in situ* extinction coefficient of phytoplankton groups from information on pigment absorption spectra (Kirk 1975b; Atlas & Bannister 1980), require a knowledge of cellular pigment composition, the spectral distribution of irradiance, and the effects on absorption of cell architecture and increased pathlength through light scattering. The quantification of all these parameters has not been achieved.

As a consequence of the inherent difficulties in obtaining field measurements of light attenuation by phytoplankton, investigations of the relationship between photosynthesis and light absorption have frequently assumed a constant specific extinction coefficient (Tyler 1975; Dubinsky & Berman 1976; Morel 1978), and the same assumption implicit in photosynthesis-irradiance models. The observed three fold range in phytoplankton extinction coefficients suggests that this assumption may frequently be invalid (Morel 1978; Atlas & Bannister 1980).

The following section attempts to assess the affect of variations in light absorption on variables of the photosynthesis-irradiance models used extensively for comparative purposes.

6.13 Theory

Using the Beer-Lambert law (equation 3.1) Duntley (1963) derived an equation to calculate the total radiant energy absorbed by all physical and chemical processes at depth Z metres. Restricting the argument here to photosynthetically active radiation (PAR, 400-700 nm)

the irradiance absorbed per volume is given by

$$\frac{dA(Z)}{dV} = \frac{d}{dZ} (I_D(Z) - I_u(Z)) \qquad 6.14$$

where $I_D(Z)$ is the downwelling irradiance and $I_u(Z)$ the upwelling irradiance at depth Z metres (Chp. 3). Rearrangement gives

$$\frac{dA(Z)}{dV} = \frac{d}{dZ} I_D(Z) \left(1 - \frac{I_u(Z)}{I_D(Z)}\right) \qquad 6.15$$

The ratio of upwelling to downwelling irradiance is termed reflectance, R (Chp. 3) and is often found to be virtually independent of depth (Duntley 1963). In the turbid inland waters typical of Australia, reflectance initially shows a small increase with depth but rapidly attains a constant value (Chp. 3, Fig. 3.11; Kirk 1977). Equation 6.15 can therefore be rewritten as,

$$\frac{dA(Z)}{dV} = \frac{d}{dZ} I_D(Z) \quad (1-R) \qquad 6.16$$

A further consequence of turbid waters is the minimal interference of spectral shifts on the exponential decline of PAR with depth after the first few centimetres. As a result the Beer-Lambert law accurately describes light attenuation over most of the euphotic zone with a single vertical extinction coefficient (Fig. 3.1, equation 3.1).

Incorporating the Beer-Lambert law into equation 6.16 and differentiating with respect to depth,

$$A(Z) = \varepsilon I_o' e^{-\varepsilon Z} (1-R) \qquad 6.17$$

where A(Z) is the total absorbed PAR per unit volume at depth Z metres ($\mu E\ m^{-3}\ s^{-1}$), ε the vertical extinction coefficient (ℓn units m^{-1}) and I_o' the incident irradiance corrected for surface reflection (Chp. 2).

The proportion of total absorbed irradiance (equation 6.17) attenuated by phytoplankton alone is given by the ratio of the phytoplankton extinction coefficient to the total extinction coefficient (Bannister 1974). In terms of equation 3.3 the fraction is $\frac{\varepsilon_s b}{\varepsilon}$, where ε_s is the specific extinction coefficient per unit chlorophyll a (m^2 mg $chla^{-1}$) and b, the chlorophyll a concentration (mg chla m^{-3}). The irradiance absorbed by the phytoplankton at depth Z metres, $A^*(Z)$ ($\mu E\ m^{-3}\ s^{-1}$) is therefore,

$$A^*(Z) = \varepsilon_s b I_o' e^{-\varepsilon Z} (1-R) \qquad 6.18$$

As R is frequently found to be small (ca. 0.02) the equation can be simplified to that derived by Bannister (1974). However values of R regularly approach 0.1 (Kirk 1977) and may exceed 0.3 (Fig. 3.6) in turbid waters, therefore R is incorporated in the following equations.

The depth integral of equation 6.18 provides an estimate of the irradiance absorbed by chlorophyll a per unit surface area,

$$\int_o^{Z_m} A^*(Z)dZ = \frac{\varepsilon_s b I_o'}{\varepsilon} (1-e^{-\varepsilon Z_m}) (1-R) \qquad 6.19a$$

where Z_m is the mixed depth in metres. If Z_m is equal to the euphotic depth, Z_{eu}, then from equation 6.12, $Z_m = \frac{4.605}{\varepsilon}$, and the term in brackets equals 0.99. When Z_m is greater than Z_{eu} the

bracketed term is close to unity and equation 6.19a reduces to,

$$\int_{o}^{Z_m > Z_{eu}} A^*(Z)\, dZ = \frac{\varepsilon_s b I_o'}{\varepsilon} (1-R) \qquad 6.19b$$

The light absorbed per unit chlorophyll a at depth Z, $A_b^*(Z)$ (μE mg $chla^{-1} s^{-1}$) follows simply from equation 6.18,

$$A_b^*(Z) = \varepsilon_s I_o' e^{-\varepsilon Z} (1-R) \qquad 6.20$$

It is evident from this equation that for a given light intensity and reflectance value, the energy absorbed per unit chlorophyll a, and so the effectiveness of the incident irradiance, varies with the specific extinction coefficient per unit chlorophyll a (ε_s). Consequently those variables describing photosynthesis-irradiance relationships which incorporate light intensity will be functions of ε_s. Two such variables are α' (mg C mg $chla^{-1}$ per E m^{-2}) the initial slope of the photosynthesis-irradiance curve (Platt & Jassby 1976), and I_k ($\mu E\ m^{-2}\ s^{-1}$) the light intensity characterizing the onset of light saturation (Talling 1957a). Note that α' varies from α (mg C mg $chla^{-1}\ h^{-1}$ per $\mu E\ m^{-2}\ s^{-1}$) used in the previous section, by incorporating the trivial conversions for time units and μ Einsteins to Einsteins, that is at low light intensities

$$\alpha' = \frac{P(Z)}{I(Z)} \times \frac{10^6}{3600} \qquad 6.21$$

where P(Z) (mg C mg $chla^{-1}\ h^{-1}$) is the specific rate of photosynthesis.

Converting light intensity at depth Z (I(Z)), to the light absorbed

per unit chlorophyll *a* using equation 6.20, yields the relationship,

$$\alpha_m^* = \frac{\alpha'}{\varepsilon_s(1-R)} \qquad 6.22$$

where α_m^* (mg C per E) is the weight of carbon fixed per unit light absorbed by phytoplankton at low light intensities. The quantum yield $\emptyset$ is defined as the moles of carbon fixed per Einstein of light absorbed (Bannister 1974; Dubinsky & Berman 1976). The maximum quantum yield $\emptyset_m$ is therefore proportional to α_m^*,

$$\emptyset_m = \frac{\alpha'}{\varepsilon_s(1-R).12000} \qquad 6.23$$

Direct substitution of I_k into equation 6.20 provides an estimate of I_k^*, the level of absorbed irradiance per unit chlorophyll *a* depicting the onset of light saturation.

As described in previous sections, models of integral photosynthesis are frequently used to provide insight to the causes of variation in areal carbon fixation rates. The model of Talling (1957b) accurately assessed integral photosynthesis in Mt. Bold Reservoir, however the parameters in the function (equation 6.1) provided little information on the types of mechanisms frequently cited as controlling rates of photosynthesis, viz. light absorption and the efficiency of energy transformation. In an attempt to provide further insight to the significance of variations in these mechanisms, the semi-empirical model of Talling was recast into more functional components. The slightly modified original model, described by equation 6.1, is restated here,

$$\Sigma P = \frac{bPm}{\epsilon} \ln \left(\frac{I_o'}{0.5I_k}\right)$$

By definition $P_m = \alpha I_k = 0.0036\ \alpha'\ I_k$ (equation 6.2 & 6.21) and,

$$\Sigma P = 0.0036\ \frac{b\alpha' I_k}{\epsilon} \ln \left(\frac{I_o'}{0.5I_k}\right) \qquad 6.24$$

Substituting for α' in this equation using equation 6.23,

$$\Sigma P = (12000\ .\ 0.0036)\ \frac{\epsilon_s b \phi_m}{\epsilon} (1-R)\ I_k \ln\left(\frac{I_o'}{0.5I_k}\right) \qquad 6.25$$

Multiplying the right hand side of the expression by $\frac{I_o'}{I_o'}$,

$$\Sigma P = 43.2\ \left[\frac{\epsilon_s b I_o'}{\epsilon} (1-R)\right]\ \phi_m \frac{I_k}{I_o'} \ln \left(\frac{I_o'}{0.5I_k}\right) \qquad 6.26$$

The term in square brackets will be recognized from equation 6.19a & b as the total light absorbed by chlorophyll *a* per unit surface area when the mixed depth is greater than the euphotic depth. ϕ_m is the maximum quantum yield which is proportional to the initial slope of the photosynthesis irradiance curve expressed on an absorption basis (equation 6.22 & 6.23). The remaining parameters

$$\int = \frac{I_k}{I_o'} \ln \left(\frac{I_o'}{0.5I_k}\right) \qquad 6.27$$

provide a measure of the restriction that light saturation places upon integral photosynthesis (Talling 1957b). This is readily shown by considering a photosynthesis-depth profile where photosynthesis remains proportional to light intensity at all depths,

$$P = b\alpha I_o' e^{-\varepsilon Z} \qquad 6.28$$

Integrating with depth and substituting for α(equation 6.2) yields,

$$\int_0^\infty P \, dZ = \frac{b\alpha I_o'}{\varepsilon} = \frac{bP_m I_o'}{\varepsilon I_k} \qquad 6.29$$

The fraction of this represented by the normal integral (equation 6.1), is given by equation 6.27.

The average quantum yield of a photosynthesis-depth profile may be calculated from the ratio of areal photosynthesis to the light absorbed by phytoplankton per unit surface area. Consequently the ratio of equation 6.1 to equation 6.19a or b, provides an estimate of $\overline{\phi}$, the average quantum yield for a profile showing saturation behaviour. However the ratio of equation 6.29 to equation 6.19 provides an estimate of ϕ_m, the maximum quantum yield. As a result it follows that,

$$\frac{\overline{\phi}}{\phi_m} = \int \qquad 6.30$$

and equation 6.26 may be rewritten as,

$$\Sigma P = 43.2 \left[\frac{\varepsilon_s b I_o'}{\varepsilon} (1-R) \right] \overline{\phi} \qquad 6.31$$

As discussed in Section 6.5, the equation derived by Talling (1957b) to describe integral photosynthesis (equation 6.1) only applies when $I_o' >> I_k$. If data are to be considered at low ratios of I_o'/I_k, then the equation derived by Vollenweider (1965) (equation 6.10) provides

the correct integral, assuming that the photosynthesis-irradiance relationship is adequately described by the equation of Smith (1936).

Beginning with the function for integral photosynthesis derived by Vollenweider (equation 6.10), an analogous series of equations to those depicted by equations 6.24 to 6.27 may be derived. The equation analogous to 6.26 becomes,

$$\Sigma P = 43.2 \left[\frac{\varepsilon_s b I_o'}{\varepsilon} (1-R) \right] \phi_m \frac{I_k}{I_o'} \text{ Arcsinh } \left(\frac{I_o'}{I_k}\right) \qquad 6.32$$

where $\text{Arcsinh } \left(\frac{I_o'}{I_k}\right) = \ell n \left(\frac{I_o'}{I_k} + \sqrt{\left(\frac{I_o'}{I_k}\right)^2 + 1}\right)$ (Vollenweider 1965), while the function $\int$, describing the restriction of light saturation on integral photosynthesis (equation 6.27) converts to,

$$\int = \frac{I_k}{I_o'} \text{ Arcsinh } \left(\frac{I_o'}{I_k}\right) \qquad 6.33$$

Equations 6.30 and 6.31 appear in the same form, although calculated using the $\int$ function of equation 6.33.

6.14 Results

The Beer-Lambert law accurately described the exponential decline of PAR with depth, yielding linear regression correlation coefficients (r^2)> 0.97 (Fig. 3.1). The vertical extinction coefficients were partitioned into the component due to phytoplankton ($\varepsilon_s b$) and that due to other material (εq) (equation 3.3) for periods when ε_s and εq remained constant (Section 3.2). Four such periods were identified from the data on Mt. Bold Reservoir and the specific extinction

coefficient per unit chlorophyll *a* (ε_s) estimated from the incremental change of ε with b the chlorophyll *a* concentration (Section 3.2, Fig. 3.5, Table 3.1). The choice of chlorophyll *a* as the independent variable is supported by its central role in photosynthesis, and its close relationship with cell volume (Fig. 6.22).

Similar data for Lough Neagh, was obtained from figures in Jones (1977a, b) for the period August-June 1973. Vertical extinction coefficients for PAR (ε) were estimated from the minimum extinction coefficient (εmin) using the factor of 1.2 calculated by Jones (1977b), and ε_s estimated from the linear regression of extinction coefficient on chlorophyll *a* concentration (Fig. 6.23).

All estimated ε_s values were significantly different from zero ($P<0.02$). The values of 0.0122, 0.0133 and 0.016 (Table 3.1) were not significantly different from each other ($P>0.05$) however all other combinations were.

The ε_s values from Mt. Bold Reservoir fell within the range of previously reported estimates, ca. 0.01-0.02 m^2 mg $chla^{-1}$ (Talling 1960; Bindloss 1974; Ganf 1974; Megard *et al*. 1979) whereas the value from Lough Neagh (0.029 m^2 mg $chla^{-1}$) was significantly larger.

Carbon fixation rates were measured directly in Mt. Bold Reservoir using the ^{14}C technique (Chp. 2), while the oxygen results from Lough Neagh (Jones 1977b) were converted to a carbon basis assuming a P.Q. ratio ($\frac{O_2}{CO_2}$ molar) of 1.1 (Harris & Piccinin 1977).

The interconversion of energy and quantum irradiance measurements depends upon the underwater-irradiance spectral distribution. In Mt. Bold Reservoir the spectral distribution at 1.0 and 2.0m, caused solely by water and dissolved coloured compounds (Fig. 3.9), showed strong absorption in the blue-wavelengths due to the presence of "gelbstoff" (Section 3.3). Filtrates from Lough Neagh (Jewson & Taylor 1978) also showed absorption due to "gelbstoff", and *in situ* spectra were further modified by high chlorophyll a concentrations (Jewson 1977; Jewson & Taylor 1978). Consideration of these data in relation to conversion factors measured by Morel and Smith (1974) resulted in use of the relationship,

$$1.0 \text{ watt} = 2.77 \times 10^{18} \text{ quanta } s^{-1} = 4.6013 \ \mu E \ s^{-1} = 1 \text{ Joule } s^{-1}$$

The quantum yield ($\emptyset$, mole C per Einstein absorbed) was calculated for each depth from the ratio of the measured carbon fixation rate (mole C mg $chla^{-1}$ h^{-1}) to the light absorbed by phytoplankton (equation 6.20 in Einsteins mg $chla^{-1}$ h^{-1}) and plotted against the natural logarithm of I(Z) (Fig. 6.24). As expected quantum yield increased with depth (Tyler 1975; Dubinsky & Berman 1976; Morel 1978), the maximum ($\emptyset_m$) occurring at low light intensities. Equation 6.23 indicates that in the low light region, where photosynthesis is linearly related to light intensity, $\emptyset_m$ should remain constant. However, very few of the profiles showed a distinct plateau (Fig. 6.24) despite the inclusion of data points below ca. 50 $\mu E \ m^{-2} \ s^{-1}$ which frequently appear linearly related to photosynthesis (Platt & Jassby 1976; this data). The lack of a plateau region was evident with both the ^{14}C technique employed here

(Fig. 6.24a-c), and the O_2 technique used by Jones (1977b) (Fig. 6.24d).

For the data from Mt. Bold Reservoir, ϕ_m was calculated from the initial slope of photosynthesis-irradiance curves using equation 6.23, and varied between 0.014 and 0.075 mole C (Einstein)$^{-1}$ (Table 6.8). Taking a value of 8 as the minimum quantum requirement of photosynthesis, the largest value ϕ_m can attain is 0.125 mole C Einstein^{-1} (Rabinowitch & Govindjee 1969). The average value for the data from Mt. Bold Reservoir was 0.037 mole C Einstein^{-1}, which fell far short of the theoretical maximum, and was less than the average value suggested as typical by Bannister (1974) and estimated by Platt & Jassby (1976) of 0.06 mole C Einstein^{-1}.

Substitution of ϕ_m = 0.125 into equation 6.23, enabled an estimate to be made of the minimum theoretical value of ε_s for a given value of α'. Data from Kinnego Bay for the 26 April 1973 (Jones 1977b) gave a maximum α' value for the period under consideration of ca. 45.3 mg C mg chla^{-1} Einstein^{-1}, and a minimum ε_s value from equation 6.23 of 0.03 m^2 (mg chla)$^{-1}$. This supported the ε_s value of 0.029 obtained from the incremental change of ε with b (Fig. 6.23).

Mixing depth (Z_m) was greater than the euphotic depth (Z_{eu}) in both Mt. Bold Reservoir (Fig. 6.14) and Lough Neagh (Jones 1977a, b), and photosynthesis incubations covered the entire euphotic zone. Therefore the total light absorbed by phytoplankton per unit surface area was calculated using equation 6.19b (Table 6.7 & 6.8), and the average quantum yield for the water column $\overline{\phi}$, estimated from the

ratio of planimetrically measured integral photosynthesis to the areal absorbed light (Table 6.8 & 6.9). In Mt. Bold Reservoir $\overline{\emptyset}$ varied between 0.005 and 0.047 mole C (Einstein)$^{-1}$ (Table 6.8) while the available Lough Neagh data covered the range 0.004 to 0.01 mole C (Einstein)$^{-1}$ (Table 6.9).

Values of the fraction $\int$ calculated using equation 6.33 ranged between 0.26 and 0.71 for Mt. Bold Reservoir (Table 6.8) and 0.19 and 0.32 for Lough Neagh (Table 6.9). The $\int$ function obtained from the shortened form of the integral used by Talling (1957b) (equation 6.27) provided similar values, as in all cases incident irradiance (I_o') was much larger than I_k (Table 6.8 & 6.9). The difference between the two functions of $\int$ for varying incident irradiance and fixed I_k values is illustrated in Fig. 6.25a & b.

6.15 Discussion

The effect of variations in the specific extinction coefficient per unit chlorophyll a (ε_s) on the interpretation of variables from photosynthesis-irradiance relationships, can be illustrated using data from Mt. Bold Reservoir and Lough Neagh.

Applying equation 6.20, the maximum observed I_k value of 344 µEinstein m^{-2} s^{-1} (Table 6.8, 12/12/78) represented an absorbed irradiance of 4.5 µEinstein (mg chla)$^{-1}$ s^{-1}, while the lower value of 306 µEinstein m^{-2} s^{-1} measured on the 28 February 1980 (Table 6.8), represented an increased absorption of 5.6 µEinstein (mg chla)$^{-1}$ s^{-1}.

Similar I_k values of 207.5 and 201.9 μEinstein m^{-2} s^{-1} obtained from two experimental periods (Table 6.8, 10/5/78 & 16/1/80) implied a similar response to light saturation, however in terms of absorbed irradiance the values were respectively 2.3 and 4.1 μEinstein (mg chla)$^{-1}$ s^{-1}.

The 2.2 fold greater I_k value (230.2 μEinstein m^{-2} s^{-1}) from Mt. Bold Reservoir on 6 December 1978 (Table 6.8) compared with Kinnego Bay (106 μEinstein m^{-2} s^{-1}) on 30 May 1973 (Table 6.9) might be interpreted as indicating a physiological variation between the two populations, yet in terms of absorbed irradiance the values were 3.0 and 3.1 μEinstein mg chla^{-1} s^{-1} respectively.

These examples clearly demonstrate the marked difference between comparisons of the effective absorbed irradiance and simple measures of irradiance intensity. As the effectiveness of a given light intensity is determined by ϵ_s, which in turn is determined by both biological (Kirk 1975a, b, 1976a) and environmental factors (Morel 1978; Atlas & Bannister 1980), light intensity based photosynthetic parameters such as I_k, may not be valid indicators of the physiological condition of phytoplankton. The onset of light saturation defined as a function of irradiance absorbed per unit chlorophyll a, provides a more satisfactory parameter.

Similar arguments apply to comparisons of the initial slope of photosynthesis-irradiance curves (α'). For example α' values from the 11 December 1979 and 1 April 1980 (Table 6.8) suggested a 25% difference in the photosynthetic rate at low light intensities. On

an absorption basis however, (equation 6.22) the difference was less than 4%, indicating that the variation was due to light absorption ability, and not to utilization efficiency of absorbed irradiance. As variations in light absorption are a function of ε_s, the difference may have been physiologically based or equally well resulted from physical differences in the light regime. To distinguish between these alternatives requires data on the underwater-irradiance spectral distribution (Morel 1978; Atlas & Bannister 1980) as well as cellular pigment content and architecture (Kirk 1975a, b; Platt & Jassby 1976; Taguchi 1976). For the two dates in question there was a significant difference in the irradiance spectral distribution determined from filtrates. This change, illustrated by Fig. 3.9e & g, coincided with the change in ε_s over the 1979/80 season (Table 6.8). However there was also a shift in species composition, from a population dominated by *Microcystis* but with *Ceratium* comprising 25% of total cell volume, to a population entirely composed of *Microcystis* (Fig. 5.11). Data on *in situ* spectral distributions, and specific species ε_s values would be required for further analysis of these changes.

The rearranged form of Talling's (1957b) model (equation 6.26 & 6.31) focuses attention on mechanisms underlying the photosynthetic response of phytoplankton to the light environment. Using this model variations in integral photosynthesis may be attributed proportionately to changes in the absorption or utilization of absorbed irradiance. For example, the 44% decrease in integral photosynthesis (ΣP) observed on Mt. Bold Reservoir between 4 and 11 December 1979 (Table 6.10) was due entirely to the 50% decrease in light absorbed by phytoplankton, the change in average quantum yield ($\bar{\phi}$) being insignificant. Analysis

of the factors affecting the quantity of light absorbed (equation 6.19b) indicated that the reduction was due to a 67% decrease in chlorophyll _a_ concentration (Table 6.10) acting through its effect on both b and ε.

Although average quantum yield increased only slightly, it was noteworthy that the components $\int$ and ϕ_m each changed by ca. 30%. However as the changes were equal and opposite the effect on the integral was negligible.

A similar analysis indicated that the eight fold increase in integral photosynthesis between 27 November and 4 December 1979 (Table 6.10) was due to both a 2.1 fold increase in the average quantum efficiency ($\overline{\phi}$) of the population, and a 3.7 fold increase in the light absorbed by chlorophyll _a_.

The increased light absorption resulted from a 5.9 fold increase in chlorophyll _a_ concentration (Table 6.10). Although the chlorophyll per cell volume increased by 37% this was insignificant compared to the increased concentration in the water.

The change in average quantum yield was due largely to an increase in ϕ_m, the maximum quantum yield. The relatively small change in $\int$ implied that variations in P_m and α were compensatory.

In the examples considered above changes in incident irradiance (I_o') were insignificant while ε_s, the specific extinction coefficient per unit chlorophyll _a_ and εq the background extinction coefficient, remained constant.

Integral photosynthesis for Mt. Bold Reservoir on 11 March 1980 was 3.48 fold higher than on 30 November 1978, despite the same average quantum efficiencies and chlorophyll a concentrations (Table 6.10). Comparison of absorbed irradiances indicated that this was the source of the variation, which resulted in part from a 2.2 fold higher light intensity and in part from a 1.6 fold higher ε_s value. Insufficient data was available to assess the source of variation in ε_s.

As the average quantum efficiency ($\overline{\phi}$) is likely to vary between relatively narrow limits (Bannister 1974) equation 6.31 predicts a close relationship between integral photosynthesis and the total light absorbed by the phytoplankton. The data from Mt. Bold Reservoir (Table 6.8) and Kinnego Bay (Table 6.9) were plotted in Fig. 6.26 along with a single point from Lake George, Uganda (Ganf 1975, $\frac{\varepsilon_s b I'_o}{\varepsilon}$ = 842.8 μEinstein m^{-2} s^{-1}, ΣP = 462.8 mgC m^{-2} h^{-1}).

At absorption values less than 1000 μEinstein m^{-2} s^{-1}, integral photosynthesis and light absorption were closely related, an increase in one generally causing an increase in the other (Fig. 6.26). However, for values above 1000 μEinstein m^{-2} s^{-1}, as observed in Kinnego Bay (Table 6.9), integral photosynthesis decreased due to a reduction in average quantum yield ($\overline{\phi}$). For example, on the 16 May 1973 when absorbed irradiance was greater than 1000 μEinstein m^{-2} s^{-1}, integral photosynthesis was depressed. One week later on the 23 May, absorbed irradiance was less than 1000 μEinstein m^{-2} s^{-1} and the rate of integral photosynthesis comparable to levels obtained from Mt. Bold Reservoir. The following week absorbed irradiance was again high and

integral photosynthesis depressed. Analysis of data in Table 6.9 & 6.11 indicated that variation in the irradiance absorbed by phytoplankton was due entirely to variations in incident irradiance (I_o'). Changes in chlorophyll a concentration (b) did occur, but these were counteracted by similar changes in the extinction coefficient ε, as a result of the linear relationship between b and ε, and the relatively small value of εq (Fig. 6.23, Table 6.9).

Changes in both $\int$ and ϕ_m affected the average quantum yield, $\overline{\phi}$, however, variations in the maximum quantum yield ϕ_m, were generally more significant (Table 6.9). Thus it appeared that in Kinnego Bay there was a critical PAR absorption value above which physiological changes in the phytoplankton caused a decrease in ϕ_m.

In Fig. 6.26 integral photosynthesis was depicted as a function of total light absorbed by phytoplankton. Dividing each of the axis values by the chlorophyll a content of the mixed zone (bZ_m), indicates that the average rate of carbon fixation per unit chlorophyll a was closely correlated with the average irradiance absorbed per unit chlorophyll a. Exceptions to the relationship were the depressed values for Kinnego Bay.

From equation 6.19a, the average light absorbed per unit chlorophyll a in the mixed zone is given by,

$$\overline{A}^* = \frac{\varepsilon_s I_o'}{\varepsilon Z_m} (1-e^{-\varepsilon Z_m}) (1-R)$$

Comparing this with the equation for calculating the mean irradiance of

the mixed zone ($\bar{I}$)(equation 5.1; Riley 1957) indicates that when R, the reflectance, and ε_s remain constant, variation in $\bar{I}$ will be proportional to variation in average light absorbed per unit chlorophyll _a_.

ε_s values measured after the vernal increase of 1978/79 (ε_s=0.0133) and 1979/80 (ε_s=0.0160) were not significantly different (Fig. 3.5b & c). Assuming these values applied during the period of increase, then previous discussion on the relationship between $\bar{I}$ and both chlorophyll _a_ concentration (Section 5.2) and integral photosynthesis (Section 6.8) may be considered in terms of light absorption per unit chlorophyll _a_. This makes more explicable the notion of a critical $\bar{I}$ value above which biomass and integral photosynthesis appear independent of further increases in mean irradiance.

In terms of irradiance absorbed per unit chlorophyll _a_ the critical value implies a saturation effect, which is well known from laboratory studies (Paasche 1968; Gons & Mur 1975, 1978; Bannister 1979).

Paasche (1968) measured the growth rate of two marine diatoms at varying light intensities and daylengths. Growth was strongly light limited below a value of 0.03 gcal cm^{-2} min^{-1}, but approached saturation above this level. In standard units this light intensity equals 1.8 MJ m^{-2} d^{-1}.

Bannister (1979) using the data on *Chlorella pyrenoidosa* embodied in a series of papers, (Phillips (1953), Phillips & Myers (1954a, b) and Myers & Graham (1971), cited in Bannister 1979) calculated incident

irradiance and absorbed irradiance per unit chlorophyll *a* in Einsteins, and illustrated their relationship with growth. The data suggested that growth was virtually saturated at an incident irradiance of 8.1 E m^{-2} d^{-1}. The critical field value of 1.6 MJ m^{-2} d^{-1} was converted to Einsteins using the above-surface conversion factor of Morel & Smith (1974) (1 Joule = 4.60132 μE), and yielded a value of 7.36 E m^{-2} d^{-1}.

Bannister (1979) calculated absorbed irradiance to be 0.086 E $mgchla^{-1}$ d^{-1}. The mean irradiance of the mixed zone ($\bar{I}$) may be converted to absorbed irradiance by multiplication with ε_s (equation 6.19a). Assuming ε_s = 0.013, the critical value was equivalent to 0.096 E $mgchla^{-1}.d^{-1}$.

It is apparent from these comparisons that the critical value of 1.6 MJ m^{-2} d^{-1} represents an important boundary between light limiting and non-limiting conditions.

Fig. 6.1: Correlation between rates of photosynthesis measured using the oxygen light-dark bottle technique (gross photosynthesis) and ^{14}C techniques, for a series of depth profiles.

a) ● P (mgC)= 0.069+0.336 GP(mg O_2) r^2= 0.99

○ P (mgC)= -0.15+0.402 GP(mg O_2) r^2= 0.96

b) ● P (mgC)= -0.51+0.32 GP(mg O_2) r^2= 0.99

c) ● P (mgC)= 0.14+0.194 GP(mg O_2) r^2= 0.98

○ P (mgC)=-0.02+0.211 GP(mg O_2) r^2= 0.93

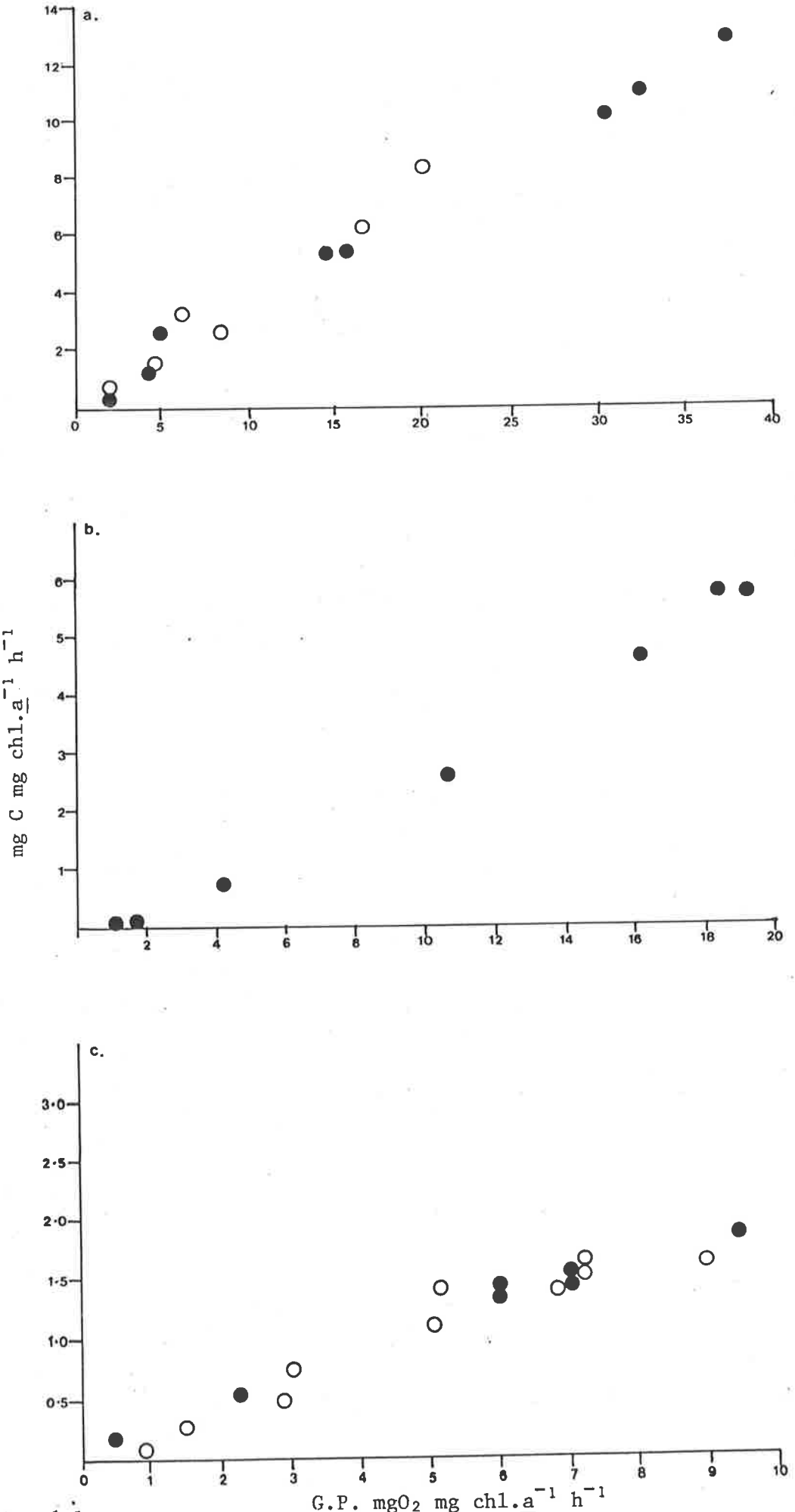

Fig. 6.1:

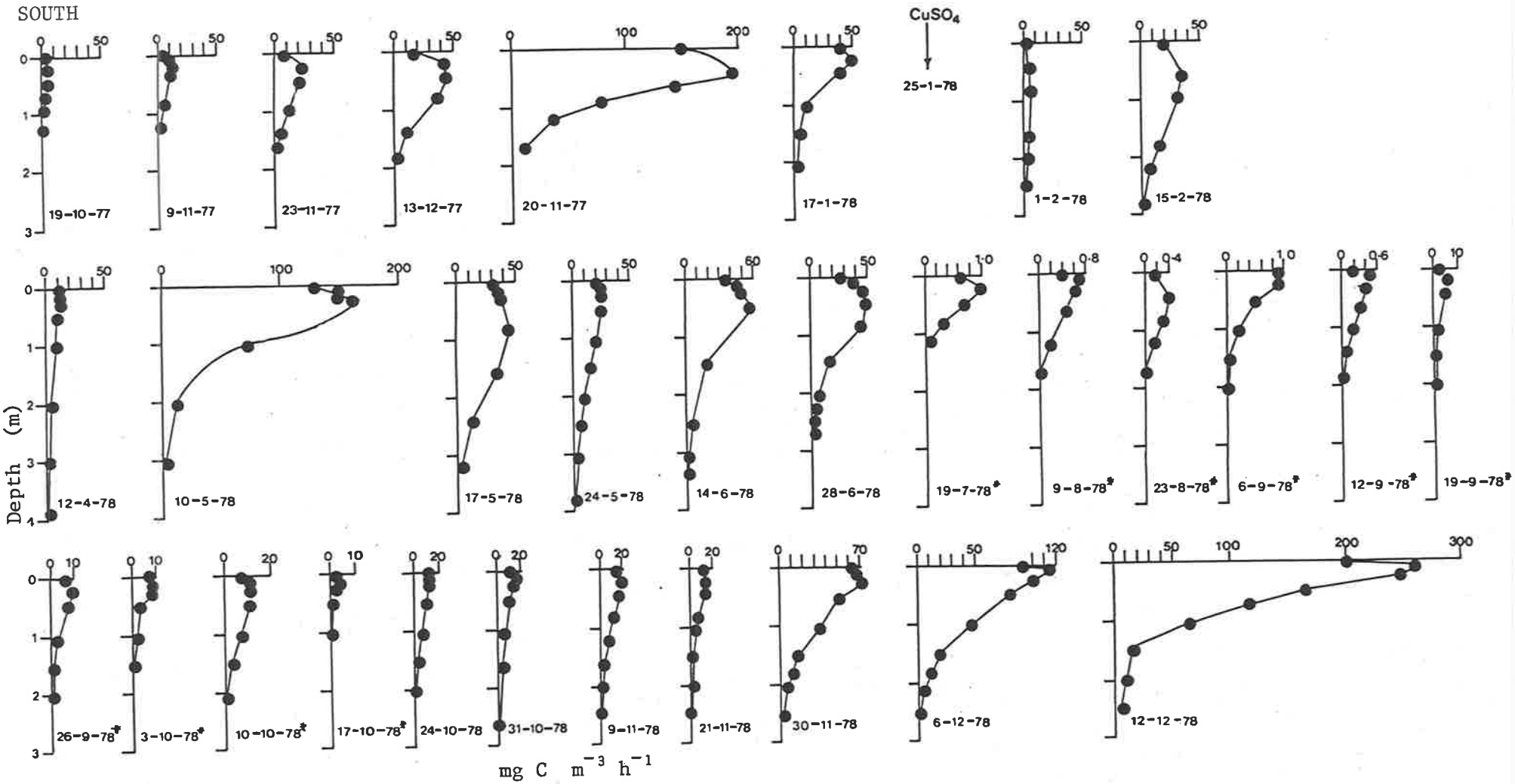

Fig. 6.2: Seasonal variation in the depth distribution of photosynthesis at the north and south sampling sites measured using ^{14}C techniques.

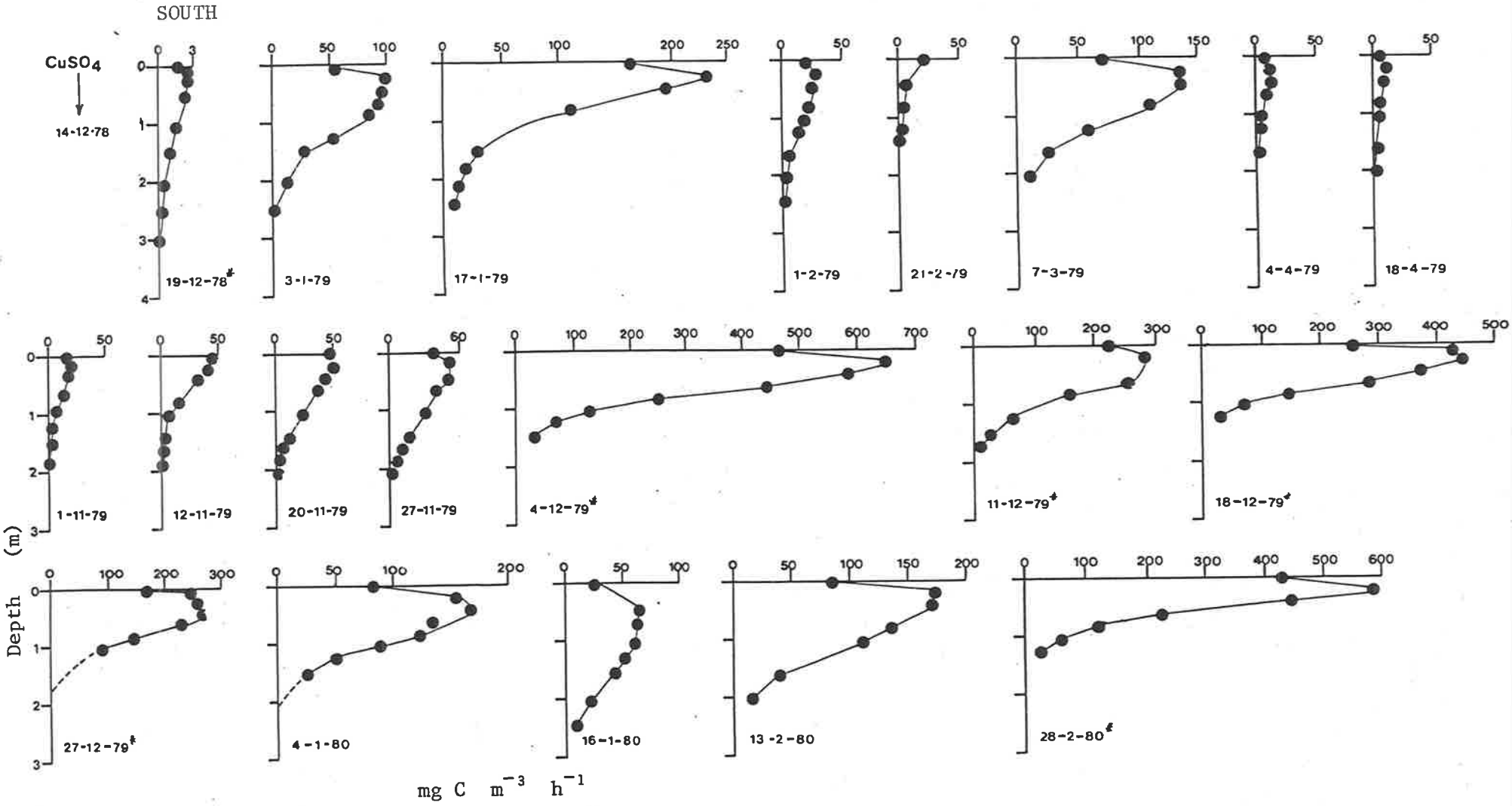
SOUTH
CuSO4
14-12-78
19-12-78*
3-1-79
17-1-79
1-2-79
21-2-79
7-3-79
4-4-79
18-4-79
1-11-79
12-11-79
20-11-79
27-11-79
4-12-79*
11-12-79*
18-12-79*
27-12-79*
4-1-80
16-1-80
13-2-80
28-2-80*
Depth (m)
mg C m⁻³ h⁻¹

Fig. 6.2: (cont.)

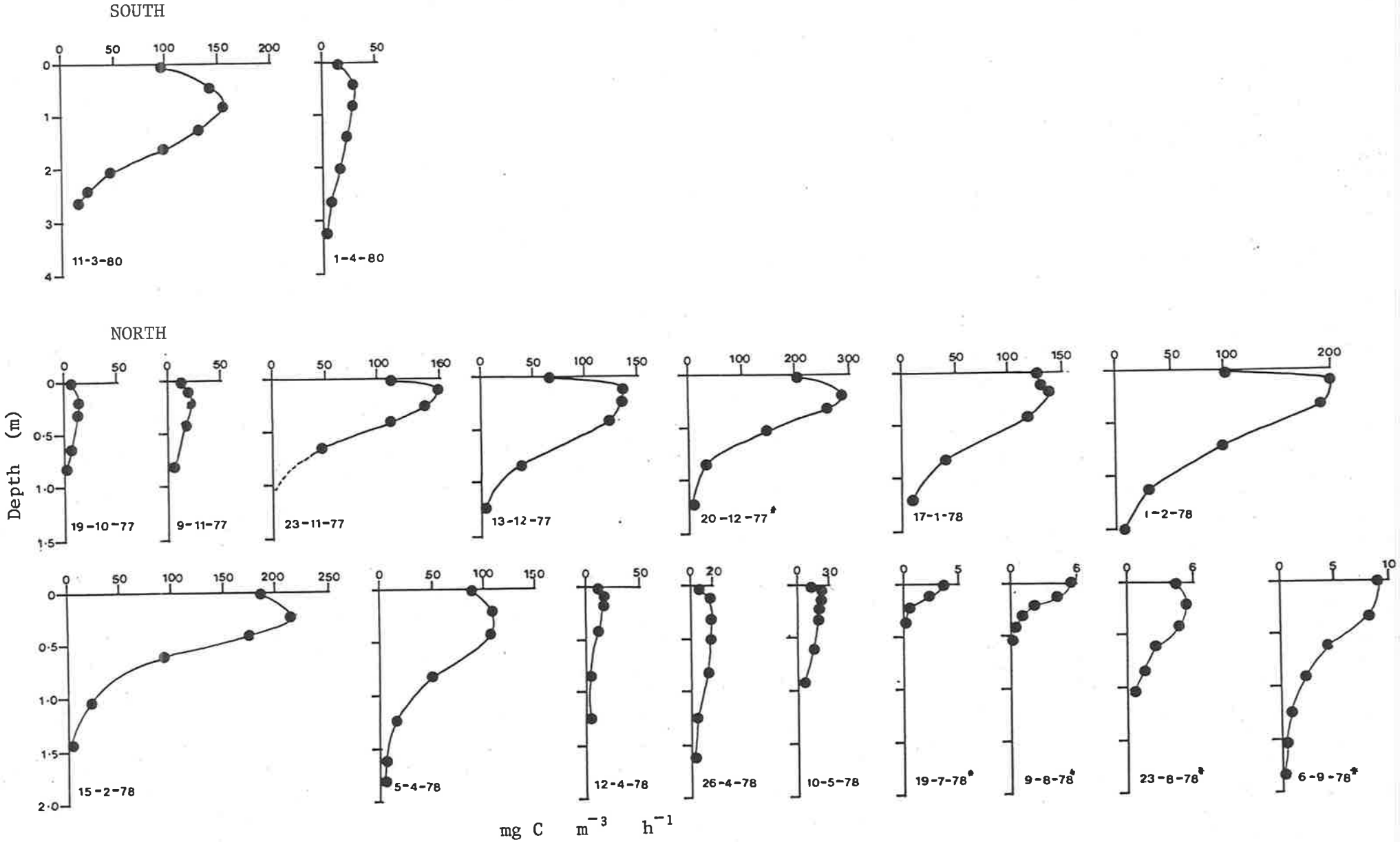
SOUTH
NORTH
Depth (m)
11-3-80
1-4-80
19-10-77
9-11-77
23-11-77
13-12-77
20-12-77*
17-1-78
1-2-78
15-2-78
5-4-78
12-4-78
26-4-78
10-5-78
19-7-78*
9-8-78*
23-8-78*
6-9-78*
mg C m⁻³ h⁻¹

Fig. 6.2: (cont.)

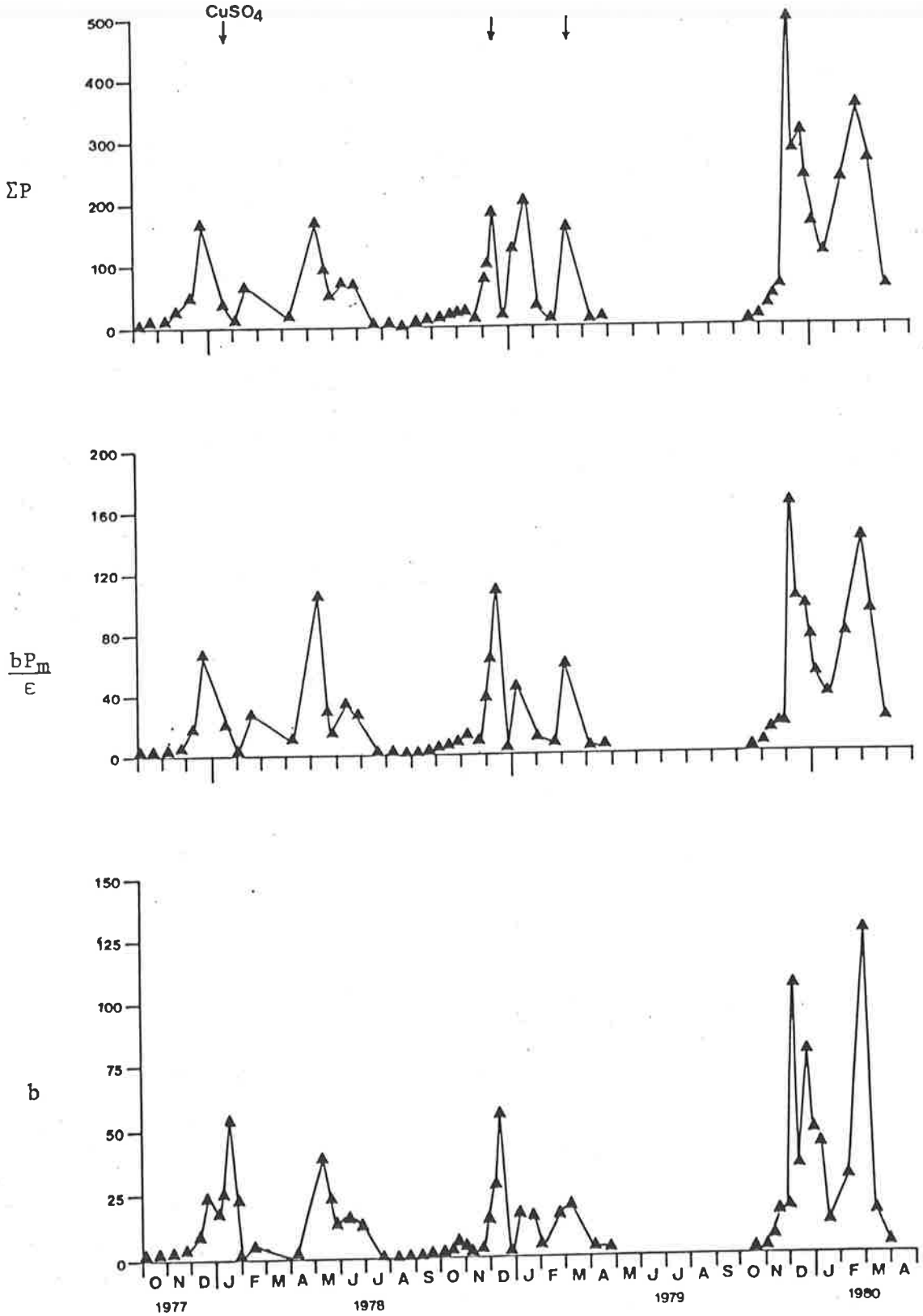

Fig. 6.3: Seasonal variation at the south sampling site of:
a. hourly rate of integral photosynthesis (ΣP), the ratio $\frac{bP_m}{\varepsilon}$ and chlorophyll *a* concentration (b).

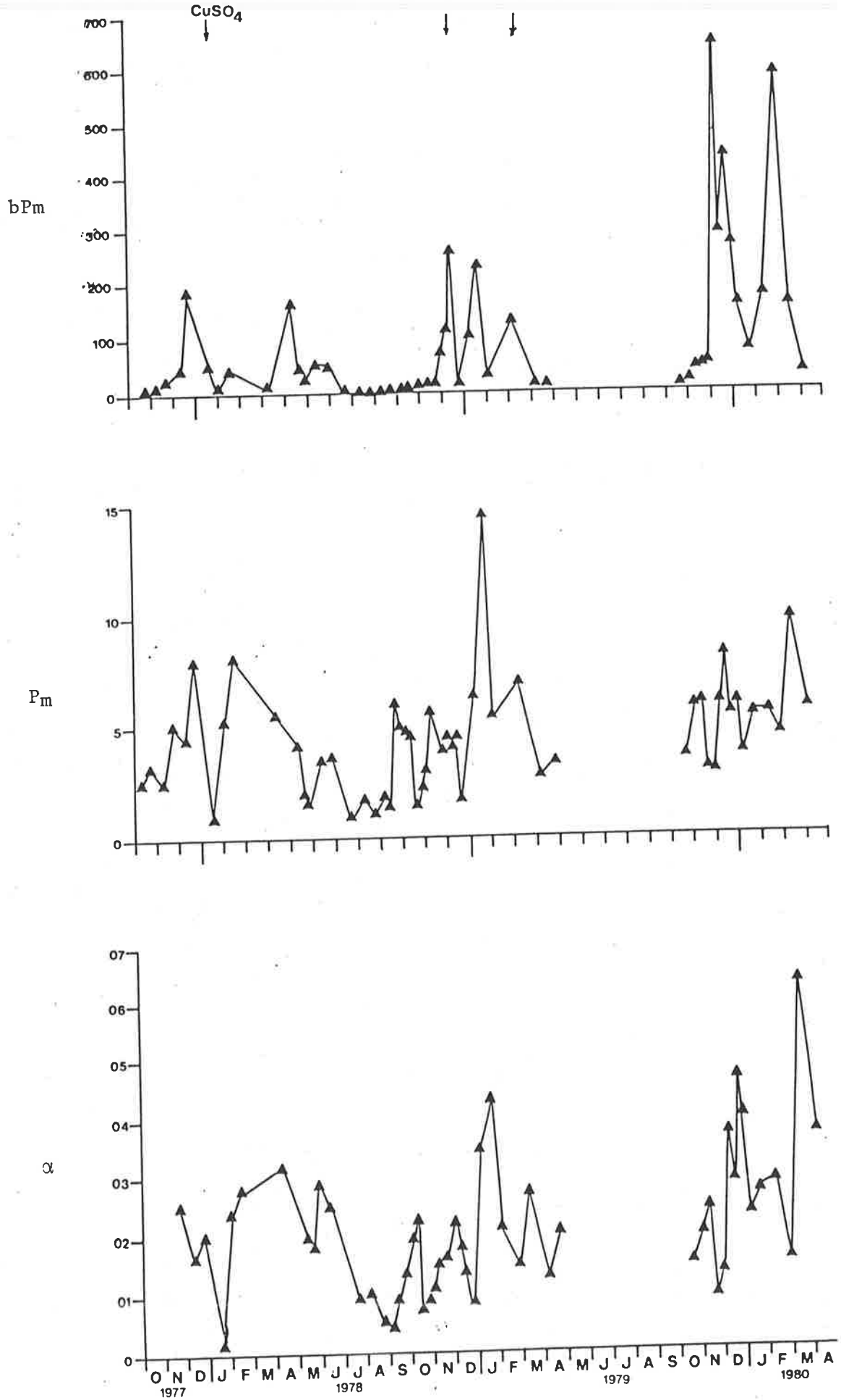

Fig. 6.3 (cont.)

b. maximum volumetric rate of photosynthesis (bPm), photosynthetic capacity (Pm) and photosynthetic efficiency (α).

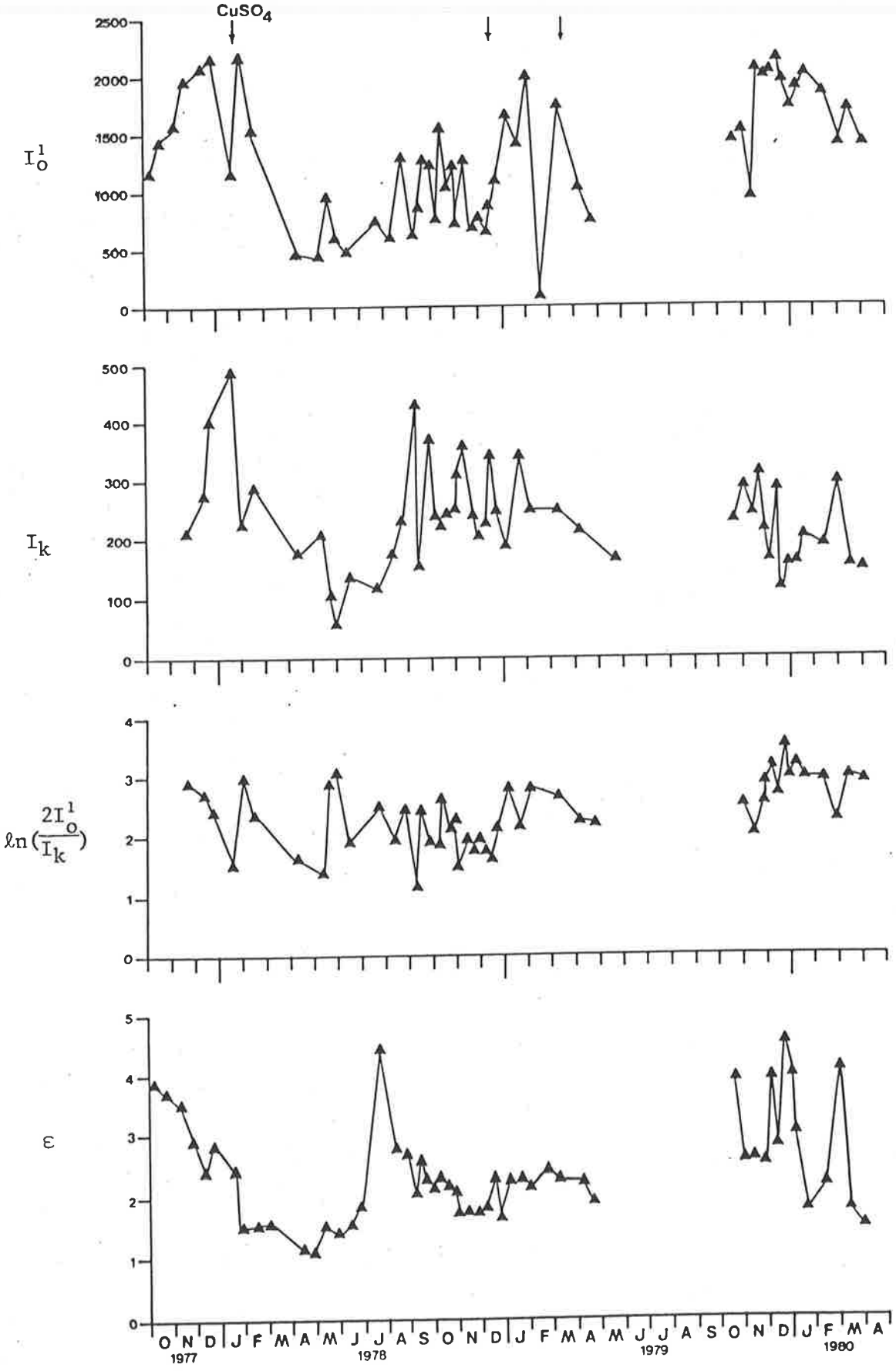

Fig. 6.3 (cont.)

c. Incident irradiance (I_o^1), irradiance characterizing onset of saturation (I_k), logarithmic light function $(\ell n(\frac{2I_o^1}{I_k}))$ and vertical extinction coefficient (ε).

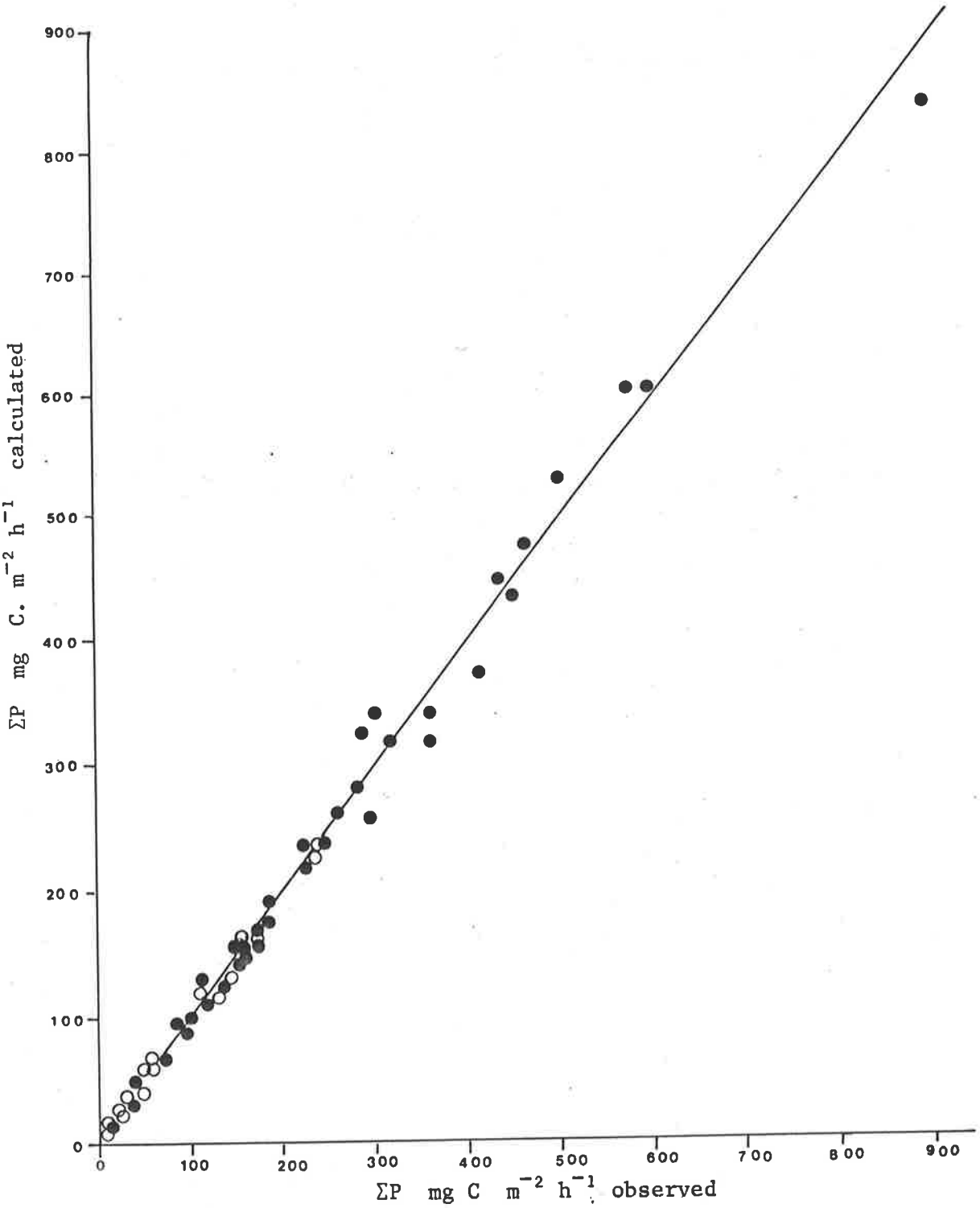

Fig. 6.4: Correlation between hourly integral photosynthesis (ΣP) measured planimetrically from photosynthesis-depth curves, and calculated using equation 6.1 (Talling 1957b).

Fig. 6.5: Correlation between hourly integral rates of photosynthesis (P) and the ratio $\frac{bP_m}{\varepsilon}$ (equation 6.1) for the north (O) and south (▲) sampling sites.

a. All data 1977-1980

$\Sigma P = -2.1 + 2.55 \frac{bP_m}{\varepsilon}$ $r^2 = 0.93$ n=76

b. 1977-1978

$\Sigma P = 1.82 + 2.29 \frac{bP_m}{\varepsilon}$ $r^2 = 0.98$ n=26

c. 1978-1979

$\Sigma P = 4 + 2.04 \frac{bP_m}{\varepsilon}$ $r^2 = 0.922$ n=36

d. 1979-1980

$\Sigma P = 1.75 + 2.89 \frac{bP_m}{\varepsilon}$ $r^2 = 0.98$ n=14

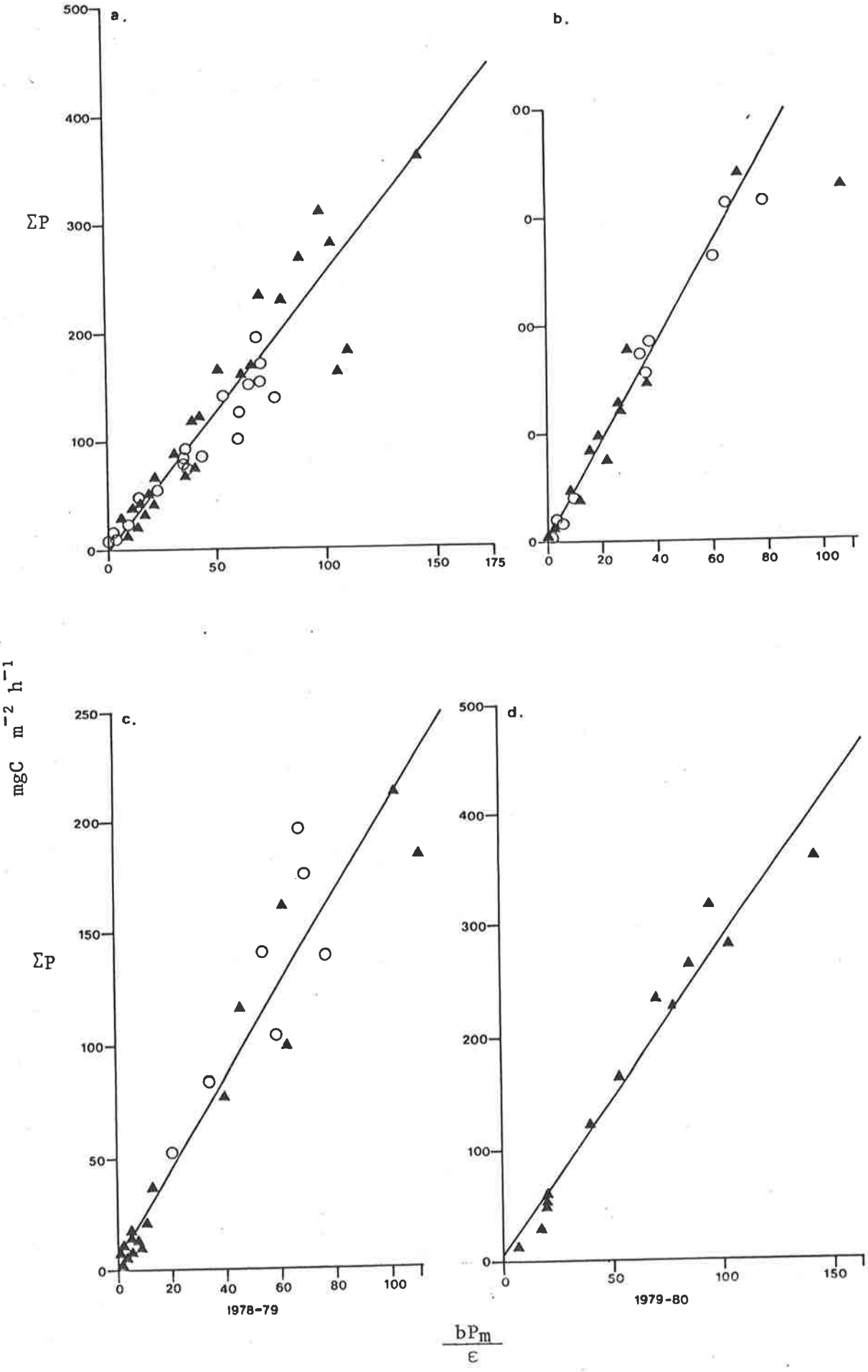

Fig. 6.5:

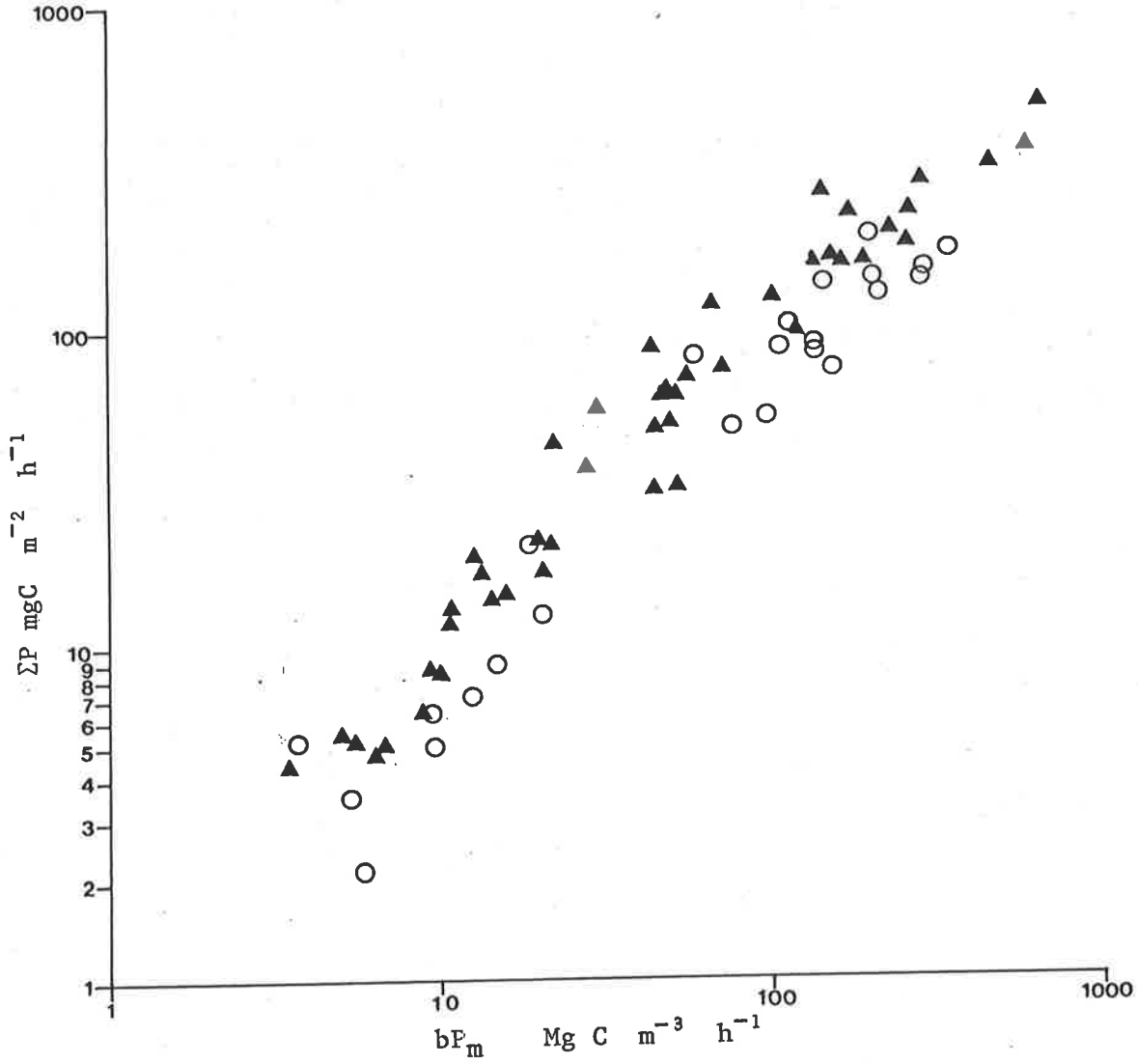

Fig. 6.6 a: Logarithmic plot of integral photosynthesis (ΣP) against maximum volumetric rate of photosynthesis (bP_m).

Linear regression of original data,

$\Sigma P = 17.1 + 0.689\ bP_m$ $\quad r^2 = 0.87$ $\quad n = 70$

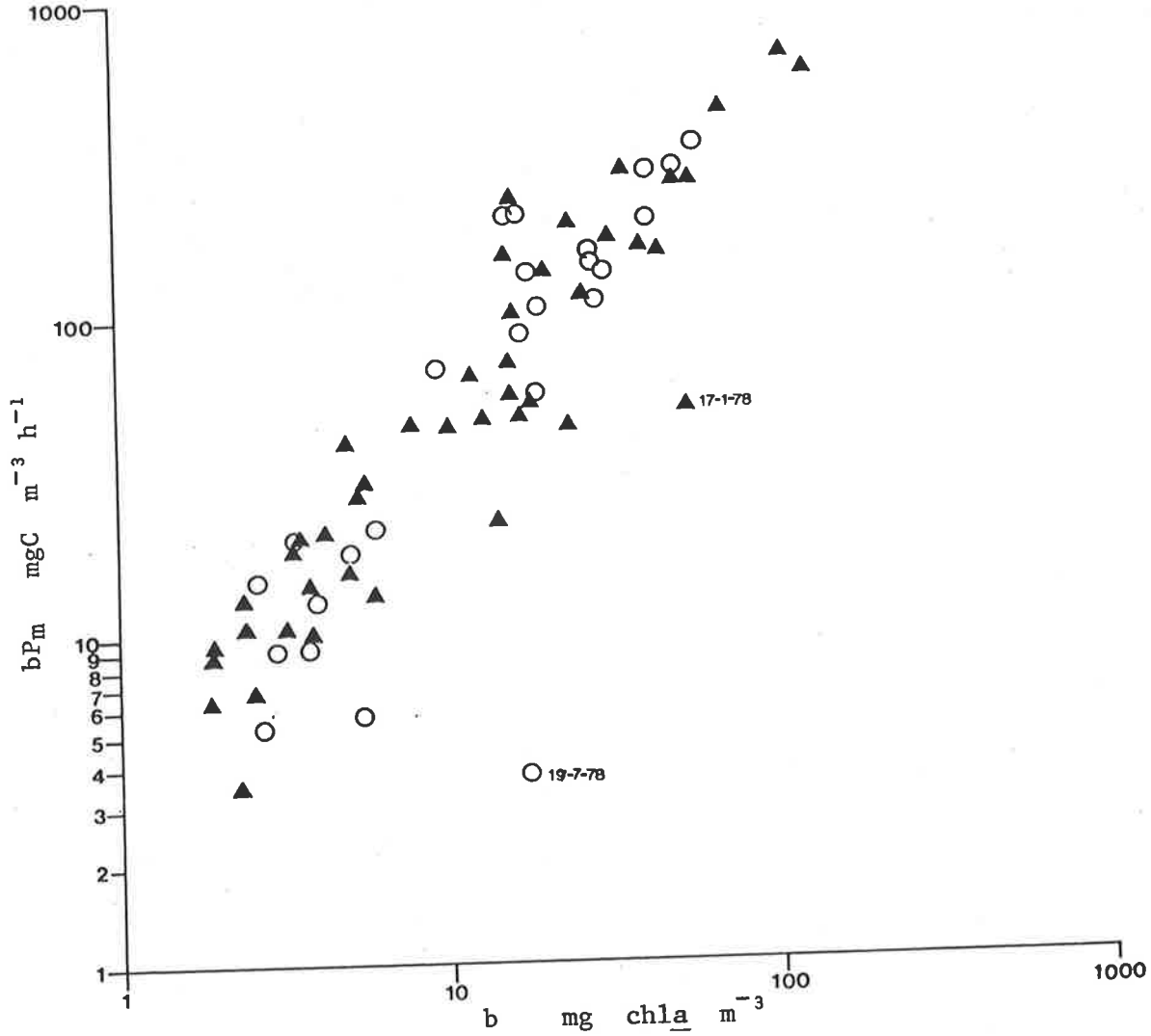

Fig. 6.6 b: Logarithmic plot of maximum volumetric rate of photosynthesis (bP_m) against chlorophyll a concentration (b). Linear regression of original data

$bP_m = 1.91 + 5.15\ b \qquad r^2 = 0.85 \qquad n=75$

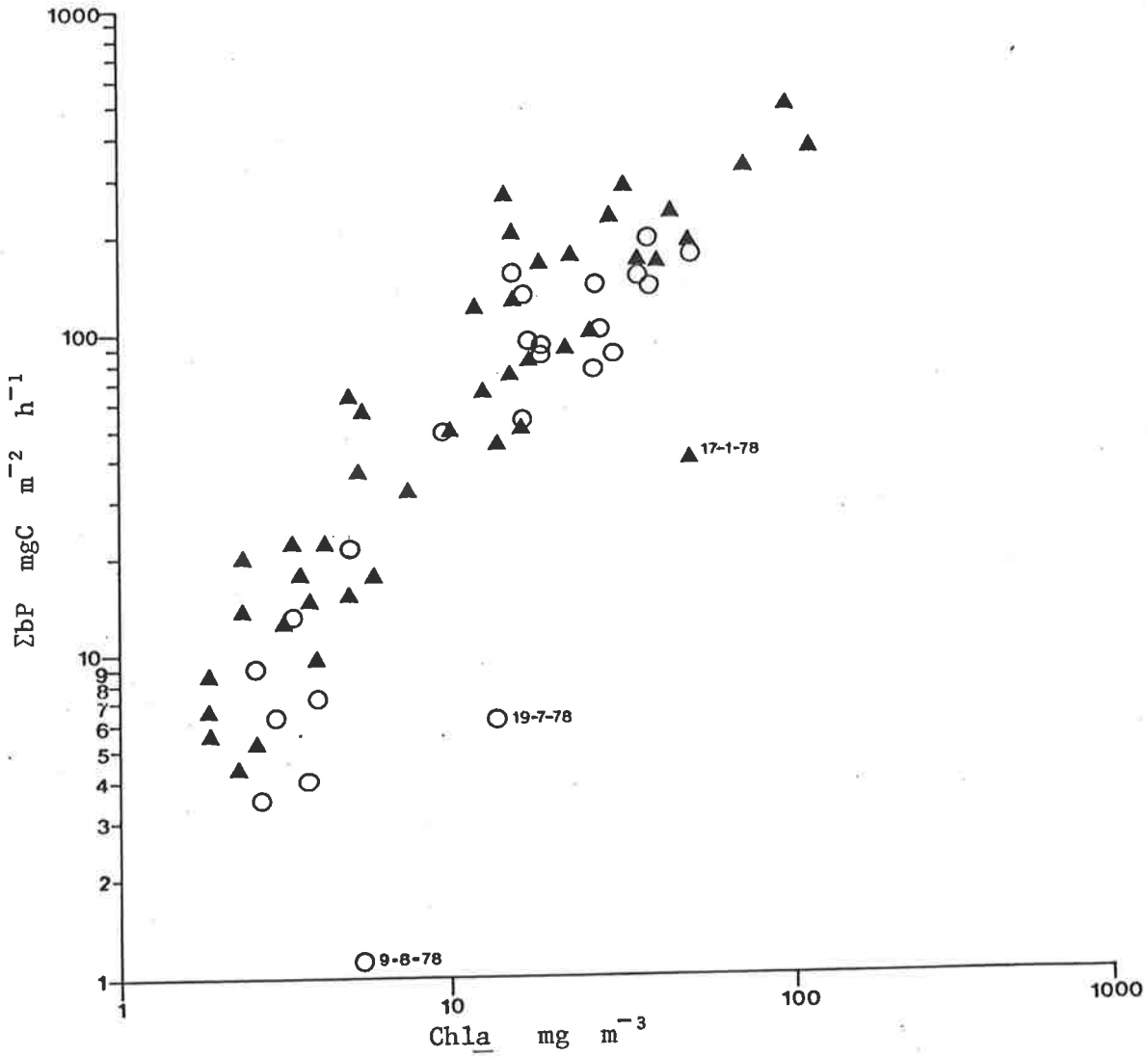

Fig. 6.7: Logarithmic plot of the relationship between hourly rate of integral photosynthesis (ΣP)and chlorophyll a concentration (b). Linear regression on original data (excluding labelled points)

$\Sigma P = 19.3 + 3.66\ b \qquad r^2 = 0.77 \qquad n = 70$

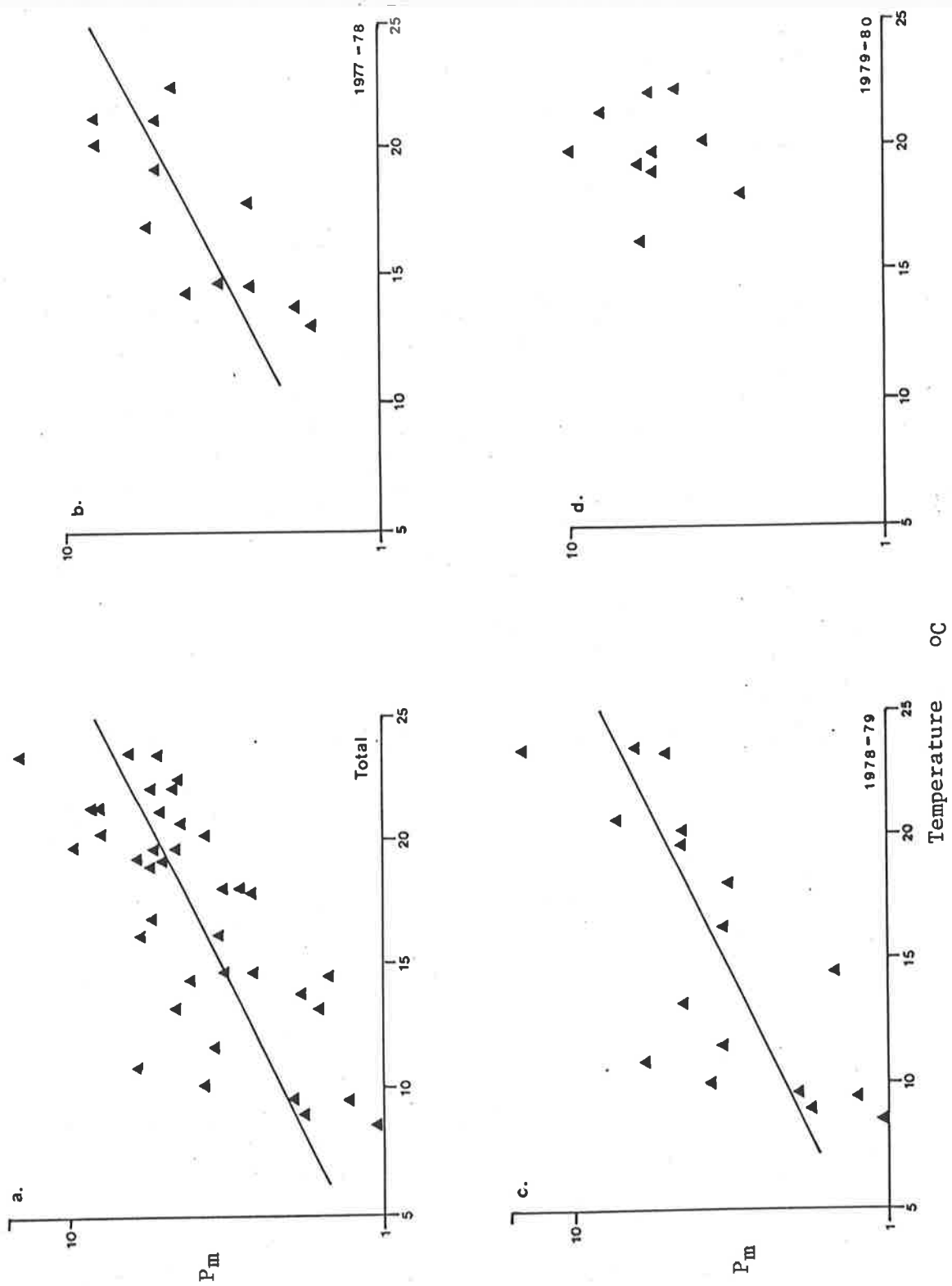

Fig. 6.8: Semilogarithmic plots of variation in maximum specific rate of photosynthesis (P_m) with temperature at the south sampling site.

a. All data 1977-80

log P_m = -0.06 + 0.039°C r^2 = 0.47 n=39 P<0.001

b. 1977-78

log P_m = -0.108 + 0.041 °C r^2 = 0.52 n=52 P<0.01

c. 1978-79

log P_m = -0.06 + 0.039 °C r^2 = 0.53 n=15 P<0.01

d. 1979-80

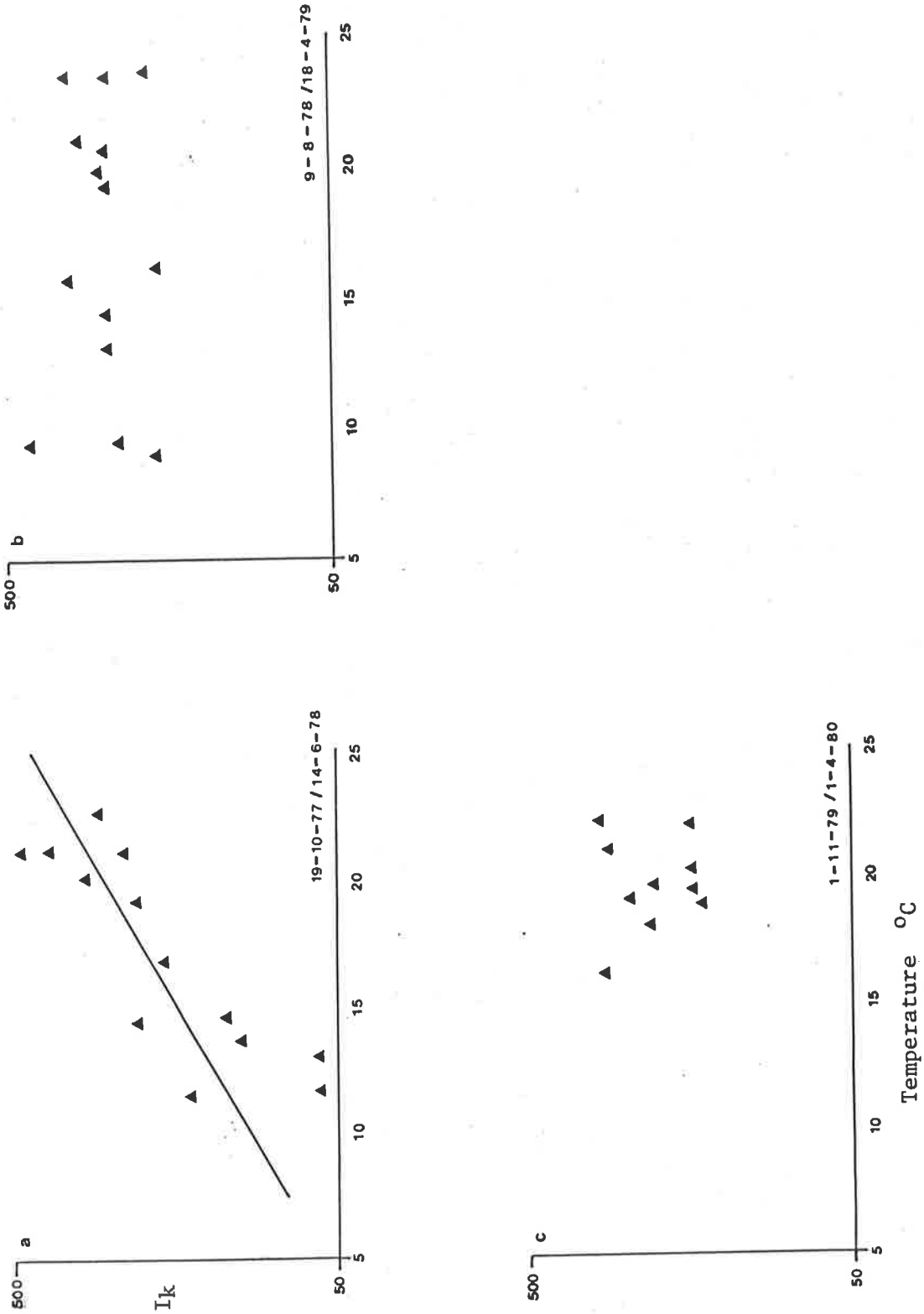

Fig. 6.9: Semilogarithmic plot of the variation in the saturation characteristic (I_k) with temperature at the south sampling site.

a. 1977-78
$\log I_k = 1.54 + 0.044\ ^oC \quad r^2 = 0.59 \quad n = 12$

b. 1978-79

c. 1979-80

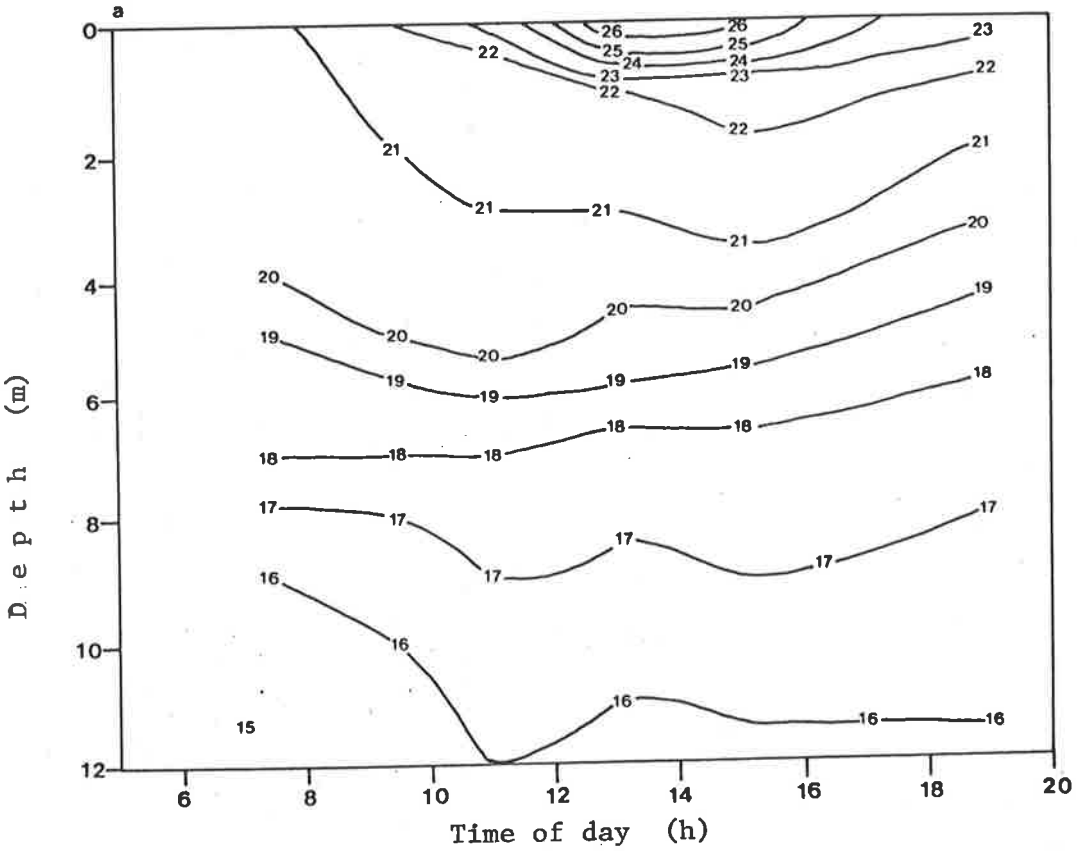

Fig. 6.10: Depth-time distributions for the 27 December 1979 of

a. Temperature

b. Chlorophyll a concentration

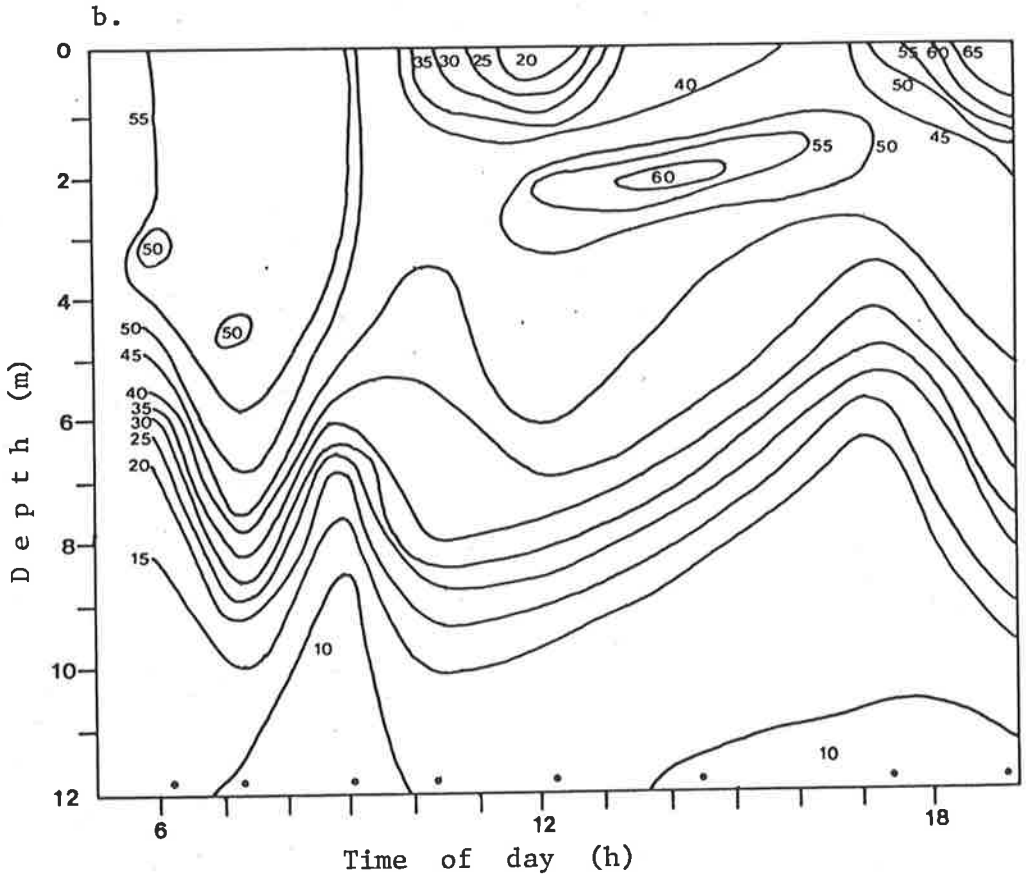
b.
0
2
4
6
8
10
12
Depth (m)
6
12
18
Time of day (h)
55
50
50
50
45
40
35
30
25
20
15
10
35 30 25 20
40
55 60 65
50
55
50
45
60
10

Fig. 6.10 (cont.)

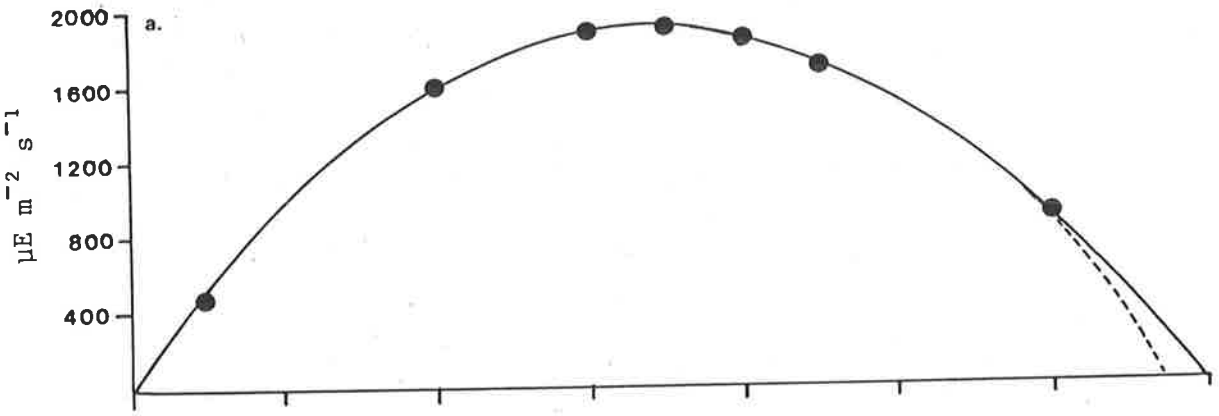

a. Incident solar irradiance

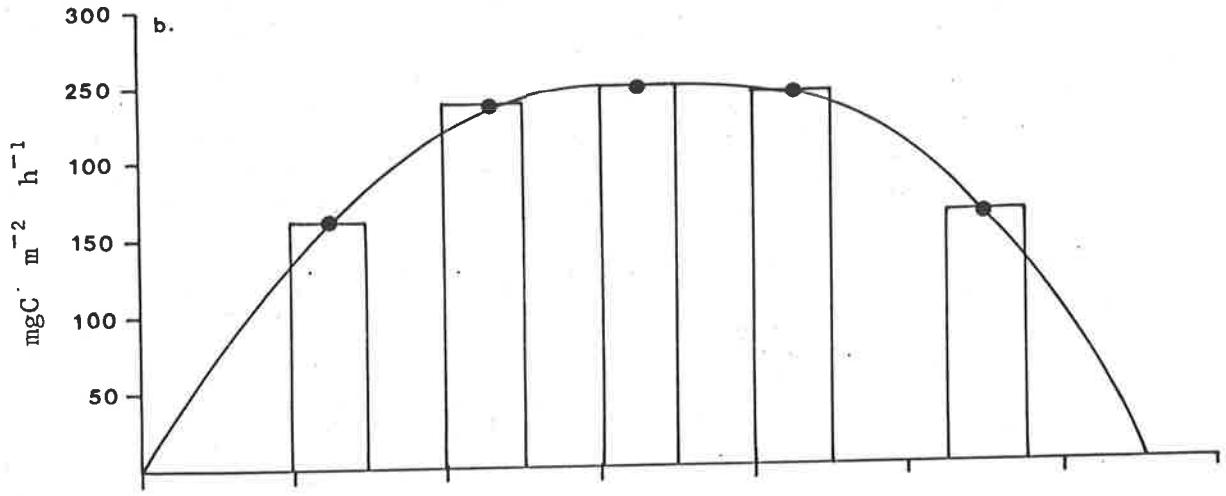

b. Hourly rate of integral photosynthesis (ΣP)

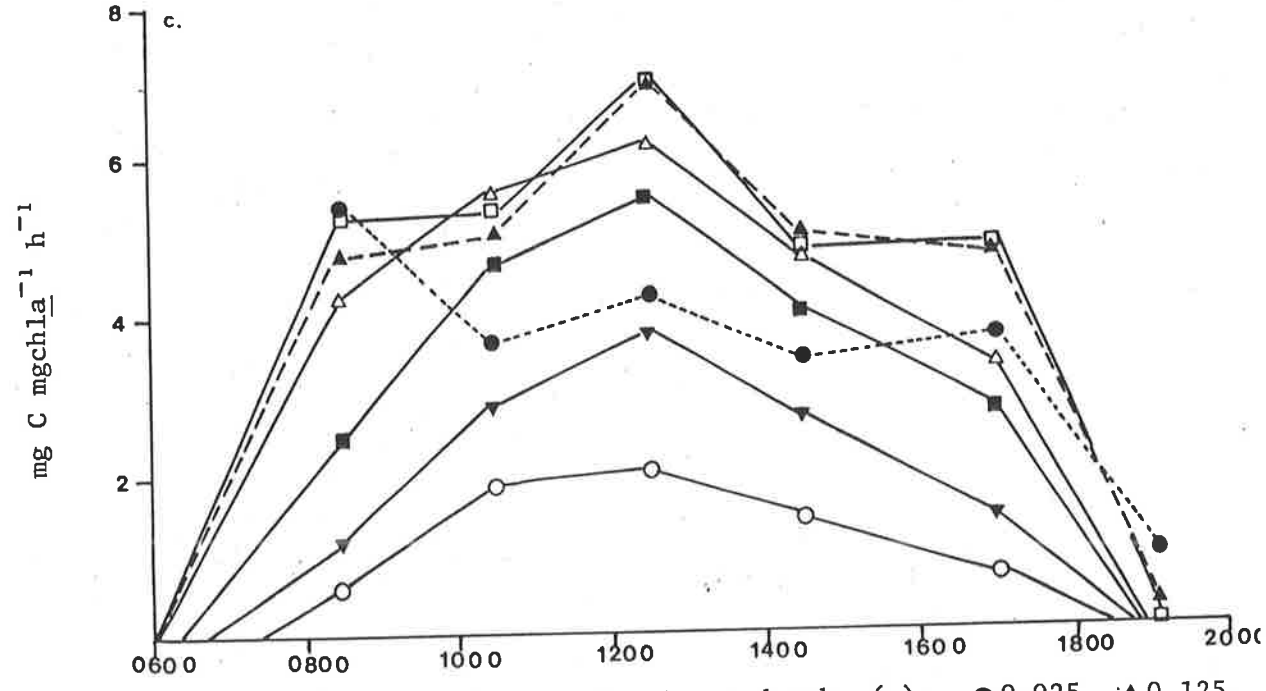

Fig. 6.11: c. Hourly rate of photosynthesis at depths (m): ●0.025, ▲0.125, □0.225, △0.425, ■0.625, ▼0.825, ○1.025.

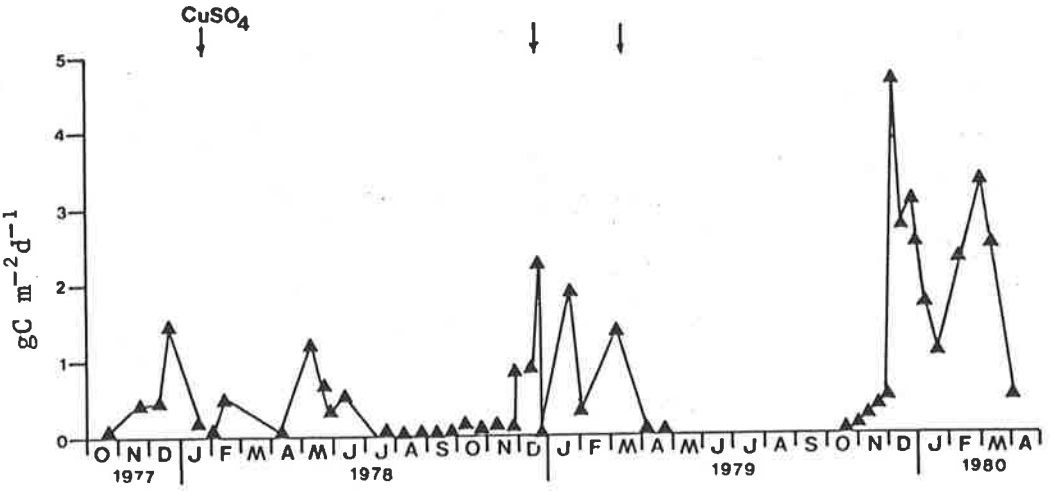

Fig. 6.12: Seasonal variation in daily integral rates of photosynthesis ($\Sigma\Sigma P$) estimated from short term incubations (equation 6.6)

Fig. 6.13: Light conditions for phytoplankton at the south sampling site shown in terms of the optical depth of the mixed zone $\frac{\varepsilon Z_m}{\ell n 2}$, and the daily logarithmic function $[LDH]^{day}$. Lines indicate the critical ratio (q_c) of the two functions for various relative respiration rates. Numbers in brackets are the critical relative respiration rates for each of the points numbered 1-8 in 1978-79 (see text).

a. 1978-79

b. 1979-80

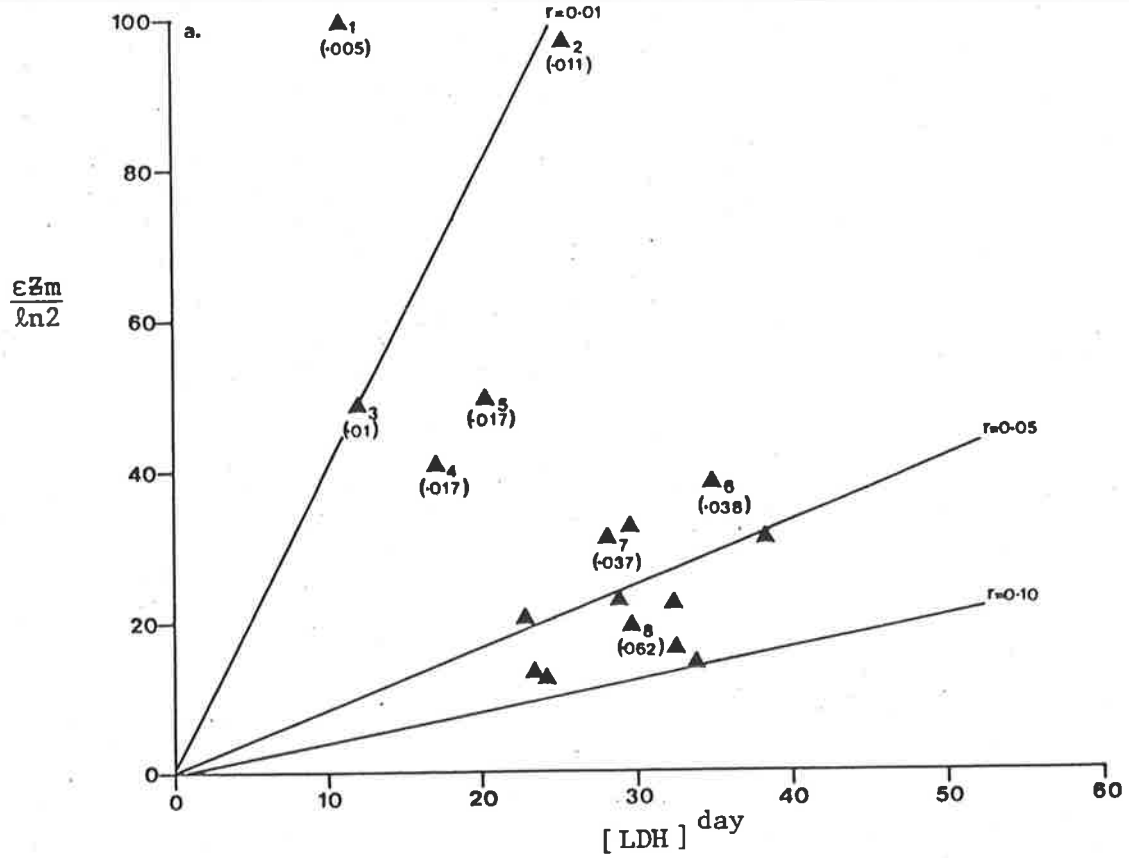
a.
r=0·01
r=0·05
r=0·10
1 (·005)
2 (·011)
3 (·01)
4 (·017)
5 (·017)
6 (·038)
7 (·037)
8 (·062)
εZm / ln2
[LDH] day

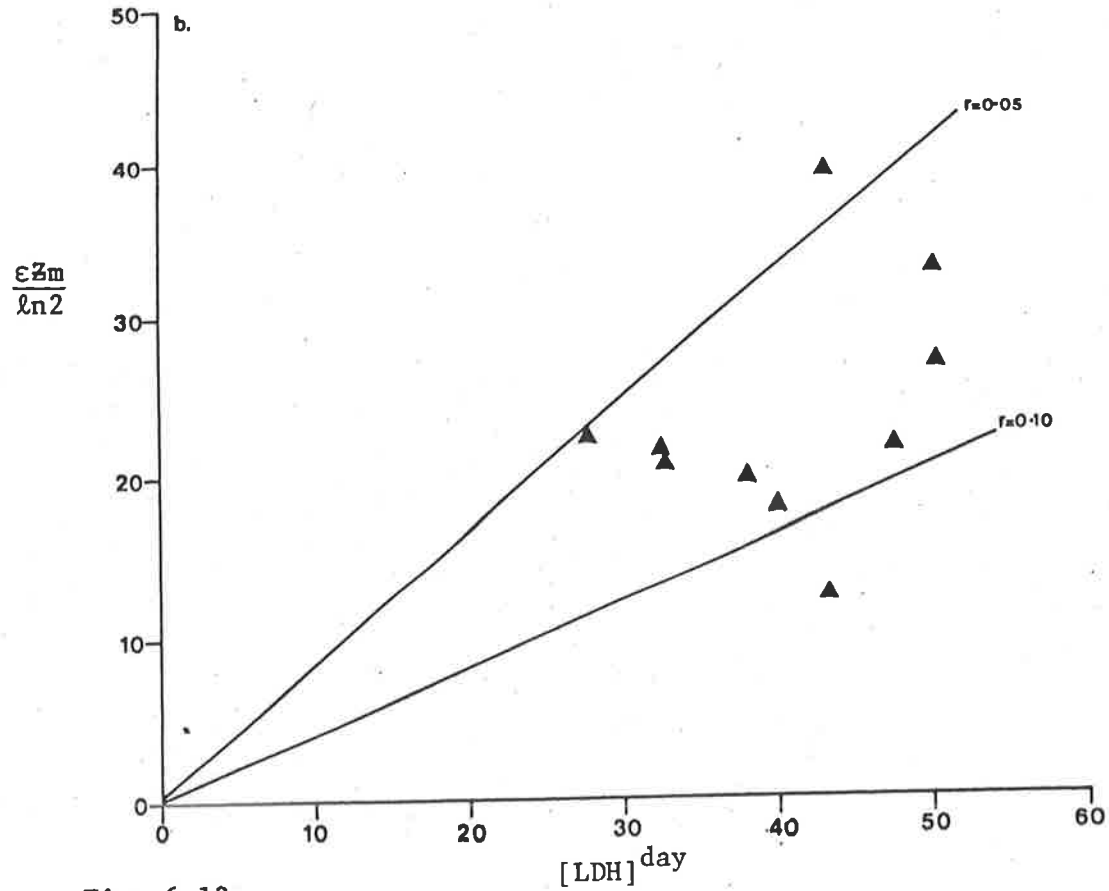
b.
r=0·05
r=0·10
εZm / ln2
[LDH] day

Fig. 6.13:

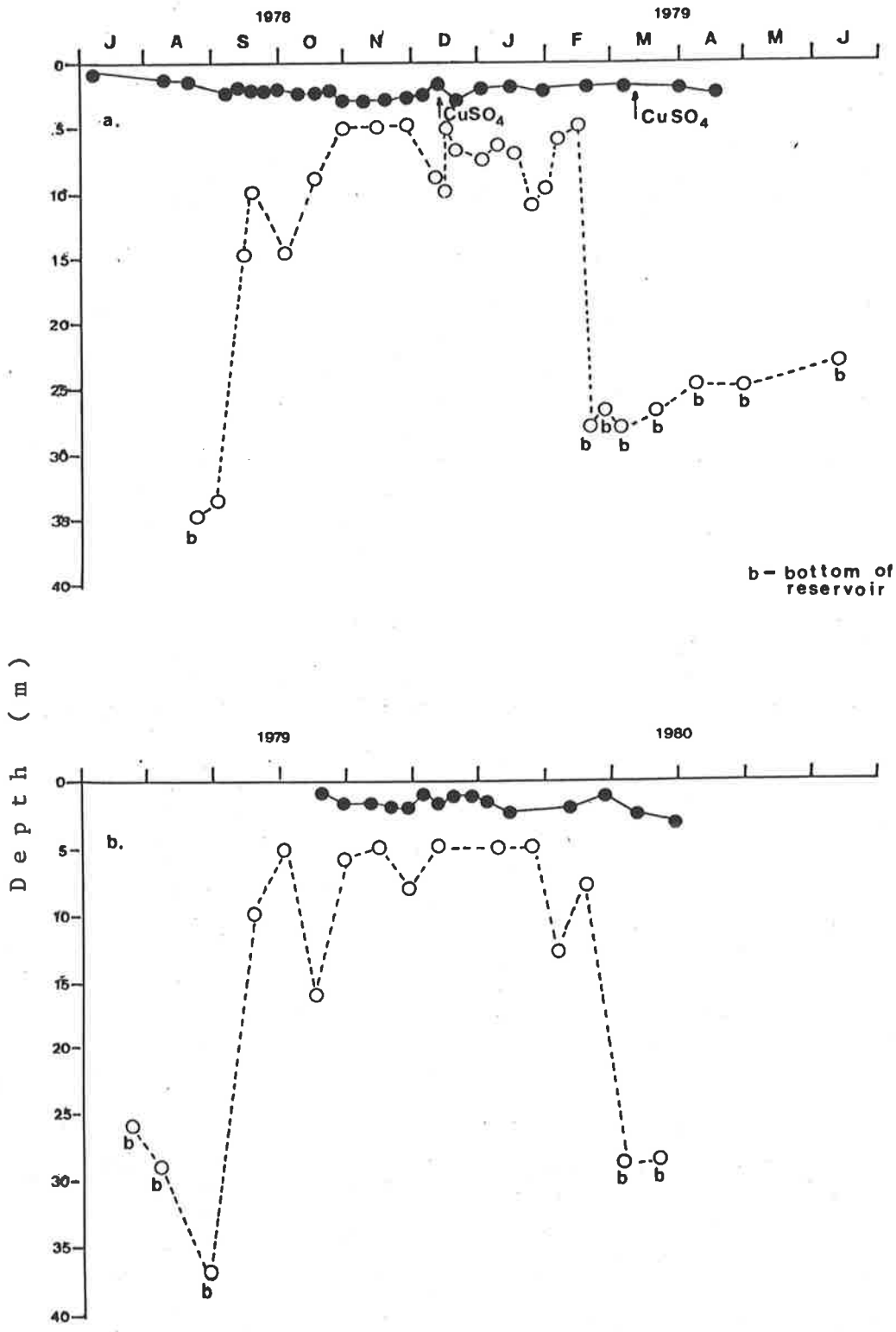

Fig. 6.14: Seasonal variation in euphotic depth (● z_{eu}) and the depth of the mixed zone (O z_m) at the south sampling site.

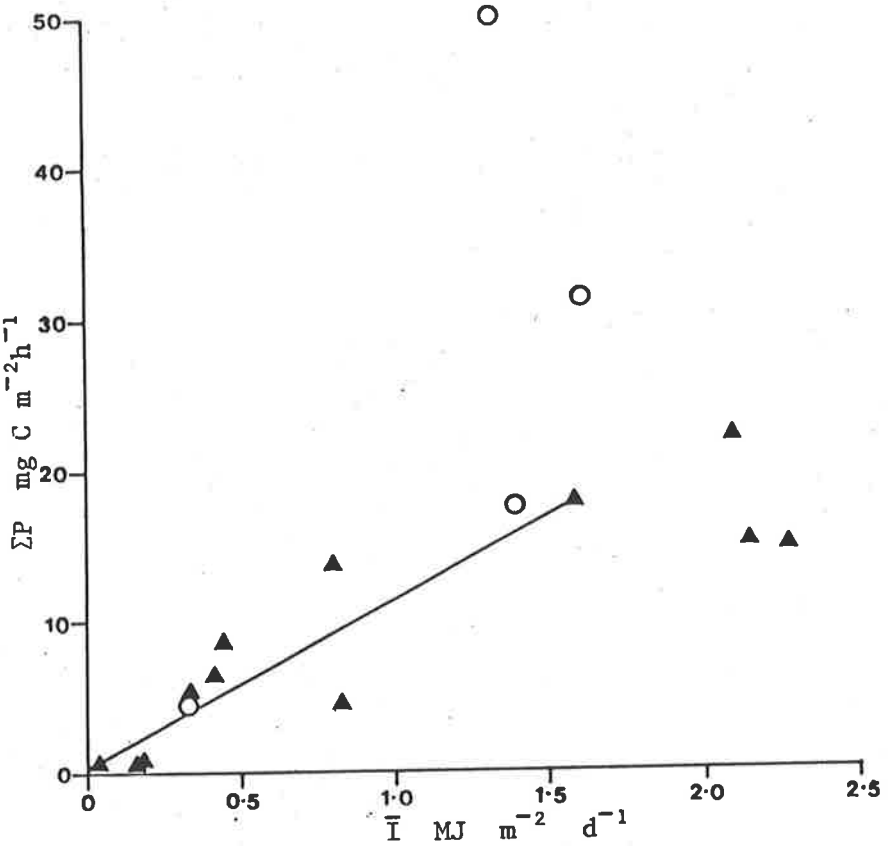

Fig. 6.15: Correlation between the hourly rate of integral photosynthesis (ΣP) and mean irradiance of the mixed zone ($\bar{I}$) during initiation of the spring biomass increase of 1978 (▲) and 1979 (○).

23.8-24.10.78 $\Sigma P = 0.299 + 11.39\ (\bar{I})$ $r^2 = 0.77$ $n=9$ $P<0.01$

Fig. 6.16:

Comparison of the calculated theoretical maximum areal biomass (estimated as $\frac{1}{\varepsilon_s}$) with measured values (estimated as $\frac{b}{\varepsilon}$) for periods when the specific extinction coefficient per unit chlorophyll a (ε_s) was known. Theoretical maxima are shown as horizontal dashed lines for respective ε_s values.

12.4 - 17.5.78 ε_s= 0.0122
21.11- 19.12.78 ε_s= 0.0133
20.11- 11.12.79 ε_s= 0.016
16. 1- 1. 4.80 ε_s= 0.021

Fig. 6.17:

Correlation between maximum specific rate of photosynthesis (P_m) and the protein to carbohydrate ratio over the nutrient depleted period (December-March) of 1979-80.

$P_m = 3.43 + 1.197 \frac{\text{Protein}}{\text{Carbohyd.}}$ $r^2 = 0.59$ $P < 0.05$

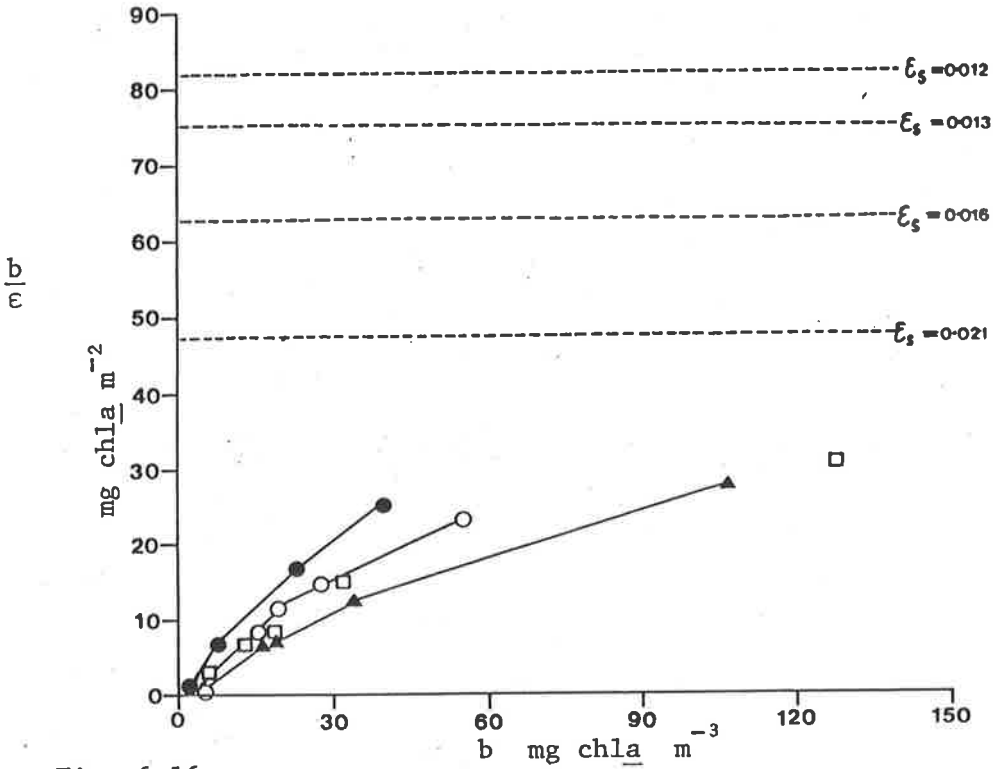

Fig. 6.16:

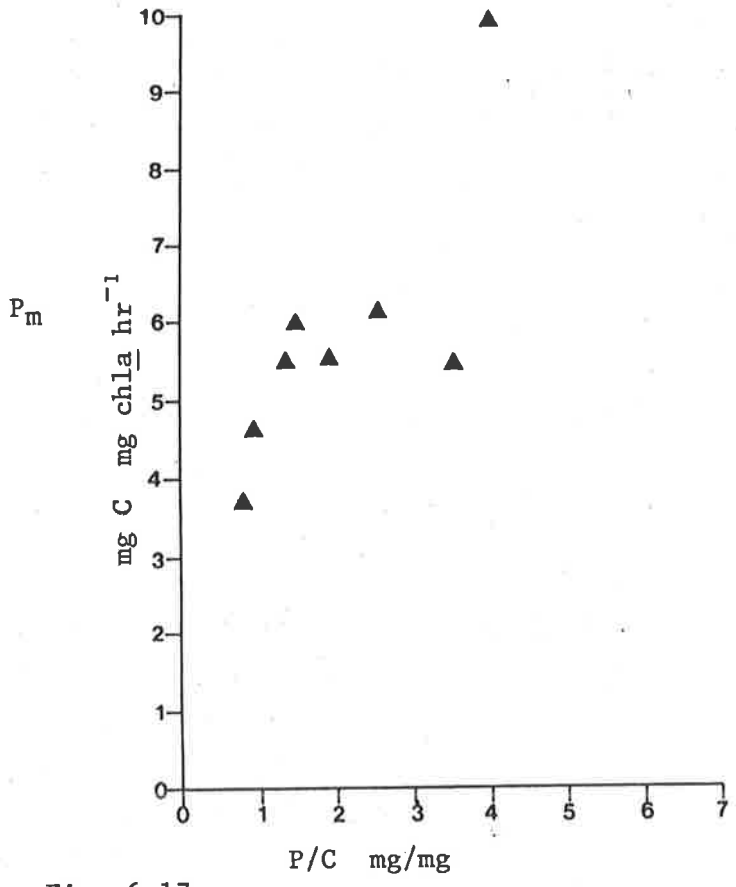

Fig. 6.17:

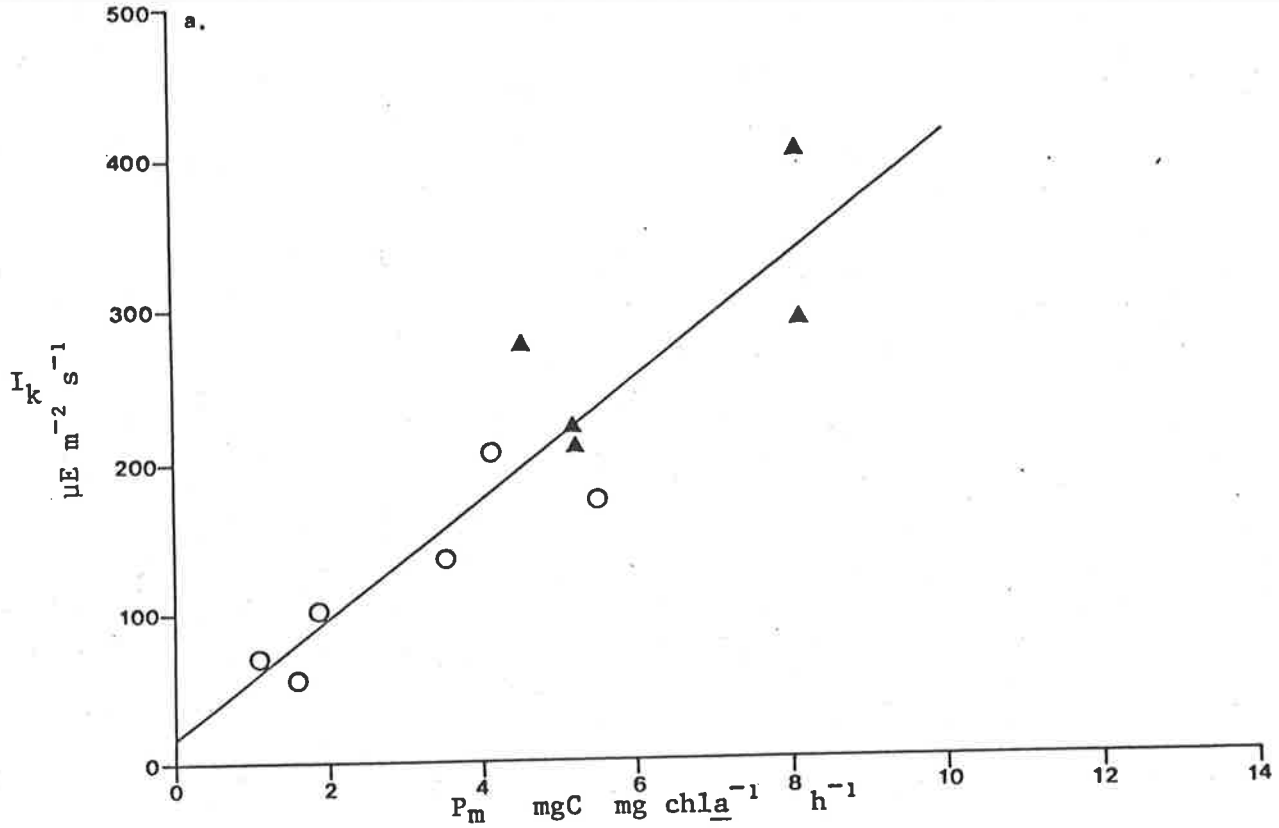

a. I_k and the maximum specific rate of photosynthesis (P_m)

$I_k = 15.1 + 40.37P_m$ $r^2 = 0.79$ $n = 10$ $P < 0.001$

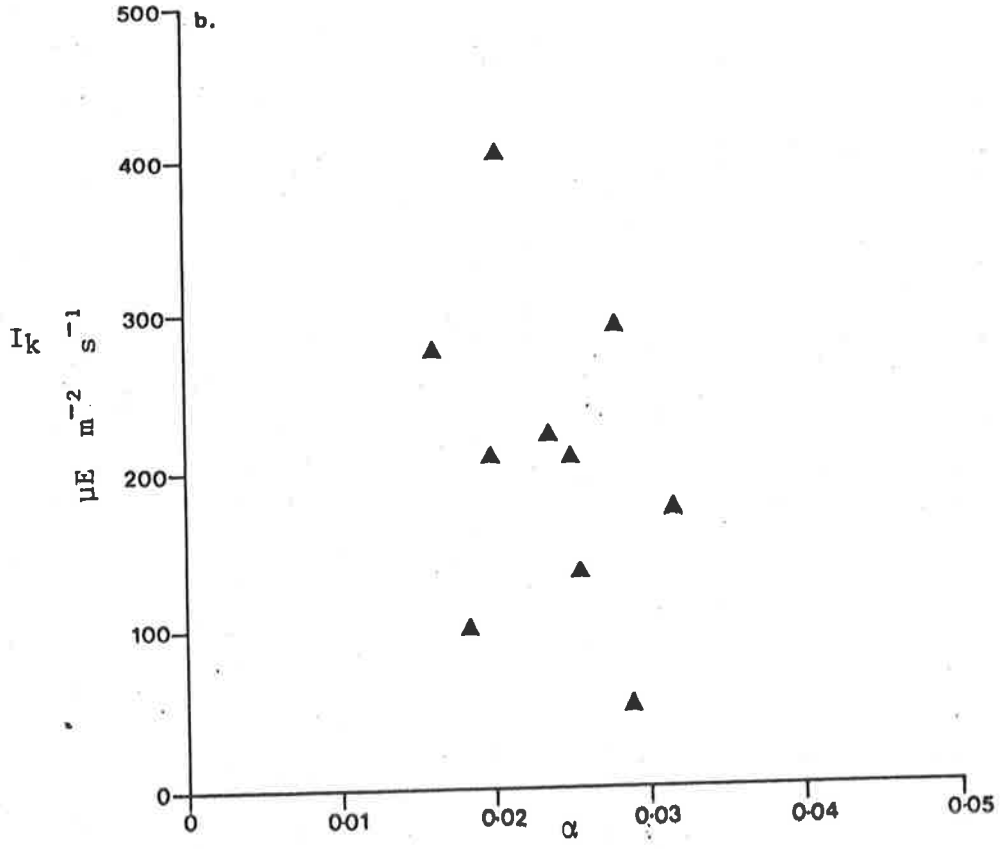

b. I_k and photosynthetic efficiency (α)

Fig. 6.18: Correlations for the 1977-78 growing season between a. I_k and P_m, b. I_k and α, and c. P_m and α.

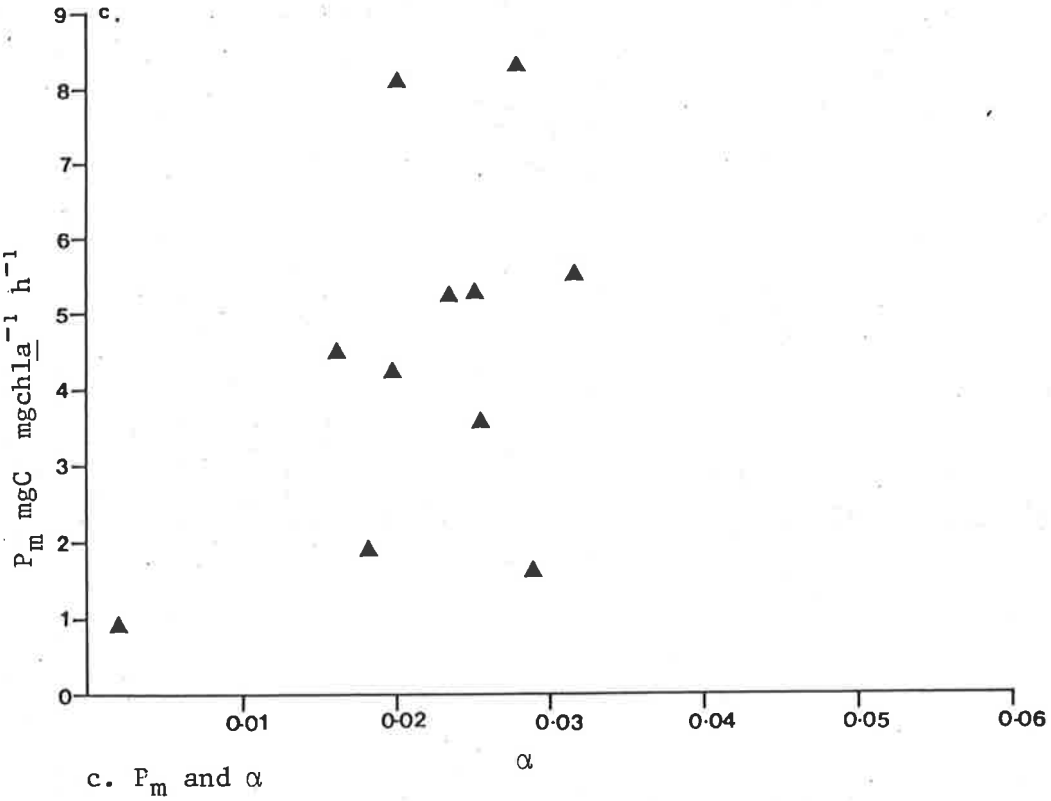

c. P_m and α

Fig. 6.18 (cont.)

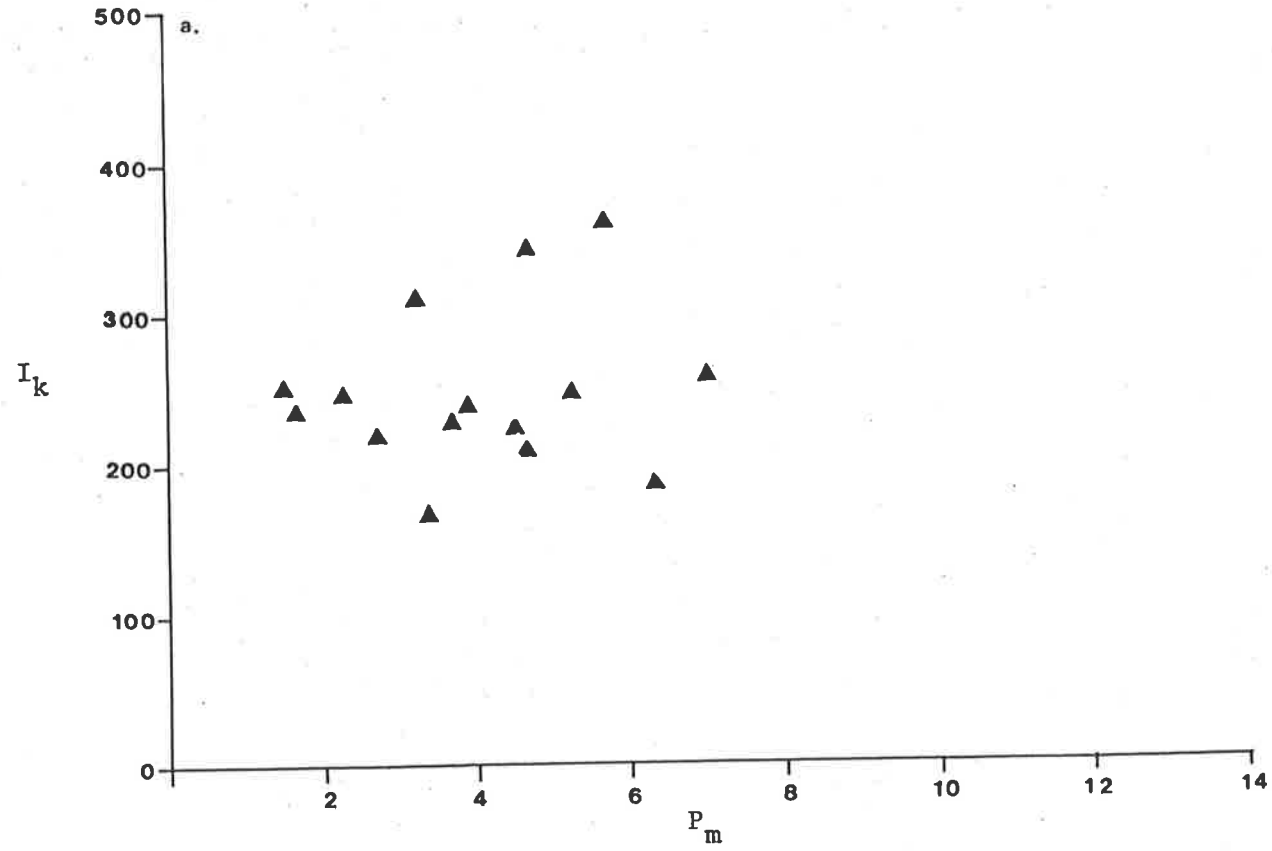

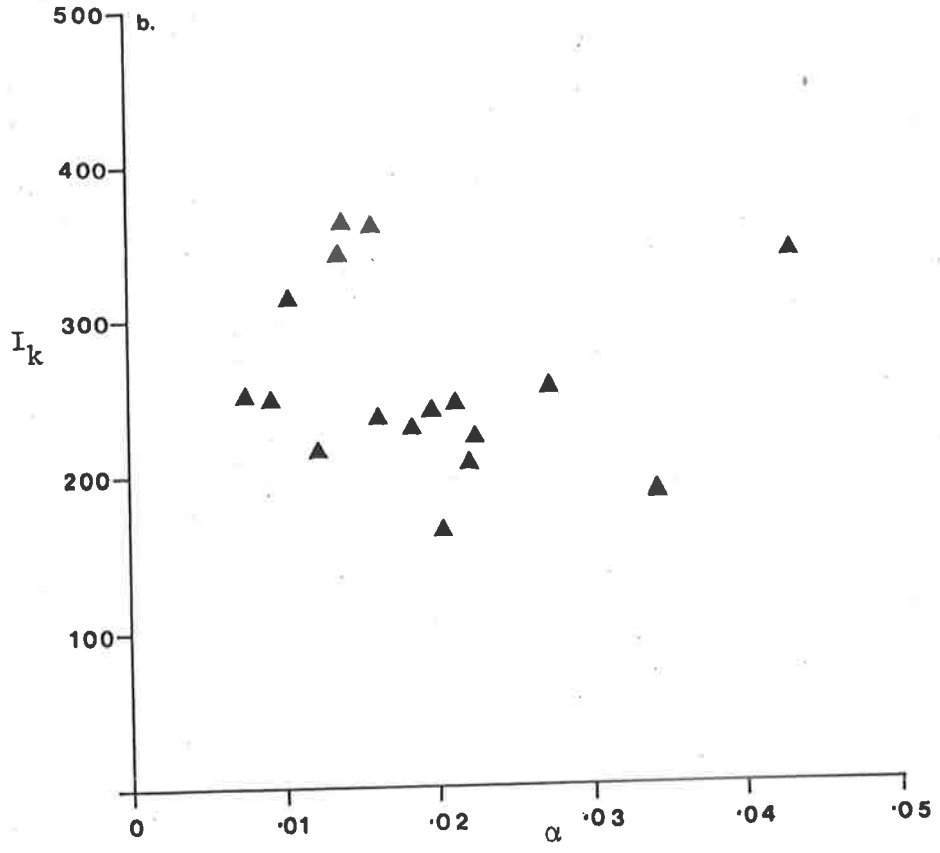

Fig. 6.19: Correlations for the 1979-80 growing season between

a. I_k and the maximum specific rate of photosynthesis (P_m)

b. I_k and the photosynthetic efficiency (α)

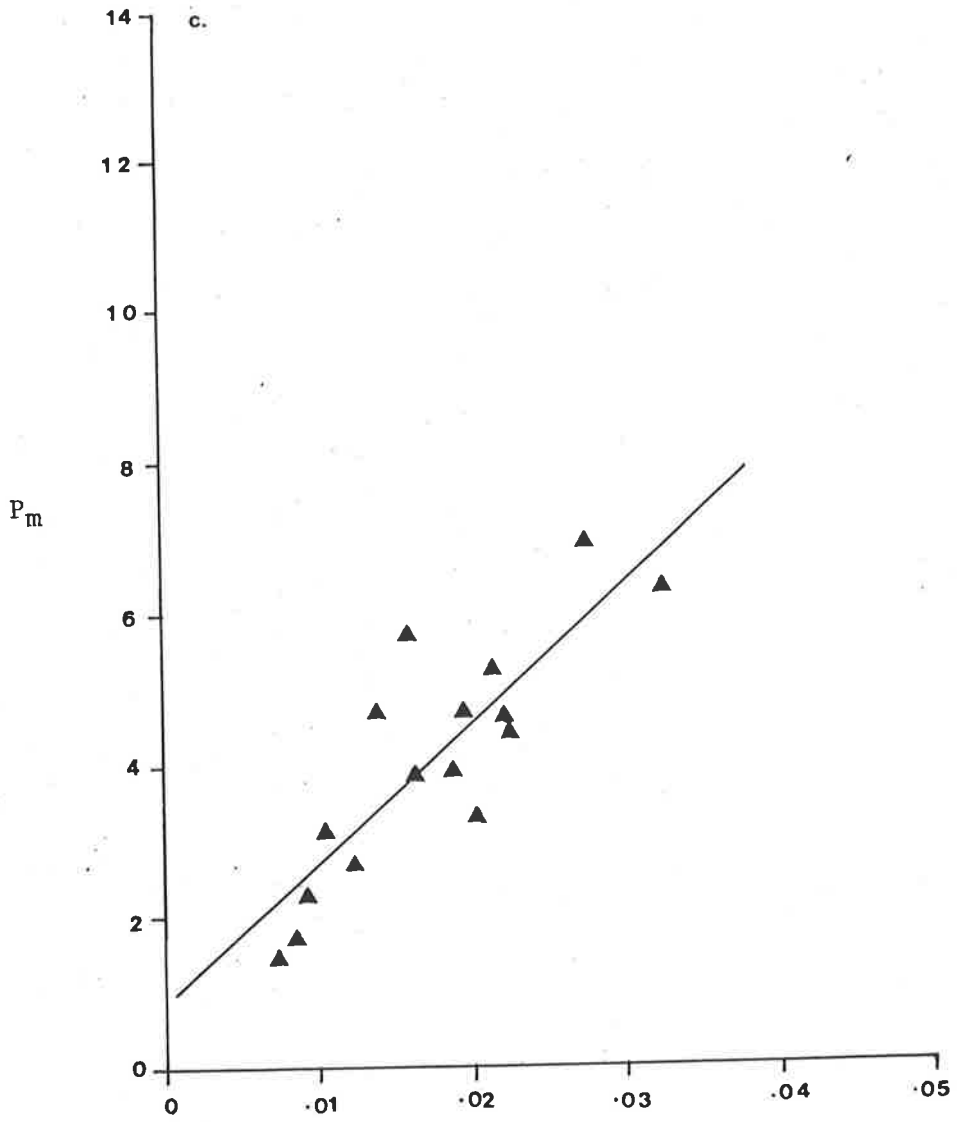

Fig. 6.19: (cont.) c. P_m and α

$P_m = 0.4 + 184.4\,\alpha$ $r^2 = 0.71$, n=16 $P < 0.001$

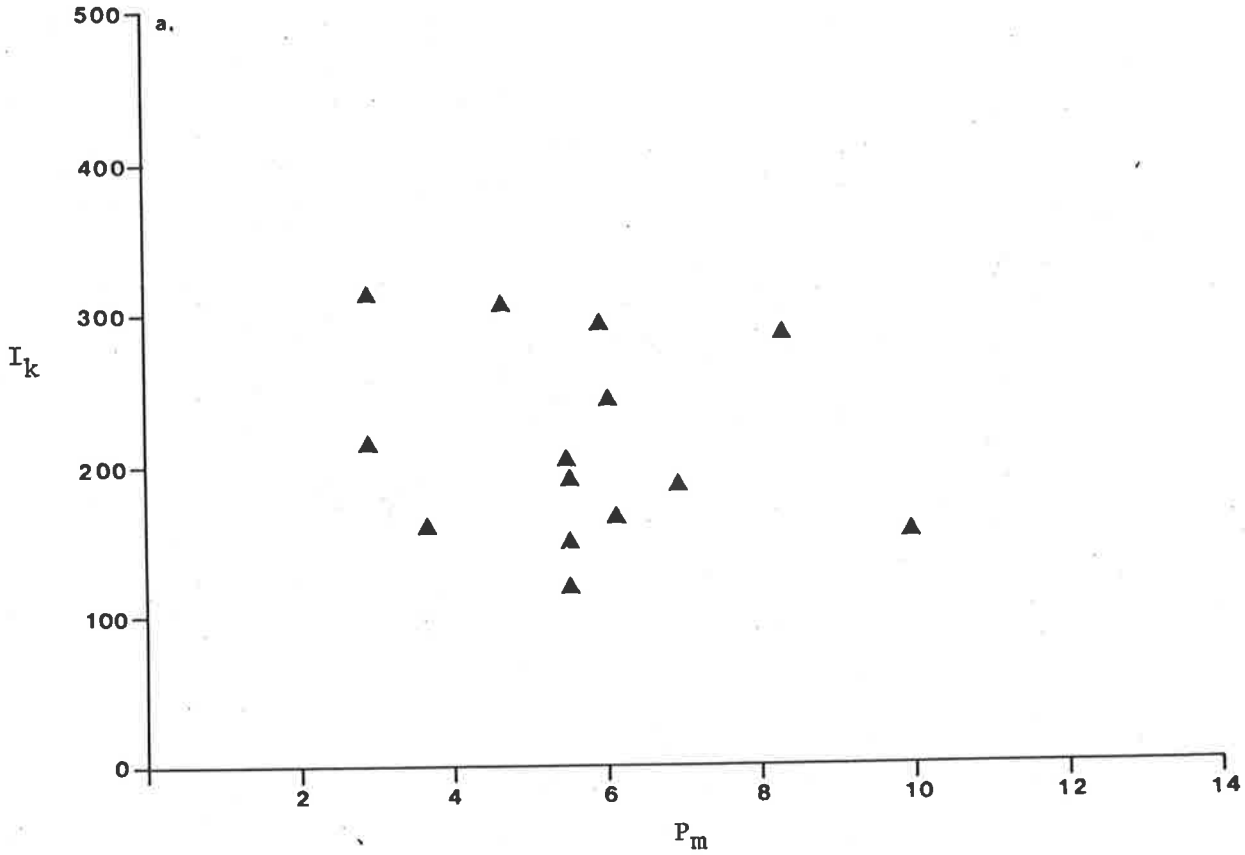

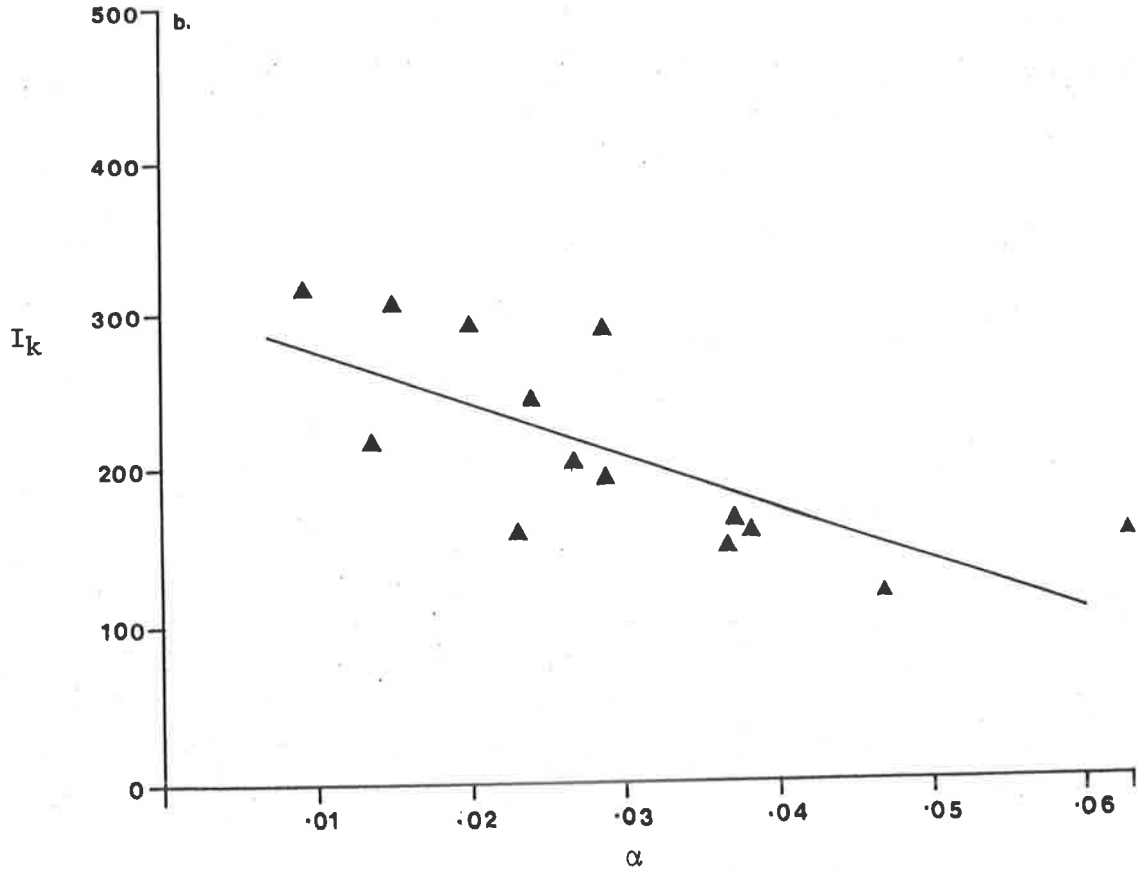

Fig. 6.20: Correlations for the 1979-80 growing season between

a. I_k and maximum specific rate of photosynthesis (P_m)

b. I_k and photosynthetic efficiency (α)
$I_k = 309.8 - 3331.65\ \alpha$ $r^2 = 0.52$ n = 14 $P < 0.01$

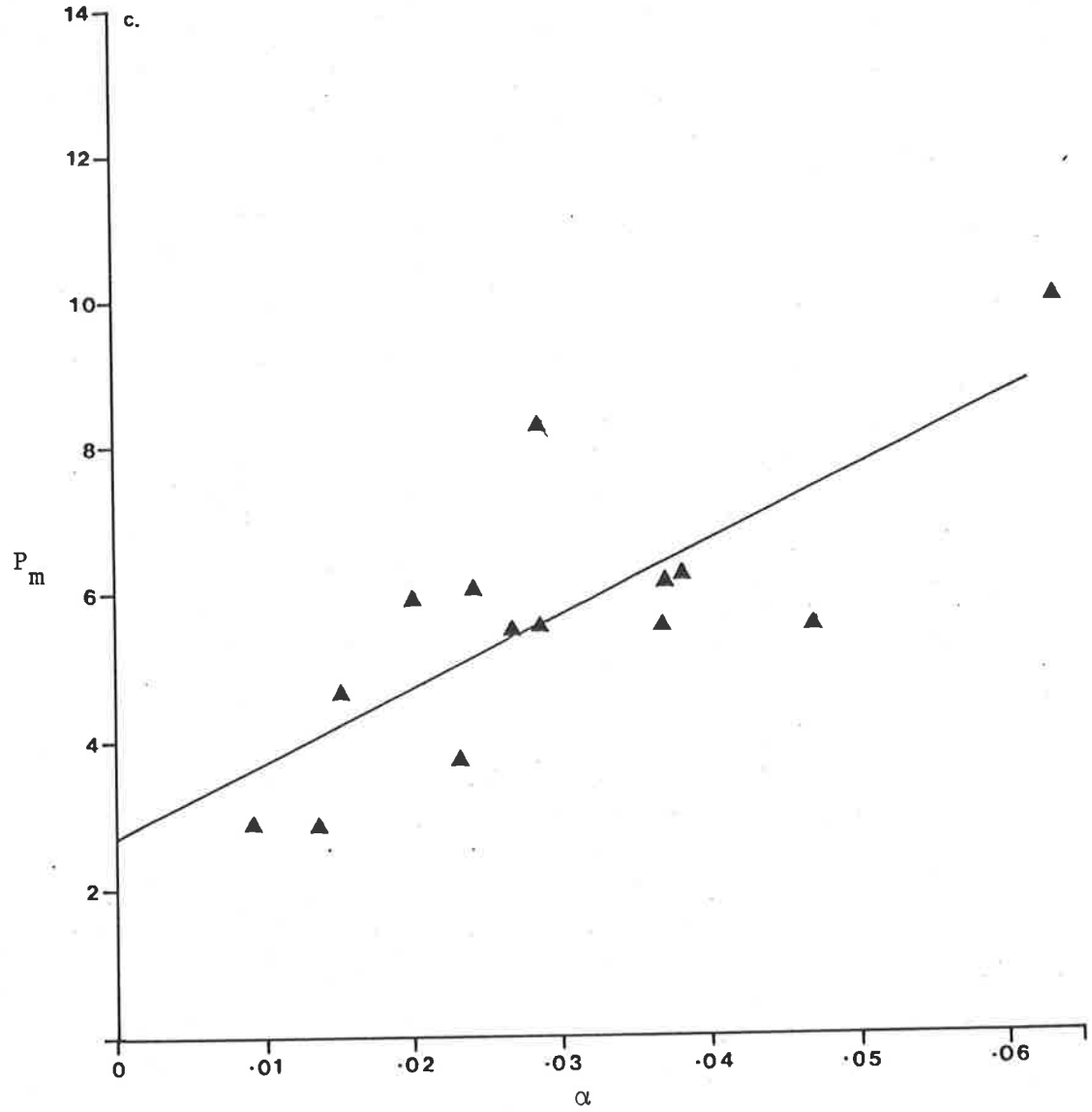

Fig. 6.20: (cont.)

c. P_m and α

$P_m = 2.61 + 102.2\ \alpha$ $r^2 = 0.6$ n = 14 $P < 0.01$

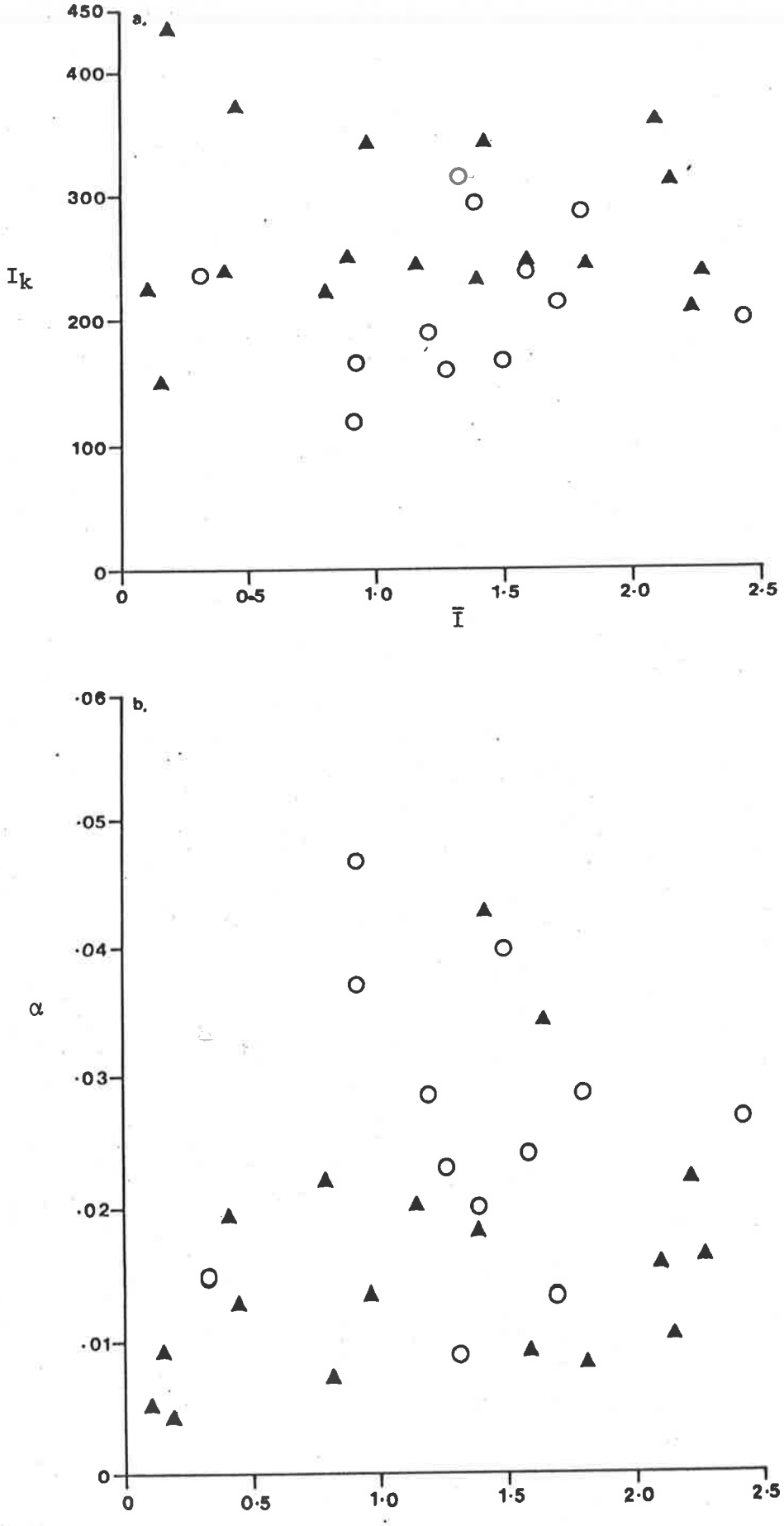

Fig. 6.21: Correlations for the seasons 1978-79 (▲) and 1979-80 (o) between

a. I_k and the mean irradiance of the mixed zone $\bar{I}$

b. Photosynthetic efficiency (α) and $\bar{I}$

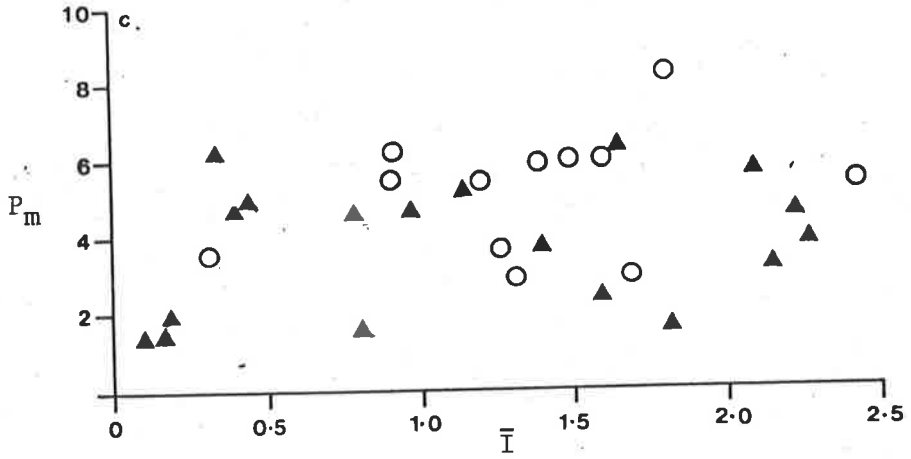

Fig. 6.21 (cont.)

c. maximum specific rate of photosynthesis (P_m) and $\bar{I}$.

Fig. 6.22: Relationship between chlorophyll a concentration and cell volume within the euphotic zone for periods when ε_s could be determined (excludes single disparate point)

[chla] = 3.7 + 2.97 [cell vol] $r^2 = 0.97$ n = 19

○ 16 Jan - 1 April 1980

● 17 Oct 1979 - 04 Jan 1980

▲ 21 Nov - 12 Dec 1978

Fig. 6.23: The relationship between the vertical extinction coefficient (ε) and the chlorophyll a concentration within the euphotic zone of Kinnego Bay, Lough Neagh, derived from the data of Jones (1977a, b) (see text).

$\varepsilon = 0.313 + 0.029$[chla] $r^2 = 0.97$

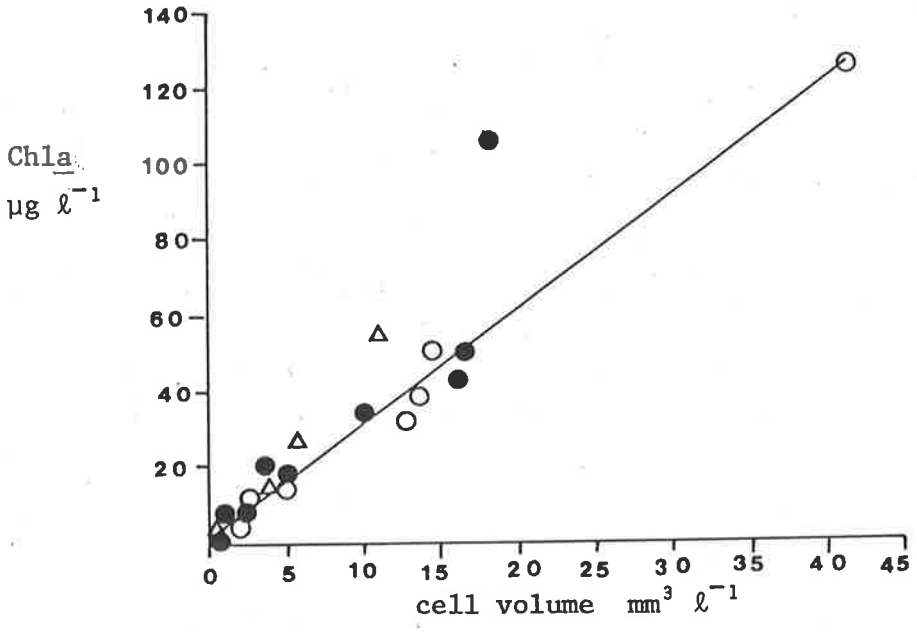

Fig. 6.22:

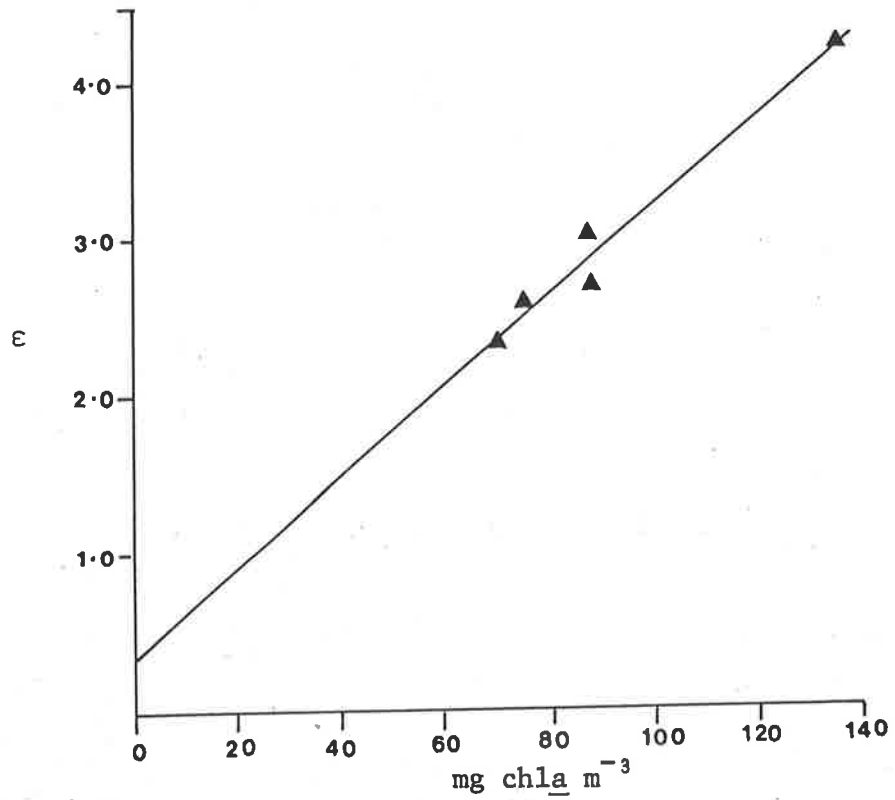

Fig. 6.23:

Fig. 6.24: The relationship between quantum yield (Ø) and the natural logarithm of light intensity (ℓnI(z)) for photosynthetic profiles from Mt Bold Reservoir.

a. □ 21 November 1978
○ 30 November 1978
● 19 December 1978

b. □ 20 November 1979
○ 27 November 1979
△ 4 December 1979
● 11 December 1979

c. □ 16 January 1980
○ 13 February 1980
△ 28 February 1980
● 11 March 1980

Kinnego Bay, Lough Neagh

d. □ 26 April 1973
△ 16 May 1973
● 20 June 1973

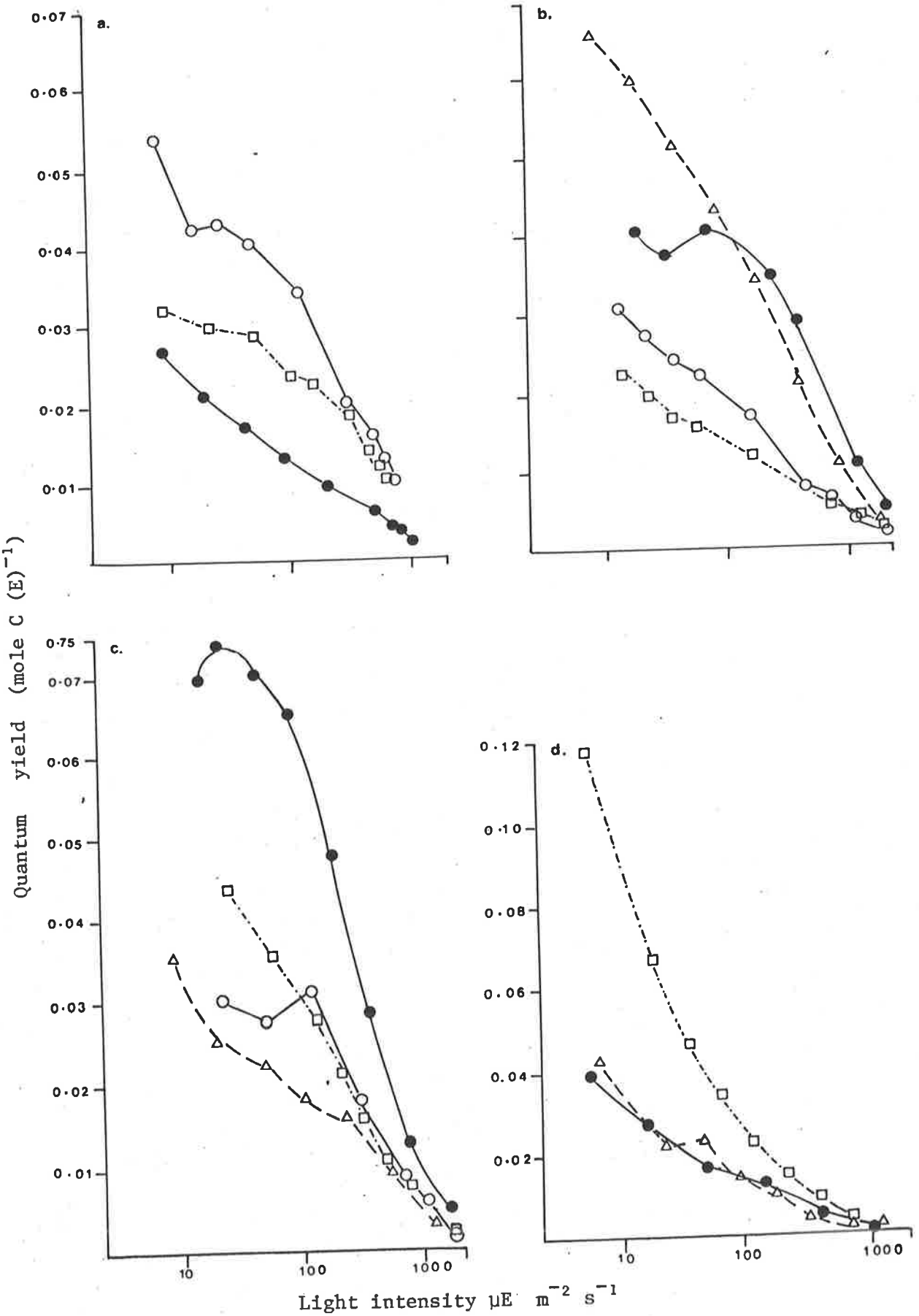
a.
b.
c.
d.
0·07
0·06
0·05
0·04
0·03
0·02
0·01
0·75
0·12
0·10
0·08
0·06
0·04
0·02
10
100
1000
Quantum yield (mole C (E)$^{-1}$)
Light intensity μE m^{-2} s^{-1}

Fig. 6.24:

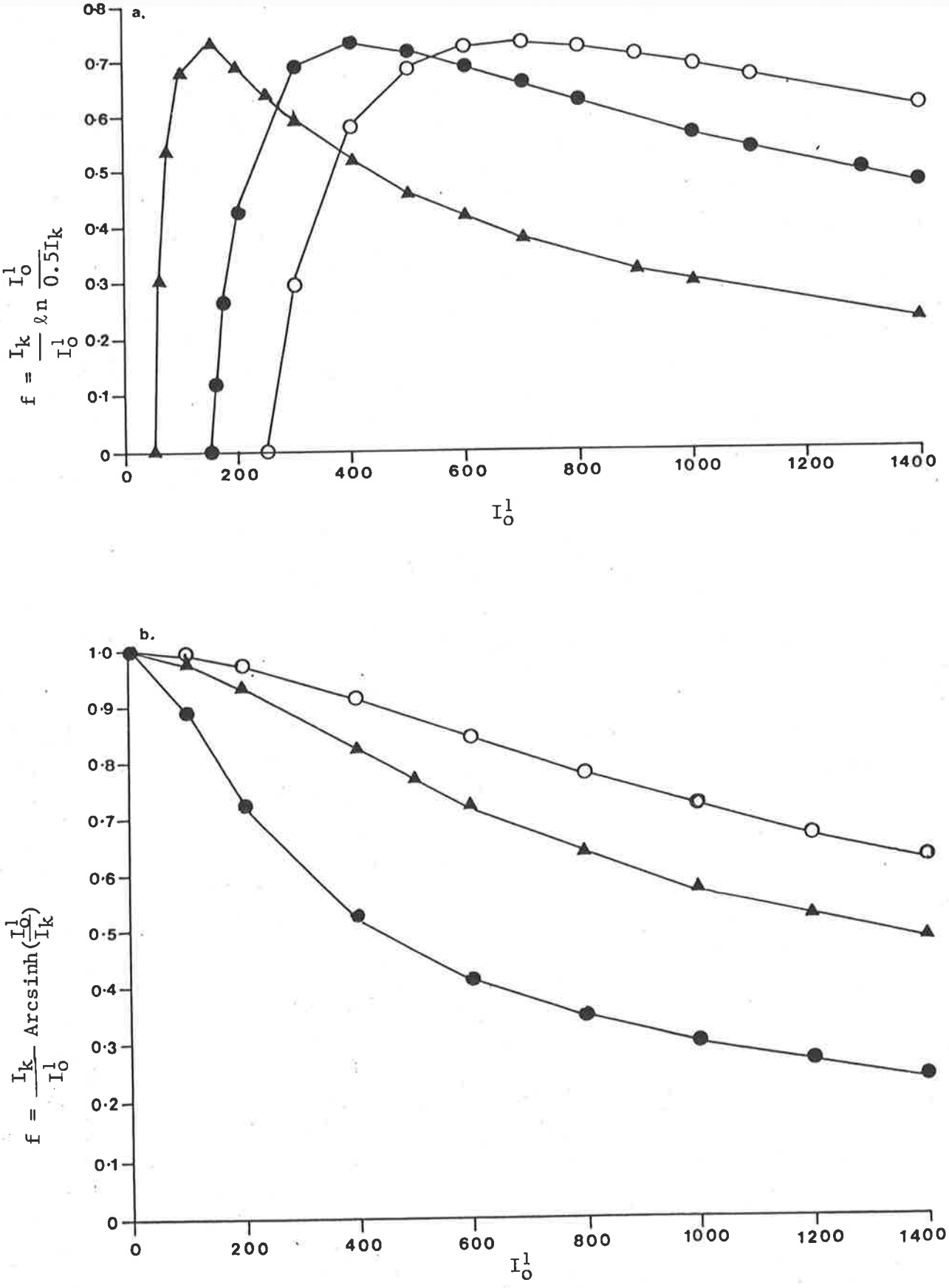

Fig. 6.25: Variation in the two functions of f for a given I_k value and changing incident irradiance intensities.

a. ▲ I_k = 100, ● I_k = 300, ○ I_k = 500

b. ● I_k = 100, ▲ I_k = 300, ○ I_k = 500

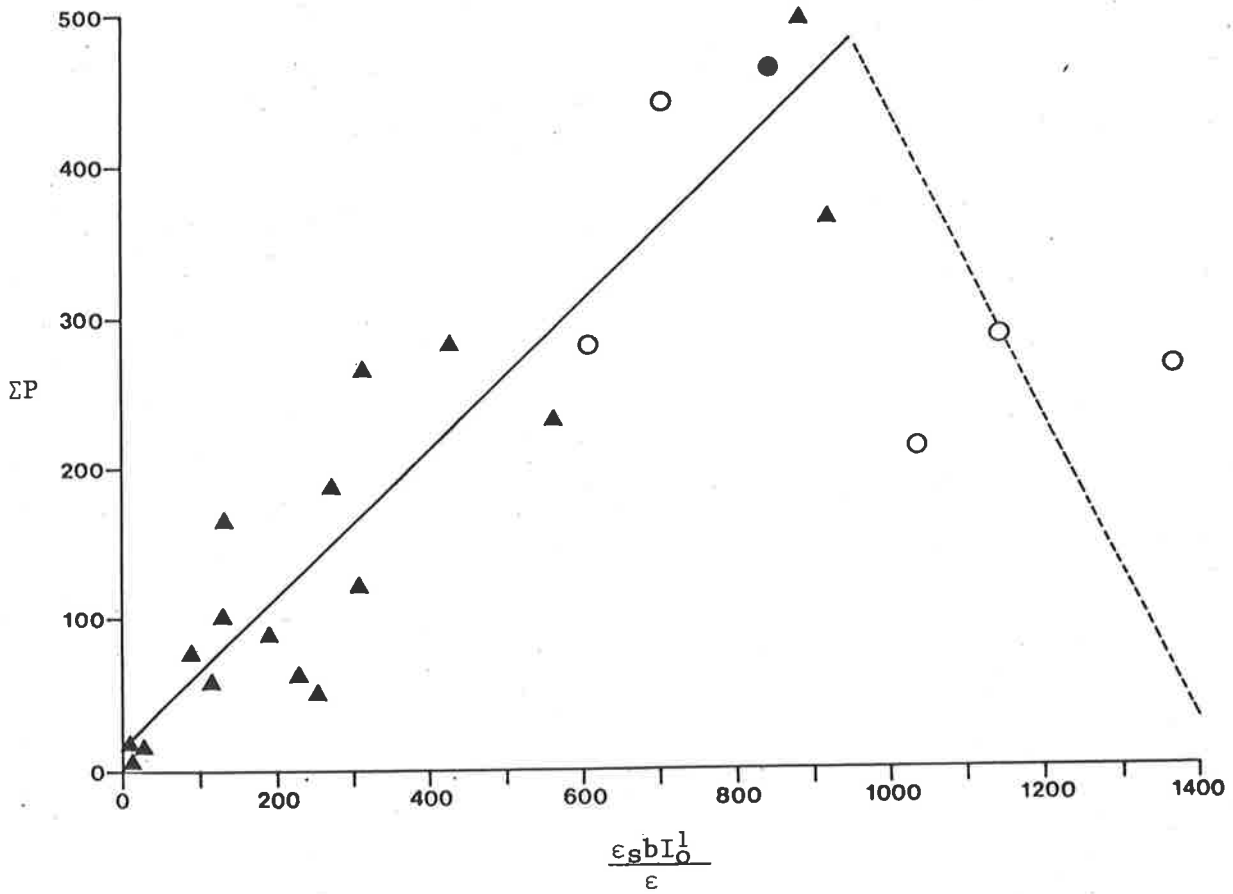

Fig. 6.26: The relationship between rate of integral photosynthesis (ΣP) and rate of integral light absorption $\frac{\varepsilon_s b I_o^1}{\varepsilon}$ for Mt Bold Reservoir (▲), Lough Neagh (○) (Jones 1977a,b) and (●) Lake George, Uganda (Ganf 1975). Linear regression on all points below an absorption rate of 1000 μEinstein $m^{-2}s^{-1}$

$\Sigma P = 17.9 + 0.478 \frac{\varepsilon_s b I_o}{\varepsilon}$ $\quad r^2 = 0.88$

Date	Site	b	R'	P_m	$\frac{R'}{P_m}$	P.Q.
15.02.78	N	17	6.0	38	.16	1.12
15.02.78	S	5	18.0	20	.90	0.93
05.04.78	N	19	2.1	19.3	.11	1.17
17.05.78	S	23.6	undet.	9.4	-	1.93
24.05.78	S	14.4	0.25	8.9	.03	1.78

Table 6.1: Chlorophyll *a* concentration (b mg $chla^{-1}m^{-3}$), specific respiration rate (R'$mgO_2mgchla^{-1}h^{-1}$), maximum gross photosynthesis ($P_m mgO_2 mgchla^{-1}h^{-1}$)and the R'/P_m ratio for experimental dates when ^{14}C and oxygen incubations were run in parallel. The photosynthetic quotient (P.Q.mole) was determined as described in the text.

Lake	P_m	Source
Victoria	av.≃8.3	Talling 1965
Kilotes	5.4-11.2	Talling *et al.* 1973
Windermere	1 - 5.3	Talling 1966
Loch Leven	0.5- 6.5	Bindloss 1974
Lough Neagh	1 - 4	Jewson 1976
Joseph	N.S.-15	Hickman 1979
Minnetonka	2.5- 5.6	Megard 1972
Hamilton Harbour	N.S.-3.5	Harris *et al.* 1980
Mt Bold Reservoir	1 - 7	

Table 6.2: Variation in maximum rates of photosynthesis (P_m mgC $mgChla^{-1}h^{-1}$) observed in a variety of lakes. Where necessary, oxygen data were converted to carbon assuming PQ=1.12.

Incubation start (h)	α	I_o'	I_k	b	P_m	ε	ΣP Planimetric	ΣP Equation 6.1	$\frac{\Sigma P}{I_o'}$
0800	0.040	1060	131	49.2	5.2	4.48	163	160	0.15
1000	0.039	1650	141	48.8	5.5	3.7	235	228	0.14
1200	0.037	1840	188.6	42.1	7.0	3.7	246	237	0.13
1400	0.044	1711	112.3	60	4.9	4.1	245	245	0.14
1630	0.027	1141	176.6	52	4.8	4.1	163.2	155.8	0.14
1840	-	311	-	57	-	4.48	5.1	-	-

Table 6.3: Variables determining integral photosynthesis (ΣP mgC $m^{-2}h^{-1}$, equation 6.1) and their variation over a diurnal series of short term (1.0 h) ^{14}C incubations. Calculated and planimetrically determined integrals are compared. The ratio of integral photosynthesis to incident irradiance (I_o', $\mu Em^{-2}s^{-1}$) provides a measure of efficiency.

Experimental period	ΣΣP from eq. 6.3	% of observed day integral	ΣΣP from proportion of radiation	% of observed day integral
0800-0900	2068	89	2272	98
1000-1100	2530	109	2105	91
1200-1300	2489	107	1976	85
1400-1500	2714	117	2116	91
1630-1730	1943	84	2114	91
1830-1930	-	-	-	-

Table 6.4: Estimates of daily integral photosynthesis (ΣΣP mgC $m^{-2}d^{-1}$), calculated from each of the 1.0 h incubation periods described in Table 6.3, using equation 6.3, and also expressed as a percentage of the observed day integral (2321.3 $mgCm^{-2}d^{-1}$, Fig. 6.11b). Estimates of ΣΣP obtained from the proportion of daily radiation received during each incubation period, also expressed as a percentage of the observed day integral.

1978	ΣP	$\bar{I}$
23.08.78	0.45	0.019
06.09.78	0.63	0.172
12.09.78	0.45	0.164
19.09.78	5.2	0.336
26.09.78	8.7	0.449
03.10.78	6.6	0.420
10.10.78	13.7	0.789
17.10.78	4.4	0.822
24.10.78	17.6	1.573
31.10.78	15.2	2.144
09.11.78	22.2	2.098
21.11.78	14.9	2.266
30.11.78	77.3	2.224
06.12.78	100.4	1.385
12.12.78	185.5	0.965
1979		
17.10.79	4.8	0.315
01.11.79	17.8	1.385
12.11.79	31.8	1.573
20.11.79	50.1	1.313
27.11.79	62.5	1.695

Table 6.5: Variation in integral photosynthesis (ΣP mgC $m^{-2}h^{-1}$) and the mean irradiance of the mixed zone ($\bar{I}$ $MJm^{-2}d^{-1}$) during initiation of the spring biomass increase of 1978 and 1979.

Lake	mgC $m^{-2}h^{-1}$	Source
Kilotes	155 - 800	Talling *et al.* 1973
Victoria	110 - 500	Talling 1965
George	300 - 670	Ganf 1975
Lough Neagh	17 - 330	Jewson 1976
" " Kinnego Bay	30 - 450	Jones 1977 b
Loch Leven	20 - 530	Bindloss 1974
Minnetonka	57 - 355	Megard 1972
Hamilton Harbour	25 - 220	Harris *et al.* 1980
Toom	0.25-2.5	Croome & Tyler 1975
Mt Bold Reservoir	0.5- 300	

Table 6.6: Variation in hourly rates of integral photosynthesis (ΣP mgC $m^{-2}h^{-1}$) observed from *in situ* exposures for a variety of lakes. Where necessary oxygen data were converted to carbon assuming P.Q.=1.12.

Lake	ΣΣP	Annual	Source
Lough Neagh	0.2 - 3.9	500	Jewson 1976
Kinnego Bay	0.3 - 5.2	600	Jewson 1976
Lanao	0.4 - 5.0	620	Lewis 1974
George	1.0 - 5.3	-	Ganf 1975
Victoria (offshore)	1.6 - 3.8		Talling 1965
Minnetonka, Browns Bay	1 - 4	470	Megard 1972
Loch Leven	0.1 - 7	700	Bindloss 1974
Toom	.003 - 0.03	9	Croome & Tyler 1975
Mt Bold Reservoir	not signif.-4.7	≃300	

Table 6.7 Variation in daily rates of integral photosynthesis (ΣΣP mgC $m^{-2}d^{-1}$) and estimates of annual carbon fixation (gC m^{-2}) for a variety of lakes. Where necessary, oxygen data were converted to carbon assuming P.Q.=1.12.

TABLE 6.8

Date	I_o'	b	ε	R	α'	I_k	ΣP	$\frac{\varepsilon_s b I_o'}{\varepsilon}$	$\emptyset_m$	$\int$	$\bar{\emptyset}$
Average ε_s = 0.0122 Average εq = 1.10											
12/4/78	459	2.4	1.15	0.175	8.72	174.2	20.0	11.7	0.072	0.64	0.0481
26/4/78	-	8.0	1.13	-	-	-	-	-	-	-	-
10/5/78	440	39.5	1.55	0.122	5.53	207.5	164.0	136.8	0.043	0.71	0.0317
17/5/78	955	23.6	1.45	0.100	5.08	101.6	89.6	189.6	0.039	0.31	0.0122
Average ε_s = 0.0133 Average εq = 1.59											
21/11/78	699	3.8	1.71	0.020	4.53	238.7	14.9	20.7	0.029	0.61	0.0170
30/11/78	778	15.5	1.81	0.020	6.11	209.9	77.3	88.6	0.039	0.55	0.0207
6/12/78	655	27.6	1.86	0.020	5.11	230.2	100.4	129.2	0.033	0.62	0.0184
12/12/78	901	55.2	2.37	0.020	3.81	344.0	185.5	278.9	0.024	0.65	0.0158
19/12/78	1076	1.6	1.59	0.020	2.33	246.4	3.9	14.4	0.015	0.50	0.0064
Average ε_s = 0.0160 Average εq = 2.21											
20/11/79	2052	17.0	2.48	0.020	2.58	315.1	50.1	255.1	0.014	0.40	0.0047
27/11/79	2005	18.0	2.50	0.020	3.78	214.7	62.5	231.0	0.020	0.31	0.0064
4/12/79	2031	106.7	3.93	0.040	10.31	165.2	498.4	882.3	0.056	0.26	0.0137
11/12/79	2169	34.7	2.78	0.030	7.94	288.8	280.4	433.3	0.043	0.36	0.0155
Average ε_s = 0.0210 Average εq = 1.44											
16/1/80	2003	12.5	1.72	0.030	7.47	201.9	121.5	305.7	0.031	0.30	0.0095
13/2/80	1855	31.7	2.20	0.079	7.97	192.3	230.9	561.2	0.034	0.31	0.0104
28/2/80	1411	127.9	4.13	0.130	4.19	306.0	360.9	917.4	0.019	0.48	0.0105
11/3/80	1712	15.5	1.78	0.075	17.56	156.6	268.7	313.0	0.075	0.28	0.0215
1/4/80	1400	5.5	1.44	0.075	10.25	149.9	58.6	112.3	0.044	0.31	0.0131

Mt. Bold Reservoir

Incident irradiance (I_o' μEm^{-2} s^{-1}), chlorophyll a concentration (b mg chla m^{-3}), vertical extinction coefficient (ε ℓn units m^{-1}) reflectance ratio (R), efficiency of photosynthesis at low light intensity (α' mgC mg $chla^{-1}E^{-1}m^{-2}$) & I_k($\mu Em^{-2}s^{-1}$) for experimental periods when ε_s(m^2mg $chla^{-1}$) could be determined. Derived from these variables were, integral photosynthesis (ΣP $mgCm^{-2}h^{-1}$), the irradiance absorbed by phytoplankton per unit surface area ($\frac{\varepsilon_s b I_o'}{\varepsilon}$ $\mu Em^{-2}s^{-1}$), maximum quantum yield ($\emptyset_m$ mole C E^{-1}) the function $\int$ (equation 6.33) and the average quantum yield ($\bar{\emptyset}$ mole C E^{-1}).

TABLE 6.9

Date	I_o'	b	ε	I_k	ΣP	$\frac{\varepsilon_s b I_o'}{\varepsilon}$	$\int$	$\bar{\phi}$
Average ε_s = 0.029		Average εq = 0.313						
26/4/73	832.8	75.0	2.57	69	441.6	704.8	0.26	0.0145
16/5/73	1426.4	89.0	2.70	74	266.7	1363.5	0.19	0.0045
23/5/73	717.8	87.5	3.00	78	280.0	607.1	0.32	0.0107
30/5/73	1191.7	70.3	2.35	106	212.5	1033.8	0.28	0.0048
20/6/73	1242.4	136.0	4.30	101	287.7	1139.5	0.26	0.0059

Kinnego Bay

Measured and derived variables of integral photosynthesis for an experimental period when ε_s could be determined (Symbols as for Fig. 6.8).

TABLE 6.10

Fractional change in variables between dates

Variable	27 November & 4 December 1979	4-11 December 1979	30 November 1978 & 11 March 1980
ΣP	7.97	0.56	3.48
$\frac{\varepsilon_s b I_o' (1-R)}{\varepsilon}$	3.74	0.5	3.33
$\overline{\emptyset}$	2.14	1.13	1.04
$\int$	0.84	1.38	0.51
$\emptyset_m$	2.8	0.77	1.92
ε_s	1.0	1.0	1.58
I_o'	1.01	1.07	2.2
b	5.93	0.33	1.0
ε	1.57	0.71	0.98

An analysis for several dates of the fractional change in variables determining integral photosynthesis in Mt. Bold Reservoir (see Table 6.8 & equation 6.26, 6.27 & 6.31).

TABLE 6.11

Fractional change in variables between dates

Variable	16-23 May	23-30 May	30 May & 20 June
ΣbP^b	1.05	0.76	1.35
$\frac{\varepsilon_s b I_o'}{\varepsilon}$	0.45	1.70	1.10
$\overline{\emptyset}$	2.38	0.45	1.23
ε_s	1.0	1.0	1.0
I_o'	0.50	1.66	1.04
b	0.98	0.80	1.93
ε	1.11	0.78	1.83

Fractional change in variables determining integral photosynthesis in Kinnego Bay, Lough Neagh over a two month period in 1973 (see Table 6.9 & equation 6.31).

PHYTOPLANKTON CELL DENSITY

7.0 Introduction

To grow successfully phytoplankton must spend sufficient time within the euphotic zone for photosynthesis to occur in excess of loss rates. The high background extinction coefficients typical of Mt. Bold Reservoir (Chp. 3) restrict the depth of the euphotic zone, and as a result relatively shallow mixing depths lead to light limitation of biomass accumulation (Chp. 5) and photosynthesis (Chp. 6).

The reduction in mixing depth resulting from thermal stratification during spring and summer causes an improvement in the mean irradiance of the mixed zone which leads to the spring biomass increase and summer growth period (Chp. 5). However the associated decline in water turbulence has important consequences for algal sedimentation.

Apart from blue-green algae, freshwater phytoplankton are denser than water and therefore tend to sink (Lund 1959; Hutchinson 1967; Walsby & Reynolds 1980). Sinking rates vary within and between species and are dependent on both physiological state (Smayda & Boleyn 1965, 1966(a) & (b); Eppley *et al*. 1967; Titman & Kilham 1976) which causes changes in cell density, and morphological characteristics (Smayda 1970) which change surface area to volume ratios and particle orientation. The discrimination between density and morphological effects on sinking rate is prerequisite to an understanding of phytoplankton adaptations to suspension.

As most phytoplankton have a particle Reynolds Number of less than 0.5, the terminal sinking velocities of spherical forms in non-turbulent conditions will be described by Stokes Law (Smith 1975). However, few phytoplankton are spherical and McNown & Malaika (1950) introduced a coefficient of form resistance ($\emptyset_f$) which modified Stokes' Law to give

$$V = \frac{gD^2(p^1-p)}{18\eta\emptyset_f} \qquad (7.1)$$

(Terms defined in Table 7.1)

This equation describes the relationship between the terminal sinking velocity, density and form of phytoplankton. The coefficient of form resistance ($\emptyset_f$) as defined in Table 7.1 is a measure of the effect on sinking velocity of a deformation from the spherical form, and is of interest in considering the adaptive advantages of phytoplankton shapes. However theoretical and model estimates of $\emptyset_f$ vary considerably between workers (Eppley et al. 1967).

Research on the gas-vesicles of blue-green algae has highlighted the importance of cell density as a factor determining their vertical distribution in lakes (Reynolds & Walsby 1975). Steel and Yentsch (1960) also implied the importance of density as a factor governing the depth distribution of phytoplankton. In groups other than the blue-greens physiologically induced changes in cell density are often inferred but few direct measurements are available (Gross & Zeuthen 1948, Smayda & Boleyn 1965, 1966(a) & (b)), due to the lack of a suitable technique.

A possible method for the measurement of cell density is isopycnic gradient centrifugation (Pertoft et al. 1978). The use of this technique was previously limited by lack of suitable gradient materials, most available substances forming solutions of undesirably high osmolality or viscosity. The relatively recent advent of silica-sols (reviewed by Wolff 1975) has provided a high molecular weight, colloidal material which does not penetrate cell membranes, and which forms solutions of low osmotic pressure and viscosity (Mateyko & Kopac 1963).

Using a silica-sol, Price et al. (1974) collected marine phytoplankton by continuous flow centrifugation. Although the algae formed distinct isopycnic bands, evidence was later given (St. Onge and Price 1975; Morgenthaler and Price 1976) which suggested that the banding densities did not necessarily correspond to the true densities of the cells.

The following section describes a series of experiments undertaken to test the possibility of using Percoll (Pharmacia Fine Chemicals), a modified silica sol (Pertoft et al. 1978), for phytoplankton density measurements. The success of the technique enabled investigation of density changes resulting from nutrient limitation, and the measurement of cellular densities in field populations.

MATERIALS AND METHODS

7.1 Organisms and Conditions of Growth

The green algae *Chlorococcum* sp. and *Chlorella vulgaris* Beyerinck

were cultured in ASM-I medium (Gorham et al. 1964) at 20°C on 12:12 light-dark cycle at a light intensity of ca.210 $\mu\varepsilon\ m^{-2}\ s^{-1}$.

A population of *Cyclotella meneghiniana* Kuetzing was obtained by enriching lake water with $N\text{-}NO_3$ (1000 $\mu g\ \ell^{-1}$), $P\text{-}PO_4$ (100 $\mu g\ \ell^{-1}$) and EDTA (1000 $\mu g\ \ell^{-1}$) and incubating at 12°C and 70 $\mu\varepsilon\ m^{-2}\ s^{-1}$ on a 12:12 light-dark cycle. Under these conditions *C. meneghiniana* became one of the dominant species of the sample.

Variation in cellular density due to nutrient limitation was investigated in *Scenedesmus quadricauda* Turp (Cambridge Culture Collection). A senescent population was enriched 1:1 with ASM I medium made to 3mM $NaHCO_3$, but containing 20% of the normal NO_3-N concentration (5.6 $\mu g\ NO_3\text{-}N\ \ell^{-1}$). The culture was continually stirred and maintained on a 10:14 h light-dark cycle at 20°C. Sub-samples taken at regular intervals were assayed for protein and carbohydrate (Stone unpublished thesis) and cell numbers counted following Lugol's iodine sedimentation. Dry weight was determined by filtering 25-50ml samples onto preweighed , 4.25cm Whatman GF/C filters, drying at 105°C, and re-weighing on a Cahn electro-balance.

Where necessary concentrations of cultured phytoplankton were increased by centrifugation in a bench centrifuge and resuspension in a small volume. Samples containing clumped material were passed through a 15μ net.

Integrated euphotic zone samples (Chp. 2) from Mt. Bold Reservoir normally required concentrating before cell density measurements

could be attempted. Concentration by centrifugation was not possible due to the presence of gas-vacuolated blue-green algae. Instead the sample was filtered sequentially through a 15μ mesh and 0.45μ Millipore filter, and phytoplankton resuspended using a magnetic stirring bar.

Microscopic measurements of cell size were made at 1000 x magnification, or under Nomarsky illumination at 400 x magnification. To avoid distortion cells were sized under a raised coverslip. Cell volumes were calculated using equations appropriate to the cell geometry.

7.2 Measurement of Sinking Velocities

Sinking velocities were measured by both a microscopic and fluorometric technique.

Microscopic measurements of sinking rate were made with a Nikon inverted microscope and a settling tube. The experimental design was similar to that of Smayda & Boleyn (1965), but the method varied significantly in the handling of the sample and the counting of cells arriving at the bottom of the settling tube.

Smayda (1974) was able to layer freshwater phytoplankton onto the surface of filtered lake water by lowering the density of the algal sample with distilled water. Attempts to use the layering technique without a density difference have been unsuccessful (Smayda & Boleyn 1965; Titman 1975). To avoid adding distilled water to the algal samples, and to standardize sample handling, the

layering technique was abandoned and completely mixed samples were used in both the microscopic and fluorometric methods.

Although a complete scan of the settling tube base is recommended for cell enumeration, it is known that the proximity of the walls distorts sinking rate. To avoid this only cells in the centre of the settling tube were recorded, this being done photographically with an Olympus PM-6 camera. Sample concentration was adjusted to maximise cell counts and minimise cell overlap.

The fluorometric method followed that of Titman (1975) using either a 10 or 20mm sinking zone. The fluorescence component due to neutrally buoyant cells was considered part of background fluorescence and subtracted from all traces. Sinking velocity estimates therefore gave the mean rate for those cells that sink, a result analogous to that obtained by the microscopic technique. The rate will vary from the mean sinking rate of the total population in accord with the proportion of neutrally bouyant cells present. This proportion was estimated either by comparing cell counts from the microscopic technique with those from a sample settled with Lugol's iodine, or by the percentage of cells remaining above the density gradient after centrifugation (Fig. 7.1).

All experiments were run at 20°C for a minimum of 12 h. When the two techniques were run in parallel the fluorometer cuvette and the settling tube had identical dimensions.

7.3 Formation and Calibration of Density Gradients

Phytoplankton densities are likely to range from ca. 1.0-1.3 g cm^{-3} (Eppley et al. 1967). Percoll has an initial density of 1.13 g ml^{-1}. To extend the density range, gradients were formed by high speed centrifugation (Pertoft et al. 1978) in a Sorvall Superspeed RC-2 centrifuge fitted with an SM-24 rotor. A spin time of 2 hours at 14,500 rpm (ca. 25,300 g) and 0°C produced gradients in 15ml centrifuge tubes ranging in density from ca. 1.0-1.20 g cm^{-3} (Fig. 7.1). For cultured material grown in ASM-I, Percoll solutions loaded into the centrifuge were prepared by mixing 5ml Percoll, 4ml of water and 1ml of ten times concentrated ASM-I. The mixture for field populations was 5ml Percoll, 4.5ml of filtered lake water and 0.5ml of 10xASM-I, while experiments with *S. quadricauda* used mixtures of 5ml Percoll, 4.5ml of culture filtrate and 0.5ml of 10 x ASM-I containing 20% of the normal NO_3-N concentration.

The absolute density of each Percoll layer was measured using a CCl_4:Kerosene organic column formed in a one litre measuring cylinder in the manner outlined by Wolff (1975) (see also Miller & Gasek 1960). This column was calibrated using standard sucrose solutions.

7.4 Banding of Algae in Density Gradients

Following preparation of the Percoll gradients a 90 minute minimum period was allowed for equilibration to room temperature (20°C). A 2 or 3ml algal sample was layered on top and forced down through the gradient at ca. 300g in a swing-out head bench centrifuge.

Perturbation of the gradient was avoided by gentle acceleration and deceleration (Price, Reardon & Guillard 1978). Fractionation of the gradients was achieved by upward displacement with fluorinert (3M Cσ., density 1.93 g ml^{-1}).

For culture material, bands of algae were easily identified by measuring the fluorescence of small (ca. 0.3ml) volumes in a Turner III fluorometer fitted with a micro-cuvette holder. Identification of *Cyclotella* bands was not so easily achieved with the fluorometer, and layers were examined microscopically. Banding of field material was also determined microscopically.

RESULTS

A comparison of sinking rate and cellular density estimates on laboratory cultures.

7.5 Cell Sizes

Frequency distributions of cell sizes approximated to normality and were analyzed accordingly. The two measured diameters, a and b, of *Chlorococcum* were generally equal. Where they were not a nominal diameter (D, defined in Table 7.1) was calculated by,

$$D = \sqrt{a.b}$$

The mean cell diameters are given in Table 7.2. Experiments 3-6 show the progressive increase in mean-cell diameter with age,

experiment 6 representing a senescent *Chlorococcum* population.

Chlorella has the shape of a prolate spheroid and axes were labelled according to McNown & Malaika (1950), with the a semi-axis parallel to the direction of motion. *Chlorella* cells were found by microscopic examination to sink with the major axis horizontal, therefore the b semi-axis is half the length of the major axis, and the c and a semi-axes are equal and half the length of the minor axis. Nominal diameters (D) of *Chlorella* samples were calculated from,

$$D = 2\ (a.b.c)^{1/3}$$

where a, b & c are the appropriate semi-axis. Results are shown in Table 7.3.

Cyclotella average cell dimensions and nominal diameter are shown in Table 7.4. The nominal diameter was calculated from,

$$D = \left(\frac{3a^2b}{2}\right)^{1/3}$$

where a is the diameter of the cylinder base and b its height.

Cell volumes and surface areas are shown in Table 7.5.

7.6 Sinking Velocities

Typical results from the inverted microscope and fluorometric techniques for measuring sinking velocity are presented in Fig. 7.2

and 7.3 a-d. Figure 7.2 indicates the number of *Chlorococcum* cells arriving at the bottom of the settling tube with time, while Fig. 7.3 a-d, shows the decrease in fluorescence with time.

The time (t_{50}) for either fluorescence to halve, or cell number to reach half maximum value, was measured from the appropriate graph. The average sinking velocity was calculated using this time (t_{50}) and half the length of the sinking zone (Eppley et al. 1967; Titman 1975). These estimates ranged from 4.38×10^{-5} to 1.4×10^{-3} cm s^{-1} (Table 7.2, 7.3 & 7.4).

In experiments 4, 5, 7 & 8, (Table 7.2 & 7.3) where the data allow direct comparison of the sinking velocities from the two techniques, a large disparity is apparent. It is evident from the results that the fluorometric method gives an estimate of sinking rate 2 to 5 times smaller than that of the inverted microscope technique.

An assumption of the fluorometric method is that fluorescence is proportional to cell concentration (Eppley et al. 1967). To test this, the inverted microscope results were converted to fluorescence units assuming a constant ratio of fluorescence to cell number. It was evident from the results of this conversion (Fig. 7.3 a-d) that corresponding calculated and measured traces were not identical, which implied that fluorescence per cell was not constant. Part of the discrepancy may be explained by the shoulders of fluorescence between 0.5 and 2 h in Fig. 7.3 b & d.

7.7 Density Measurements and Calculations

Fluorescence was found to be a suitable indicator of algal bands in Percoll. The plot of fluorescence against density was generally normally distributed (Fig. 7.4 a & b), as was the plot of cell number against density for the *Cyclotella* experiment (Fig. 7.4c). The mean cell densities obtained in Percoll ranged from 1.044 to 1.101 g cm^{-3} (Table 7.2, 7.3 & 7.4).

The validity of the Percoll density measurements cannot be assumed due to the possibility of anomalous banding resulting from both osmotic effects and interactions between the gradient medium and the cells (St Onge & Price 1975; Morgenthaler & Price 1976). Samples of phytoplankton removed from the Percoll gradients were viable when recultured, indicating the absence of large osmotic effects.

To further check the validity of the Percoll measurements, densities were calculated from the observed sinking rates using the generalized form of Stokes' Law (equation 7.1), nominal diameter, and an assumed $\emptyset_f$ value of one (Table 7.2, 7.3 & 7.4). The assumption of $\emptyset_f = 1$ implies that the cells sink in the same manner as a sphere of equal volume. For spherical *Chlorococcum* cells this assumption is valid, whereas for *Chlorella* and *Cyclotella* it is not necessarily true.

McNown and Malaika (1950) provide equations to calculate form resistance $\emptyset_f$, for ellipsoidal particles. Using their equation (3), $\emptyset_f$ values for two *Chlorella* experiments were calculated as 1.01 for experiment 9, and 1.04 for experiment 10 (Table 7.3). As these

corrections are small calculated densities assuming $\emptyset_f$=1 should be close to true densities.

McNown and Malaika (1950, fig 4) also showed experimentally that a cylindrical form with a particle Reynolds Number less than ca. 0.1, and diameter equivalent to length, will settle at the same velocity as a sphere of equal volume. The *Cyclotella* dimensions (Table 7.4) show it is only slightly wider than long and therefore might be expected to fall at a similar velocity to a sphere of equal volume. For all three species the cell densities calculated from the inverted microscope results, assuming $\emptyset_f$=1, were equivalent to the mean densities measured in Percoll (Table 7.2, 7.3 & 7.4). As would be expected from the earlier comparison of sinking rates obtained fluorometrically and microscopically, the density estimates calculated from the fluorometer data vary significantly from the others.

Neutrally buoyant cells were found only in *Chlorococcum* experiments 3, 4 & 5 (Table 7.2), where they comprised 3.5, 2 and 7% of the population. These values do not significantly alter the average sinking rate for the total population from those measured directly with either the microscopic or fluorometric techniques.

DENSITY VARIATIONS UNDER INCREASING NUTRIENT LIMITATION

7.8 Changes in Cell Number and Composition of *S. quadricauda* in Batch Culture.

Enrichment of the senescent *S. quadricauda* culture resulted in an

exponential increase in cell number over an eight day period (Fig. 7.5). The increase in cell number then ceased, but dry weight continued to rise due to the formation of carbohydrate (Table 7.6). As protein formation stopped with cell growth, the protein to carbohydrate ratio progressively decreased in the stationary phase, indicating nutrient limitation (Chp. 4), which under the culture conditions described was most likely nitrogen. The average dry weight per cell was high in the senescent population, decreased over the growth period, but increased again in the stationary phase.

On day 2, 5 and 8 measurements were taken just prior to the onset of the light period (AM), and the dark period (PM) (Table 7.6). Cell counts were similar for morning and afternoon samples indicating that cell division was occurring at night. Carbohydrate content increased over each light period, while protein showed increases over day 2 and 5 but not day 8. In response to these changes, average dry weight per cell increased ca. three times over the light period of day 2, but showed only a small increase over day 5 and 8 (Table 7.6).

7.9 Density Variations

The distribution of *Scenedesmus* cells in Percoll gradients was determined fluorometrically and generally approximated normality (Fig. 7.6 a-g). The mean density of the population varied between 1.070 and 1.122 g cm^{-3} (Table 7.6).

Enrichment of the original culture (density = 1.096 g cm^{-3}) resulted in daily fluctuations in the mean population cellular density. For

example on day 2 (Fig. 7.6b, Table 7.6) the morning sample had a mean density of 1.070 g cm^{-3} and the afternoon sample 1.103 g cm^{-3}. By day 5 these fluctuations were reduced (Fig. 7.6c, Table 7.6) and the population maintained a mean cell density between ca. 1.08-1.09 g cm^{-3} for the remainder of the exponential growth period.

At the beginning of stationary phase (day 12), the mean cell density increased to the maximum observed value (Fig. 7.6e). Thereafter densities remained relatively high but continued to vary around a value close to the density of the original culture (Fig. 7.6f & g).

Between day 0 and 5 the mean dry weight per cell was correlated with mean cell density. (Fig. 7.7) indicating that cell volume was remaining relatively constant. As stationary phase was approached cell volume decreased and the relationship between mean dry weight and cell density changed (Fig. 7.7).

It has been demonstrated that the protein to carbohydrate ratio provides a measure of nutrient availability (Chp. 4). The relationship between this index and cell density was exponential in form (Fig. 7.8), an increase in the ratio coinciding with a decrease in density.

APPLICATION TO FIELD SAMPLES

7.10 Cellular Densities of Phytoplankton from Field Populations

The cellular density of major phytoplankton species occurring in Mt. Bold Reservoir was measured on six occasions during the 1979/80 growing season (Table 7.7). Cell counts were used to estimate the

range and modal density for each species, and converted to a fraction of a species total number for the graphical description of density distribution (Fig. 7.9 a-f).

Samples taken early in the season required concentrating. As soon as cell numbers were sufficiently high this step was removed to minimize handling effects. In most cases cell densities measured with and without the concentrating procedure were of similar magnitude (cf. 22/11/79 and 16/1/80 Table 7.7).

7.11 Discussion

The excellent agreement between density results calculated from the inverted microscope technique and densities measured directly in Percoll gradients, clearly demonstrates the successful use of these gradients for such measurements.

The effects of various aspects of cell size on sinking rates can be drawn from Table 7.5. The relationship between sinking velocity, cell diameter and the surface area to volume ratio fell within the range shown by Smayda (1970, Fig. 1 and 3). Although the data supports these broad relationships the scatter of points indicates significant changes in density, morphology, or both. The ability to directly but independently measure the density and sinking velocity of phytoplankton allows for discrimination between density and form affects. An example of this is provided by the age sequence experiments conducted with *Chlorococcum* (Table 7.2, experiments 3-6). The cell sinking veolcity increased with culture age from 3.05×10^{-4} cm s^{-1} (calculated

for experiment 3 from Stokes' Law using the Percoll density and average nominal cell size) to 8.17 x 10^{-4} cm s^{-1}, while the cell diameter correspondingly increased from 8.94 to 18.79 µm. Cell density, however, as indicated by measurements in Percoll, at first increased from 1.070 to 1.089 gm cm^{-3}, but then fell in the senescent population to 1.044 gm cm^{-3} (Fig. 7.4a). The fast sinking rate of the senescent population was therefore a result of the large cell size rather than cell density. Increased sinking velocity with culture age has been demonstrated in a number of phytoplankton (Eppey et al. 1967; Smayda 1970) leading to the view that older cells are denser than younger cells. The *Chlorococcum* results suggest that this may not be generally correct.

Senescent *Chlorococcum* cells differed markedly in appearance from young cells. In experiment 5 the cell constituents filled the cell volume completely, whereas in the senescent population of experiment 6 the cell constituents were maintained in a central sphere surrounded by a thick colourless layer. This outer layer made up 50% of the cell diameter and was equivalent to the increase in cell size from experiment 5 to experiment 6. If the increased size of the senescent cells is considered to be the result of addition of a thick outer layer to a *Chlorococcum* cell which otherwise maintains its density and size, then the density of the added layer can be calculated from,

$$\text{New cell density} = \rho'' + [(\rho' - \rho'')/\hat{a}^3]$$

(Hutchinson 1967 p. 274).

ρ'' is the density of the added layer, ρ' the density of the cell prior to the addition of the layer and $\hat{a}$ the factor by which the added layer

has increased the cell radius. Using the data from experiments 5 and 6 we have,

$$1.044 = \rho'' + [(1.089-\rho'')/1.53^3]$$

and $\rho'' = 1.026$ g cm^{-3}.

Staining with acidified iodine solution and Bismark Brown Y supported the contention of an added layer and indicated that it consisted of mucin. The adaptive significance of this strategy is unclear. The decrease in absolute density from 1.089 to 1.044 g cm^{-3} decreased the excess density, and so the sinking rate by a factor of 2.0 (assuming that cell size had remained constant), however, the concomitant increase in cell size from 12.3 to 18.79 µm increased sinking rate by a factor of ca. 2.3 (assuming that cell density had remained constant). The final result was the observed ca. 17% increase in sinking rate of the senescent population. Although this may not appear to be directly an adaptation to aid flotation it is remarkable that with the relatively large changes in cell diameter and excess density (ca. 50% for both) sinking rate should only vary by 17%. It is possible that the cells were maintaining a critical sinking velocity by size adjustment overcoming the effect of adding a mucin layer which itself has some other function such as protection. Increase in cell size of senescent populations, particularly when forming resting stages, has been shown for *Ditylum brightwelli* and *Rhizosolenia setigera* (Eppley et al. 1967).

The independent measurements of cell density and sinking velocity further allow the calculation from equation (1) of the form factor $\emptyset_f$, indicating the adaptive significance of non-spherical shapes. This

method of determining the parameter ϕ_f also includes other factors which might affect sinking rate, such as cell oscillation or rotation, therefore care must be taken in its interpretation. Values of ϕ_f calculated from equation 2 are shown for *Chlorella* and *Cyclotella* (Tables 7.3 and 7.4) and as would be expected are trivial for these test organisms where the three dimensions are similar.

Previously most estimates of cell density have relied upon the derivation of a mean cell density by the application of Stokes' Law (e.g. Eppley et al. 1967). Although Smayda (1970, Fig. 3) has attempted to define minimum and maximum sinking velocities, and hence by interpolation maximum and minimum densities, these still rely upon a deterministic calculation based upon Stokes' Law. The direct measurements of cell density presented here not only confirm the implied density ranges of Eppley et al. and Smayda but also quantify the absolute range and distribution.

For the young *Chlorococcum* population the density range was remarkably small (1.065 - 1.09 g cm^{-3}), as the population aged, so the range of densities initially increased (1.04 - 1.14) but then fell in the senescent population (1.02 - 1.06). Both *Chlorella* populations showed a wide density range (1.02 - 1.18) as did the population of *Cyclotella* (1.02 - 1.2). The range of densities found in this single diatom population covers much of the range found in the literature (Hutchinson 1967 p. 248; Eppley et al. 1967). This density distribution pattern along with the distribution of cell dimensions suggest that a wide range of sinking rates may occur within a single field population.

Phytoplankton sinking rates are generally observed to increase with a decline in growth rate (Smayda & Boleyn 1965, 1966a, b; Eppley et al. 1967; Titman & Kilham 1976). These variations frequently occur independently of changes in morphological characteristics but are closely associated with nutrient availability, suggesting a physiological cause. The occurrence of this phenomenon in a wide range of algal groups suggests a common mechanism, although this has not yet been described.

The density changes in *Scenedesmus* following nutrient enrichment, paralleled the expected changes in sinking velocity (Titman & Kilham 1976). Density decreased during the period of logarithmic growth (Fig. 7.5 & 7.6) and increased as the stationary phase was approached. The maximum change in density (ca. 1.07 to 1.12, Table 7.6) was sufficient to cause a 70% increase in sinking rate, assuming a constant cell volume and morphology. The relationship between cell density and the ratio of protein to carbohydrate (Fig. 7.8), suggested that increased density was a function of increased carbohydrate reserves accumulated by phytoplankton under nutrient poor conditions (Table 7.6; Healey 1975; Myklestad 1977; Gibson 1978; Stone unpublished thesis). This mechanism provides an explanation for the increased sinking rate observed with culture age (Smayda & Boleyn 1965, 1966a, b; Eppley et al. 1967; Titman & Kilham 1976), however it cannot be assumed that these fluctuations are necessarily an adaptation for buoyancy control.

The *Chlorococcum* results discussed earlier demonstrate that the postulated mechanism is not evident in all algae.

Although the density changes observed for *Scenedesmus* paralleled expected variations in sinking rate, concomitant changes in cell

volume following day 8 (Fig. 7.7) made interpretation of the actual effect on sinking rate difficult. A comparison of the data for the afternoon of day 8 and day 12 (Table 7.6) suggested that cell volume had decreased without a significant change in cell number. Despite this apparently anomalous result, a comparison of dry weight per cell with cellular density measurements (Fig. 7.7), from day 8 onwards, indicated that cell volume had decreased.

The daily variation observed in cellular density (day 2 & 5) can be explained in terms of variation in the protein and carbohydrate content. During these measurements changes in density were proportional to changes in dry weight per cell, implying a small variation in cell volume (Fig. 7.7). Consequently the accumulation over the light period of both protein and carbohydrate, but mainly the latter, increased cellular density, while overnight cell division and utilization of carbohydrate reserves decreased it. As nutrients became limiting and growth diminished the density oscillations were reduced.

7.12 Cellular Densities of Field Populations

The largest variation in cellular density was unexpectedly shown by *Ceratium* (Table 7.7; Fig. 7.9e), with modal values ranging from 1.033 to 1.162 g cm^{-3}. The larger densities were observed in mid-November and the smaller values in late November and January suggesting a decline in cellular density as thermal stratification increased. The results however do not unequivocally demonstrate active adaptation by individual cells of the population. Only a

small absolute number of *Ceratium* cells were present in January (Fig. 7.9e shows relative numbers), and may simply have been the lower density cells of the original population. The data suggest however that cellular density may be an important factor even to a flagellated alga such as *Ceratium*.

In contrast *Sphaerocystis* with a modal density of 1.015 g cm^{-3} varied only slightly over the same period (Fig. 7.9f), as did *Trachelomonas* (Table 7.7) with a modal density of ca. 1.03-1.04 g cm^{-3}.

Cyclotella and *Melosira* both gave maximum cell numbers at densities between 1.15 and 1.18 g cm^{-3} (Fig. 7.9a & b), however low cell numbers were frequently observed at much smaller cellular densities (Table 7.7). On occasions some cells appeared to be almost neutrally bouyant occurring in the uppermost layers of Percoll gradients. On the 20/2/80 cell numbers of both *Melosira* and *Cyclotella* were low, but indicated a modal value of 1.068 - 1.078 g cm^{-3}, with neutrally bouyant cells of both species evident. The sample of *Cyclotella* cultured in lake water by addition of nutrients, gave a modal density of ca. 1.095 g cm^{-3} (Fig. 7.4c) while earlier experiments on *Cyclotella* maintained in the culture collection gave estimates of 1.062 - 1.068 g cm^{-3}. Part of this variation probably resulted from differences in nutrient conditions.

As expected the blue-green algae showed low modal densities (Fig. 7.9c & d). Values for *Microcystis* ranged from bouyant to 1.025 g cm^{-3} while *Anabaena* showed a more restrictive range from bouyant to 1.01 g cm^{-3}.

The density distributions of the species supports presently accepted ideas on the role of differential sedimentation rates in seasonal succession. In natural populations where an increase in cell numbers is a balance between production of new cells and their loss via sinking, a decrease in water turbulence will result in a progressive loss of cells in order of sinking rates (Knoechel & Kalff 1975). If morphological effects are small then the relative sinking rates of the different species may be estimated from the product of their excess density ($\rho'-\rho$), and the square of their nominal diameter (D^2) (equation 7.1), assuming viscosity equivalent for all species. As a result of the large density differences between the non-motile species (Fig. 7.9), volume had little effect on relative sinking rates which decreased from the diatoms through *Sphaerocystis* to the blue-green algae.

Attempts to relate changes in average population sinking rate, estimated using values of $D^2(\rho'-\rho)$, to variation in the index of succession rate (S.D., Section 5.7) were handicapped by the limited data, and no significant correlations were obtained.

Reynolds (1979) and Walsby & Reynolds (1980) derived an expression to estimate the *in situ* sinking rate (V', md^{-1}) of particles sedimenting from a zone sufficiently well mixed as to keep the population within the zone evenly dispersed,

$$V' = Z_m \left[1 - \left(\frac{P_t}{P_o}\right)^{1/t}\right] \qquad 7.2$$

P_o and P_t are the population size within the mixed zone $Z_m(m)$ at

time o and t respectively. The function $(\frac{P_t}{P_o})^{1/t}$ is a measure of the daily fractional retention rate of the mixed zone (Walsby & Reynolds 1980).

Qualitatively the model envisages that particles are lost from suspension where water currents are slowed by friction, for example at the upper layers of the metalimnion (≡ thermocline *sensu* Hutchinson 1941; Chp. 3, Fig. 3.24). Assuming that the sinking velocity of the particles and the degree of turbulence remains constant over t days the decline in population size will be exponential.

During the period 20/11 - 4/12/79 the *Cyclotella* population of euphotic zone samples decreased exponentially, the linear form of the exponential growth equation (equation 5) giving a correlation coefficient, $r^2 > 0.99$. On the assumption that population growth was minimal, equation 7.2 was used to calculate the *in situ* sinking rate. Over the 14 day period the population size of the mixed zone (Z_m = 6.0m, Fig. 6.14b) decreased from 5609 to 578 cell ml^{-1} (Fig. 5.6) and the calculated sinking rate, $V' = 0.9$ m d^{-1}.

The expected sinking rate of *Cyclotella* cells in non-turbulent conditions, assuming a form factor $\emptyset_f$=1, was calculated from equation 7.1 using the density estimate obtained from Percoll gradients (1.175 g cm^{-3}, Fig. 7.9a). Water temperature was between 19-20°C allowing use of the constants in Table 7.1, average cell volume was 234 μm^3 giving a nominal diameter of 7.64 μm, and the expected sinking rate calculated from these values, 0.5 m d^{-1}.

The similarity of the two values is encouraging, implying that when water turbulence is minimal the modified form of Stokes' equation enables empirical calculation of *in situ* sinking rates.

The capability to measure cell density, combined with laboratory measurements of sinking rate, allows quantification of cellular sinking characteristics, and provides the basis for modelling *in situ* sinking rates under more turbulent conditions. However the statistical quantification of variation in water turbulence provides a formidable impediment.

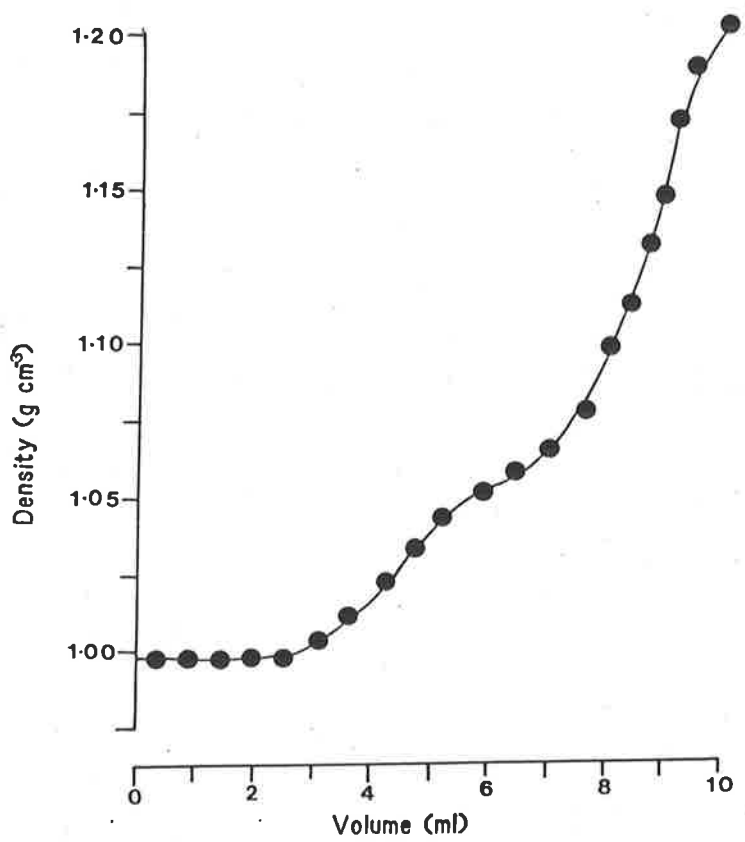

Fig. 7.1: Shape of Percoll density gradients formed as described in the text. Increasing volumes represent sequential layers down the centrifuge tube. (Total depth = ca. 5 cm).

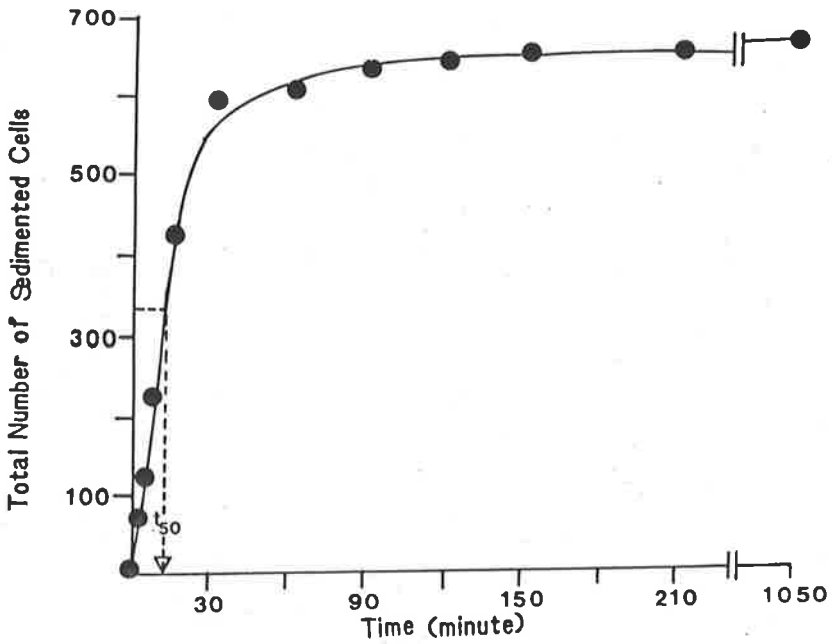

Fig. 7.2: The relationship between total number of sedimented *Chlorococcum* cells and time (Table 7.2, exp. 5). t_{50} represents the time required for 50% of the cells to sediment through an average distance of half the sample height.

Fig. 7.3: The decrease in fluorescence with time measured in the fluorometer (●—●) compared with the decrease in fluorescence with time calculated from the parallel inverted microscope results, assuming a constant fluorescence per cell (o---o).

a. *Chlorella*, Table 7.3, experiment 7

b. *Chlorella*, Table 7.3, experiment 8

c. *Chlorococcum*, Table 7.2, experiment 4

d. *Chlorococcum*, Table 7.2, experiment 5

Fig. 7.3

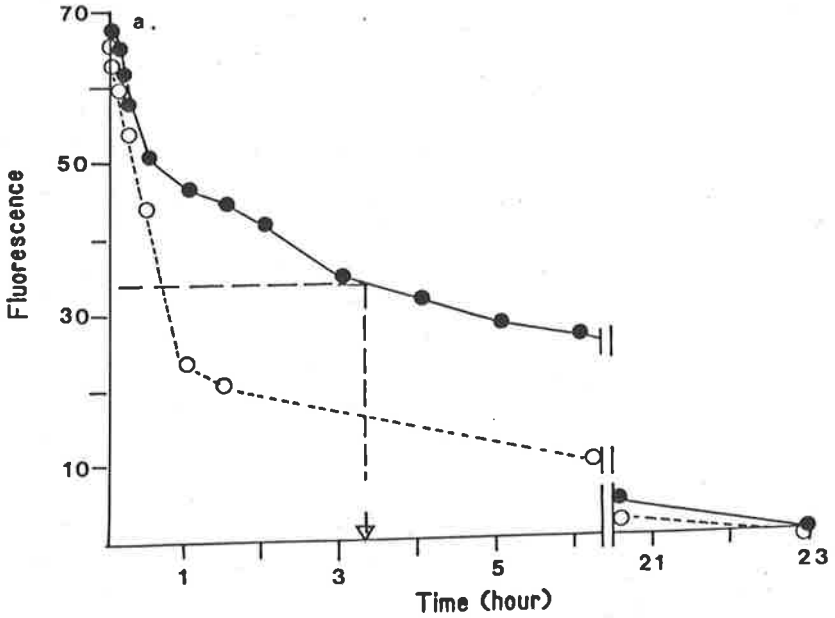
a.
70
50
30
10
Fluorescence
1
3
5
21
23
Time (hour)

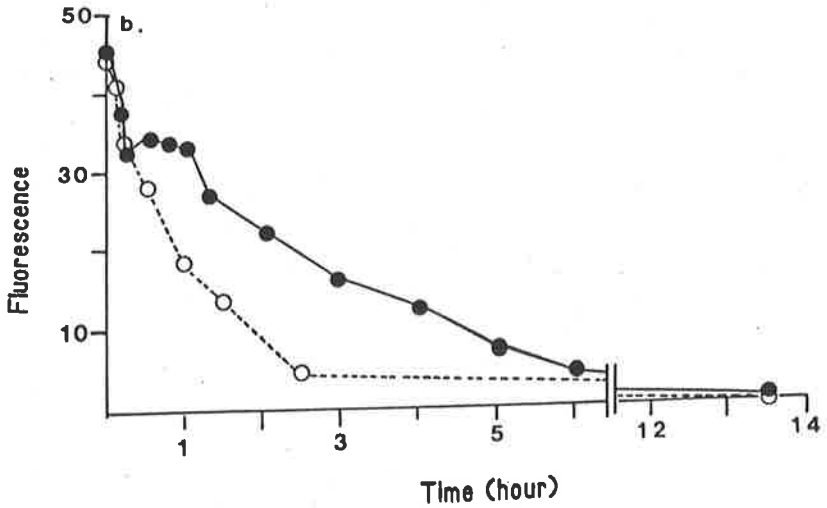
b.
50
30
10
Fluorescence
1
3
5
12
14
Time (hour)

Fig. 7.3

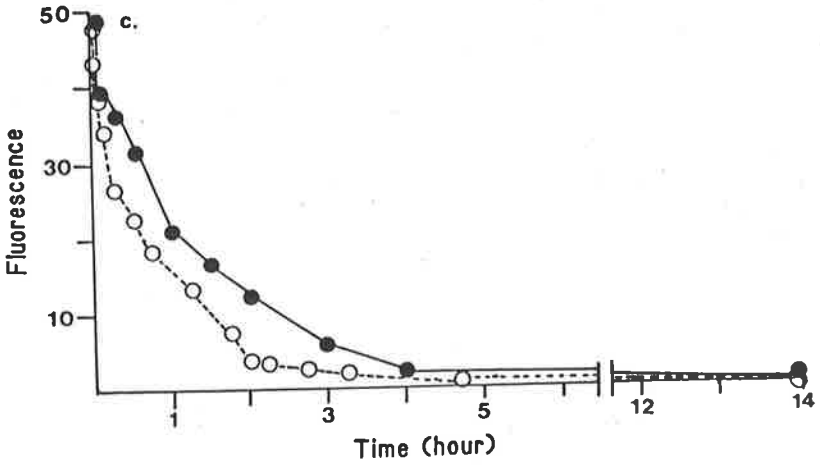
c.
50
30
10
Fluorescence
1
3
5
12
14
Time (hour)

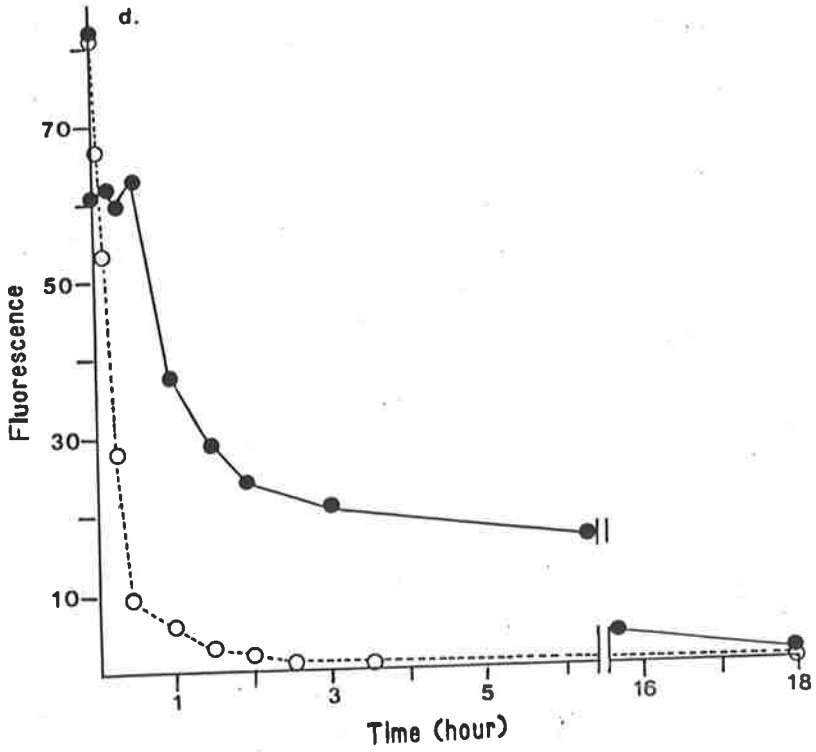
d.
70
50
30
10
Fluorescence
1
3
5
16
18
Time (hour)

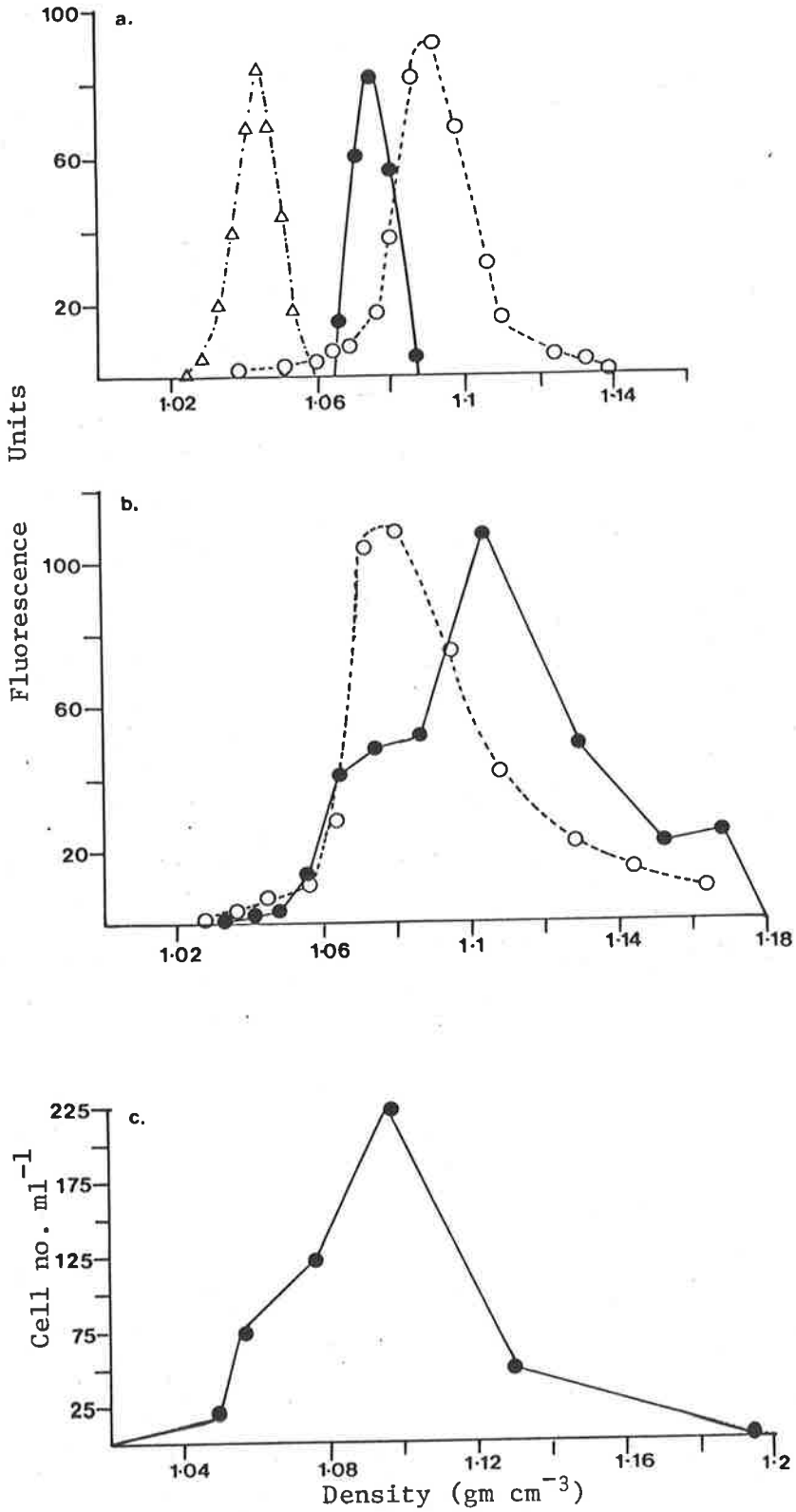

Fig. 7.4: The density distribution of

a. three *Chlorococcum* populations of varying age; (●—●) exp. 2, $\bar{x}$ = 1.074; (○···○) exp. 5, $\bar{x}$ = 1.089; (△-·-△) exp. 6 (senescent population), $\bar{x}$ = 1.044.

b. two *Chlorella* populations; (●—●) exp. 9, $\bar{x}$ = 1.101; (○···○) exp. 10, $\bar{x}$ = 1.088.

c. the *Cyclotella* population.

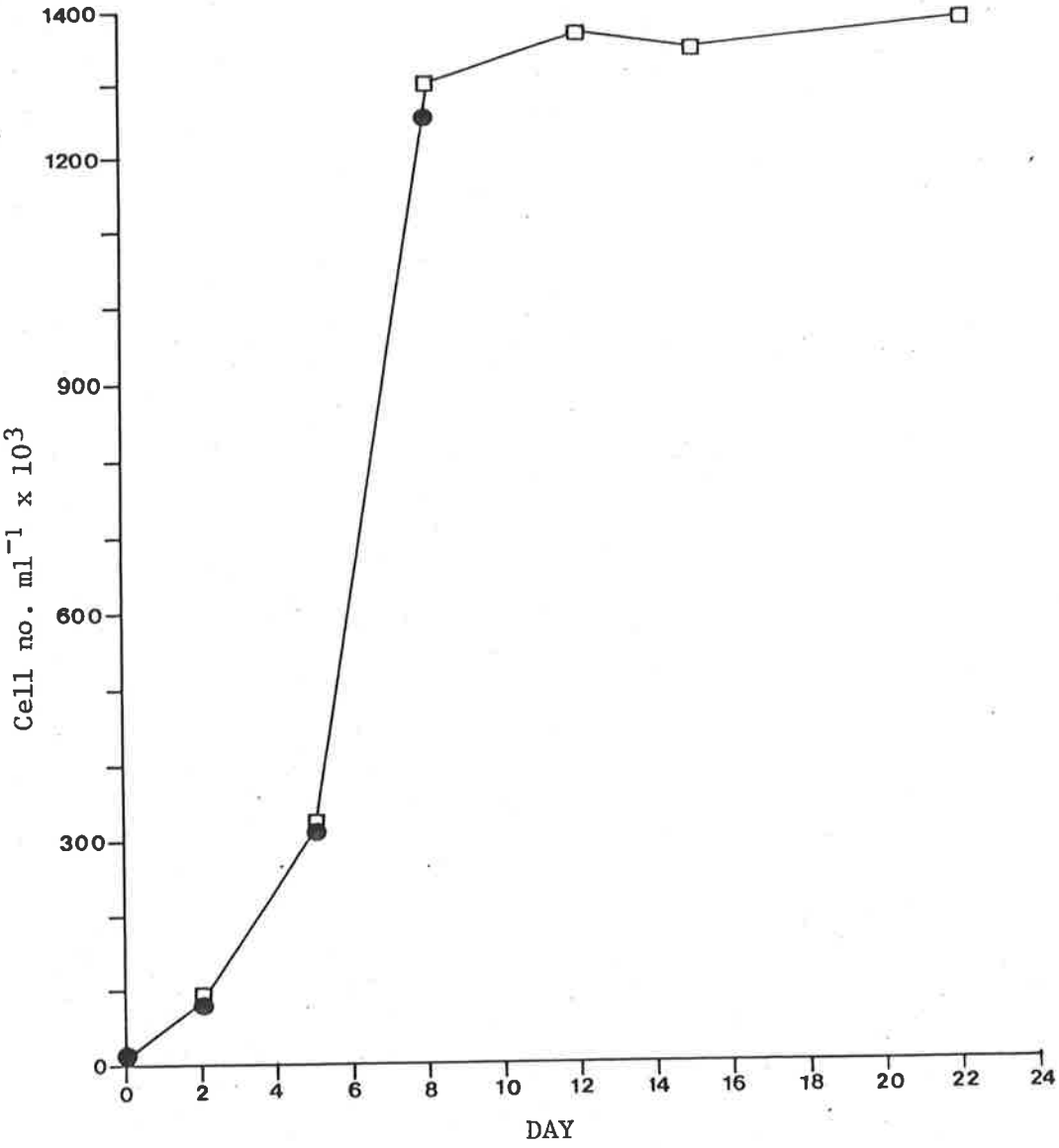

Fig. 7.5: Change in cell number with time of *S. quadricauda* grown in batch culture. (●)AM, (□)PM

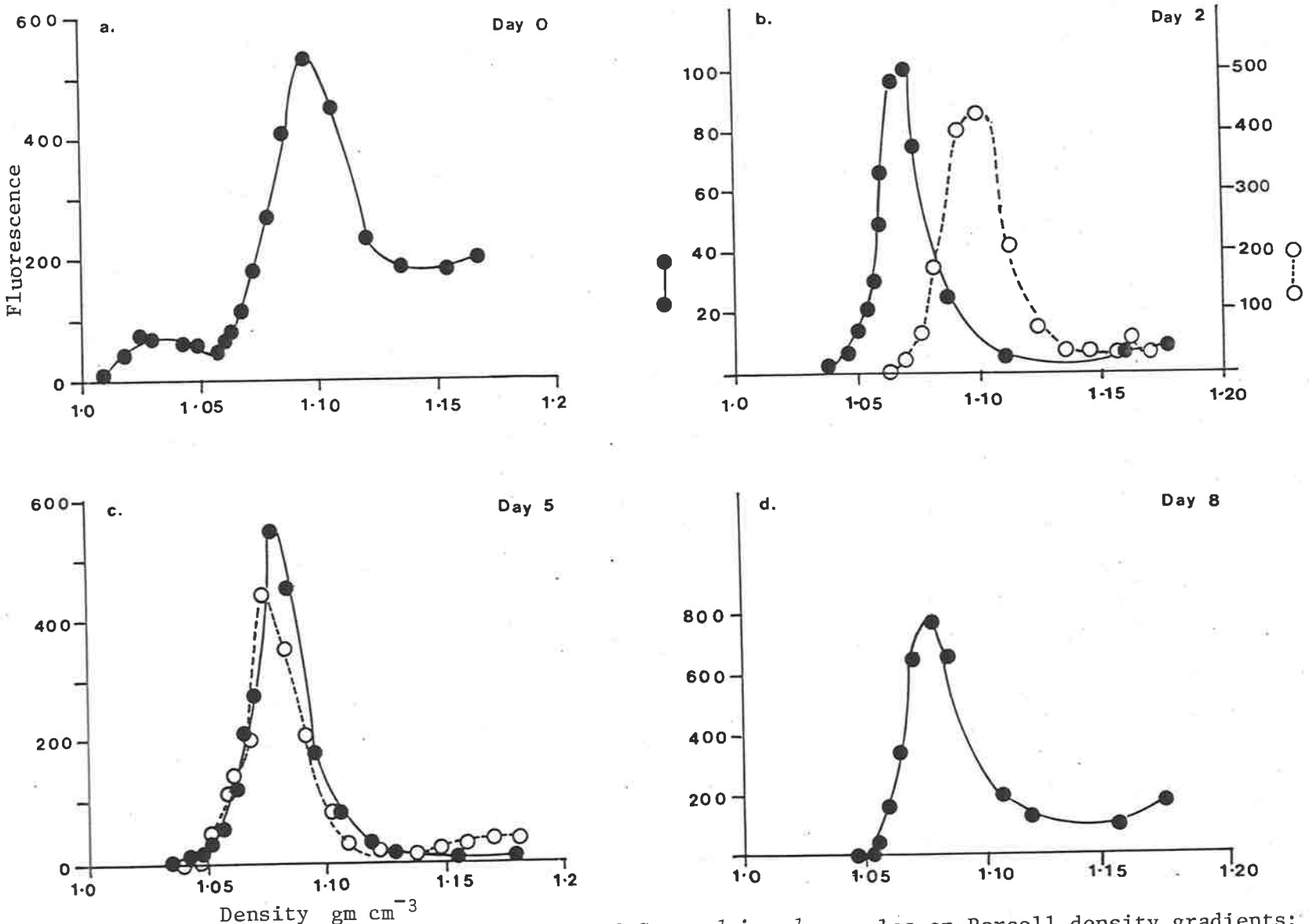

Fig. 7.6: Fluorometrically determined distribution of *S. quadricauda* samples on Percoll density gradients; a. original sample; b. Day 2, AM (●), PM (○); c. Day 5, AM (●), PM (○); d. Day 8, PM;

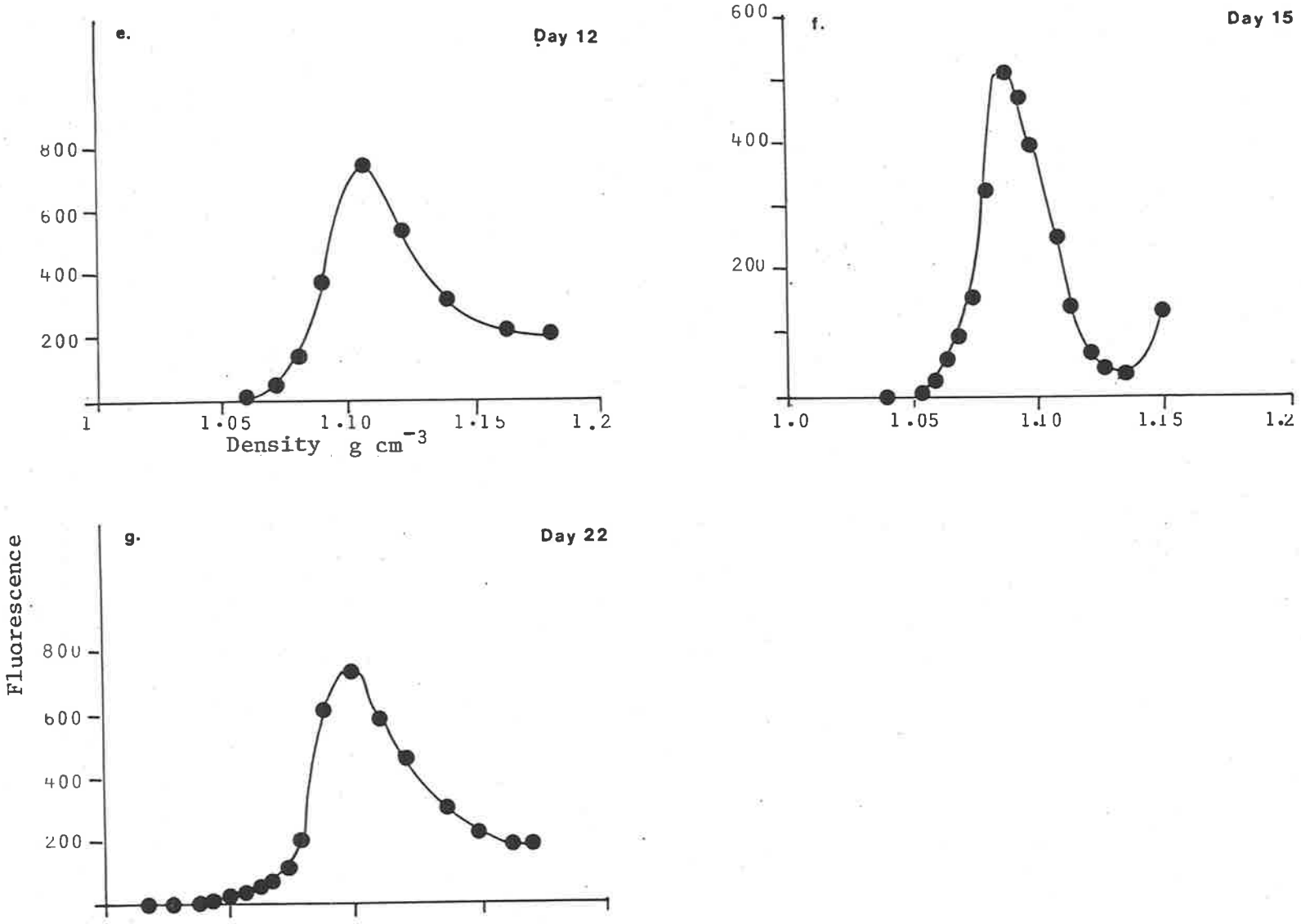

Fig. 7.6: (cont.) e. Day 12, PM; f. Day 15, AM; g. Day 22, AM.

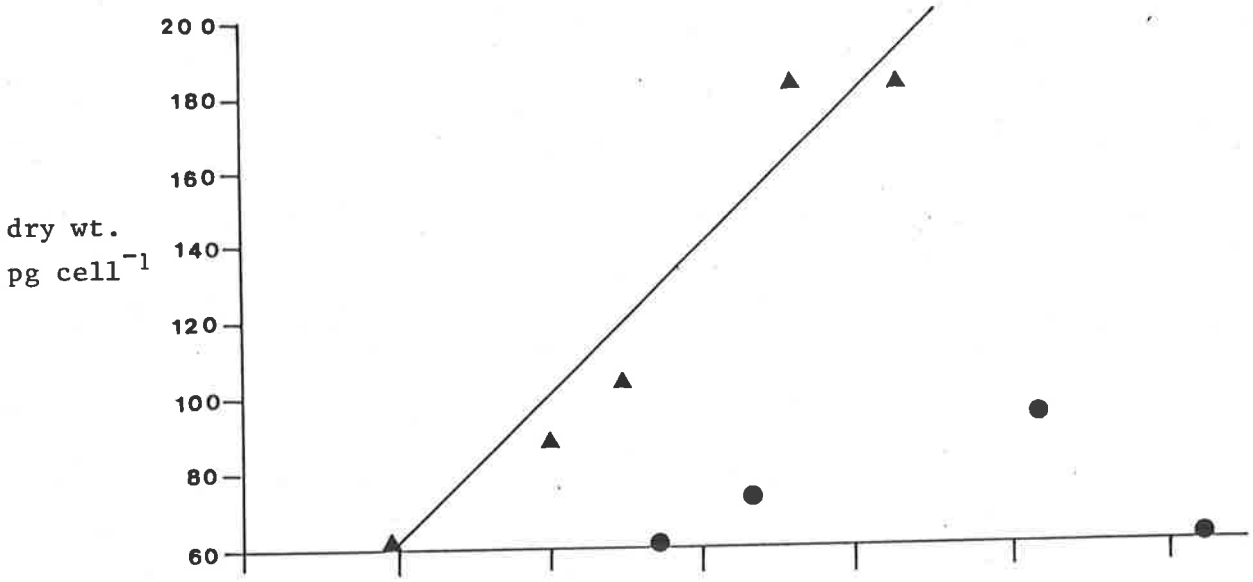

Fig. 7.7: Relationship between cell dry weight and cell density for day 0-5 (▲) and day 8-22 (●). Line relates to symbol ▲.

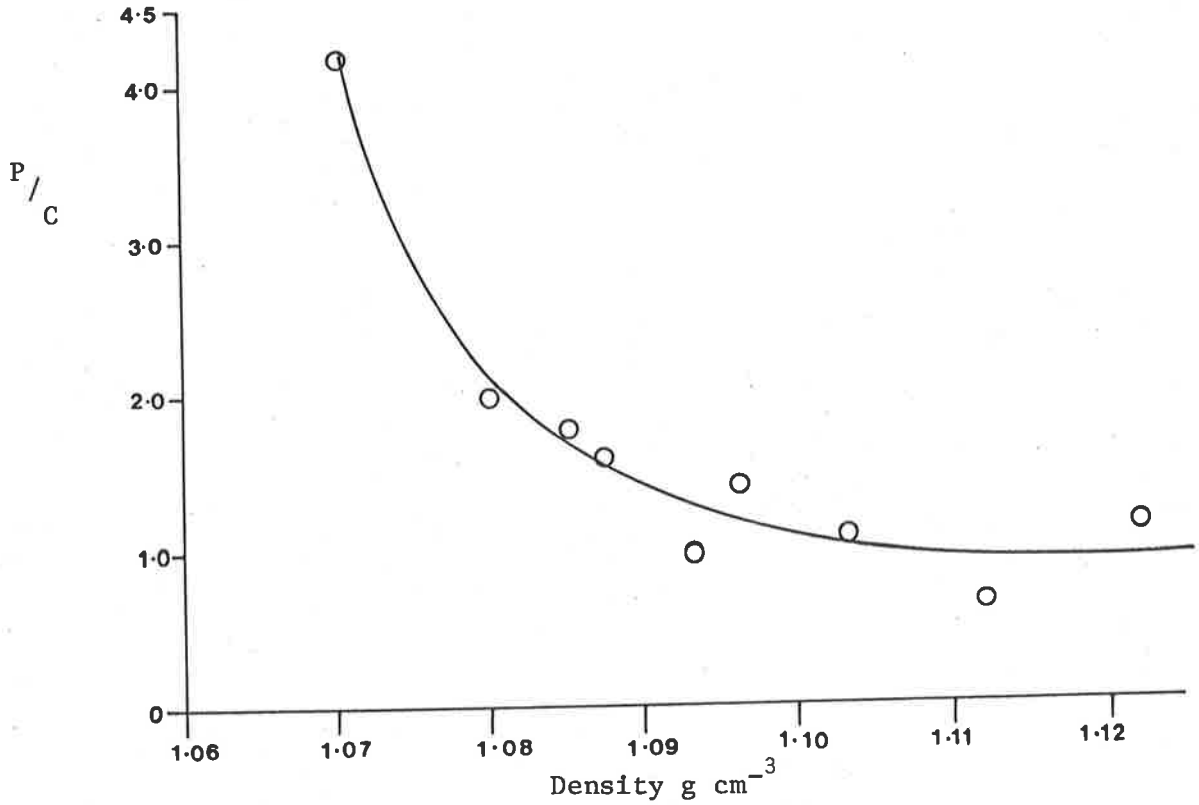

Fig. 7.8: Correlation between the ratio of cell protein to carbohydrate content and cell density.

Fig. 7.9: Density distribution of phytoplankton species from Mt Bold Reservoir

a. *Cyclotella*

b. *Melosira*

c. *Anabaena*

d. *Microcystis*

e. *Ceratium*

f. *Sphaerocystis*

Results are shown as the fraction of a species in each layer.

Symbols refer to samples taken at various times through the summer period 1979-80.

b = buoyant

nb = neutrally buoyant.

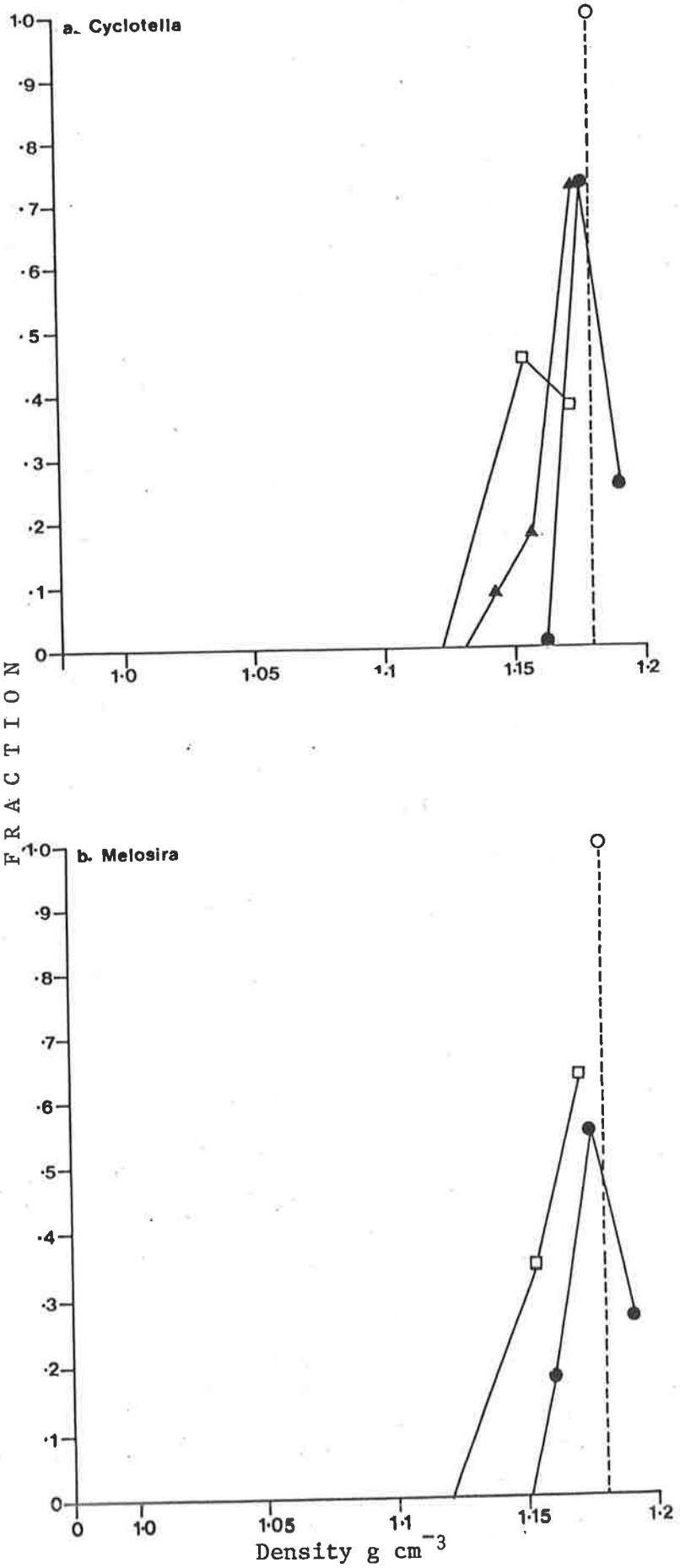
a. Cyclotella
b. Melosira
FRACTION
1·0
·9
·8
·7
·6
·5
·4
·3
·2
·1
0
1·0
1·05
1·1
1·15
1·2
Density g cm⁻³

Fig. 7.9:

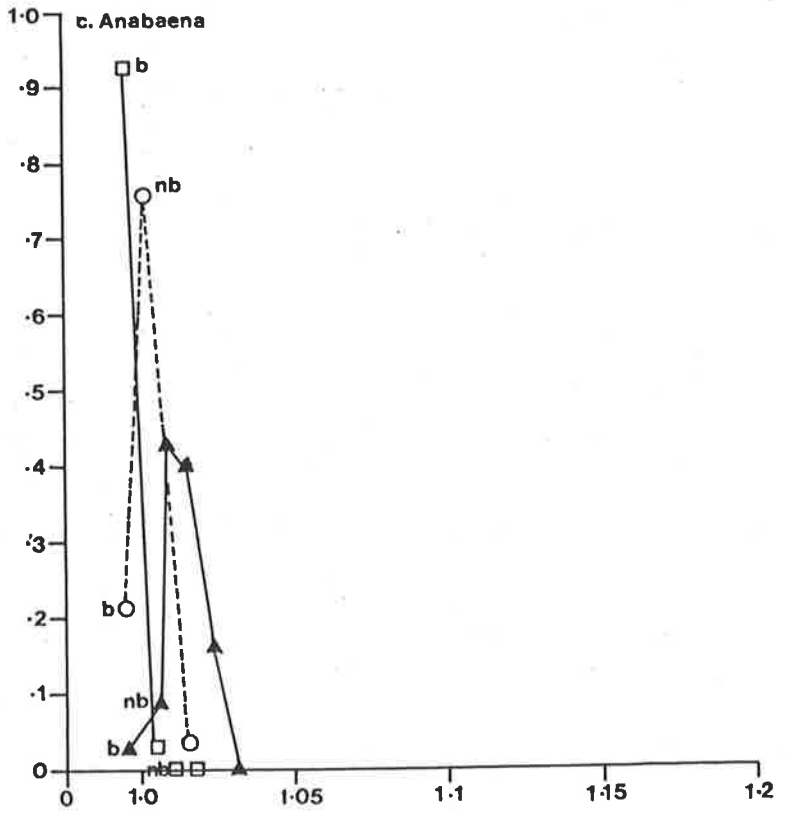
c. Anabaena
1·0
·9
·8
·7
·6
·5
·4
·3
·2
·1
0
b
nb
b
nb
b
nb
0
1·0
1·05
1·1
1·15
1·2

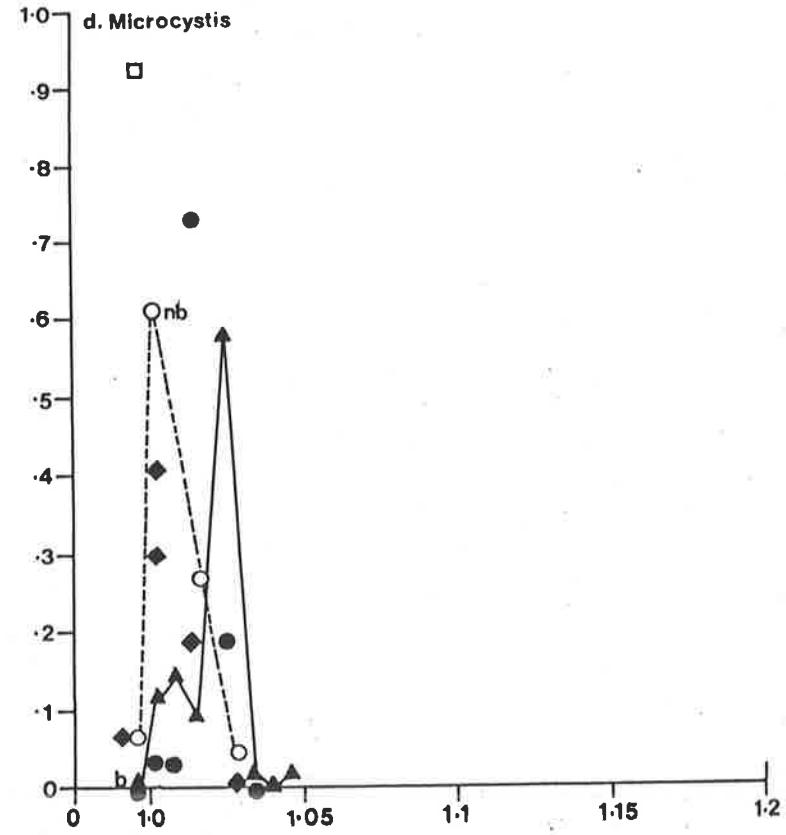
d. Microcystis
1·0
·9
·8
·7
·6
·5
·4
·3
·2
·1
0
nb
b
0
1·0
1·05
1·1
1·15
1·2

Fig. 7.9: (cont.)

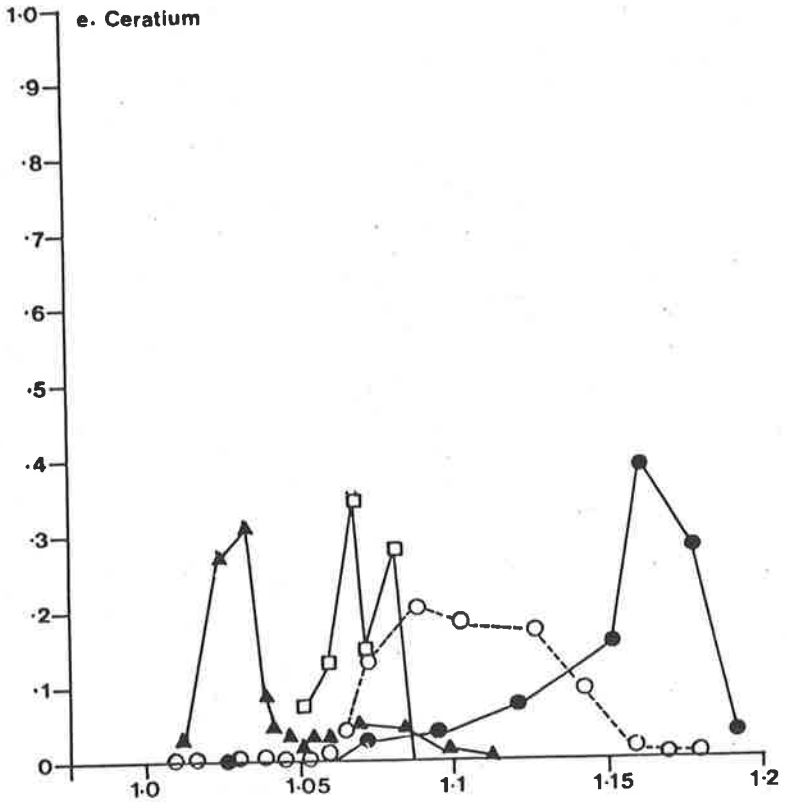
e. Ceratium
1·0
·9
·8
·7
·6
·5
·4
·3
·2
·1
0
1·0
1·05
1·1
1·15
1·2

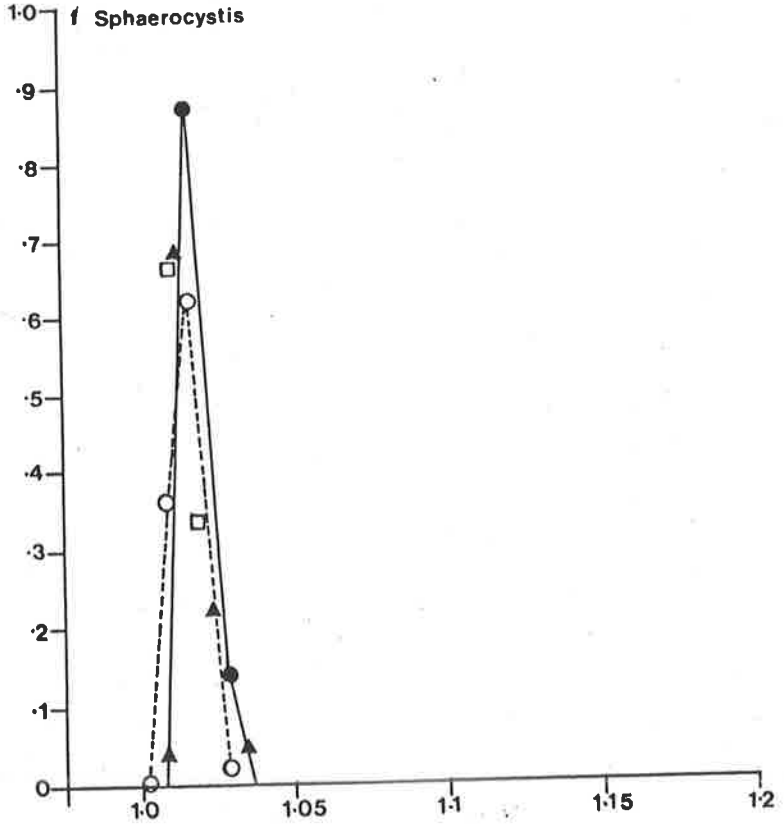
f Sphaerocystis
1·0
·9
·8
·7
·6
·5
·4
·3
·2
·1
0
1·0
1·05
1·1
1·15
1·2

Fig. 7.9: (cont.)

TABLE 7.1

Symbol	Definition	Units
V_s	Terminal sinking velocity of a sphere falling through a fluid.	cm s^{-1}
V	Terminal sinking velocity of a non-spherical body falling through a fluid.	cm s^{-1}
D	Nominal diameter of a non-spherical body, defined as the diameter of a sphere with volume equal to that of the body.	cm
$\emptyset_f$	Coefficient of form resistance, defined as $\emptyset_f = V_s/V$ where V_s represents the terminal sinking velocity of a sphere with diameter equal to the nominal diameter (D) of the particle (McNown & Malaika 1950).	
P'	Density of body	g cm^{-3}
P	Density of water (0.9998 at 20°C).	g cm^{-3}
g	Acceleration due to gravity (980.665).	cm s^{-2}
η	Viscosity of water (0.02002 at 20°C).	poise

Definition of symbols, and values of constants referred to in text.

TABLE 7.2

Experiment Number	Mean Cell Diameter (μm)	FLUOROMETER Sinking Velocity (cm s^{-1})	FLUOROMETER Calculated Density (gm cm^{-3})	INVERTED MICROSCOPE Sinking Velocity (cm s^{-1})	INVERTED MICROSCOPE Calculated Density (gm cm^{-3})	PERCOLL Mean Density (gm cm^{-3})
1	11.25±0.33	3.35×10^{-4}	1.048	-	-	1.072
2	11.25±0.33	3.788×10^{-4}	1.055	-	-	1.074
3	8.94±0.22	1.449×10^{-4}	1.033	-	-	1.070
4	9.36±0.29	1.667×10^{-4}	1.035	3.33×10^{-4}	1.070	1.071
5	12.30±0.32	1.515×10^{-4}	1.018	6.94×10^{-4}	1.084	1.089
6	18.79±0.41	-	-	8.17×10^{-4}	1.042	1.044

A comparison of *Chlorococcum* cell densities calculated from Stokes' Law using a fluorometric and microscopic technique with those determined directly from density gradient centrifugation in Percoll, over a range of cell sizes (± S.E.). Note agreement between data derived from the inverted microscope and Percoll techniques.

TABLE 7.3

Experiment Number	Mean Length of Semi-axes (μm) a	b	c	Nominal Diameter (μm)	FLUOROMETER Sinking Velocity cm s^{-1}	Calculated Density gm cm^{-3}	INVERTED MICROSCOPE Sinking Velocity cm s^{-1}	Calculated Density gm cm^{-3}	PERCOLL MEAN Density gm cm^{-3}	$\emptyset_f$ McNown & Malaika (1950)	$\emptyset_f$ From equation 7.1
7	2.74 ±.07	3.13 ±.01	.274 ±.07	5.73	4.38×10^{-5}	1.024	1.852×10^{-4}	1.104	-		-
8	2.89 ±0.1	3.22 ±.06	2.89 ±0.1	5.99	7.16×10^{-5}	1.037	1.812×10^{-4}	1.093	-		-
9	2.89 ±0.05	3.32 ±0.06	2.89 ±0.05	6.05	-	-	2.058×10^{-4}	1.103	1.101	1.01	0.98
10	2.25 ±0.04	3.20 ±0.05	2.25 ±0.04	5.06	-	-	1.142×10^{-4}	1.082	1.088	1.04	1.07

A comparison of *Chlorella* cell densities calculated from Stokes' Law using two independently measured sinking velocities and nominal cell diameters (D), with direct density measurements in Percoll. Form resistance ($\emptyset_f$) calculated from equation 1 using Percoll densities, and sinking velocities measured using the inverted microscope technique, are compared with the theoretical values of McNown & Malaika (1950). Mean semi-axis lengths are shown ± S.E.

TABLE 7.4

Experiment Number	Mean Cell Dimensions (μm) a	b	Nominal Diameter (μm)	Sinking Velocity (cm s^{-1})	Calculated Density (gm cm^{-3})	Percoll Mean Density (gm cm^{-3})	$\emptyset_f$
11	15.04 ±0.31	13.28 ±0.25	16.52	1.389×10^{-3}	1.093	1.096	1.03

A comparison of *Cyclotella* cell density calculated from Stokes' Law using the measured sinking velocity and nominal cell diameter (D), with direct density measurement in Percoll.

The form resistance factor ($\emptyset_f$) was calculated from equation 7.1.

TABLE 7.5

Experiment Number	Species	Sinking Velocity ($m\ day^{-1}$)	Diameter (μm)	Surface Area (μm^2)	Volume (μm^3)	$\mu m^2 : \mu m^3$
3	Chlorococcum	0.26	8.94	251	374	0.67
4	"	0.29	9.36	275	429	0.64
5	"	0.60	12.30	475	974	0.49
6	"	0.71	18.79	1109	3474	0.32
7	Chlorella	0.16	5.73	103	99	1.05
8	"	0.16	5.99	113	113	1.00
9	"	0.18	6.05	116	116	1.00
10	"	0.10	5.06	82	68	1.21
11	Cyclotella	1.20	16.52	983	2359	0.42

Cell surface area, volume and surface area to volume ratios compared with the microscopically measured sinking rate in metres day^{-1} for laboratory experiments with *Chlorococcum*, *Chlorella* and *Cyclotella*.

Day	Time	Protein mg ℓ^{-1}	Carbohydrate mg ℓ^{-1}	Protein / Carbohy. mg/mg	Dry weight mg ℓ^{-1}	Cell No. x10^3 ml^{-1}	Dry wt / cell pg $cell^{-1}$	Density g cm^{-3}
0	-	0.474	0.339	1.4	2.06	11.17	184	1.096
2	AM	2.904	0.691	4.2	5.33	85.56	62.3	1.070
	PM	5.99	5.65	1.06	16.15	88.72	182	1.103
5	AM	13.32	6.59	2.02	31.33	319	98.2	1.080
	PM	15.40	8.74	1.76	38.27	321	119.2	1.085
8	AM	26.21	14.54	1.8	76.28	1258	60.6	-
	PM	26.43	17.04	1.55	79.78	1304	61.2	1.087
12	PM	26.33	22.62	1.16	84.65	1369	61.8	1.122
15	AM	26.59	27.26	0.975	97.30	1343	72.4	1.093
22	AM	28.00	41.91	0.670	136.95	1388	93.7	1.112

Table 7.6: Fluctuations in cellular composition and Percoll gradient estimates of cell density during growth of *Scenedesmus quadricauda* in batch culture.

TABLE 7.7

Date	Conc^{n} Factor	Ceratium	Cyclotella	Melosira	Sphaerocystis	Trachelomonas
1/11/79	80X	1.0734-1.162-1.18*	1.162-1.177-1.18*	- 1.177 -	- 1.015-1.027	1.027 -
13/11/79	78X	1.01 -1.087-1.17*	1.17* -	- 1.17* -	1.001-1.015-1.028	1.028-1.037
22/11/79	50X	1.014 -1.033-1.114	1.047- 1.16*	- 1.16* -	1.008-1.014-1.033	
16/1/80	1	1.045 -1.067-1.083	1.153-1.173*	- 1.15 -1.17*	- 1.015 -	
20/2/80	1		1.006-1.078-	1.006-1.068-		
29/3/80	1					1.041 -

		Melosira sp	Peridinium	Microcystis	Anabaena
1/11/79	80X	- 1.162 -	- 1.162 -		
13/11/79	78X	1.087-1.141-1.169	1.103-1.169-1.17*	1.001*- 1.015 -1.028	1.001*-1.015
22/11/79	50X	1.100-1.133-1.16*		1.006*- 1.024 -1.047	1.006*-1.011 -1.047
16/1/80	1			Bouyant-1.03	Bouyant-1.05
20/2/80	1			1.005*- 1.014 -1.046	
29/3/80	1			0.999*- 1.000 -1.061	

Range and modal density for phytoplankton collected from Mt. Bold Reservoir. Asterix (*) indicates maximum and minimum densities of the Percoll gradient. Cells collected in the first gradient layer were classed as bouyant.

8. CONCLUSION

It is evident from the data presented in previous chapters, that the complex interplay of physical, chemical and biological factors which determine phytoplankton growth and seasonal succession in Mt Bold Reservoir are intimately related to the degree of turbulence within the water column. This has been demonstrated by studies on temperate lakes in the northern hemisphere (Lund 1965, Round 1971, Kalff & Knoechel 1978). The singular importance of this factor suggests that successional sequences of phytoplankton, occurring in response to conditions resulting from variation in turbulence, might be similar between lakes. The data from Mt Bold Reservoir confirms the general successional pattern described by Lewis (1978a) for tropical Lake Lanao, and Reynolds (1980) for a series of English lakes, and provides a description of the major influences.

The turbidity of the reservoir focussed attention on the importance of assessing phytoplankton irradiance absorption, and a series of mathematical functions were derived for this purpose. Application of these equations demonstrated that curtailment of the mixing depth in spring resulted in a mean absorbed irradiance per unit chlorophyll *a* for the mixed zone, which appeared to saturate integral photosynthesis. Consideration of laboratory experiments on the relationship between growth and irradiance (Paasche 1968, Bannister 1979, Laws & Bannister 1980) provided support for the critical value (ca. 0.08 Einstein absorbed mg chl*a*$^{-1}$ d^{-1}) and suggested that it represented the boundary condition for light limited growth.

In both 1978 and 1979 the critical irradiance value was attained prior to the onset of nutrient limitation. This was demonstrated by bioassay results and, in 1979, compositional indices. As a result, there

occurred a period of time in which growth rate was no longer light limited and nutrients were present in sufficiency. It was during this period that the explosive spring biomass increase occurred.

The sudden spring blooming of phytoplankton is a frequently described feature of seasonal biomass patterns, attributed generally to the improving light conditions, or increasing temperature or both. The necessity for a critical mean irradiance to initiate the biomass increase has previously been recognized in marine habitats (Riley 1967, Hitchcock & Smayda 1977). It is postulated from the data for Mt Bold Reservoir, that the critical value denotes the shift from light limited growth to light sufficiency.

A result of the large background extinction of irradiance in the reservoir, and the small specific extinction coefficient per unit chlorophyll a is that once the critical level has been attained, biomass can increase to high concentrations without substantially affecting the mean irradiance of the mixed zone. Coupled with the continued reduction in mixing depth, and increase in incident irradiance, this provides suitable conditions for the rapid increase in biomass.

The biomass level attained during the spring increase will depend on the optical properties and irradiance regime of the water column, and on nutrient availability. The spring biomass increase of 1979-80 reduced the mean light intensity of the mixed zone to 0.919 MJ $m^{-2}d^{-1}$ (Table 5.1, 4.12.79) following which biomass levels declined. However, algal growth simultaneously reduced the concentration of nutrients in the epilimnion, leading to increased nutrient limitation

as demonstrated by the decline in protein to carbohydrate ratios (Fig. 4.13d). Consequently the factor which had determined the peak biomass concentration could not be ascertained. It was suggested (Chp 5) that as succeeding biomass fluctuations resulted in the mean irradiance of the mixed zone oscillating around the critical value, this was indicative of the controlling influence of irradiance. Further reduction in nutrient concentrations resulted in the nutrient-limited biomass decline of mid-summer (Chp 5).

It is evident from this data that distinct periods of light-limited and nutrient-limited growth occurred, separated by a period of overlap in which both factors were maximal but declined in response to algal growth. This same sequence will very likely apply to most stratifying lakes.

The summer period of low turbulence and low epilimnial nutrient concentrations was dominated by gas-vacuolate blue-green algae. It has been suggested that the buoyancy control afforded by these structures enables vertical movement of the cells, to overcome the vertical separation of nutrients and light (Fogg & Walsby 1971, Reynolds 1973a, Ganf & Oliver in press).

During both 1978-79 and 1979-80 nutrient concentrations declined in the upper layers of the water column (Fig. 4.10a & 4.10b), and as summer progressed the vertical separation between zones of available light and available nutrients increased. For example, in December 1978-79 the euphotic zone (ca. 2 m Chp 3) was separated by a vertical distance of 5 m from water layers which bioassays demonstrated were capable of supporting growth (Fig. 4.10a). It is suggestive that this

period was dominated by *Microcystis* and *Ceratium*, two species capable of vertical migration. However, during the 1979-80 season when protein to carbohydrate ratios were used as indices of nutrient conditions, the *Microcystis* population gave ratios indicative of nutrient limitation. If vertical movement to nutrient rich layers was occurring, the capability of blue-green algae to store excess nutrients (Stewart *et al.*1978) would be expected to result in protein to carbohydrate ratios more typical of growing populations. The results suggested that the *Microcystis* population was not utilizing hypolimnetic nutrient reserves.

Further evidence for the nutrient limited condition of the population during 1979-80 was the rapid increase in the protein to carbohydrate ratio, and biomass, following phosphorus influx to the epilimnion late in January (Chp 4 & 5). This occurrence demonstrated the significance of a slight increase in mixing depth to nutrient supply within the mixed zone.

All evidence therefore points to a period of nutrient limitation throughout the stratified period. The generality of this occurrence will depend on turbulent regimes in specific lakes, and inflow conditions.

Within the sequence of events described net growth may be modified by variation in loss rates such as grazing and sedimentation. It was suggested that in Mt Bold Reservoir initiation of the 1978-79 spring biomass increase was delayed by a change in loss rate (Chp 5). Kalff & Knoechel (1978) have emphasized the importance of loss factors to an understanding of seasonal succession, and noted the lack of quantitative data available in the literature to assess these factors.

Two major loss mechanisms are grazing and sedimentation. The technique devised in this project for measuring cell density should provide

valuable data on the density variations of natural populations, and the mechanisms available to phytoplankton to aid suspension. Density measurements in combination with experimentally determined form factors enable calculation of sinking rates in non-turbulent conditions. The comparison of these expected sinking rates with those observed in the field may provide insight to the influence of water turbulence on algal suspension.

The effects of grazing on phytoplankton seasonal succession in Mt Bold Reservoir are unknown, but presently under investigation. The outcome of these studies, combined with the results presented in this project on phytoplankton dynamics, will provide a valuable example of the biology of an Australian lake.

REFERENCES

ALLISON, E.M. & WALSBY, A.E. (1981). The role of potassium in the control of turgor pressure in a gas-vacuolate blue-green alga. J.exp.Bot., 32,241-249.

ANTIA, N.J., MCALLISTER, C.D., PARSONS, T.R., STEPHENS, K. & STRICKLAND, J.D.H. (1963). Further measurements of primary production using a large volume plastic sphere. Limnol.Oceanogr.,8,166-183.

ARTHUR, C.R. & RIGLER, F.H. (1967) A possible source of error in the ^{14}C method of measuring primary productivity. Limnol.Oceanogr.,12,121-124.

ATLAS, D. & BANNISTER, T.T. (1980). Dependence of mean spectral extinction coefficient of phytoplankton on depth, water colour and species. Limnol.Oceanogr.,25,157-159.

BACHMANN, R.W. & GOLDMAN, C.R. (1965). Hypolimnetic heating in Castle Lake, California. Limnol.Oceanogr.,10,233.

BANNISTER, T.T. (1974). Production equations in terms of chlorophyll concentration, quantum yield, and upper limit to production. Limnol.Oceanogr.,19,1-12.

BANNISTER, T.T. (1979). Quantitative description of steady state, nutrient-saturated algal growth, including adaptation. Limnol.Oceanogr.,24, 76-96.

BARLOW, J.P. (1958). Spring changes in phytoplankton abundance in a deep estuary, Hood Canal, Washington. J.Mar.Res.,17,53-67.

BEARDALL, J. & MORRIS, I. (1976). The concept of light intensity adaptation in marine phytoplankton: some experiments with *Phaeodactylum tricornutum*. Mar.Biol.,37,377-387.

BINDLOSS, M.E. (1974). Primary productivity of phytoplankton in Loch Leven, Kinross. Proc.R.Soc.Edinb.(B) 74,157-181.

BINDLOSS, M.E. (1976). The light-climate of Loch Leven, a shallow Scottish lake, in relation to primary production by phytoplankton. Freshwat. Biol.,6,501-518.

BOWLES, B.A., POWLING, I.J. & BURNS, F.L. (1979). Effects on water quality of artificial aeration and destratification of Tarago Reservoir. A.W.R.C.Tech.Pap.,46. Aust.Govt.Publ.Serv.,Canberra.

BRANSOME, E.D. & GROWER, M.F. (1970). Liquid scintillation counting of (^{3}H) and (^{14}C) on solid supports: a warning. Analyt.Biochem.,38,401-408.

BUCKNEY, R.T. (1979). Chemical loadings in a small river, with observations on the role of suspended matter in the nutrient flux. A.W.R.C.Tech. Pap.40. Aust.Govt.Publ.Serv.,Canberra.

BUSH, E.T. (1963). General applicability of the channels ratio method of measuring liquid scintillation counting efficiencies. Anal.Chem.,35, 1024-1029.

CAMERON, J. & MEYER, J. (1972). Nitrogen-limited growths of marine phytoplankton. I. Changes in population characteristics with steady-state growth rate. Deep-Sea Res.,19,601-618.

CARPENTER, J.H. (1965). The accuracy of the Winkler method for dissolved oxygen analysis. Limnol.Oceanogr.,10,135-140.

CORNETT, R.J. & REGLER, F.H. (1979). Hypolimnetic oxygen deficits: their prediction and interpretation. Science 205,580-85.

CROOME, R.L. & TYLER, P.A. (1975). Phytoplankton biomass and primary productivity of Lake Leake and Tooms Lake, Tasmania. Hydrobiologia 46, 435-443.

DESORTOVA, B. (1981) . Relationship between chlorophyll-a concentration and phytoplankton biomass in several reservoirs in Czeckoslovakia. Int. Rev.ges.Hydrobiol.,66(2),153-169.

DILLON, P.J. & RIGLER, F.H. (1974). The phosphorus-chlorophyll relationship in lakes. Limnol.Oceanogr.,19,767-773.

DILLON, T.M., POWELL, T.M. & MYRUP, L.O. (1975). Low frequency turbulence and vertical temperature microstructure in Lake Tahoe, California-Nevada. Verh.Internat.Verein.Limnol.,19,110-115.

DOTY, M.S. & OGURI, M. (1957). Evidence for photosynthetic-daily periodicity. Limnol.Oceanogr.2,37-40.

DROOP, M.R. (1970). Vitamin B_{12} and marine ecology. V. Continuous culture as an approach to nutritional kinetics. Helgol.Meeres.,20,629-36.

DROOP, M.R., (1974). The nutrient status of algal cells in continuous culture. J.Mar.Biol.Assoc.U.K.,54,825-855.

DUBINSKY, Z. & BERMAN, T. (1976). Light utilization efficiencies of phytoplankton in Lake Kinneret (Sea of Galilee). Limnol.Oceanogr., 2],226-230.

DUBINSKY, Z. & BERMAN, T. (1979). Seasonal changes in the spectral composition of downwelling irradiance in Lake Kinneret (Israel). Limnol.Oceanogr. 24,652-663.

DUNTLEY, S.Q. (1963). Light in the Sea. J.Opt.Soc.Am.,53,214-233.

EPPLEY, R.W., HOLMES, R.W. & STRICKLAND, J.D.H. (1967). Sinking rates of marine phytoplankton maeasured with a fluorometer. J.exp.Mar.Biol. Ecol.,1,191-208.

EPPLEY, R.W. & RENGER, E.H. (1974). Nitrogen assimilation of an oceanic diatom in nitrogen limited continuous culture. J.Phycol.,10, 15-23.

EPPLEY, R.W. & SHARPE, J.H. (1976). Photosynthetic measurements in the central North Pacific: the dark loss of carbon in 24-h incubations. Limnol.Oceanogr.,20,981-987.

FALKOWSKI, P.G. & OWENS, T.G. (1980). Light-shade adaptation. Two strategies in marine phytoplankton. Plant Physiol.,66,592-595.

FEE, E.J. (1969). A numerical model for the estimation of photsynthetic production integrated over time and depth in natural waters. Limnol.Oceanogr.,14,906-911.

FEE, E.J. (1973a). A numerical model for determining integral primary production and its application to Lake Michigan. J.Fish.Rs.Bd. Canada 30,1447-1468.

FEE, E.J. (1973b). Modelling primary production in water bodies: a numerical approach that allows vertical inhomogeneities. J.Fish.Res.Bd.Canada 30,1469-1473.

FOGG, G.E. & WALSBY, A.E. (1971). Bouyancy regulation and the growth of planktonic blue-green algae. Mitt.Internat.Verein.Limnol.,19,182-188.

FORSBERG, C., RYDING, S-O, CLAESSON, A. & FORSBERG, A. (1978). Water chemical analyses and/or algal assay ? Sewage effluent and polluted lake water studies. Mitt.Internat.Verein.Limnol.,21,352-363.

GANF, G.G. (1972). The regulation of net primary production in Lake George, Uganda, East Africa. pp.693-709 IN Kajok, Z.& Hilbricht-Ilkowska, A. (eds.) Productivity problems of freshwaters. PWN Polish Scientific Publishers, Warsaw.

GANF, G.G. (1974). Incident solar irradiance and underwater light penetration as factors controlling the chlorophyll a content of a shallow equatorial lake (Lake George, Uganda). J.Ecol.,62,593-609.

GANF, G.G. (1975). Photosynthetic production and irradiance - photosynthesis relationships of the phytoplankton from a shallow equatorial lake (Lake George, Uganda). Oecologia 18, 165-183.

GANF, G.G. (1976). Primary production. pp.25-35 IN Proc.A.W.R.C.Symp. on eutrophication. Aust.Govt.Publ.Serv.,Canberra.

GANF, G.G. (1980). Factors controlling the growth of phytoplankton in Mount Bold Reservoir, South Australia. A.W.R.C.Tech.Pap.48. Aust.Govt. Publ.Serv.,Canberra.

GANF, G.G. & HORNE, A.J. (1975). Diurnal stratification, photosynthesis and nitrogen fixation in a shallow equatorial lake (Lake George, Uganda). Freshwat.Biol.,5,13-39.

GANF, G.G. & OLIVER, R. (in press). The vertical separation of light and available nutrients as a factor causing the shift from green to blue-green algae.

GIBSON, C.E. (1978). Field and laboratory observations on the temporal and spatial variation of carbohydrate content in planktonic blue-green algae in Lough Neagh, Northern Ireland. J.Ecol.,66,97-115.

GIESKES, W.W. & KRAAY, G.W. (1975). The phytoplankton spring bloom in Dutch coastal waters of the North Sea. Neth.J.Sea Res.,9,166-196.

GLOOSCHENKO, W.A., MOORE,J.E. MUNAWAR, M. & VOLLENWEIDER, R.A. (1974). Primary producton in Lakes Ontario and Erie: a comparative study. J.Fish.Res.Bd.Canada 31,253-263.

GOLDMAN, C.R. (1960). Primary productivity and limiting factors in three lakes of the Alaskan Peninsula. Ecol.Monogr.,30,207-230.

GOLDMAN, C.R. (1972). The role of minor nutrients in limiting the productivity of aquatic ecosystems. p.21-33 IN Likens, G.E.(ed) Nutrients and eutrophication. Am.Soc.Limnol.Oceanogr.Spec.Symp.1.

GOLDMAN, C.R. (1978). The use of natural phytoplankton populations in bioassay. Mitt.Internat.Verein.Limnol.,21,364-371.

GOLTERMAN, H.L. (1971). Methods for chemical analysis of fresh waters. IBP Handbook 8, 172 pp. Blackwell, Oxford.

GOLTERMAN, H.L. (1975) Physiological limnology. Developments in water science II. 489 pp. Elsevier Sci.Publ.Comp. Amsterdam.

GONS, H.J. & MUR, L.R. (1975). An energy balance for algal populations in light limiting conditions. Verh.Internat.Verein.Limnol.,19,2729-2733.

GONS, H.J. & MUR, L.R. (1978). On the kinetics of light limited growth of *Scenedesmus protuberans* Fritsch and ecological implications. Mitt. Internat.Verein.Limnol.,21,125-135.

GORHAM, P.R., MCLACHLAN, J., HAMMER, U.T. & KIM, W.K. (1964). Isolation and culture of toxic strains of *Anabaena flos-aquae* (Lyngb) de Breb. Verh.Internat.Verein.Limnol.,15,796-804.

GRAN, H.H. & BRAARUD, T. (1935) A quantitative study of the phytoplankton in the Bay of Fundy and the Gulf of Maine. J.Biol.Bd.Canada 1,279-467.

GROSS, F. & ZEUTHEN, E. (1948). The bouyancy of plankton diatoms: a problem of cell physiology. Proc.R.Soc.Lond.B 135,382-389.

HALL, K.J. & LEE, G.F. (1974). Molecular size and spectral characterization of organic matter in a meromictic lake. Water.Res.,8,239-251.

HALMANN, H. (1972). Chemical ecology. Evidence for phosphate as the only factor limiting algal growth in Lake Kinneret. Israel J.Chem.,10, 841-855.

HAMILTON, D.H. (1969). Nutrient limitation of summer phytoplankton growth in Cayuga Lake. Limnol.Oceanogr.,14,579-590.

HAPPEY, C.M. (1970a). Some physico-chemical investigations of stratification in Abbot's Pool, Somerset: the temperature cycle. J.Ecol.,58,419-434.

HAPPEY, C.M. (1970b). Some physico-chemical investigations of stratification in Abbot's Pool, Somerset: studies on the dissolved oxygen content. J. Ecol.,58,435-444.

HARDING, L.W., MEESON, B.W., PREZELIN, B.B., SWEENEY, B.M. (1981). Diel periodicity of photosynthesis in marine phytoplankton. Mar.Biol., 61(2/3),95.

HARRIS, G.P. (1978). Photosynthesis, productivity and growth: the physiological ecology of phytoplankton. Ergeb.Limnol.,10,1-171.

HARRIS, G.P. (1980). Temporal and spatial scales in phytoplankton ecology. Mechanisms, methods, models and management. Can.J.Fish.Aquat.Sci., 37,877-900.

HARRIS, G.P. & PICCININ, B.B. (1977). Photosynthesis by natural phytoplankton populations. Archiv.Hydrobiol.,80,405-457.

HARRIS, G.P., HAFFNER, G.D. & PICCININ, B.B. (1980). Physical variability and phytoplankton communities.II. Primary productivity by phytoplankton in a physically variable environment. Arch.Hydrobiol.,88, 393-425.

HARRIS, G.P. & PICCININ, B.B. (1980). Physical variability and phytoplankton communities. IV. Temporal changes in the phytoplankton community of a physically variable lake. Arch.Hydrobiol.,89,447-473.

HAUG, A., MYKLESTAD, S. & SAHSHAUG, E. (1973). Studies on the phytoplankton ecology of the Trondheimsfjord. I. The chemical composition of phytoplankton populations. J.exp.mar.Biol.Ecol.,11,15-26.

HEALEY, F.P. (1975). Physiological indicators of nutrient deficiency in algae. Can.Dept.Envt.Tech.Rept.585.

HEALEY, F.P. (1978). Physiological indicators of nutrient deficiency in algae. Mitt.Internat.Verein.Limnol.,21,34-41.

HENDERSON, S.T. & HODKISS, D. (1963). The spectral energy distribution of daylight. Brit.J.Appl.Phys.,14,125-131.

HEBERT, D., PHIPPS, P.J. & STRANGE, R.W. (1971). Chemical analysis of microbial cells. pp.209-344 IN Norris, J.R. & Ribbons, D.W. (Eds.) Methods in microbiology. Academic Press, London.

HESSLEIN, R. & QUAY, P. (1973). Vertical eddy diffusion studies in the thermocline of a small stratified lake. J.Fish.Res.Bd.Canada 30, 1491-1500.

HICKMAN, M. (1974). Thermal stratification and heating mechanisms in a small lake. Arch.Hydrobiol.,74,60-67.

HICKMAN, M. (1979). Phytoplankton production in a small eutrophic lake in central Alberta, Canada. Int.Rev.ges.Hydrobiol.,64,643-659.

HITCHCOCK, G.L. & SMAYDA, T.J. (1977). The importance of light in the irradiation of the 1972-1973 winter-spring diatom bloom in Narragansett Bay. Limnol.Oceanogr.,22(1),126-131.

HUTCHINSON, G.E. (1941). The mechanisms of intermediary metabolism in stratified lakes. Ecol.Monogr.,11,21-60.

HUTCHINSON, G.E. (1957). A treatise on limnology. Vol. I. Geography, physics and chemistry. Wiley, N.Y.

HUTCHINSON, G.E. (1967). A treatise on limnology. Vol.II. Introduction to lake biology and the limnoplankton. Wiley, N.Y.

HUTCHINSON, G.E. & LOFFLER, H. (1956). The thermal classification of lakes. Proc.nat.Acad.Sci.,42,84-86.

IDSO, S.B. & FOSTER, J.M. (1975). An analytical study of three characteristic forms of light-forced primary production in aquatic ecosystems. Oecologia (Berl.) 18, 145-154.

ILMAVIRTA, V. (1974). Diel periodicity in the phytoplankton community of the oligotrophic lake Pääjärvi, southern Finland. I. Phytoplanktonic primary production and related factors. Ann.Bot.Fenn.,11,136-177.

JASSBY, A.D. & GOLDMAN, C.R. (1974). A quantitative measure of succession rate and its application to the phytoplankton of lakes. Am.Nat.,108, 688-693.

JASSBY, A. & POWELL, T. (1975). Vertical patterns of eddy diffusion during stratification in Castle Lake, California. Limnol.Oceanogr.,20,530-543.

JASSBY, A.D. & PLATT, T. (1976). Mathematical formulation of the relationship between photosynthesis and light for phytoplankton. Limnol. Oceanogr.,21,540-547.

JERLOV, N.G. (1968). Optical oceanography. Elsevier, Amsterdam.

JEWSON, D.H. (1975). The relation of incident radiation to diurnal rates of photosynthesis in Lough Neagh. Int.Rev.ges.Hydrobiol.,60,759-767.

JEWSON, D.H. (1976). The interaction of components controlling net phytoplankton photosynthesis in a well-mixed lake (Lough Neagh, Northern Ireland. Freshwat.Biol.,6,551-576.

JEWSON, D.H. (1977). Light penetration in relation to phytoplankton content of the euphotic zone of Lough Neagh, Northern Ireland. Oikos 28,74-83.

JEWSON, D.H. & TAYLOR, J.A. (1978). The influence of turbidity on net phytoplankton photosynthesis in some Irish lakes. Freshwat.Biol.,8,573-584.

JONES, R.I. (1977a). Factors controlling phytoplankton production and succession in a highly eutrophic lake (Kinnego Bay, Lough Neagh). I. The phytoplankton community and its environment. J.Ecol.,65,547-559.

JONES, R.I. (1977b). Factors controlling phytoplankton production and succession in a highly eutrophic lake (Kinnego Bay, Lough Neagh). II. Phytoplankton production and its chief determinants. J.Ecol.,65, 561-577.

JONES, R.I. (1977c). Factors controlling phytoplankton production and succession in a highly eutrophic lake (kinnego Bay, Lough Neagh). III. Interspecific competition in relation to irradiance and temperature. J.Ecol.,65,579-586.

JONES, R.I. (1978). Adaptations to fluctuating irradiance by natural phytoplankton communities. Limnol.Oceanogr.,23,920-926.

JORGENSEN, E.G. & STEEMANN-NIELSEN, E. (1966). Adaptation in plankton algae. pp.37-46 IN C.R. Goldman (ed.) Primary productivity in aquatic environments. Mem.Ist.Ital.Idrobiol.,18 Suppl., Uni.Calif.Press, Berkeley.

JUDD, D.B., MACADAM, D.L. & WYSZECKI, G. (1964). Spectral distribution of typical daylight as a function of correlated colour temperature. J.Opt.Soc.Am.,54,1031-1040.

KALFF, J. & KNOECHEL, R. (1978). Phytoplankton and their dynamics in oligotrophic and eutrophic lakes. Ann.Rev.Ecol.Syst.,9,475-95.

KILHAM, P. (1971). A hypothesis concerning silica and the freshwater planktonic diatoms. Limnol.Oceanogr.,16,10-18.

KILHAM, S.S. (1978). Nutrient kinetics of freshwater planktonic algae using batch and semicontinuous methods. Mitt.Internat.Verein.Limnol.,21, 147-157.

KIRK, J.T.O. (1975a). A theoretical analysis of the contribution of algal cells to the attenuation of light within natural waters. I. General treatment of suspensions of pigmented cells. New Phytologist 75,11-20.

KIRK, J.T.O. (1975b) A theoretical analysis of the contribution of algal cells to the attenuation of light within natural waters. II. Spherical cells. New Phytologist 75,21-36.

KIRK, J.T.O. (1976a). A theoretical analysis of the contribution of algal cells to the attenuation of light within natural waters. III. Cylindrical and spheroidal cells. New Phytologist 77, 341-358.

KIRK, J.T.O. (1976b). Yellow substance (gelbstoff) and its contribution to the attenuation of photosynthetically active radiation in some inland and coastal south-eastern Australian waters. Aust.J.Mar. Freshwater Res.,27,61-71.

KIRK, J.T.O. (1977). Use of a quanta meter to measure attenuation and underwater reflectance of photsynthetically active radiation in some inland and coastal south-eastern Australian waters. Aust.J.Mar. Freshwater Res.,28,9-21.

KIRK, J.T.O. (1979). Spectral distribution of photosynthetically active radiation in some south-eastern Australian waters. Aust.J.Mar. Freshwater Res.,30,81-91.

KIRK, J.T.O. (1980). Relationship between nephelometric turbidity and scattering coefficients in certain Australian waters. Aust.J.Mar. Freshwater Res.,31,1-12.

KNOECHEL, R. & KALFF, J. (1975). Algal sedimentation: the cause of a diatom-blue-green succession. Verh.Internat.Verein.Limnol.,19,745-754.

KONDRATYEV, K.Ya. (1969). Radiation in the atmosphere. Internat.Geophys. Ser.,12. Acad.Press.

LAWS, E.A. & BANNISTER, T.T. (1980). Nutrient- and light-limited growth of *Thalassiosira fluviatilis* in continuous culture, with implications for phytoplankton growth in the ocean. Limnol.Oceanogr.,25,457-473.

LERMAN, A. & STILLER, M. (1969). Vertical eddy diffusion in Lake Tiberias. Verh.Internat.Verein.Limnol.,17,323-333.

LEWIS, W.M. Jr. (1974). Primary production in the plankton community of a tropical lake. Ecol.Monogr.,44,377-409.

LEWIS, W.M. Jr. (1978a). Dynamics and succession of the phytoplankton in a tropical lake: Lake Lanao, Philippines. J.Ecol.,66,849-880.

LEWIS, W.M.Jr. (1978b). Analysis of succession in a tropicl phytoplankton community and a new measure of succession rate. Am.Nat.,112,401-414.

LUND, J.W.G. (1950). Studies on *Asterionella formosa* Hass. II. Nutrient depletion and the spring maximum. J.Ecol.,38,1-35.

LUND, J.W.G. (1959). Bouyancy in relation to the ecology of the freshwater phytoplankton. Brit.Phycol.Bull.,1,1-17.

LUND, J.W.G. (1965). The ecology of the freshwater phytoplankton. Biol.Rev., 40,231-293.

LUND, J.W.G., KIPLING, C. & LE CREN, E.D. (1958). The inverted microscope method of estimating algal numbers and the statistical basis of estimations by counting. Hydrobiologia 11, 143-170.

LUND, J.W.G., JAWORSKI, G.H.M. & BUTTERWICK, C. (1975). Algal bioassay of waters from Belham Tarn, English Lake District, and the growth of planktonic diatoms. Arch.Hydrobiol. Suppl.49, Algological studies 14,49-69.

MCNOWN, J.S. & MALAIKA, J. (1950). Effects of particle shape on settling velocity at low Reynolds numbers. Trans.Am.Geophys.Union 31(1), 74-82.

MACCAULL, W.A. & PLATT, T. (1977). Diel variations in the photosynthetic parameters of coastal marine phytoplankton. Limnol.Oceanogr.,22(4), 723-731.

MALONE, T.C. (1971). Diurnal rhythms in netplankton and nannoplankton assimilation ratios. Mar.Biol.,10,285-289.

MATEYKO, G.M. & KOPAC, M.J. (1963). Cytophysical studies on living normal and neoplastic cells. II. Isopycnotic cushioning during high speed centrifugation. Ann.N.Y.Acad.Sci.,105(4),219-253.

MEGARD, R.O. (1972). Phytoplankton, photosynthesis and phosphorus in Lake Minnetonka, Minnesota. Limnol.Oceanogr.,17,68-87.

MEGARD, R.O., COMBS, W.S.Jr.,SMITH, P.D. & KNOLL, A.S. (1979). Attenuation in light and daily integral rates of photosynthesis attained by planktonic algae. Limnol.Oceanogr.,24,1038-1050.

MILLER, G.L. & GASEK, J.McG. (1960). Drift of drops in density gradient columns. Anal.Biochem.,1,78-87.

MOREL, A. (1978). Available, usable and stored radiant energy in relation to marine photsynthesis. Deep Sea Res.,25,673-688.

MOREL, A. & SMITH, R.C. (1974). Relation between total quanta and total energy for aquatic photsynthesis. Limnol.Oceanogr.,19(4-6),591-600.

MORGENTHALER, J.J. & PRICE, C.A. (1976). Density gradient sedimentation in silica sols. Anomalous shifts in the banding densities of polystyrene 'Latex' beads. Biochem.J.,153,487-490.

MORTIMER, C.H. (1941) The exchange of dissolved substances between mud and water in lakes. J.Ecol.,29,280-329.

MORTIMER, C.H. (1942) The exchange of dissolved substances between mud and water in lakes. J. Ecol.,30,147-201.

MYKLESTAD, S. (1977). Production of carbohydrates by marine phytoplanktonic diatoms. II. Influence of the N/P ratio in the growth medium on the assimilation ratio, growth rate, and production of extracellular carbohydrates by *Chaetoceros affinis* var. Willei (Gran) Hustedt and *Skeletonema costatum* (Grev.)Cleve. J.exp.mar.Biol.Ecol.,29,161-179.

NEWHOUSE, J. DOTY, M.S. & TSUDA, R.T. (1967). Some diurnal features of a neritic surface plankton population. Limnol.Oceanogr.,12,207-212.

NICHOLLS, K.H. & DILLON, P.J. (1978). An evaluation of phosphorus-chlorophyll phytoplankton relationships in lakes. Int.Rev.ges.Hydrobiol.,63,141-154.

NORTHCOTE, K.H. (1976). Soils. pp.61-73 IN Twidale, C.R., Tyler, M.J. & Webb, B.P. Natural history of the Adelaide region. R.Soc.S.A.Inc.

O'BRIEN, J. & deNOYELLES, F. (1976). Response of three phytoplankton bioassay techniques in experimental ponds of known limiting nutrient. Hydrobiologia 49,65-76.

OLIVER, R.L. & GANF, G.G. (unpublished) A comparison of absorbed and incident irradiance as determinants of phytoplankton photosynthesis and its depth integral. Submitted J. Ecol.

PAASCHE, E. (1968). Marine plankton algae grown with light-dark cycles. II. *Ditylum brightwelli* and *Nitszchia turgidula*. Physiol.Plant.,21,66-77.

PAASCHE, E. & ØSTERGREN, I. (1980). The annual cycle of plankton diatom growth and silica production in the inner Oslofjord. Limnol.Oceanogr., 25,481-494.

PEARSALL, W.H. (1932). Phytoplankton in the English Lakes. II. The composition of phytoplankton in relation to dissolved substances. J.Ecol.,30, 241-262.

PECHLANER, R. (1970). The phytoplankton spring outburst and its conditions in Lake Erken (Sweden). Limnol.Oceanogr.,15,113-130.

PERTOFT, H., LAURENT, T.C., LAAS, T. & KAGEDAL, L. (1978). Density gradients prepared from colloidal silica particles coated by polyvinyl-pyrrolidone (Percoll). Anal.Biochem.,88,271-282.

PLATT, T. & JASSBY, A.D. (1976). The relationship between photosynthesis and light for natural assemblages of coastal marine phytoplankton. J. Phycol.,12,421-430.

PLATT, T., GALLEGOS, C.L. & HARRISON, W.G. (1980). Photoinhibition of photosynthesis in natural assemblages of marine phytoplankton. J.Mar.Res., 38,687-701.

POWELL, T. & JASSBY, A. (1974). The estimation of vertical eddy diffusivities below the thermocline in lakes. Water Resources Research 10, 191-198.

PRICE, C.A., MENDIOLA-MORGENTHALER, L.R., GOLDSTEIN, M., BREDEN, E.N. & GUILLARD, R.R.L. (1974). Harvest of planktonic marine algae by centrifugation into gradients of silica in the CF-6 continuous-flow zonal rotor. Biol.Bull.,147,136-145

PRICE, C.A., REARDON, E.M. & GUILLARD, R.R.L. (1978). Collection of dinoflagellates and other marine microalgae by centrifugation in density gradients of a modified silica sol. Limnol.Oceanogr.,23,548-553.

PUGH, R.R. (1970). Liquid scintillation counting of ^{14}C diatom material on filter papers for use in productivity studies. Limnol.Oceanogr.,15, 652-655.

RABINOWITCH, E. & GODVINDJEE, . (1969). Photosynthesis. Wiley, N.Y.

REDFIELD, A.C. (1958). The biological control of chemical factors in the environment. Amer.Sci.,46, 205-221.

REYNOLDS, C.S. (1972). Growth gas vacuolation and bouyancy in a natural population of a planktonic blue-green alga. Freshwat.Biol.,2,87-106.

REYNOLDS, C.S. (1973a). Growth and bouyancy of *Microcystis aeruginosa* Kütz. emend. Elenkin in a shallow eutrophic lake. Proc.R.Soc.Lond.B 184, 29-50.

REYNOLDS, C.S. (1973b). The seasonal periodicity of planktonic diatoms in a shallow eutrophic lake. Freshwat.Biol.,3,89-110.

REYNOLDS, C.S. (1979). Seston sedimentation : experiments with *Lycopodium* spores in a closed system. Freshwat.Biol.,9,55-76.

REYNOLDS, C.S. (1980). Phytoplankton assemblages and their periodicity in stratifying lake systems. Holarct.Ecol.,3,141-159.

REYNOLDS, C.S. & WALSBY, A.E. (1975). Water blooms. Biol.Rev.,50,437-481.

REYNOLDS, C.S. & BUTTERWICK, C. (1979). Algal bioassay of unfertilized and artificially fertilized lake water, maintained in Lund Tubes. Arch. Hydrobiol.Suppl.56 Algological studies 23,166-183.

RILEY, G.A. (1942). The relationship of vertical turbulence and spring diatom flowerings. J.Mar.Res.,5,67-87.

RILEY, G.A. (1957). Phytoplankton of the north central Sargasso Sea. Limnol. Oceanogr.,2,252-270.

RILEY, G.A. (1967). The plankton of estuaries. pp.316-326 IN Lauff, G.H. (ed.) Estuaries. Publ.Am.Assoc.Adv.Sci.,83.

RINNE, I. & TARKIAINEN, E. (1978). Algal tests used to study the chemical factors regulating the growth of planktonic algae in the Helsinki sea area. Mitt.Internat.Verein.Limnol.,21,527-546.

RODHE, W. (1965). Standard correlations between pelagic photosynthesis and light. pp.365-381 IN Goldman, C.R. (ed.) Primary productivity in aquatic environments. Mem.Ist.Ital.Idrobiol.,18 Suppl.

ROUND, F.E. (1971). The growth and succession of algal populations in freshwaters. Mitt.Internat.Verein.Limnol.,19,70-99.

RYTHER, J. & DUNSTAN, W.M. (1971). Nitrogen, phosphorus and eutrophication in coastal marine environment. Science 171,1008-11.

ST ONGE, J.M. & PRICE, C.A. (1975). Automatic sorting of ichthyoplankton: factors controlling plankton density in gradients of silica. Mar. Biol.,29,187-194.

SAKAMOTO, M. (1966). Primary production by phytoplankton community in some Japanese lakes and its dependence on lake depth. Arch.Hydrobiol.,62, 1-28.

SAKSHAUG, E. & MYKLESTAD, S. (1973). Studies on the phytoplankton ecology of the Trondheimsfjord. III. Dynamics of phytoplankton blooms in relation to environmental factors, bioassay experiments and parameters for the physiological state of the populations. J.exp.mar.Biol.Ecol., 11,157-188.

SCHELSKE, C.L., ROTHMAN, E.D. & SIMMONS, M.S. (1978). Comparison of bioassay procedures for growth-limiting nutrients in the Laurentian Great Lakes. Mitt.Internat.Verein.Limnol.,21,65-80.

SCHINDLER, D.W. (1971). Carbon, nitrogen, and phosphorus and the eutrophication of freshwater lakes. J.Phycol.,7,321-329.

SCHINDLER, D.W. & FEE, E.J. (1975). The rates of nutrient cycling and radiant energy in aquatic communities. pp.323-343 IN Cooper, J.P. (ed.) Photosynthesis and productivity in different environments. Cambridge Uni.Press.

SCHWERDTFEGER, P. (1972). The role of meteorology in urban planning- a case study. IN The city as a life system ? Proc.Ecol.Soc.Aust.,7,143-160.

SCHWERDTFEGER, P. (1976). Climate. pp.75-86 IN Twidale, C.R., Tyler, M.J. & Webb, B.P. (eds.) Natural history of the Adelaide region. R.Soc.S.A. Inc.

SCOTT, B.D. (1978). Phytoplankton distribution and light attenuation in Port Hacking estuary. Aust.J.Mar.Freshwater Res.,29,31-44.

SENFT, W.H. (1978). Dependence of light-saturated rates of algal photosynthesis on intracellular concentrations of phosphorus. Limnol. Oceanogr.,23(4),709-718.

SMAYDA, T.J. (1970). The suspension and sinking of phytoplankton in the sea. Oceanogr.Mar.Biol.Ann.Rev.,8,353-414.

SMAYDA, T.J. (1974). Bioassay of the growth potential of the surface water of lower Narragansett Bay over an annual cycle using the diatom *Thalassiosira pseudonana* (oceanic clone, 13-1). Limnol.Oceanogr., 19,889-901.

SMAYDAM T.J. (1980). Phytoplankton species succession. pp.493-570 IN Morris, I. (ed.) The physiological ecology of phytoplankton. Studies in ecology Vol. 7.

SMAYDA, T.J. & BOLEYN, B.J. (1965). Experimental observations on the flotation of marine diatoms. I. *Thalassiosira* cf.*nana*, *Thalassiosira rotula* and *Nitszchia seriata*. Limnol.Oceanogr.,10(4),499-509.

SMAYDA, T.J. & BOLEYN, B.J. (1966b). Experimental observations on the flotation of marine diatoms. III. *Bacteriastrum hyalinum* and *Chaetoceros lauderi*. Limnol.Oceanogr.,11,35-43.

SMAYDA, T.J. & BOLEYN, B.J. (1966a). Experimental observations on the flotation of marine diatoms. II. *Skeletonema costatum* and *Rhizosolenia setigera*. Limnol.Oceanogr.,11,18-34.

SMITH, E.L. (1936). Photosynthesis in relation to light and carbon dioxide. Proc.Nat.Ac.Sci.22,504-511.

SMITH, I.R. (1975). Turbulence in lakes and rivers. Freshwat.Biol.Assoc. Sci.Publ.,29.

SMITH, R.A. (1980). The theoretical basis for estimating phytoplankton production and specific growth rate from chlorophyll, light and temperature data. Ecological Modelling 10, 243-264.

SMITH, R.C. (1968). The optical characterization of natural waters by means of an "extinction coefficient". Limnol.Oceanogr.,13,423-429.

SMITH, R.C. & TYLER, J.E. (1967). Optical properties of clear natural water. J.Opt.Soc.Am.,57,589-595.

SMITH, R.C., TYLER, J.E. & GOLDMAN, C.R. (1973). Optical properties and colour of Lake Tahoe and Crater Lake. Limnol.Oceanogr.,18,189-199.

SMITH, V.H. (1979). Nutrient dependence of primary productivity in lakes. Limnol.Oceanogr.,24,1051-1064.

SMITH, V.H. (unpublished) A variable yield chlorophyll-phosphorus model for lakes. MS for submission to Environ.Sci.Technol.

SOEDER, C.J., MULLER, H., PAYER, H.D., & SCHULLE, H. (1971). Mineral nutrition of planktonic algae: some considerations, some experiments. Mitt. Internat.Verein.Limnol., 19,39-58.

SPECHT, R.L. (1972). The vegetation of South Australia. 2nd Ed. Govt. Printer, Adelaide.

SPENCE, D.H.N., CAMPBELL, R.M. & CHRYSTAL, J. (1971). Spectral intensity in some Scottish freshwater lochs. Freshwater Biol.,1,321-337.

STADELMANN, P.,MOORE, J.E. & PICKETT, E. (1974). Primary production in relation to temperature structure, biomass concentration and light conditions at an inshore and offshore station in Lake Ontario. J. Fish.Res.Bd.Canada.,31,1215-1232.

STEEL, J.A. (1973). Reservoir algal productivity. IN The use of mathematical models in water pollution control. Symposium, Univ. of Newcastle upon Tyne, Sept. 10-14, 1973.

STEEL, J.A. (1980). Phytoplankton models. IN Le Cren, e.d. & Mc.Connell, R.H. (eds.) The functioning of freshwater ecosystems, Ch. 5. Primary production. I.B.P. 22.

STEELE, J.H. (1962). Environmental control of photsynthesis in the sea. Limnol.Oceanogr.,7,137-150.

STEELE, J.H. & YENTSCH, C.S. (1960). The vertical distribution of chlorophyll. J.Mar.Biol.Ass.U.K.,39,217-226.

STEEMAN-NIELSEN, E. (1974). Light and primary production. Ch.16, pp.361-388 IN Jerlov, N.G. & Steeman-Nielsen E. Optical aspects of oceanography. Academic Press.

STEWART, K.M. (1976). Oxygen deficits, clarity, and eutrophication in some Madison Lakes. Int.Rev.ges.Hydrobiol.,61,563-579.

STEWART, W.D.P., PEMBLE, M. & AL-UGAILY, L. (1978). Nitrogen and phosphorus storage and utilization in blue-green algae. Mitt.Internat.Verein. Limnol.,21, 224-247.

STRICKLAND, J.D.H. (1960). Measuring the production of marine phytoplankton. Bull.Fish.Res.Bd.Can.,122,1-172.

SVERDRUP, H.H. (1953). On conditions for the vernal blooming of phytoplankton. J.Cons.perm.int.Explor.Mer.,18,287-295.

TAGUCHI, S. (1976). Relationship between photosynthesis and cell size of marine diatoms. J.Phycol.,12,185-189.

TALLING, J.F. (1957a). Photosynthetic characteristics of some freshwater plankton diatoms in relation to underwater radiation. New Phytol. 56,29-50.

TALLING, J.F. (1957b). The phytoplankton population as a compound photosynthetic system. New Phytol.,56,133-149.

TALLING, J.F. (1960). Self shading effects in natural populations of a planktonic diatom. Wetter und Leben 12,235-242.

TALLING, J.F. (1965). The photosynthetic activity of phytoplankton in East African Lakes. Int.Rev.ges.Hydrobiol.,50,1-32.

TALLING, J.F. (1966). The annual cycle of stratification and phytoplankton growth in Lake Victoria (East Africa). Int.Rev.ges.Hydrobiol.,51, 545-621.

TALLING, J.F. (1969). Generalized and specialized features of phytoplankton as a form of photosynthetic cover. IN Prediction and measurement of photosynthetic productivity. Proc. IBP/PP Tech.meeting, Trebon.

TALLING, J.F. (1971). The underwater light climate as a controlling factor in the production ecology of freshwater phytoplankton. Mitt. Internat. Verein.Limnol.,19,214-243.

TALLING, J.F. (1973). The application of some electrochemical methods to the measurement of photosynthesis and respiration in fresh waters. Freshwat.Biol.,3,335-362.

TALLING, J.F. & DRIVER, D. (1963). Some problems in the estimation of chlorophyll a in phytoplankton. pp.142-146 IN Proceedings of conference on primary productivity measurement, marine and freshwater. U.S.Atomic energy commission, Division of Technical Information.

TALLING, J.F., WOOD, R.B., PROSSER, M.V. & BAXTER, R.M. (1973). The upper limit of photosynthetic productivity by phytoplankton:evidence from Ethiopian soda lakes. Freshwat.Biol.,3,53-76.

TAYLOR, A.H. & KERR, G.P. (1941). The distribution of energy in the visible spectrum of daylight. J.Opt.Soc.Am.,31,3-8.

THEKAEKARA, M.P. (1970). The solar constant and the solar spectrum measured from a research aircraft. NASA Tech.Rep.R-351.

TILMAN, D. & KILHAM, S.S. (1976). Phosphate and silicate growth and uptake kinetics of the diatoms *Asterionella formosa* and *Cyclotella meneghiniana* in batch and semi-continuous culture. J.Phycol.,12, 375-483.

TILZER, M.M. (1973). Diurnal periodicity in the phytoplankton assemblage of a high mountain lake. Limnol.Oceanogr.,18,15-30.

TITMAN, D. (1975). A fluorometric technique for measuring sinking rates of freshwater phytoplankton. Limnol.Oceanogr.,20(5),869-875.

TITMAN, D. (1976). Ecological competition between algae: experimental confirmation of resourse-based competition theory. Science 192, 463-465.

TITMAN, D. & KILHAM, P. (1976). Sinking in freshwater phytoplankton: some ecological implications of cell nutrient statues and physical mixing processes. Limnol.Oceanogr.,21(3),409-417.

TYLER, J.E. (1961) Scattering properties of distilled and natural waters. Limnol.Oceanogr., 6,451-456.

TYLER, J.E. (1975). The in situ quantum efficiency of natural phytoplankton populations. Limnol.Oceanogr.,20,976-980.

TYLER, J.E. & SMITH, R.C. (1970). Measurements of spectral irradiance underwater. Gordon & Breach, N.Y.

VOLLENWEIDER, R.A. (1965). Calculation methods of photosynthesis - depth cultures and some implications regarding day rate estimates in primary production measurements. pp.425-457 IN Goldman, C.R. (ed.) Primary productivity in aquatic environments. Mem.Ist.Ital.Idrobiol. 18 Suppl. Univ. Calif.Press, Berkeley.

VOLLENWEIDER, R.A. (1968). Scientific fundamentals of the eutrophication of lakes and flowing waters, with particular reference to phosphorus and nitrogen as factors in eutrophication. OECD Tech.Rept. Paris.

VOLLENWEIDER, R.A. (1969). A manual on methods for measuring primary production in aquatic environments. I.B.P. Handbook 12. Blackwell, Oxford.

VOLLENWEIDER, R.A. (1970). Models for calculating integral photosynthesis and some implications regarding structural properties of the community metabolism of aquatic systems. pp.455-472 IN Malick, I. (ed.) Prediction and measurement of photosynthetic productivity. Pudoc, Wageningen.

VOLLENWEIDER, R.A. & NAUWERCK, A. (1961). Some observations on the ^{14}C method for measuring primary production. Verh.Internat.Verein Limnol.,14,134-139.

WALKER, K.F. (1973). Studies on a saline lake ecosystem. Aust.J.Mar.Freshwat. Res., 24,21-71.

WALSBY, A.E. (1971). The pressure relationships of gas vacuoles. Proc.R.Soc.B. 178,301-326.

WALSBY, A.E. (1978). The properties and bouyancy-providing role of gas vacuoles in *Trichodesmium* Ehrenberg. Br.Phycol.J.,13,103-116.

WALSBY, A.E. & REYNOLDS, C.S. (1980). Sinking and floating. pp.371-412 IN Morris, I.G. (ed.) The physiological ecology of phytoplankton. Blackwell, Oxford.

WEISS, C.M. (1979). Trophic indices and their use in trophic classification of lakes and reservoirs of North Carolina. pp.141-211 IN Maloney, T.E. (ed.) Lake and reservoir classification systems. U.S.A. EPA-600/3-79-074.

WILLIAMS, W.D. (1973). Man-made lakes and the changing limnological environment in Australia. pp.495-499 IN Ackermann, W.C., White, G.F. & Worthington, E.B. (eds.) Man made lakes: their problems and environmental effects. Geophysical Monograph Series Vol.17.

WILLIAMS, W.D. (1976). The Australian inland aquatic environment: a background review for management purposes. A.W.R.C. Symp. on eutrophication.

WILLIAMS, W.D. & WAN, H.F. (1972). Some distinctive features of Australian inland waters. Water Res.,6,829-836.

WINCH, G.T., BOSHOFF, M.C., KOH, C.J. & DU TOUT, A.G. (1966). Spectro-radiometric and colorimetric characteristics of daylight in the southern hemisphere: Pretoria, South Africa. J.Opt.Soc.Am.,56,456-464.

WOLFF, D.A. (1975). The separation of cells and subcellular particles by colloidal silica-density gradient centrifugation. pp. 85-104 IN Prescott, D.M. (ed.) Methods in cell biology, Vol.X.

WRIGHT, J.C. (1960). The limnology of Canyon Ferry Reservoir. III. Some observations on the density dependence of photosynthesis and its cause. Limnol.Oceanogr.,5,356-361.

YENTSCH, C.S. & LEE, R.W. (1966). A study of photosynthetic light reactions, and a new interpretation of sun and shade phytoplankton. J.Mar.Res., 23,319-337.

APPENDIX 1

Growth rate (K, doubling d^{-1}) calculated using equation (4.8) as described in text, for bioassay flasks unenriched (C), or innoculated with sodium nitrate (+N) or potassium dihydrogen phosphate (+P) or both (N+P)(Chp. 2).

Date 10/12/79 — Growth period = 7 days

Depth (m)	0	1	2	5	10
C	0.008	0.11	0.3	0.42	0.43
+N	0.008	0.18	0.3	0.58	0.57
+P	0.01	0.15	0.17	0.43	0.44
N+P	0.55	0.56	0.57	0.59	0.57

Date 4/1/80 — Growth period = 6 days

Depth (m)	0	2.5	5	7.5	10	12.5	14.5
C	0.05	0	0.18	0.06	0.42	0.48	0.54
+N	0.01	0.01	0.10	0.14	0.56	0.69	0.68
+P	0.13	0.06	0.21	0.15	0.37	0.48	0.63
N+P	0.65	0.66	0.67	0.64	0.72	0.68	0.73

Date 16/1/80 — Growth period = 6 days

Depth (m)	0	2.5	5	7.5	10	11	12.5	15
C	0.04	0.12	0.13	0.07	0.07	0.24	0.39	0.45
+N	0.05	0.05	0.06	0.08	0.20	0.36	0.52	0.65
+P	0.26	0.17	0.22	0.24	0.24	0.24	0.40	0.46
N+P	0.66	0.73	0.76	0.72	0.73	0.69	0.78	0.74

Date 29/1/80 — Growth period = 4 days

Depth (m)	0	3	6	9	15
C	0.11	0.09	0.14	0.23	0.24
+N	0.56	0.60	0.54	0.53	0.65
+P	0.10	0.08	0.20	0.22	0.32
N+P	0.50	0.54	0.55	0.55	0.66

Date 6/2/80 — Growth period = 7 days

Depth (m)	0	5	10	12.5	15	20	25	30
C	0.07	0.01	0.14	0.21	0.24	0.29	0.29	0.29
+N	0.23	0	0.18	0.20	0.37	0.34	0.37	0.52
+P	0.22	0.15	0.20	0.25	0.19	0.24	0.25	0.21
N+P	0.49	0.46	0.52	0.57	0.48	0.60	0.55	0.46

Appendix 1 (Continued)

Date 13/2/80 — Growth period = 6 days

Depth (m)	0	5	10	14.6	20	25	30
C	0.18	0.19	0	0.29	0.34	0.36	0.6
+N	0.11	0.10	0.72	0.33	0.53	0.62	0.75
+P	0.29	0.13	0.22	0.42	0.40	0.38	0.6
N+P	0.68	0.67	0.72	0.75	0.67	0.71	0.74

Date 28/2/80 — Growth period = 7 days

Depth (m)	0	2.5	5	10	15	20	25	30
C	-0.05	-0.03	-0.05	0	0.19	0.33	0.41	0.53
+N	-0.05	-0.05	-0.04	0	0.20	0.32	0.33	0.58
+P	0.24	0.22	0.21	0.25	0.35	0.33	0.45	0.54
N+P	0.50	0.41	0.38	0.43	0.40	0.56	0.54	0.60

Date 11/3/80 — Growth period = 7 days

Depth (m)	0	2.5	5	10	15	20	25	28
C	0.07	0.08	0.04	0	0.06	0.09	0.06	0.1
+N	0.08	0.05	0.04	-0.02	0.03	0.22	0.20	0.1
+P	0.19	0.26	0.19	0.25	0.27	0.15	0.24	0.32
N+P	0.26	0.23	0.36	0.32	0.30	0.36	0.53	0.53

Date 1/4/80 — Growth period = 8 days

Depth (m)	0	2.5	5	10	15	20	25
C	0.21	0.18	0.20	0.20	0.31	0.17	0.21
+N	0.27	0.17	0.22	0.17	0.21	0.22	0.18
+P	0.32	0.31	0.28	0.34	0.29	0.29	0.29
N+P	0.53	0.41	0.52	0.49	0.53	0.53	0.43

Date 28/4/80 — Growth period = 4 days

Depth (m)	0	2.5	5	10	15
C	0.69	0.38	0.72	0.33	0.79
+N	0.33	0.44	0.41	1.11	1.15
+P	0.75	0.86	0.81	0.85	0.94
N+P	1.14	1.17	1.15	1.09	1.11

Date 13/5/80 — Growth period = 5 days

Depth (m)	0	1.0	2.5	5	10	15
C	0.22	0.34	0.31	0.24	0.21	0.19
+N	0.20	0.18	0.24	0.23	0.21	0.30
+P	0.56	0.58	0.57	0.69	0.62	0.46
N+P	0.61	0.71	0.67	0.68	0.82	0.66

Appendix 1 (Continued)

Date 18/6/80 Growth period = 5 days

Depth (m)	0	1	2.5	5	10	15
C	0.42	0.39	0.34	0.42	0.48	0.51
+N	0.45	0.38	0.32	0.42	0.49	0.35
+P	0.79	0.76	0.81	0.73	0.73	0.82
N+P	0.96	0.89	0.88	0.95	0.92	0.98

APPENDIX 2

Seasonal variations in cell volume ($mm^3\ \ell^{-1}$), chlorophyll *a* concentration ($\mu g\ \ell^{-1}$), organic-N ($mgN\ \ell^{-1}$), organic-P ($\mu gP\ \ell^{-1}$), protein ($mg\ \ell^{-1}$), carbohydrate ($mg\ \ell^{-1}$), total nitrogen (TN, $mgN\ \ell^{-1}$) and total phosphorus (TP, $\mu gP\ \ell^{-1}$)

Date	Cell volume	Chlor-a	Organic-N	Organic-P	Protein	Carbohydrate	TN	TP
3/10/79	-	-	0.86	66	-		1.49	165
17/10/79	0.18	2.2	1.09	58	-	-	1.75	166
31/10/79			0.89	50	-	-	1.53	153
1/11/79	0.46	3.5	-	-	-	-	-	-
5/11/79	0.84	7.6						
12/11/79	2.1	7.7						
14/11/79			1.04	57			1.69	140
15/11/79					1.621	0.242		
20/11/79	3.9	17			4.375	0.661(5.04)		
27/11/79	4.2	18			1.372	0.358(1.73)		
28/11/79			0.72	59			1.27	113
4/12/79	18.3	106.7			7.826	3.484(11.3)		
7/12/79		138			8.314	4.123		
10/12/79		126						
11/12/79	9.9	34.7						
12/12/79			1.82	119			1.97	143
18/12/79		80			3.948	3.440		
21/12/79					12.178	7.431		
23/12/79					8.286	6.289		
27/12/79	16.5	49.5			3.859	5.282(9.14)		
30/12/79					4.227	4.002		
2/1/80					3.064	4.005		
4/1/80	16.2	43.2			3.058	4.107(7.17)		
9/1/80			1.03	29			1.2	70
16/1/80	2.4	12.5			2.021	0.578(2.6)		
22/1/80	4.4	25			3.207	1.589(4.8)		
24/1/80			1.01	45			1.15	68
5/2/80					4.979	1.747		
6/2/80			1.03	51			1.19	71
13/2/80	12.5	31.7			2.724	1.425(4.1)		
18/2/80			1.78	104			1.89	120
19/2/80					7.680	7.944		
22/2/80					4.736	3.662		
28/2/80	41.1	127.9			9.012	9.973(18.9)		
5/3/80	13.3	38.5	1.32	41	3.489	3.475(6.9)	1.42	81
11/3/80	4.9	15.5			2.268	0.573(2.8)		
20/3/80					4.315	2.041		
28/3/80	14.4	50.2			4.736	2.676(7.4)		
1/4/80	1.3	5.5	0.81	28			1.27	44
14/4/80	4.3		0.99	19			1.21	39
16/4/80		18.9			2.260	0.499		
28/4/80	2.1		0.97	52	1.820	0.419(2.24)	1.36	77
5/5/80	8.3	39.8			2.341	0.692(3.03)		
12/5/80			0.80	51			1.41	70
13/5/80	2.1							
26/5/80	0.22		0.67	59			1.33	92

APPENDIX 3

Seasonal variation in ratios used to investigate nutrient limitation.

Date	chla / cell vol. (µg/mm³)	Protein / cell vol. (mg/mm³)	chla / carbohyd. (µg/mg)	ORG-N / cell vol. (mgN/mm³)	ORG-P / cell vol. (µgP/mm³)	ORG-N / ORG-P (µgN/µgP)	TN / TP (µgN/µgP)	min-N / sol-P (µgN/µgP)	carb / cell vol. (mg/mm³)	P / C (mg/mg)
3/10/79						13	9.03	6.4		
17/10/79	12.2			6.056	322.2	18.8	10.5	6.1		
31/10/79						17.8	10	6.2		
1/11/79	7.6			1.935	108.7					
5/11/79	9.0									
12/11/79	3.7			0.5	27.1					
14/11/79						18.2	12.1	7.8		
15/11/79										6.698
20/11/79	4.4	1.12	25.72						0.169	6.619
23/11/79										6.839
27/11/79	4.3	0.33	50.28						0.085	4.142
28/11/79				0.171	14.05	12.2	11.2	10.2		
4/12/79	5.8	0.428	30.63						0.190	2.511
7/12/79			33.47							1.876
11/12/79	3.5									
12/12/79				0.184	12.02	15.3	13.8	6.25		
18/12/79			23.26							1.338
21/12/79										1.639
23/12/79										1.318
27/12/79	3.0	0.234	9.37						0.320	1.423
30/12/79										1.056
2/1/80										0.765
4/1/80	2.7	0.189	10.52						0.254	0.745
9/1/80						35.5	17.1	4.1		
16/1/80	5.2	0.842	21.63						0.241	3.497
22/1/80	5.7	0.729	15.73						0.361	2.018

APPENDIX 3 (cont.)

24/1/80				0.23	10.2	22.4	16.9	6.09	2.850
5/2/80									
6/2/80						20.2	16.8	8	
13/2/80	2.5	0.218	22.2						0.114 1.912
18/2/80						17.11	15.8	6.9	
19/2/80									0.967
22/2/80									1.293
28/2/80	3.11	0.219	12.82						0.243 0.904
5/3/80	2.9	0.262	11.08	0.099	3.08	32.2	17.5	2.5	0.261 1.004
11/3/80	3.2	0.463	27.05						0.117 3.958
20/3/80									2.114
28/3/80	3.5	0.329	18.76						0.186 1.770
1/4/80	4.2			0.623	21.5	28.9	28.9	28.8	
14/4/80				0.23	4.4	52.1	31.0	11	
16/4/80			37.88						4.529
28/4/80		0.867		0.46	24.8	18.7	17.7	15.6	0.20 4.343
5/5/80	4.8	0.282	57.5						0.083 3.385
12/5/80				0.381	24.3	15.7	20.1	32.1	
26/5/80				3.05	268.2	11.4	14.5	20	